Documentation for the

Review Panel of the

GILDA beamline at ESRF

April 2009

Contents:

This report was written by F. d'Acapito and S. Mobilio, with the help of A. Balerna, F. Boscherini, P. Fornasini, P. Lattanzi, A. Martorana, C. Maurizio, M. Merlini, C. Meneghini, G. Polzonetti, S. Quartieri, F. Rocca and G. Venturoli, who significantly contributed to section V (Overview of the overall scientific activity) and section VII (Highlights of the scientific activity).
The technical help of V. Tullio is acknowledged.

I. Technical description of the beamline

I.1 Introduction

The Italian Collaborating Research Group GILDA at ESRF[1] is a general-purpose beamline using a bending magnet source. It is now financed by two major italian public research Institutes (Consiglio Nazionale delle Ricerche CNR, and Istituto Nazionale di Fisica Nucleare).
It is operational since Sept 1994, and is mainly dedicated to the investigation of atomic structures. At this purpose, techniques like X-ray Absorption Spectroscopy as well as X-ray Diffraction are used on the beamline in the energy range 4-90 keV. The GILDA beamline consists in four hutches: the first contains the optical elements and the others the experimental apparata. The first experimental hutch, is dedicated to X-ray Absorption Spectroscopy (XAS) and is placed in the 1:3 horizontal focal configuration to obtain the maximum flux from the sagittally focusing monochromator. The wide energy range of the beamline makes GILDA well-suited for XAS investigations on mid-heavy elements with the possibility to access the K absorption edges from Ca to Au and the L edges from Sb on. Experiments are carried out in transmission, fluorescence and total electron yield modes. For the study of highly diluted samples a 13-elements high purity Ge detector is currently used (current limit sensitivity: 10^{14} at/cm^2). Surface experiments in total reflection mode (ReflEXAFS) are performed in a dedicated experimental chamber.
The second hutch, in 1:1 focal geometry, is dedicated to X-ray scattering and diffraction. Time-resolved (10^1-10^2 minutes) powder diffraction experiments can be performed, by using a Translating Image Plate coupled to a hot air blower.
A third experimental hutch at the end of the beamline is available for users who wish to install their own apparatus. An ultra high vacuum chamber fully equipped for surface preparation and characterization is available for surface-EXAFS investigations.

I.2 Optics

The beamline, schematically shown in figure 1,

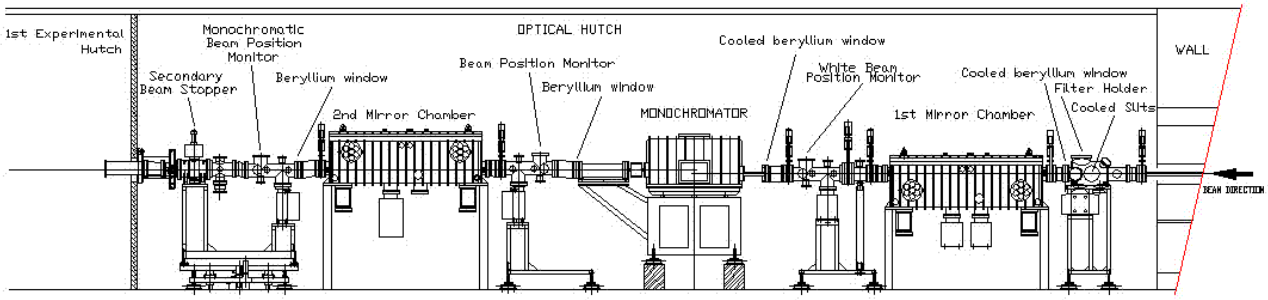

Figure 1
Layout of the optical hutch.

provides a monochromatic x-ray photon beam in the energy interval 4 - 90 keV, with an energy resolution $\Delta E/E \approx 10^{-5}$ - 10^{-4}, a spot size of about 1*1 mm and a flux at the sample position up to 10^9 - 10^{11}ph/s. To achieve these performances, the beamline works in four distinct optical configurations. At intermediate energies (7-27 keV) the first mirror intercepts the horizontal fan of radiation at a glancing angle of 3 mrad, reflecting and collimating the beam in the vertical direction.

[1] D'Acapito F., Colonna S., Pascarelli S., Antonioli G., Balerna A., Bazzini A., Boscherini, Campolungo F., Chini G., Dalba G., Davoli I., Fornasini P., Graziola R., Licheri G., Meneghini, Rocca F., Sangiorgio L., Sciarra V., Tullio V., Mobilio S., ESRF Newsletter **30** (1998), 42.

The monochromator is a double-crystal and double rotation axis device with fixed-exit. The second crystal is sagittally curved to focus the beam in the horizontal plane; dynamical focusing[2] is used to keep beam dimensions in the focal point constant throughout a full energy scan and can be used in the whole energy range of the beamline. By using a wide fan the minimum horizontal size Full Width Half Maximum (h-FWHM) for the beam on the sample is limited, due to the slope error induced by the second crystal ribs, to about 1-2 mm. When needed the part of the crystal between two ribs can be used to achieve a beam horizontal FWHM of only 100 μm.

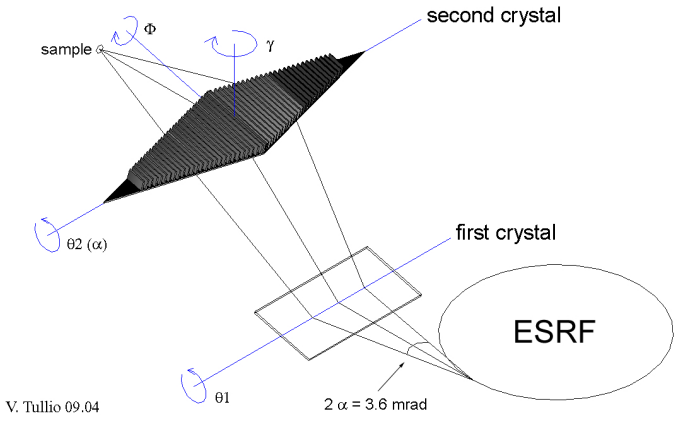

Figure 2
Schematic view of the sagittally focussing monochromator operative at GILDA

The second mirror focuses the beam in the vertical direction in three focal points at the interior of each of the three experimental cabins. The mirrors have a double coating to achieve efficient harmonic rejection in the 7-21 keV(Pd coat) or 21-27 keV (Pt coat) when working at 3 mrads. With the new second mirror we achieved a good focalization of the beam v-FWHM in the vertical direction with values of about 100 μm. At low energies (4 - 7 keV), Si(111) monochromating crystals are used together with a further pair of Pt coated mirrors working at 10 mrad for an efficient rejection of the harmonics. At high energy (27 - 50 keV), mirrors are removed and Si(511) crystals are used.

Recently, some additional operating modes have been added in order to improve the quality of the beam on the sample. In particular we have started using a flat crystal for carrying out highest quality measurements in transmission mode. In this configuration the ribbed second crystal is left un-bent. In this way a noticeable improvement in the beam homogeneity has been achieved, that revealed to be crucial in the study of slightly inhomogeneous samples (ground powders, high absorption levels) requiring very low levels of noise ($<2*10^{-4}$). The considerable intensity loss (about 50-200) is not critical as in the case of transmission mode data the noise is dominated by other sources than the statistical fluctuations. A further working mode involves the use of the mirrors. Considered that the use of the small pair of Pt coated mirrors for harmonic rejection lead to a too high beam intensity reduction (about 70%) the use of the Pd coated mirrors at an angle of 3.6 mrad was decided. In this way we increased the harmonic-free range of the beamline down to 6 keV so including the Mn-K edge that in the last years was hugely used by the users.

[2] Pascarelli S., Boscherini F., D'acapito F., Hrdy J., Meneghini C., Mobilio S., J. Synchrotron Rad. **3** (1996) 147.

I.3 The XAS facility

The x-ray absorption spectroscopy (XAS) hutch has been designed to carry out XAS experiments in different ways, ranging from concentrated to dilute samples (limit dilution 10 ppm or 10^14 at/cm^2) and from bulk to surfaces (limit thickness 0.2 Ml). The conventional XAS apparatus consists in two experimental high vacuum chambers

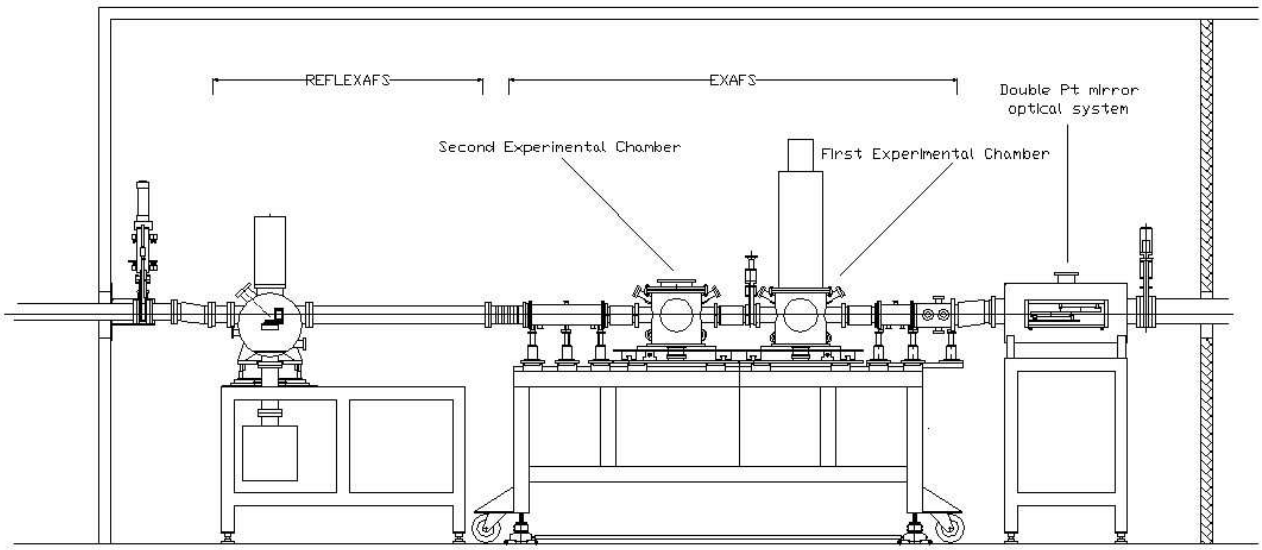

Figure 3
. Layout of the EXAFS Hutch

the first chamber is used for standard experiments, while the second one is available for the installation of bulky/heavy cells from the users (Figure 3). Depending on the nature of the samples a number of different detectors are available at the beamline, namely:

1) Ion Chambers: two chambers are used for measurements in transmission mode. They can be filled with N, Ar or Kr gases to ensure a good efficiency in the whole energy range.

2) High Purity Ge multidetector (13 elements): this detector is used for the collection of high quality fluorescence spectra with a typical energy resolution of 200 eV and maximum count rate of 100 kcps/element. A digital pulse processing permits a fast and reliable calibration of the device , an easy correction for dead time effects [Ciatto et al. 2004] as well as an effective subtraction of the background [D'Acapito et al. 2007e].

3) Electron detectors to perform measurements with surface sensitivity. In particular the measurement of the sample current, the detection of electrons with a channel multiplier (with possibility to perform partial yield) and detection of electrons amplified by a He chamber are available.

XAS measurements can be carried out in a wide temperature range using a liquid He cryostat (4-500 K). A translation/rotation stage mounted on top the liquid nitrogen cryostat allows the accurate positioning of the sample respect to the beam polarization direction, so permitting to easily carry out "polarized EXAFS" experiments; the use of a vibrating sample holder helps in minimizing the effect of coherent scattering when analyzing single crystals[3]. A cell, specially

[3] A. Martorana, G. Deganello, A. Longo, F. Deganello, L. Liotta, A. Macaluso, G.Pantaleo, A. Balerna, C. Meneghini and S. Mobilio, J. Synchrotron Rad. **10** (2003). 177.

conceived for gas-solid reactions, has been realized in collaboration with the Palermo university and is now available to all users [Longo et al. 2005].

A further experimental chamber is dedicated to total reflection EXAFS (ReflEXAFS) measurements for the investigation of surfaces or buried interfaces. The sample is oriented with the surface parallel to the polarization vector and the incidence angle can be adjusted within $1.2*10^{-3}$ deg. The size of the incident beam is about 50 μm. The intensity of the "incoming" and "specularly reflected" beams is measured by ion chambers whereas the fluorescence signal can be collected using the multielement Hp-Ge detector. Samples can be also prepared in situ by evaporation and an oven permits the sample treatment in controlled gas atmosphere up to 700 K. The main limitation on the use of ReflEXAFS technique is represented by the stringent conditions required on the samples in terms of length (a few cm), roughness and flatness, conditions that not always are satisfied. Therefore, to avoid the use of the REFLEXAFS apparatus when total reflection in not possible an alternative data collection system that permits measurements in grazing incidence (ϕ = 2 deg) mode inside the first EXAFS chamber was recently developed

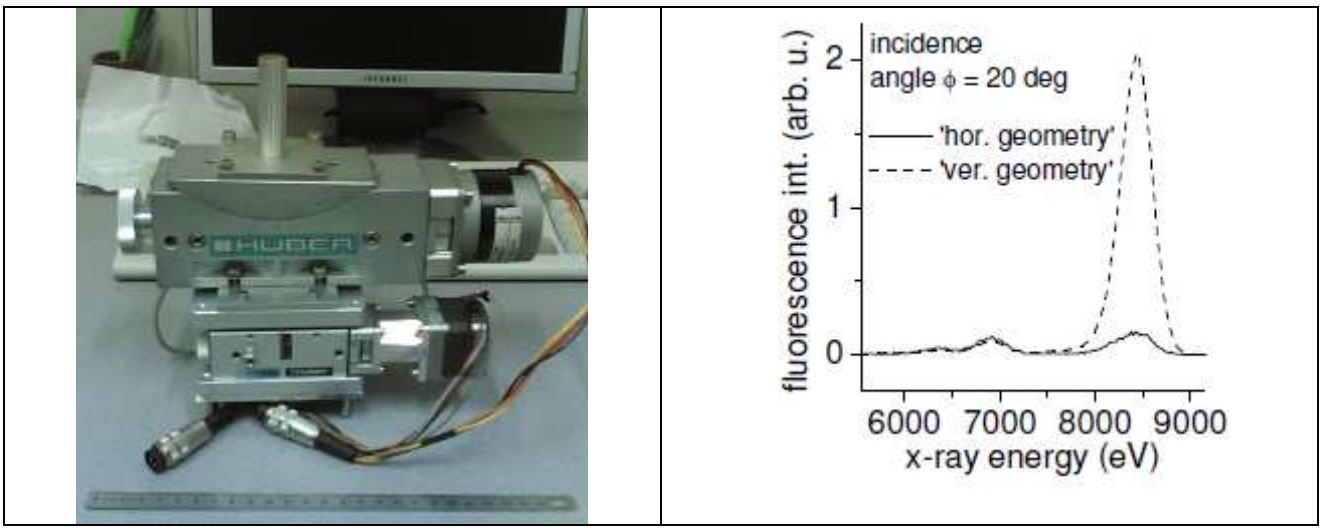

Figure 4.

Left: picture of the sample holder for measurements in grazing incidence mode. Right: comparison between the Er-L_α emission from a thin layer of Er doped glass onto a pure glass substrate. Here two collection geometries are compared with a common value for the incidence angle (20 deg): Hor geometry i.e. with the sample surface on an horizontal plane (as realized by the holder presented here) and Ver geometry i.e. with the sample surface on a vertical plane. Note the improvement of the ratio between the elastic and fluorescence peak in the former case respect to the latter.

The apparatus has demonstrated to be highly effective in reducing the spurious signal from the substrate in the case of analysis of samples in thin film form.

I.4 The X-ray Diffraction Facility

The diffraction hutch is equipped with a Translating Image Plate (TIP) detector to carry out experiments of time resolved x-ray diffraction[4].

[4] C. Meneghini, G. Artioli, A. Balerna, A. F. Gualtieri, P. Norby and S. Mobilio, J. Synchrotron Rad. **8**, (2001) 1162.

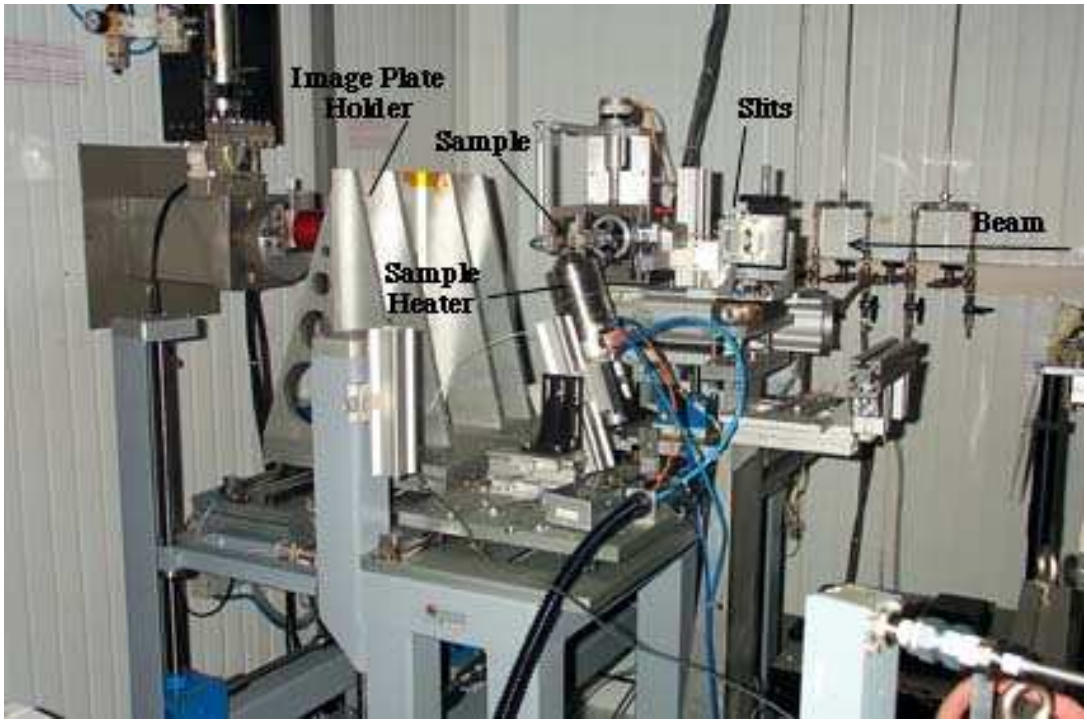

Figure 5
The apparatus for Time resolved x-ray Diffraction

The Image plate has a resolution of 100 *100 μm and is placed at about 30 cm from the sample: this permits the collection of data up to a scattering angle of about 40 deg. Phase transitions in the range of 10^1-10^2 minutes can be studied in samples contained in thin capillaries (0.2-1 mm) and undergoing heat treatments via an air blower (up to 1000 deg) or chemical reactions. In front of the TIP a slit selects a vertical slice of the diffracted beam; the TIP can translate horizontally so permitting the collection of time resolved data. An IP reader is available in the terminal room of the beamline. A MAR345 Image Plate detector has been recently purchased in order to replace the old IP system.

I.5 Third Hutch

The third experimental hutch was conceived for users wishing install their own apparata on the beamline. At present, an apparatus dedicated to EXAFS in Ultra High Vacuum conditions is mounted.

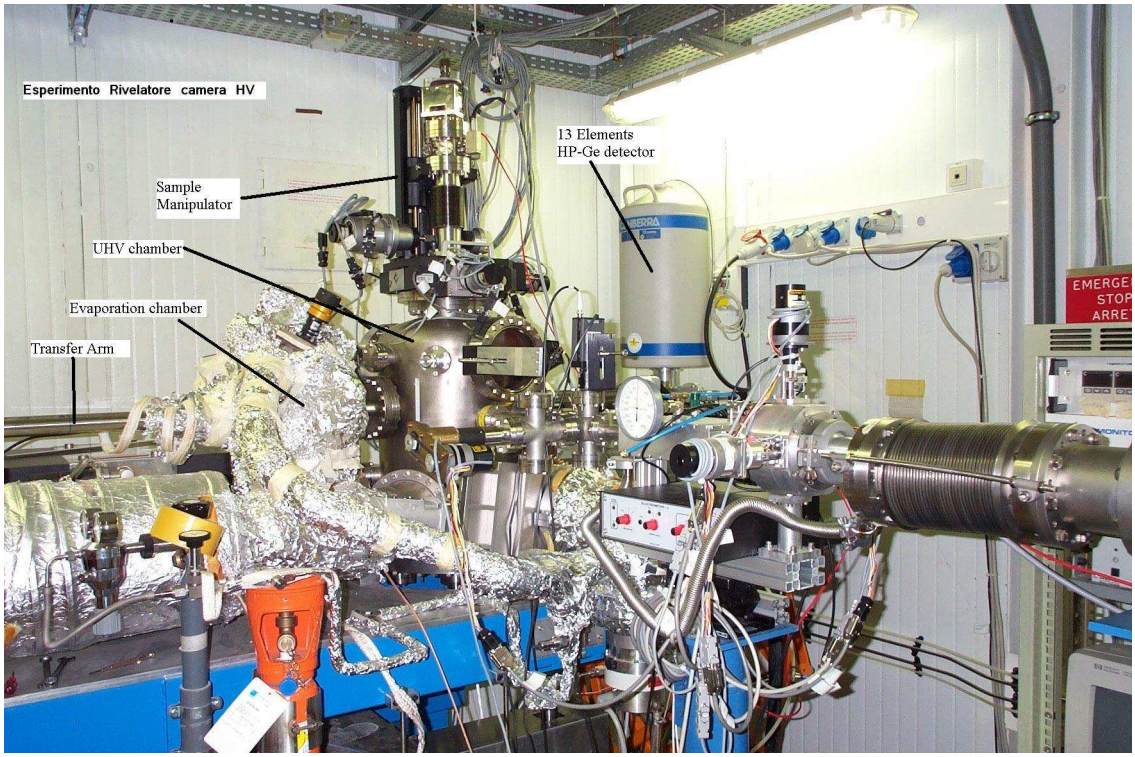

Figure 6.

Picture of the UHV chamber. It is capable to reach a base pressure of 10^{-10} mbar, containing an angular resolved electron detector, an Auger electron analysis system and a manipulator to align the sample and keep it at temperatures between LNT and 700 K. A side chamber is used for sample preparation using an evaporator and a transfer arm connects the two chambers. Detectors like multielement HP-Ge or a channeltron can be used for the collection of surface EXAFS data.

Due to lack of staff, the instrument is not operative at present.

II. Staff and associated roles

Gilda has two kinds of staff, the personnel permanently resident in Grenoble and the Italian collaborators.

At Grenoble at the moment two scientists with permanent positions (F. d'Acapito and C. Maurizio) of the Consiglio Nazionale delle Ricerche (CNR) are present. Francesco D'Acapito is a senior scientist and is Habilité à Diriger des Recherches on behalf of the Université Joseph Fourier – UJF– of Grenoble . He is responsible of the management of the beamline; his scientific activity regards mainly the study of optoelectronic materials, nanostructured systems and Diluted Magnetic Semiconductors. Chiara Maurizio is a scientist; her scientific activity regards the study of optoelectronic materials, ion-implanted glasses and clusters. A further permanent position as scientist is under decision following an open call of CNR; however due to burocratic formalities but there is no guarantee that the winning candidate will accept the transfer to Grenoble.

In the period 2003-2008 F. Bardelli worked at GILDA firstly as a PhD student of the UJF (up to 2006) and in the following years as post-doc. Other post-doc positions were given to C. Battocchio (2005, dedicated to EXAFS activities) and M. Merlini (engaged at 50% in 2006 on diffraction activities). Since 2006 Mauro Rovezzi is the PHD student from UJF; his thesis concerns the study of Diluted Magnetic Semiconductors under the responsibility of F. d'Acapito. The end of this thesis is foreseen for September 2009.

At present there is no perspective of hiring neither a new PhD student nor a post-doc due to the recent freezing of the funds dedicated to the personnel by the CNR administration.

In 2004 there were two technicians (F. Danca and F. la Manna both engaged at 50%) with permanent positions and dedicated to the support to the activities at GILDA. Since 2006 one of them (F. Danca) transfered in Italy and the other one was dedicated to other activities.

The technical operation of the beamline have been ensured till Jan 2009 by a Fixed-Term technician (H. Pais). The renewal or extension of this position was not possible due to lack of financial contribution from the partners so at present there is no technical personnel permanently resident at GILDA. A few basic technical issues are covered by the ESRF technician charged for the CRG operations, E. Dettona.

For what concerns the associated personnel they gave an un-valuable contribution to the design, construction, installation and commissioning of the beamline in the beginning phase. Now they are assuming more and more the role of external users, with strong scientific interaction with the permanent staff. At the moment their role in an eventual new project of the beamline is not defined.

In the period 2004-2008 the contributions came mainly from the Frascati National Laboratory of INFN with two technicians (engagement at 25%) reduced to one since June 2008 and University of Roma TRE, with two scientist, S. Mobilio who is in charge of the overall project responsibility (engagement at 25%) and C. Meneghini dedicated to the management of the diffraction instrumentation (engagement at 15%).

University of Trento contributed with technical support to the EXAFS instrumentation developed by this group in the initial phase.

Finally also A. Balerna and F. Boscherini gave occasionally their help in the management of the beamline instrumentation.

III. Statistical data of the GILDA Users and Scientific Production

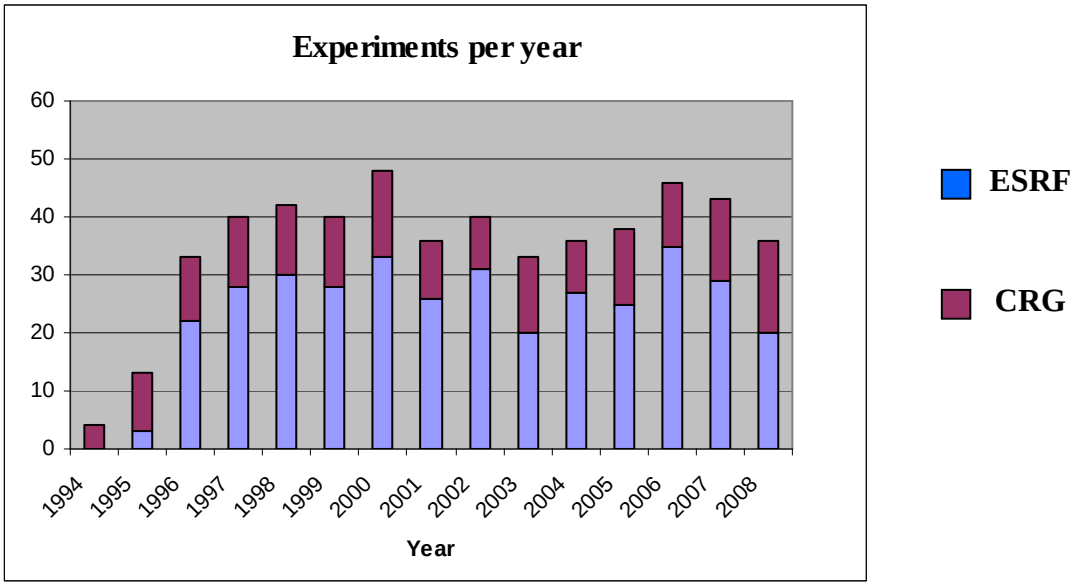

Figure 1
Number of experiment approved and performed per year divided between ESRF and CRG users

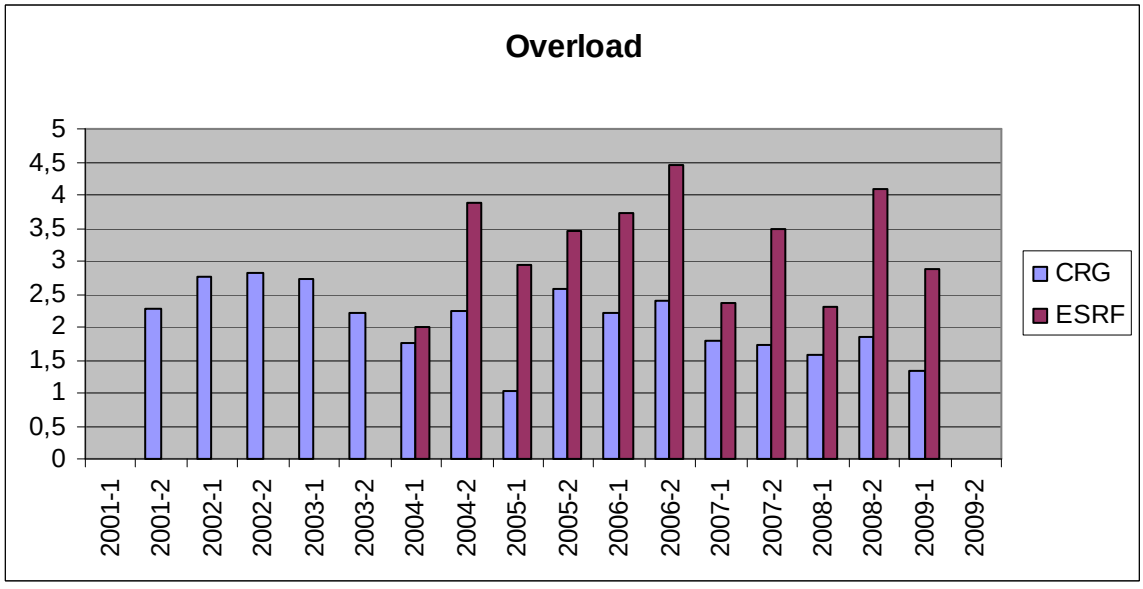

Figure 2
Overload of the request in term of number of shifts

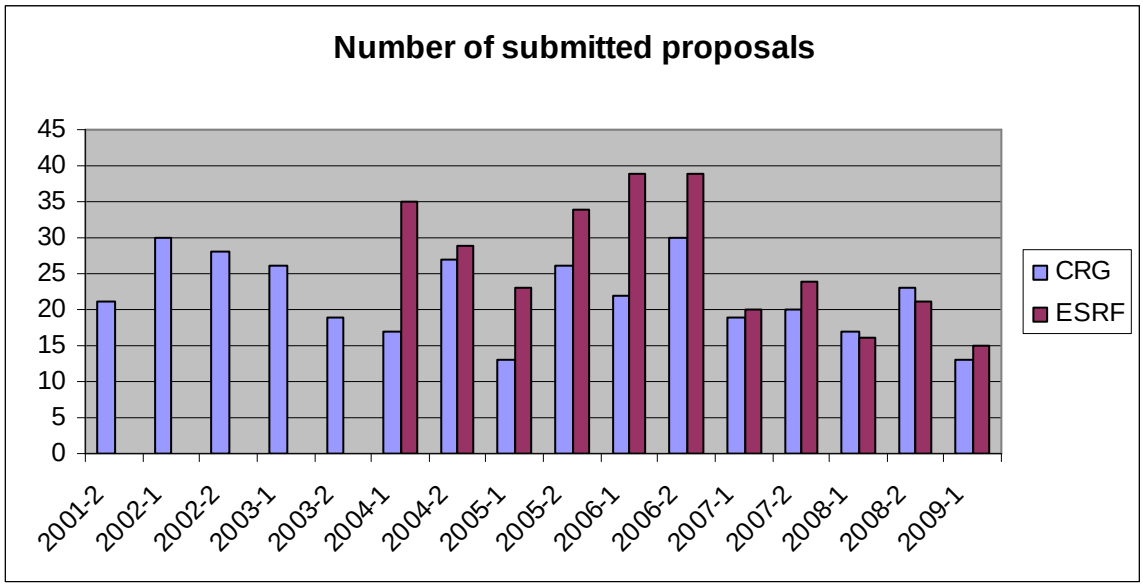

Figure 3
Number of the submitted proposal per period

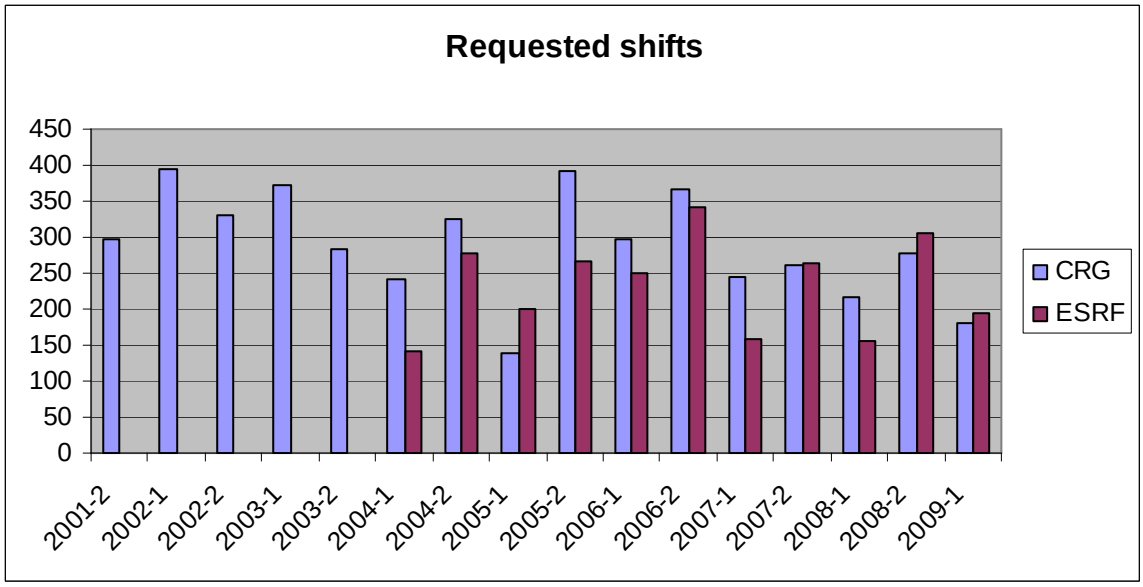

Figure 4
Number of the requested shifts per period

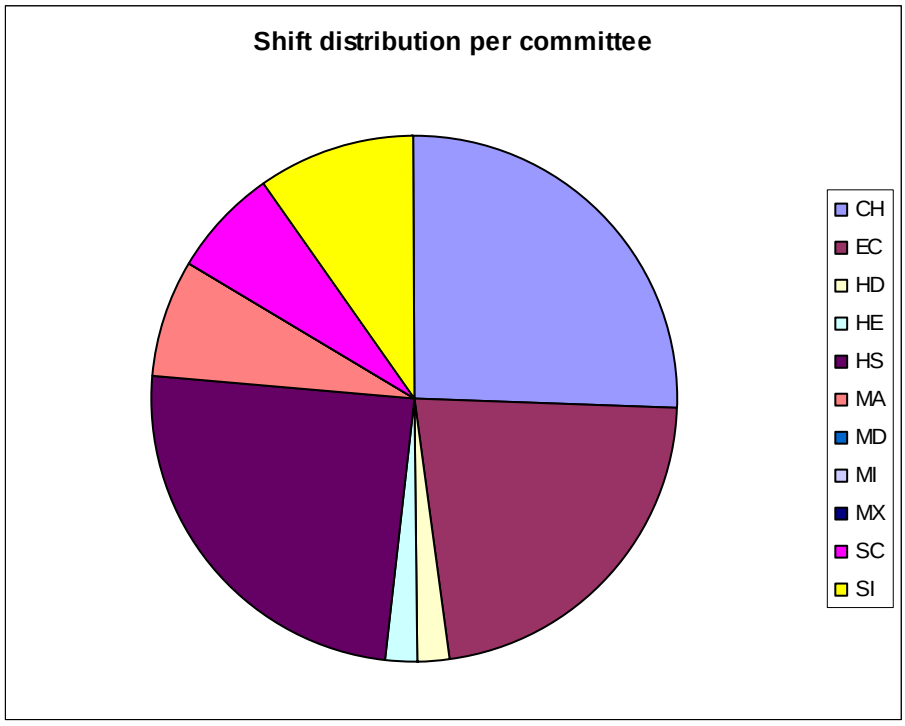

Figure 5
Distribution of requested shifts per committee (including italian experiments)

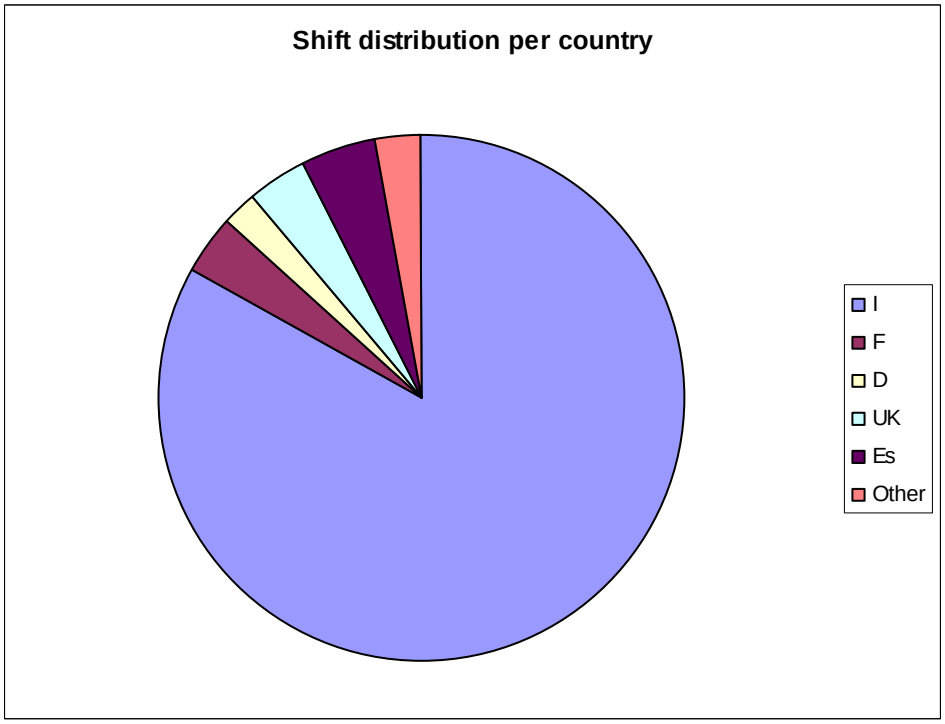

Figure 6
Distribution of requested shifts per main proposer country (ESRF proposal only)

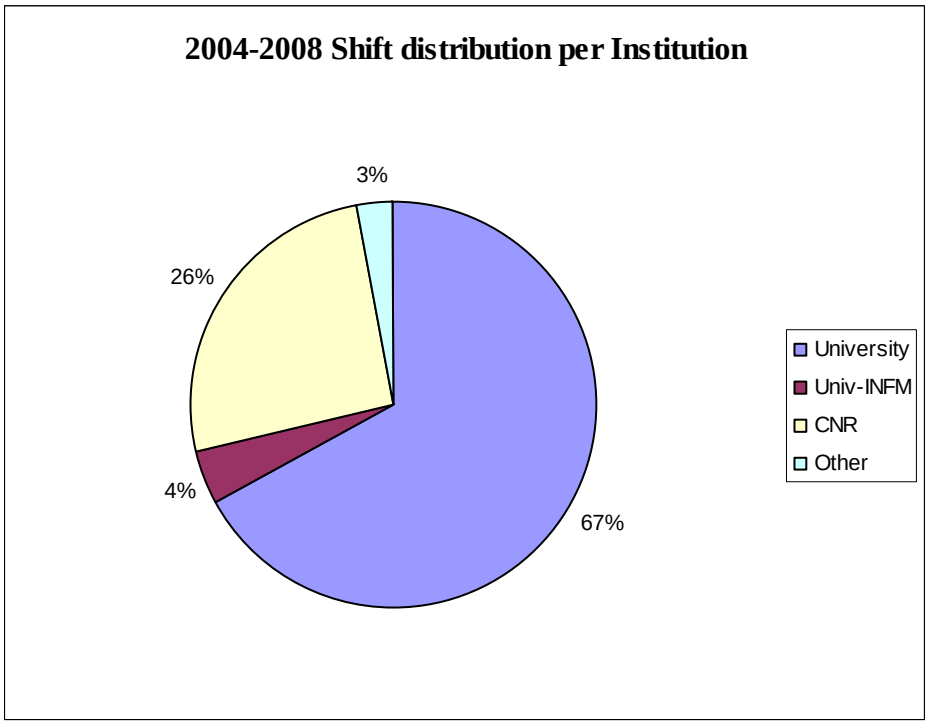

Figure 7
Distribution of the shifts per Institutions (all experiments, based on the affiliation of the Italian main proposer)

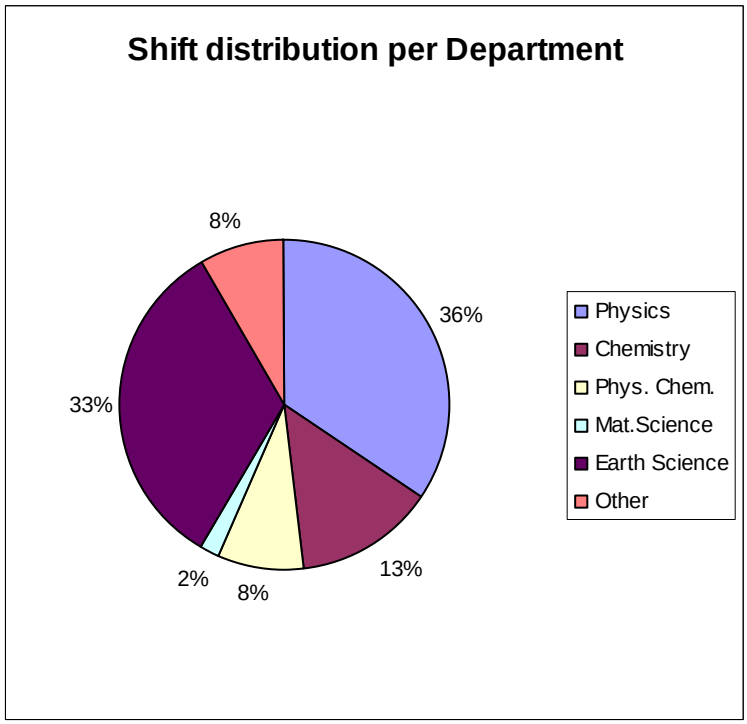

Figure 8
Distribution of the shifts per Department (all experiments, based on the affiliation of the Italian main proposer)

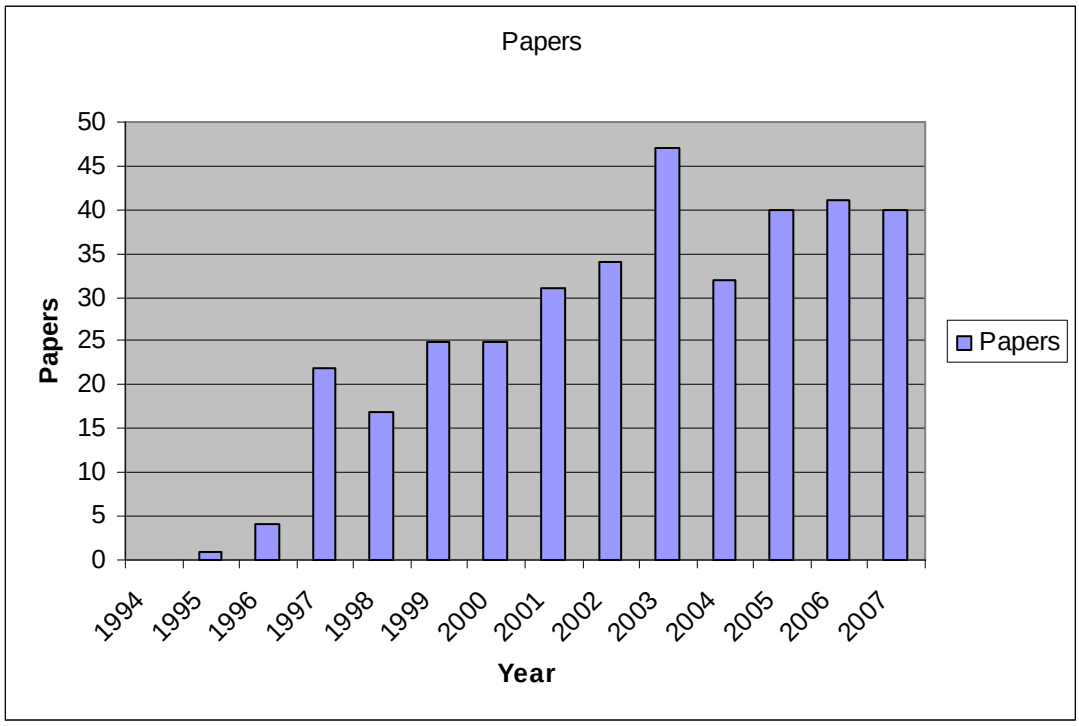

Figure 9
Annual distribution of the papers published on international journals

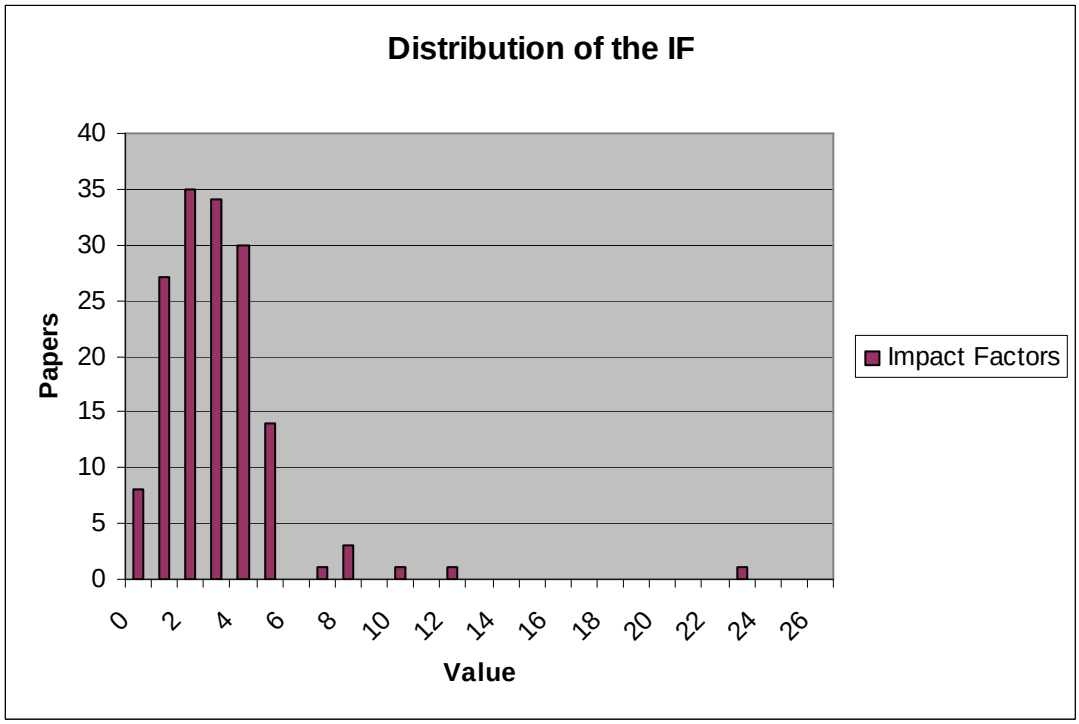

Figure 10
Distribution of the Impact Factors of the 2004-2008 GILDA publications

IV. Future perspectives and plans for upgrade

GILDA was realized more than 15 years ago and since then no major refurbishment action has been carried out on the instrumentation apart for the change of the second mirror; during these years the instrumentation of the beamline was continuously upgraded to ameliorate the overall performances in terms of spectra signal to noise ratio, dilution limits, stability, spot dimension. Now the bulk of the instrumentation overcome its reasonable operating lifetime and a deep refurbishment of the beamline is needed.

At present some refurbishment actions are in progress and regards the beamline stepper motor drivers and vacuum control system. We are dismissing the old stepper motor drivers, which run under OS-9 operating system, and we are installing the new ICEPAP cards under SPEC control. Moreover we purchased the standard ESRF instrumentation for beamline vacuum control (PLC, gauges and related readers, …) and the whole system will be installed during the summer shutdown 2009.

To continue the beamline operation in a reliable condition for the next five years additional refurbishment is needed, in particular the change of the monochromator and the replacement of the old Ge multi-detectors with a new one.

A proposal to the Italian Institution supporting GILDA (CNR and INFN) for the financial support of these refurbishments has been submitted and now is under evaluation.

We are defining a project for a radical reconstruction of the beamline. The X-ray optics is being designed and optimized for a beam with low divergence-and-size as well as possessing a high spatial homogeneity and temporal stability. This will permit to us to take advantage of the Upgrade Plan of the ESRF by realizing a beamline that makes a better use of the high brilliance of the source as well as of the noticeable stability that will be available with the forthcoming *top-up* filling mode. The new beamline will give a contribution in some of the strategic areas defined in the *ESRF Science and Technology programme 2008-2017* (in short referred to as the *Purple Book*) mainly "Nanoscience and nanotechnology" and "Science at Extreme conditions". The design criteria will make the beamline particularly adapted to measurements in total-reflection/glancing-angle conditions as well as to high quality (low-noise) conventional EXAFS measurements. The former data collection mode is of paramount importance for the analysis of surfaces of materials as it permits the minimization of the spurious signal coming from the substrate. Materials consisting in low-level doping (bulk materials in nm sized layers or, alternatively, depositions of $\leq$ 1atom/nm^2) need necessarily this kind of data collection that allows also the realization of experiments in real (i.e. non UHV) conditions. There are several research issues of strategic importance, as underlined by the recent *European White book of Fundamental Research in Materials Science* (edited by the Max Planck Institute), that will benefit from a beamline optimized for glancing angle measurements. Just to cite a few cases: in the field of electronics where the realization of devices below the 90nm node need both the realization of shallow junctions and new low-dielectric constant oxides for the replacement of SiO_2. Also in the case of surface heterogeneous catalysis the same publication evidenced the need of moving beyond the commonly used methods for surface analysis based on UHV environment by developing investigation techniques capable to realize real working conditions for the material. Both issues need surface structural investigations of materials for which the new beamline will be particularly adapted.

A design for the x-ray optics has been defined with the aim of obtaining a beamline with focused beam operating in the range 5-40 keV with a beam size of about 200 μm and a divergence below 0.01 deg. The beamline will provide an intense and stable beam also in an energy range

(E=20-40 keV) still poorly covered by gap-scanning undulator sources. The high beam intensity will be achieved by focalization using toroidal mirrors. This technical solution has the advantage of being achromatic so it will ensure a high homogeneity and spatial stability of the beam. The beamline layout will be compatible with the existing lead hutches. A schematic layout of the beamline is the following.

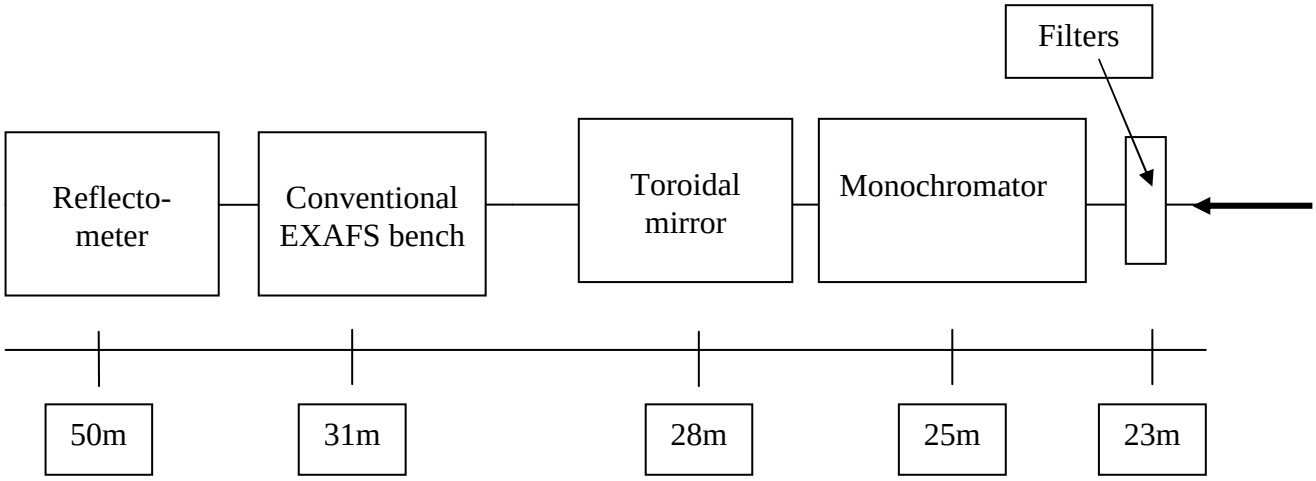

Figure 1.
Schematic layout of the new beamline (not to scale). The distances in meters are relative to the source.

- **Attenuating filters** and slits. These will be necessary in order to reduce the thermal load on the monochromator at the highest energies.
- **Monochromator**. It will use flat crystals and will host at least two or three pairs that will be possible to change by simply shifting horizontally the device. The cooling will be of cryogenic type in order to minimize the thermal bump.
- **Toroidal mirror** in 1:1 focusing configuration. The mirror will be realized starting from the substrate of the present one and will consist in two cylindrical channel with coverage of Pt and Si. The incidence angle will be 2mrad so permitting a full harmonic free operation range of 5-15 kev (Si mirror) and 15-40 keV (Pt mirror).
- **First experimental hutch** placed in the same position as the present one. This will host the instrumentation for the data collection in transmission mode already operative on the beamline. The beam in this zone will be unfocused as in this case no high intensity or reduced dimensions are needed.
- **Second experimental hutch** that will result from the merging of the present second and third hutches. In this zone the beam will be fully focused and here we will place the instrumentation for the EXAFS data collection from thin films. The instrumentation will consist in a reflectometer that will permit the orientation of the sample respect to the beam in total reflection conditions. The purchase of a new fluorescence detector will be needed in order to ensure reliable operation of the experimental station. Time resolved diffraction experiments will be still possible with the calculated beam parameters.

A simulation of the beam shape on the sample location (2^{nd} hutch) is show below:

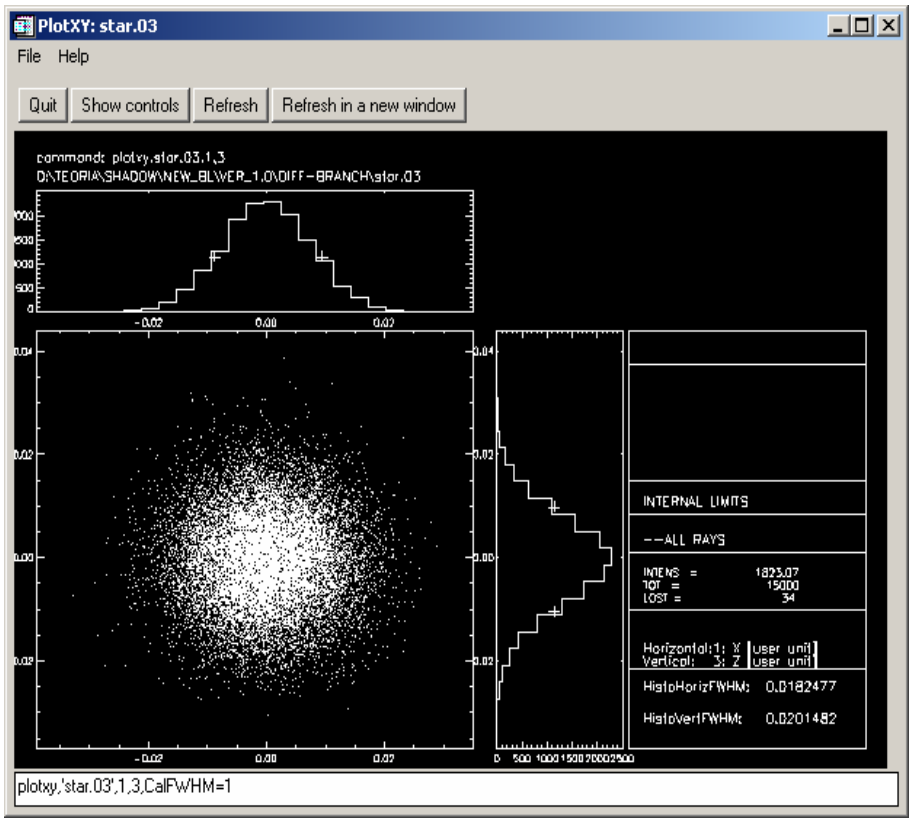

Figure. 2.
Simulation of the beam shape at 20 keV in the sample position. The computation was carried out using the SHADOW code. For the toroidal mirror the slope error data relative to the actual GILDA cylindrical mirror were used. Simulations based on more realistic slope error data aer in progress.

The beam will have a size of about 200 * 200 mm^2 and an intensity in the range of 10^{10} ph/s .

V. Overview of the overall scientific activity of GILDA 2004 – 2008

In this section we give a complete overview of the scientific activity performed at GILDA beamline during the five years 2004-2008, based on the experiments performed, on the experiments reports and on the published paper. The overall material is presented according to the following research fields:

A. Information and Communication technologies, with the subfields Material science for optoelectronics, Materials with peculiar magnetic behavior and semiconductor;
B. Nanoscience and Nanotechnology, with the subfields Semiconductors nanoparticles and Metallic nanoparticles;
C. Materials for energy production and transport;
D. Environment with the subfields of Earth Science, Pollution and Archeological and Cultural Heritage;
E. Life Science;
F. Soft Condensed Matter;
G. Catalysis;
H. Miscellanea with the topics of thermal expansion, phase transition and local lattice distortions;
I. Instrumentation and data treatment methods.

A. Information and Communication Technologies

A1. Material science for optoelectronics

In recent years, the material science for Information and Communication Technology has taken progressively more advantage from synchrotron radiation based techniques. This class of materials are often in form of thin films that are intentionally doped with one or more chemical species that are used to tailor a specific macroscopic property. Since the macroscopic properties of the obtained composite system often depend on the nano and sub-nano structures formed around the dopant, the x-ray absorption spectroscopy (XAS) is an elective tool to correlate the macroscopic response of the system with its structure at the atomic scale. Moreover, due to the irrelevance of any long-range (crystalline) order considerations in interpreting the XAS data, the XAS is also successfully used in investigating the atomic structure of glassy systems: in particular, it has been demonstrated to efficiently complement x-ray diffraction analyses in case of amorphous systems that are in the proximity of the crystallization.

The experiments carried out at the GILDA beamline on the materials for the Information and Communication Technology in the last five years focussed on the investigation of the link between their peculiar optical response and the local structure around the dopant atoms. In fact, the luminescence emission of materials is mainly dependent on the local structure and site symmetry of the luminescent centers that have to be controlled to finely tune the optical properties of the systems, in term of luminescent efficiency and/or of the emission wavelength.

The experiments performed at the GILDA beamline are mainly based on the x-ray absorption spectroscopy. The high flux available on the beamline in a wide x-ray energy range (in this case from the Er L_{III}-edge, 8358 eV to the Er K-edge, 57486 eV), together with the use of a state-of-the art fluorescence detector allowed to perform high-quality experiments that leaded to significant steps forward in this field of research. In specific cases the x-ray diffraction also allowed a structural characterization of the composite systems.

The papers published focussed on three main subjects.

The first one is on Er-doped glasses for optical amplifiers. The second subject addressed by the GILDA users is the study of light waveguides obtained by metal-for-alkali ion exchange in glass matrices. The third is on the x-ray excited optical luminescence experiments, that, in some specific cases, have proved their capability to investigate preferentially the luminescent sites of a selected atomic species.

Rare-earth doped materials

The Er^{3+} ions emission (1.5 μm) matches the low-absorption range of the silica glass, so that Er-doped silica-based glasses are very promising in the field of optoelectronics. To this respect, the research performed by different groups at the GILDA beamline was aimed i) to investigate the incorporation of Er in different glasses and glass-ceramics and with different techniques, to overcome as most as possible the low solubility limit of the rare-earth in the pure silica glass; ii) to explore the possibility of using efficient sensitizers for the Er ions to overcome the low cross section of the Er 1.5 μm emission.

Rare-earth doped materials: Overcoming of the Er solubility limit.

To overcome as most as possible the low solubility limit of Er ions in silica or silicon, the incorporation of Er in glasses and glass ceramics with different techniques was explored. In fact, the Er photoluminescence (PL) efficiency drops down if the Er site symmetry is centrosymmetric and/or in the presence of non-radiative de-excitation channels for the Er ions.

When embedded in crystalline Si by ion implantation, the concentration quenching effect occurs because the Er atoms form silicides, in which the Er site is centrosymmetric, and the 1.5 μm transition is forbidden. One possibility to overcome this problem is the co-doping with Er and O atoms. The EXAFS experiments performed at the Er L_{III}-edge on this kind of systems, prepared by different synthesis routes (ion implantation or MBE), revealed that the Er ions are five or six fold oxygen coordinated, with a bond length of 2.24 Å (to be compared with 6 O atoms at about 2.27 Å in the crystalline Er_2O_3); moreover, a well defined Er-O-Si bond was found, of about 135 deg, leading to an Er-Si distance of 3.58 Å [D'Acapito et al. 2004a, D'Acapito et al. 2005].

The use of non-equilibrium techniques for the Er incorporation into a matrix, as the cited ion implantation, is quite promising because the concentration threshold for the PL quenching can be raised. For this reason, the field-assisted solid-state ion exchange technique was also explored for the first time to prepare Er-doped silicate glasses: the first experimental results indicate that the Er site is similar to what found when Er is embedded in crystalline Si [Cattaruzza et al. 2009].

To investigate the possible structural modification of the Er site correlated with the PL quenching induced by the Er concentration, an EXAFS experiment was performed on a phosphate glass doped with Er at different concentration values, below and above the concentration threshold (that in this glass is about 2 at%). To have access to a larger range in the photoelectron wave number, the EXAFS spectra were recorded in this case at the Er K-edge (E_0 = 57486 eV). It has been found that no significant changes in the Er site occurred at varying the Er concentration around the concentration quenching threshold; moreover, no Er-Er direct coordination was visible passing from the lowest Er concentration (0.2%) to the highest (5%): these facts demonstrate that the rare-earth clustering, evident from the PL response, does not take place at short distances [D'Acapito et al. 2007a].

As host materials for Er ions for applications in optoelectronics, the use of glass-ceramics has been widely explored. It has been shown that the Er concentration has an effect on the early stages of the crystallization of chloro-tellurite glasses: a combined EXAFS and in situ XRD experiment showed that the α-TeO_2 and $Zn_2Te_3O_8$ crystalline phases, formed upon in-situ annealing in the matrix without Er, where not present if $ErCl_3$ (2-10 mol%) was introduced. The first O shell around Er is similar to what found in the previous examples [Fortes et al. 2004]. If the presence of Er ions can modify the glass-ceramic structure, the inverse was also observed: in SiO_2-GeO_2-P_2O_5 Er-doped optical fiber performs, the addition of CaO in the glass modifies the Er local environment. In

particular, without CaO, the EXAFS analysis showed that the Er site is crystalline and very similar to that one of $ErPO_4$; upon addition of CaO, the Er site is locally disordered and similar to what observed in silicate or phosphate glasses. Correspondingly, the width of the PL emission increases due to the inhomogeneous broadening induced by the amorphous environment [D'Acapito et al. 2008].

The site of Er ions in glass and glass-ceramics waveguides has been investigated by the EXAFS spectroscopy by the research group of the Trento University and CNR. They focussed on binary matrices formed by SiO_2-Al_2O_3, SiO_2-TiO_2 and SiO_2-HfO_2. They found that the first atomic shell of O around the Er ions is essentially independent on the matrix composition; the second shell is formed of Si atoms (as in pure silica) in SiO_2-TiO_2, and it is probably constituted of Al atoms in SiO_2-Al_2O_3, even for Al_2O_3 concentration as low as 2% mol [Afify et al. 2006a, Afify et al. 2007a]. A special behaviour is reserved to Er-doped SiO_2-HfO_2 glass-ceramics. In this case, as usual the first coordination shell around Er^{3+} ions is composed of oxygen atoms, but it is observed that hafnium is the main constituent of the second coordination shell of Er^{3+}. Moreover, the local structure around Er^{3+} ions is found to be independent of the HfO_2 concentration and the Er^{3+} ions are found to be preferentially dispersed in HfO_2-rich regions of the glassy waveguide, even at the lowest HfO_2 concentration. This behaviour explains the PL properties of the considered waveguides: in fact, the observed PL spectra and shortened lifetimes can be explained by considering that the incorporation of HfO_2 in SiO_2 strongly modifies the next-nearest shell environment around Er^{3+}, inducing an increase of the electric dipole component of the ${}^4I_{13/2} \rightarrow {}^4I_{15/2}$ transition probability. The independence of the luminescence process on the HfO_2 content (10-40 mol %) means that the crystal-field-dependent component of the luminescence process remains unchanged, and in fact the local structure around Er^{3+} remains unchanged as well [Afify et al. 2007b].

Finally, an amphoteric behaviour for Er^{3+} ions in $BaTiO_3$ ceramic has been enlightened by a Er L_{III}-edge XANES and EXAFS investigation on Er-doped ceramics with different Ba/Ti ratio (=1 or >1): in the case Ba/Ti >1, the Er ions mostly substitute Ti ions in the perovskite structure, while in the other case almost equal occupancy of Er on Ba and Ti sites is found, thus assessing the ability of the stoichiometry to control the doping mechanism [Buscaglia et al. 2004].

Rare-earth doped materials: Sensitizing effect for the Er^{3+} emission.

To overcome the intrinsic small cross section for Er excitation in Er-doped SiO_2-based materials, a useful strategy is represented by the interaction with sensitizing species such as other rare earths, or nanostructures like Si, Au or Ag nano-aggregates. The effect of the atomic-scale structure on the PL properties of these composite systems has been investigated at the GILDA beamline by the EXAFS spectroscopy. The Er site has been determined in Er-doped SiO_x layers ($1<x<2$), and the corresponding 1.5 μm PL emission interpreted. The substochiometric SiO_x matrix is an effective sensitizer for the Er PL emission, whose cross section can increase of several orders of magnitude, tuned by the segregation of Si clusters that preferentially transfer their energy to the Er-ions that subsequently de-excite radiatively. It has been shown that, in the presence of an extensive phase separation between Si and SiO_2 the local environment around Er plays a crucial role on the efficiency of the PL emission at 1.54 μm, which is significantly increased when the first shell of atoms around Er is closer to that one of Er_2O_3 [Maurizio et al. 2005, Maurizio 2006]. Later on, for similar systems with x =1 (silicon rich oxide Er-doped layer), it has been shown that the energy transfer effect from the Si-containing nanostructures is very efficient, especially when N atoms are incorporated into the matrix. The incorporation of nitrogen atoms with Er during the SiO layer deposition induced a shortening of the Er-Si interatomic distance as compared to samples grown in O_2 atmosphere or in vacuum. These facts have strongly suggested that the Er-Si interatomic distance has an effect on the energy transfer between Si and Er in the SiO:Er layers [Noe et al. 2007] (Figure 1).

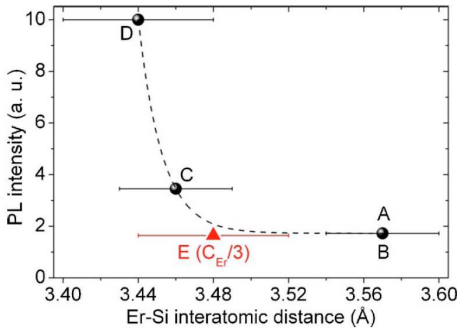

Figure 1. 1.55 μm Er PL intensity and corresponding Er-Si second shell distance in different Er-doped Si-rich oxide layers: the samples A-D have the same Er concentration, while the Er concentration in sample E is lower of a factor of 3.

The EXAFS spectroscopy has been used to investigate both the Er site and the metal nanostructures in metal and Er co-doped glasses, where the metallic nanostructures were introduced into the matrix to enhance the Er PL emission efficiency. The question to be answered was if the size of the metallic aggregates played a role in the sensitizing effect. The point was first investigated for the case of Er+Ag doped sol-gel films, where Er was directly introduced in the glass preparation, while the Ag doping was realized upon subsequent Ag-for-Na ion exchange. It has been shown that the Er^{3+} excitation is significantly increased (by a factor of about 7) when Ag was incorporated into the matrix: in particular, Ag multimers, only detectable by the EXAFS spectroscopy, are found to be efficient sensitizers for the Er PL emission, while the effect of Ag clusters in the nanometer range of size is not so remarkable [Mazzoldi et al. 2004]. A similar investigation was carried out for Er-Au co-doped silica by ion implantation. The EXAFS analysis performed at both the rare-earth and Au L_{III}-edges support the hypothesis that the energy transfer process is mediated by sub-nanometric Au aggregates with a metallic character that are optically activated mostly through electron interband transitions between *d* and *sp*-conduction levels [Trave et al. 2006].

Metal-for-alkali ion-exchanged waveguides.

Metal-for-alkali ion-exchange is largely used to dope surface layer of glass with metal ions so inducing a modification of the optical properties of the doped layer, useful to fabricate low-loss optical waveguides. Even if this procedure is already technologically used; nevertheless, basic questions about the stability of the metallic dopant and in some cases about its oxidation state were still unanswered. X-ray absorption spectroscopy is a particularly important technique used to investigate the site of the metal ions introduced into the matrix, in specific cases also singling out the dopant oxidation state. Since the optical waveguides are few-μm thin films doped with metal at low concentration, the use of high flux beamline is mandatory; in some cases, the use of grazing incidence geometry near the total reflection condition is needed to enhance the fluorescence signal of the metallic dopant and to investigate the oxidation state of the dopant as a function of the depth.

When the metal ions that diffuse into the matrix can have different oxidation states, as in the case of Cu, the dopant distribution within the matrix follows a rather complex behaviour, critically dependent on both glass and bath composition as well as on the process parameters. In this case, the use of x-ray absorption spectroscopy in grazing incidence mode allow a proper investigation of the waveguide structure: by selecting a specific incidence angle near the critical one for the incoming x-ray beam, a specific layer thickness can be probed, so that the measured x-ray absorption spectrum gives information on the chemical state (XANES region) and of the site (EXAFS region) of the dopant in a selected layer below the surface [Gonella et al. 2005a]. The EXAFS results, coupled with the measured concentration depth profiles (by secondary ion mass spectrometry) indicate that the Cu^{2+}/Cu^{+} ratio is strongly depth-dependent, being the Cu^{2+} ions preferentially located close to the glass surface. The relative presence of the two species throughout the exchanged region turns out to be governed by their different diffusion regimes, while the chemistry of the redox process is

shown to play a minor role; moreover, on the basis of the experimental results, a phenomenological model has been proposed to describe the diffusion process [Gonella et al. 2005b].

Among the most technologically used and mastered metal-for-alkali ion exchange processes, an important part is taken by Ag-for-Na ion exchange: together with K-for-Na one, it allow the realization of both surface and buried waveguides. Nevertheless, one of the main drawback is the potential reduction of Ag^+ ions into metallic Ag, that involves undesirable optical losses in the waveguides. To this respect, it is clear that a careful control of the dopant site and of its stability upon specific post-exchange treatments (specific thermal annealing, laser or ion irradiation as well as possible natural aging) is mandatory, because they can have an effect on the optical properties of the system. In these years different EXAFS experiments have been carried out at the GILDA beamline to investigate the Ag site in ion-exchanged waveguides and its stability upon specific annealing treatments. It has been evidenced a quite general behaviour, that is found in different kind of glasses (soda-lime, boro-silicate and germanate) [Maurizio et al. 2008a, Maurizio et al. 2009]. In particular, it has been found that in all of the matrices the Ag site resulted strongly dependent on the Ag doping level: the first shell, formed of about 2 O atoms, exhibits an Ag-O distance that increases from about 2.2 Å (for the samples with the lowest concentration, corresponding to an Ag/Na average exchange ratio less than 0.2) to about 2.3 Å for high level doping (for the samples with Ag/Na average exchange ratio of about 0.7). It has been demonstrated that this variation is related to a structural rearrangement of the Ag site in the whole doped layer; the EXAFS results on the samples that underwent the ion-exchange at higher temperatures, together with the comparison with literature data suggest that the sites with shorter distances are more stable. Moreover, in the case of borosilicate waveguides the correlation between local structure around Ag and its photoluminescence emission is established: in particular, the UV emission has been related to the presence of short Ag-O distances (2.1-2.2 Å) and the red-shift of the blue band observed in the absorption and excitation spectra by increasing the Ag concentration has been univocally related to the increase of the Ag-O bond length [Maurizio et al. 2009] (Figure 2).

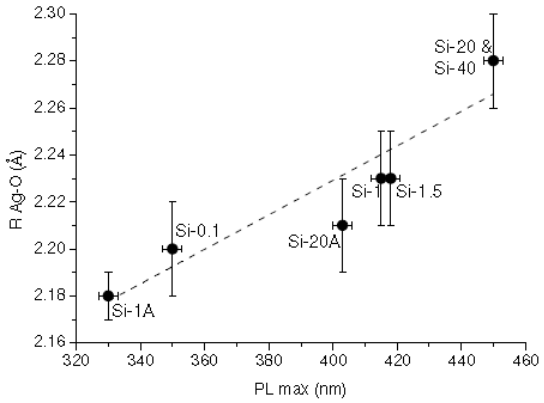

Figure 2. Ag-O distance in different Ag-for-Na borosilicate waveguides (from EXAFS) as a function of the wavelength corresponding to the maximum of the photoluminescence emission.

Finally, the Tl-for-Na ion exchange process has been investigated by the EXAFS spectroscopy in grazing incidence mode: due to the high polarizability of the Tl ions and despite its toxicity, Tl is a good candidate for the waveguide fabrication. The EXAFS results indicate that the site of Tl ions is extremely disordered, with a Tl-O distance lower than what found for the corresponding crystalline oxides. On the other hand, it has also been shown that the effect of air annealing is to induce a relaxation of the metal site towards the metal-oxygen distance typical of the crystalline oxides, as also found for Ag-for-Na ion exchanged glasses [Maurizio et al. 2008b].

X-ray excited optical luminescence.

About the investigation of the relationship between the local structure around a light emitting center and its photoluminescence emission, it would be extremely interesting to have a local structural probe sensitive only to the luminescent centers of a selected atomic species; this possibility is still debated in literature. At the GILDA beamline a series of x-ray excited optical luminescence (XEOL) experiments have been performed on different materials; in the case of nanostructured ZnO, by collecting both the x-ray absorption spectrum in fluorescence mode and the XEOL spectrum in the visible range, it has been shown that it is possible to study the local environment only of those Zn atoms that are in the proximity of or directly related to the light emitting centers [Larcheri et al. 2006].

A2. Materials with peculiar magnetic and magneto-transport behaviour

In the recent years broad scientific interest is attracted by materials presenting peculiar magnetic and magnetotransport properties such as magnetoresistance (giant and colossal), semi-metallic features, low field magnetoresistance, bias exchange effect and so on.

These physical properties often originate from a delicate and fascinating balance among magnetic, electronic and structural properties, whose understanding represent a stimulating challenge for the fundamental research. On the other hand proper understanding these special features is mandatory in perspective of applicative purposes.

X-ray absorption spectroscopy (XAS) is a well ascribed technique to finely investigate the local atomic structure around specific atomic species. Indeed several research groups exploited the GILDA beamline capabilities, and in particular XAS, to carefully investigate materials having special magnetic properties, in order to seed light on the relationships between local atomic structure and peculiar physical response. These studies can be roughly grouped in four classes: Manganese oxide perovskites, characterized by colossal magnetoresistance effect; double perovskites, characterized by strong spin polarization of charge carriers and large tunnel type magnetoresistance; exchange bias effect; diluted magnetic semiconductors.

Manganese oxide perovskites

Manganese oxides with perovskite structure are solid solutions: $(Re\mathrm{MnO_3})_{1-x}(\mathrm{MeMnO_3})_x$ in which trivalent rare earth ions (*Re* = La, Pr, Y,…) are substituted with divalent metal ions (Me=Ca, Ba, Sr,…). This substitution produces a mixed-valence state of Mn^{3+} and Mn^{4+} ions giving rise to complex phase diagram in the space of magnetic, structural and electronic transport properties that stimulated a wide interest of fundamental research. On the other hand the major interest of the applied research were stimulated from the discovering of the so called colossal magnetoresistance (CMR) effect in some of these compounds, opening many applicative possibilities such as sensors, mass storage devices, magnetic memories and so on. The larger effort of the fundamental research is dedicated to fully understand the complex interplay among structural, electronic and magnetic degrees of freedom responsible for the observed peculiar properties. The theories proposed to explain the complex magnetotransport properties of these compounds, rely on a delicate balance between double-exchange (DE) interaction, promoting the charge mobility and ferromagnetic coupling, the electron-phonon (EP) coupling which depress the charge mobility favouring the insulating state, and the superexchange (SE) interaction promoting charge ordering and antiferromagnetic state. The clear understanding of these compounds requires the precise and detailed characterization of their local atomic structure. In this research the x-ray absorption spectroscopy plays a fundamental role thanks to its chemical selectivity and local order sensitivity. The study of local structure in different manganese oxide perovskites is an issue addressed by

several groups which worked on GILDA [Bardelli et al. 2003, Dezanneau et al. 2004, Ghigna et al. 2005, Malavasi et al. 2005, Malavasi et al. 2006, Monesi et al. 2005, Monesi et al. 2006].

In [Dezanneau et al. 2004] defective manganese oxide compounds $La_{1-x}MnO_{1+\delta}$ have been investigated combining XAS and x-ray diffraction. In these compounds the Mn^{3+} / Mn^{4+} mixed valence state is achieved acting on the La/Mn ratio and O stoichiometry. These compounds are prepared by high-temperature pyrolysis of precursor aerosol, a technique widely used for the production of fine electro-ceramic materials like ZrO_2 TiO_2 and PZT. The technological interest for these compounds stem out from the possibility of a massive production and from the good reproducibility of the physical properties (magnetoresistance and metal to insulator transition temperature) weakly dependent on the composition in a wide range of La/Mn ratios. The study reveals the segregation of different phases instead of a homogeneous sample composition. Interesting is the segregation of a vacancy-doped phase La_yMnO_3 whose composition is nearly the same (y~0.9) for all the investigated samples, independently of the average sample composition. Since this phase is found to be principally responsible for the magnetic properties, such a phase separation scenario would explain the largely composition independent magnetic properties observed in the range 0.9>La/Mn>0.7.

A strong interest in mixed-valent manganite has been triggered by the possibility of tuning their structural, magnetic, and electrical properties by cation doping on the Mn site instead of the more commonly followed route of A-site substitutions. This has led to the discovery of new phenomena when a magnetic ion partially replaces the manganese, as the appearance of a metallic and ferromagnetic state in insulating and antiferromagnetic manganites when doping with ions such as Cr, Co, Ni or Ru. In case of Ru larger doping ratios can be achieved keeping the material single phase. Moreover three different Ru oxidation states (Ru^{3+}, Ru^{4+} and Ru^{5+}) can be found and the low-spin configuration of Ru ions makes them suitable for a FM coupling with Mn ions. XAS measurements at Mn and Ru K edges [Malavasi et al. 2005] clearly indicated that a simple Mn reduction is not the only mechanism involved in charge compensation in Ru doped $La_{1-x}Na_xMn_{1-y}Ru_yO_{3+\delta}$ manganites. In particular, at a relatively low intrinsic hole doping (x=0.05) a stronger influence of oxygen stoichiometry variation seems to play a considerable role in keeping the system neutral while at higher holes concentration a more direct electron exchange between Mn^{3+}/Mn^{4+} and Ru^{3+}/Ru^{4+} couples is present.

An interesting possibility in the study of these complex compounds is represented by the possibility, recently provided by advanced data analysis packages, to quantitatively refine the near edge region of XAS spectra (XANES). In fact the analysis of the XANES regions can provide detailed information on the electronic structure and local atomic topology around the absorber complementary to that obtained from EXAFS analysis. However, the complexity of the XANES analysis usually prevents a quantitative understanding of the data. The quantitative refinements of Mn K edge on $LaMnO_3$ and $CaMnO_3$ samples [Monesi et al. 2005, Monesi et al. 2006] in the extended and edge regions has been performed demonstrating that a quantitative picture of the local structure can be obtained from XANES in these crystalline compounds. Moreover, the quantitative XANES analysis provided topological information not directly achievable from EXAFS data analysis. This work demonstrates that combining the analysis of extended and near-edge regions of Mn K-edge XAS spectra could provide a complete and accurate description of Mn local atomic environment.

Double perovskites

The observation of large negative magnetoresistance (MR) at higher temperatures and lower applied magnetic fields in Sr_2FeMoO_6 oxides has stimulated extensive research activities on the double perovskite $A_2BB'O_6$ family of materials, where A could be alkaline earth metals and B/B' are transition metal ions. The basic nomenclature *double perovskite* presumes a perfect alternate occupancy of the B and B' ions along the three cube axes giving rise to the effect of doubling the basic unit perovskite cell, while in reality deviations from this ideal scenario, modifying the long

range crystallographic order, is often observed. Sr_2FeMoO_6 exhibits unique trends both in its magnetic as well as MR behaviours where the degree of disorder is also found to play critical role other than just influencing the crystal structure. Moreover, the electronic structure of Sr_2FeMoO_6 has also been recently shown to get strongly affected by Fe/Mo cationic disorder.

The Fe/Mo disorder i.e. creating crystal imperfections by interchanging Fe and Mo ionic positions in a perfectly ordered structure, is usually termed as antisite (AS) defects. Normally, two different distributions of such defects are discussed. In one they are considered to be placed randomly throughout the lattice leading to a homogeneous distribution of defects. In the other, instead of being randomly distributed, defects prefer to segregate as patches in some parts of the crystal. Segregated defects recover the perfect periodicity of the original lattice except that within these patches Fe occupies the notional Mo site and vice versa. It is reasonable to expect the ordered patches arising from a segregation of defects to have almost identical properties as the original ordered lattice, since the two are connected by a simple translation. Nevertheless the inversion of B/B' order at the boundary regions (antiphase boundaries: APB) is expected to affect the magnetic response of the system (figure 3). The properties of Sr_2FeMoO_6 are indeed profoundly affected by changing the extent of disorder, however most reports in the literature implicitly assumed a homogeneous disorder distribution of AS as the appropriate description of disorder in this class of compounds.

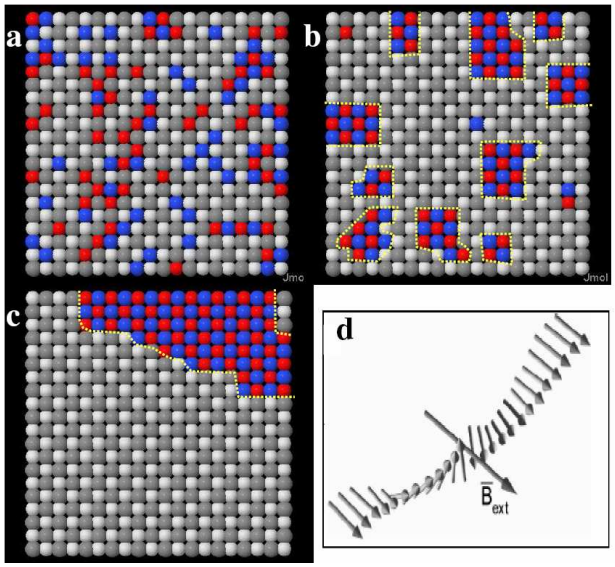

Figure 3(left): In panels a to c are shown the planes of ideal Fe/Mo cubic lattices (light and dark grey sites representing the Fe and Mo ordered positions) with different kind of disorder: red (blue) sites being Fe (Mo) on the Mo (Fe) sublattice: a) random AS distribution, b) small antiphase domains and c) large antiphase regions. Antiphase boundaries (APBs) are highlighted by dashed lines (yellow). d) effect of APB (pictorial view): the applied B_{ext} aligns neighbour domains while AFM coupling persist in the vicinity of APB.

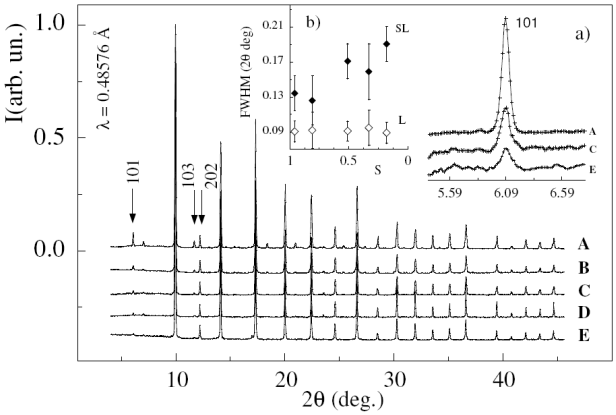

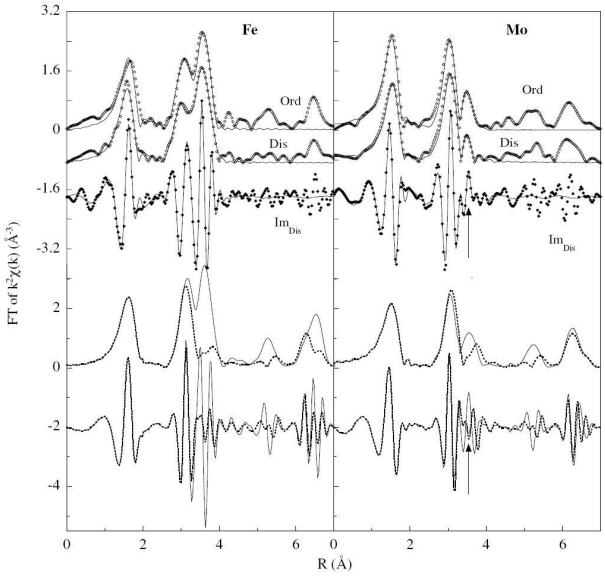

*Figure 4: **left**: XRD patterns for all the investigated samples. The inset a) show the region corresponding to the (101) superlattice peak for samples A, B and E. The inset b) reports the FWHM of lattice (open diamonds) and superlattice (filled diamonds) peaks. **Right** (Upper curves) moduli of k^2-weighted FT of experimental (diamonds) and best fit (full lines) spectra are shown for Ord and Dis samples at Fe and Mo (right panel) K edges. The imaginary part of FT of experimental (diamonds) and best fit (full lines) are shown only for disordered sample. The lower curves represent the k^2-weighted FTs of simulated XAFS spectra at the Fe and Mo K edges calculated for fully ordered (full thin lines) and chemically disordered (dot lines) Sr_2FeMoO_6 structures.*

Fe and Mo K edge XAFS studies in Sr_2FeMoO_6 [Liscio et al. 2006, Meneghini et al. 2009] demonstrates that a high degree of cation order is preserved locally (atomic scale) even in samples with high degree of long range crystallographic disorder. This indicates that the formation of APB patches will be favoured compared to homogeneous distribution of AS defects and the chemical short (SRO) and long range order (LRO) features in Sr_2FeMoO_6 can be understood in terms of locally ordered regions, connected to each other with phase differences. The analysis of the diffraction data, with the help of simulations, establishes the presence of nanosized antiphase domains in the system which eventually controls the magnetic properties of this material.

Exchange Bias

Exchange bias, i.e., the shift of the hysteresis loop of a ferromagnetic (FM) layer in contact with an antiferromagnetic (AFM) layer in the direction of the applied field, has attracted a lot of attention since its discovery in 1957. This interest is stimulated by its widespread application in information storage technology and to the intriguing and still not fully understood physics of the problem (Luches 2006, Del Bianco 2008). Although several models for the description of the process have been proposed, a general quantitative description is still lacking. In order to seed more light on this effect the FeNi(001) interface has been studied by Fe K edge EXAFS exploiting the directional sensitivity of polarized EXAFS measurements to distinguish the Fe local structure perpendicular and parallel the interface (Luches 2006).

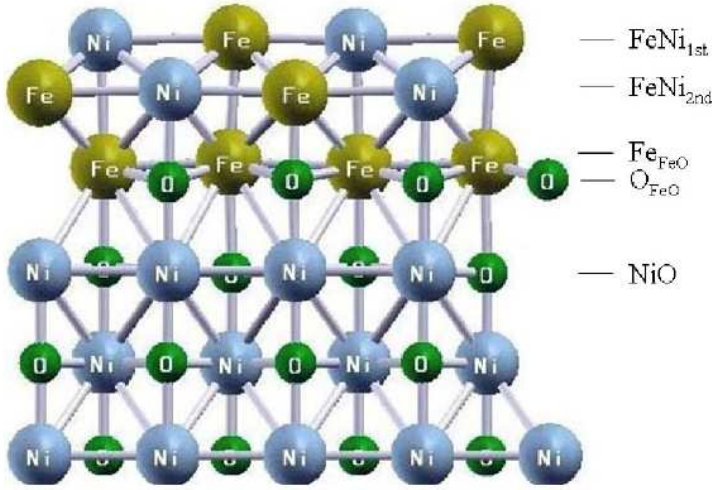

Figure5. Relaxed interface structure of 2 ML FeNi on NiO, with an FeO interface layer, as calculated by DFT, in agreement with polarized EXAFS results.

XAFS results were compared with DFT calculations which also allowed to evaluate the spin magnetic moment of the Fe atoms at the interface, providing original insight into the relation between structure and magnetic properties on these systems.

In particular, combining polarized EXAFS and theoretical DFT models it has been proved the presence of a Fe-Ni bct alloyed phase on top of a two-dimensional FeO layer situated at the interface, characterized by a 7% expansion of the interplanar distance at the interface with NiO and by a 0.3 A° buckling in the Fe and O atomic positions. The presence of such a structurally distorted

FeO layer is found to increase the spin magnetic moment of Fe atoms by $0.6\mu_B$. The very good agreement between theoretical and experimental structural parameters gives confidence that the proposed model is correct, under the chosen experimental conditions. This work provides the atomic level characterization necessary in order to provide a structural basis for a physical understanding of exchange bias in metal/magnetic-oxide interfaces.

Diluted Magnetic Semiconductors

Diluted magnetic semiconductors represent a particularly interesting class of materials that have received a considerable interest from the scientific community in the latest years. This research aims to the realization of devices capable of manipulating at the same time the charge and the spin of the carriers so permitting to realize a vast variety of functionalities. There are several still open issues to be addressed before moving to a practical exploitation of these materials:

- The value of the Curie temperature TC. Indeed it is necessary that in the FerroMagnetic (FM) state the device should be capable of working at ambient conditions so values of TC well above 300 K are necessary. Up to now DMS systems exhibit TC of about 170K at most, so new solutions for increasing this value should be found
- The overall structure of the material. In the latest years several claims of new DMS with high TC have appeared in the literature that, after a careful structural investigation, revealed to be

composite materials consisting in a semiconducting matrix with segregated magnetic phases. This no longer corresponds to a DMS and in principle should be avoided although the possibility of exploiting such composite materials is presently under debate.

- The micro-structure of the magnetic phase. Actually the magnetic species can be incorporated in the semiconducting matrix in sites magnetically active (namely substitutional) or magnetically inactive (interstitial) or even create preferential aggregation. This behavior must to be controlled if aiming in realizing a device.

Clearly all these issues are tightly interconnected because from the (micro)structure all the magneto-transport properties are derived. Moreover, the presence of codopants, altering the value of the Fermi energy, can modify the behavior of these systems. Thus, an experimental technique like XAS, capable of describing the microstructure around the magnetic species, is particularly effective in this research. GILDA revealed to be particularly well suited to the study of this class of materials for the intensity of the beam available (usually the Mn content is a few at % in a few 10^2 nm so resulting in a total amount of 10^{15} Mn/cm^2), for the limited beam size (samples of less that 1 cm^2 are normally produced) and good energy resolution. Moreover, being grown on single crystal substrates, the data collection equipment available on the beamline (Energy-dispersive multielement detector, vibrating sample holder, grazing incidence data collection) revealed to be extremely useful in this research. The investigations carried out at GILDA regarded the following materials: Mn in GaAs, Mn in Ge, Fe in GaN

Diluted Magnetic Semiconductors : Mn in GaAs

Mn in GaAs represents the most widely studied system in the field of DMS. In one of our papers [Dacapito et al. 2006c] we investigated the site of the metal in the matrix when introduced via the δ-doping technique. This procedure should assure a high local concentration of magnetic ions as well as an overall low Mn density. In this paper we confirmed that Mn substitutes for Ga in the matrix and by an analysis of the XANES part of the spectrum we ruled out the possibility of having Mn replacing an As ion. The analysis of samples co-doped with Be permitted to reveal the presence of Mn in tetrahedral interstitial site whose local structure was quantitatively described. The effect of stabilization of interstitial sites by a raise of the Fermi Energy was previously foreseen theoretically and represents a serious problem in Mn:GaAs because, being the T_C proportional to the hole density as well as the EF, the latter cannot be raised too much via external doping (namely by Be doping) otherwise the formation of interstitial Mn, behaving as an acceptor in GaAs, seriously degrades the magnetic properties of the material.

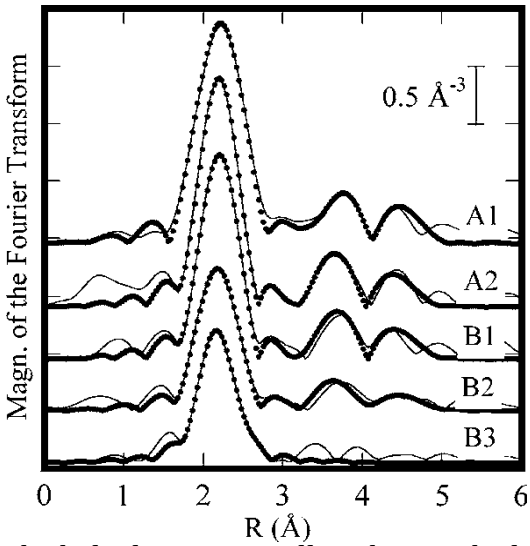

Figure 6.. Fourier Transforms (FT) of the EXAFS data relative to Mn δ-doped GaAs. The first 3 coordination shells (appearing at about 2.2, 3.8 and 4.5 Å) are visible so denoting a well ordered environment around Mn. The lower curve is relative to the Be codoped sample; it appears to be less ordered as the peaks of the higher coordination shells are missing and the tail at high R in the main peak of the FT is due to the appearance of interstitial sites.

One of the main points of this paper was the observation, in the Be-doped sample, of an additional Mn-Ga bond at 2.80 Å that is due to the interstitial Mn. This represented a direct observation for this site and a confirmation of the theoretical predictions.

As a further issue we investigated the possibility of growing GaAs nanowires on Si that are doped with Mn [Martelli et al. 2006]. The novelty in the growing technique was that Mn was directly used as catalyst for the wire growth in place of Au that is commonly used at this purpose. The result was that Mn was indeed found linked to As so demonstrating the incorporation of the metal in the wires. However, EXAFS revealed that the Mn-As bond length was longer that that found in bulk GaAs (2.56 Å in place of 2.49 Å) so suggesting the formation of nuclei of MnAs typical of high temperature annealed Mn:GaAs rather that centers with Mn in a substitutional site.

Diluted Magnetic Semiconductors : Mn in Ge

Another system that has been deeply investigated in the present years is the Mn:Ge DMS. This is particularly interesting because this technology is directly applicable to the standard Silicon production processes whereas it is not the case for GaAs. The problem is that Mn is hardly embedded in Ge as it exhibits a marked tendency in forming the Ge3Mn5 compound unless extremely low growth temperatures (50-150 ºC) are used in case of an MBE process. A clear evolution from the diluted form to the precipitated form was shown in [Gunnella et al. 2005] by comparing XAS data on samples grown at temperatures between 160 and 350 ºC. The same authors in [Ottaviano et al. 2006] evidenced as ion implantation can be an effective mean to obtain Mn diluted in Ge with the metal occupying substitutional sites.

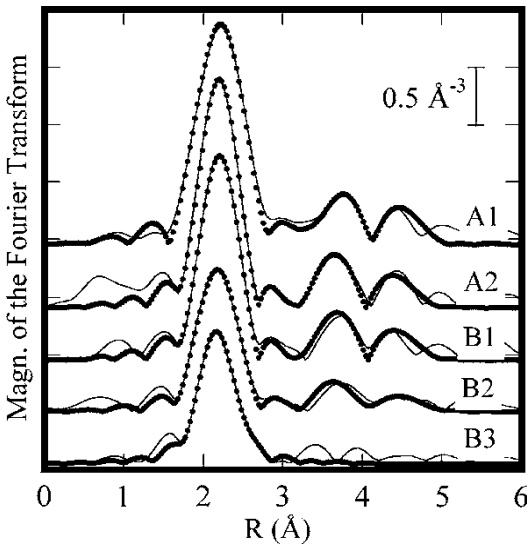

Figure 7. Fourier Transforms (FT) of the EXAFS data relative to Mn δ–doped GaAs. The first 3 coordination shells (appearing at about 2.2, 3.8 and 4.5 Å) are visible so denoting a well ordered environment around Mn. The lower curve is relative to the Be codoped sample; it appears to be less ordered as the peaks of the higher coordination shells are missing and the tail at high R in the main peak of the FT is due to the appearance of interstitial sites.

Anyways the simple "diluted" form is not really interesting from an applicative point of view as these samples exhibit a paramagnetic behavior. Taking apart the case when Ge3Mn5 is formed, FM properties are found in samples where Mn ions come close to each other forming columnar Mn-rich zones[5]. The local structure of these zones has been the topic investigated in [Rovezzi et al. 2008]. Actually, as diffraction presents only features typical of crystalline diamond Ge, EXAFS revealed to be of great utility in shading a light on these columns. The result was that the Mn is incorporated in Ge via the formation of Mn_3Ge tetrahedra that are also the building blocks of the Ge_3Mn_5 structure. This structure is particularly affine to the Ge{111} face as commented in a recent publication (Figure 8).

[5] M. Jamet et al. Nat. Mater. 5 (2006), 653

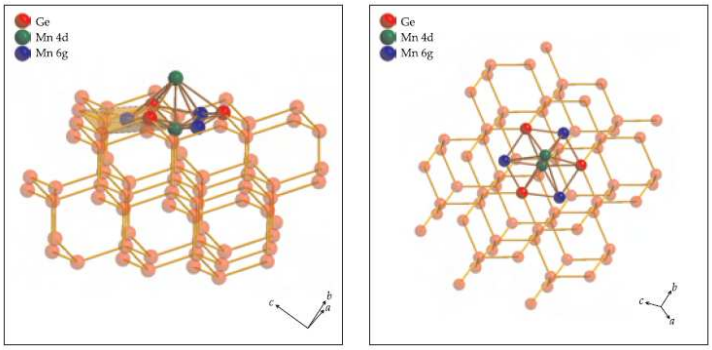

Figure 8. Pictorial view of how Mn_3Ge tetrahedral units taken from the Ge_3Mn_5 structure can be combined to match the Ge{111} face. The structural parameters that can be derived from this cluster are in good agreement with the experimental results of [Rovezzi et al. 2008]. Picture taken from [Selected Topics of Semiconductor Physics and Technology, Vol. 96 S. Ahlers Magnetic and electrical properties of epitaxial GeMn Walter Schottky Institut, Technische Universität München 2009].

Diluted Magnetic Semiconductors : Fe in GaN

Nitrides has received a great attention since a theoretical study[6] predicted that semiconductors with the widest gap values possess T_C well above Room Temperature when doped with magnetic species. Among the various possible systems in this class we concentrated our attention on Fe:GaN. This material can exhibit isolated substitutional Fe [Rovezzi et al. unpublished] as well as precipitated of Fe_3N particles or a *spinodal decomposition* phase in between these two. The Fe concentration or the velocity of growth have been shown to influence this behaviour. In a recent paper [Bonanni et al. 2008a, Bonanni et al. 2008b] it has been shown that the position of the Fermi energy, changed by adding electrically active co-dopants to the system, can drive the kinetics of formation of precipitates. In particular it was

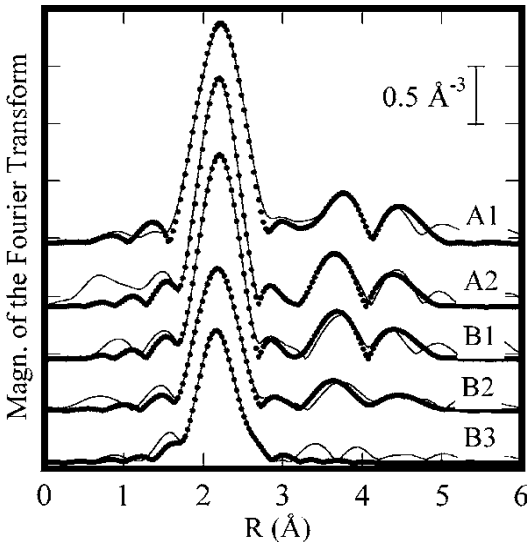

Figure 9:. Fourier Transforms (FT) of the EXAFS data relative to Mn δ-doped GaAs. The first 3 coordination shells (appearing at about 2.2, 3.8 and 4.5 Å) are visible so denoting a well ordered environment around Mn. The lower curve is relative to the Be codoped sample; it appears to be less ordered as the peaks of the higher coordination shells are missing and the tail at high R in the main peak of the FT is due to the appearance of interstitial sites.

shown that by adding Si to the Fe:GaN the precipitation of Fe_3N is hampered and from a fine analysis of the XANES spectrum we realized that the co-dopant also affects the valence state of the metal that partially shifts from 3^+ to 2^+. A complete and systematic characterization of Fe doped GaN in different growth conditions has been carried out in the latest months and a paper is in preparation [Rovezzi et al., unpublished].

[6] T. Dietl et al. Science 87 (1019), 2000

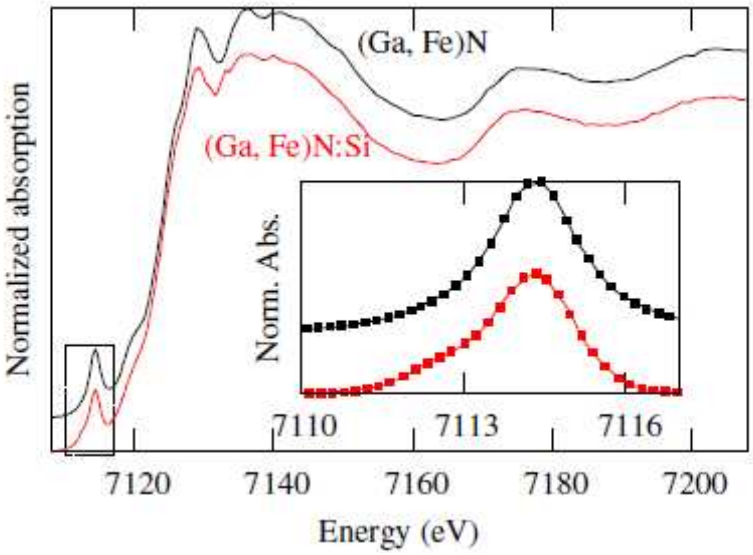

Figure 10. XANES spectra of the Fe:GaN samples in pure form (black line) or co-doped with Silicon (red line). The pre-edge peak, due to 1s-3d dipole forbidden transition, is analyzed in detail and fitted (dots) with one or two pseudo-voigt lines as shown in the inset. The presence in the Si-codoped sample of an additional line at 7112 eV demonstrates the presence of Fe^{2+} ions together with the dominating Fe^{3+} species. The partial reduction of Fe in the matrix is thus linked to the presence of the codopant.

A3. Semiconductors

In the field of semiconductor science and technology, new growth and deposition schemes are continuously devised, with the objective of obtaining samples and devices with novel and potentially useful physical properties. The role of highly sensitive and sophisticated methods such as XAFS is to provide a description of the local atomic environment which can form the structural basis for an understanding of the physical properties and, ultimately, insightful materials design. In fact, in the past twenty years, XAFS has developed from an intriguing physical phenomenon to a *tool* which is used in many branches of science, including semiconductor physics. XAFS is advantageously coupled to more traditional structural tools which are available in-house, such as high resolution X-ray diffraction (HRXRD), ion – based techniques (Rutherford back scattering RBS, channeling, proton induced X-ray emission PIXE), Mössbauer spectroscopy (for Fe), transmission electron microscopy (TEM) and various surface science techniques (for surface related problems). It is applied when the crucial issue is the local structure of a particular element, which cannot often be obtained by other means.

In this field in the period 2004 – 2008 at GILDA there have been three main areas of activity namely Ion implantation and dopants, Dilute alloys and Thin and ultra thin films.

The characteristic of XAFS which are exploited for these studies are the chemical selectivity, the applicability to relatively dilute samples and to surfaces and interfaces and the sensitivity to very small structural distortions (high resolution in the first few coordination shells). Specific instrumentation at GILDA which has made this research possible include the 13 element HP-Ge fluorescence detector with its fast digital electronics, the grazing incidence XAFS chamber and the low temperature sample holder allowing for polarization studies and sample vibration.

Over the past years, scientific collaborations have been established between the GILDA group and many Italian groups active in the area of semiconductor physics: TASC (Trieste), MDM (Agrate, Milan), University of Padova, University of Catania, University of Rome “La Sapienza” and others.

Scientific activity in this field has been the subject of two review papers [Lamberti 2004 and Boscherini 2008] and one Ph.D. dissertation [Ciatto 2004].

Ion implantation and dopants

Especially when fluorescence detection is employed, XAFS can most effectively be used as a probe of the local structure of dopants in semiconductors. Its main advantage is that it offers direct structural information on most atoms in the periodic table in any semiconductor matrix; it can be used to concentrations of the order of 10^{18} atoms/cm^3. The objective of an XAFS investigation of dopants is not only to describe the local structure of the foreign atom but also to relate the local structure to the physical properties of the system. A common finding is that the doping efficiency is often far from ideal (the ideal, textbook, case being one charge carrier released per dopant) due to the formation of defect structures of various nature.

Ion implantation and dopants: Fe in III-V alloys

Ion implantation, followed by appropriate thermal annealing, is a commonly used method to insert a doping atom in a semiconductor matrix. Its main advantage is that most atoms in the periodic table can be implanted, that the dose can be reliably determined and that the implantation profile (concentration versus depth) can be changed by variation of the beam energy.

The atomic environment of Fe impurities introduced in III-V alloys (InP and InGaP alloys) by high-temperature ion implantation has been the subject of a series of experiments [Cesca et al. 2003, Ciatto et al. 2003a, Cesca et al. 2007, Fraboni et al. 2007]. Due to its near-midgap deep acceptor level Fe acts very efficiently as electron trap and is therefore routinely used in bulk and epitaxial crystal growth to produce semi-insulating (SI) substrates or SI current blocking layers in various device structures. The same singly charged Fe^{2+} trap state responsible of electrical compensation also shows interesting optical properties due to internal d-shell transitions between $^5T_2$ and ^5E states which give rise to a sharp photoluminescence spectrum centred at 3.5 μm which could be exploited to produce an emitting device in the mid-IR region. The XAFS results have been complemented with studies by ion – based techniques (RBS, PIXE), HRXRD and TEM. In InP it has been found that the high-temperature implantation process favors the incorporation of Fe in high-symmetry sites. Conversely, the point defect flux occurring during high-temperature annealing controls the kick-out of the Fe atoms from substitutional locations, leading to the formation of Fe-P complexes. In InGaP substrates, an increased thermal stability of the substitutional Fe atoms with respect to InP has been observed, whereas no effect related to the n-doping has been pointed out.

Ion implantation and dopants Ultra – shallow junctions: As in Si

Arsenic in silicon can be considered one of the prototypical semiconductor dopant system and it has been the subject of numerous investigations in the past. Recently, by using very low (~ 1 keV) energy implantation, it has been possible to fabricate ultra – shallow (~ 10 nm) junctions in which a very high dopant density (~ 10^{21} atoms/cm2) is realized; this kind of junction is required for ultra scaled devices. At GILDA, it has been possible to determine the local order around As dopants in these junctions by exploiting the grazing incidence geometry which allows varying the penetration of the beam in the sample [D'Acapito et al. 2004b; D'Acapito et al. 2007b,c]. It was possible to identify different As sites along its concentration profile. In the deeper parts of the sample, As mainly occupies substitutional sites and vacancy – arsenic complexes, whereas in the region close to the surface a mixed phase of aggregates and impurities is present. First principles structural calculations supported the experimental observations.

The specific issue of As deactivation in ultra – shallow implants due to moderate temperature (500 – 800 °C) processes such as solid phase epitaxial regrowth (SPER) or laser sub-melt annealing has been also studied [Giubertoni et al. 2006]. It was found that spike annealing produces a surface accumulation with a local order around As atoms similar to the amorphous structure observed in the as implanted sample. After removal of the surface accumulation, XAFS spectra are typical of a sample with a high level of activation. This was also observed for samples processed with laser sub-

melt annealing before the spike anneal. Samples treated with only the laser process show an intermediate level of crystal order.

Ion implantation and dopants: Co – doping: C and In in Si

Among p-type dopants in Si, In is particularly attractive as it possesses a low diffusion coefficient that makes it ideal for the realization of sharp doping profiles. Its main drawbacks are the low solubility in Si and the high ionization energy. However, co – doping with C leads to an acceptor state with an appreciably lower energy so that the electrical activation is greatly enhanced. XAFS studies performed at GILDA in the grazing incidence set – up [D'Acapito et al. 2006a, D'Acapito et al. 2006b] have provided the first direct experimental determination of the sites of In and In – C complexes in Si. The experiment was particularly challenging because, due to the low solubility of the impurity and to the high energy of the K edge, an original experimental procedure was developed to separate the fluorescence signal from the substrate scattering. It was found that without C co – doping In occupies substitutional sites with a local expansion; with C co – doping an In–C bond appears at 2.31 Å and the site is greatly disordered.

Dilute alloys

The detection of local structural distortions in ternary semiconductor alloys (e.g. InGaAs) in the 1980's was one of the first clear illustrations of the high resolution afforded by XAFS in the structural determination for the first few coordination shells. Another characteristic of XAFS which is most useful in the study of alloys is the possibility of quantitatively distinguishing various degrees of atomic ordering; by atomic ordering we mean the relative disposition of atoms in an alloy, opposite cases of which are a random arrangement or the maximization of heteroatomic bonds. It is therefore not surprising that XAFS has been used in recent years to probe the structure of dilute nitrides, a new class of semiconductor alloys in which a small fraction of N isoelectronic impurities substitute for As in GaAs or similar matrix, leading to novel and useful physical properties (most notably a counterintuitive red shift of the band gap).

Dilute alloys: Local strain and ordering

The degree of static disorder brought about by the incorporation of N in a GaAs matrix has been studied by Ga K – edge XAFS recorded in the total electron yield mode [Ciatto et al. 2005a], including a comparison with density-functional supercell calculations and with the predictions of valence force field models. It was found that inclusion of N induces static disorder in the Ga-As bond length distribution and an increase of the Ga-As bond length; the latter is due to the competing effects of the decrease of the free lattice parameter and the tensile strain due to pseudomorphic growth.

Short-range ordering, in the form of an excess of In-N bonds with respect to the random case, has been predicted for the dilute nitride alloy InGaAsN. A detrimental consequence of this ordering is thought to be a blue shift of the optical band gap and this could represent a fundamental limitation since it would increase the band gap over the range for useful applications. Using In K – edge XAFS it was possible [Ciatto et al. 2003b and Ciatto et al. 2003c] to provide a quantitative determination of the effect of annealing on the short-range ordering in InGaAsN; complementary information was obtained from N edge XANES recorded at ELETTRA. It was found that in annealed samples short-range ordering is only weak, in fact one order of magnitude smaller than predicted. Ordering studies have also been performed on another quarternary alloy, namely GaAsSbN; the Sb K – edge XAFS data was complemented by N K – edge and Sb L – edge XANES recorded at ELETTRA and ID26. Ordering is one of the potential origins of the huge blueshift of the band gap observed upon annealing in GaAsSbN. It was found that neither strong Sb clustering nor preferential Sb-N association are present, and that Sb atoms see a random number of N next nearest neighbors except for growth temperatures smaller than 400 °C, for which Sb-N neighbors in the type-V sublattice are in excess with respect to statistical disorder [Ciatto et al. 2007].

Related to dilute nitrides are dilute oxide semiconductor alloys, which are obtained by adding oxygen to II - VI binary compounds; they are of potential applicative interest for blue-light emitters in which the oxygen content could be used to tune the band gap. In order to provide a structural basis for an understanding of their physical properties, Zn and Se XAFS measurements in the total electron yield mode have been performed on a set of ZnSeO and ZnSeOS epilayers on GaAs [Boscherini et al. 2007]; these measurements performed at GILDA were complemented by N edge XANES performed at ELETTRA and HRXRD. It was found that the variation of the Zn-Se bond length with O and S concentration is in agreement with estimates based on models of local distortions in strained and relaxed epilayers; an increase of the mean-square relative displacement is detected at high O and S concentration and is related to both intrinsic and extrinsic factors.

Dilute alloys: Hydrogenation

Hydrogenation of dilute nitrides has been recently found to be a powerful tool to tune the materials properties, since it reversibly alters the band gap. The effects of hydrogenation on the local structure of InGaAsN quantum wells has been studied by combining In K-edge XAFS and Ga K-edge x-ray diffraction anomalous fine structure performed on the BM1 beamline [Ciatto et al. 2005b]. It was found that the cation-As bond lengths in hydrogenated samples are systematically longer than the values predicted by a valence force field model corrected for the epitaxial strain, an effect of the formation of NH complexes. Moreover, it was found that hydrogenation removes the static disorder induced by N incorporation in GaAs, an effect due to the unique characteristics of the N substitutional anion and to the breaking of the ionic GaN bonds upon hydrogenation.

Thin and ultra thin films

As material dimensions shrink towards the nanoscale, the atomic arrangement at the surface and in the near interface region or at interface between different materials plays a crucial role in determining their physical properties. Important issues are atomic interdiffusion and strain due to epitaxial growth. XAFS can probe precisely these structural aspects. Sensitivity to very low thicknesses is possible in XAFS by using specific experimental set – ups existing on the GILDA beamline, such as grazing incidence, fluorescence or electron yield detection. Moreover, it is easy to obtain directional information, parallel or perpendicular to the growth plane, by exploiting the angular dependence of the cross section and the linear polarization of synchrotron radiation. These characteristics have been used on the GILDA beamline to study high dielectric ultra thin films on Si and II – VI alloys deposited by electrochemical methods.

Thin and ultra thin films: High dielectric constant oxides on Si

Various oxides are actively studied as replacements of amorphous silicon oxide in downscaled microelectronic devices. This stems from the competition between the requirement of a high gate capacitance and a low tunneling current; when the physical thickness of the insulator is decreased below 2 nm in order to increase the capacitance, the tunneling current across amorphous silicon oxide becomes unacceptably large (> 1 A/cm^2). It therefore seems desirable to use an alternative dielectric, characterized by a high relative dielectric constant ("high-κ") which might guarantee a high capacitance at a thickness which reduces the tunneling current to acceptable levels. An understanding of the physical properties of these ultra – thin epilayers on silicon is both a required prerequisite for applications and of fundamental interest. On the GILDA beamline, Y_2O_3, Yb_2O_3 and Lu_2O_3 ultra thin films on Si have been studied.

Regarding Y_2O_3/Si(001), Y K – edge XAFS data recorded in grazing incidence were used to study interdiffusion and local order [Spiga et al. 2004; Malvestuto et al. 2005]; data acquired at GILDA were complemented by O K – edge XAFS data recorded at ELETTRA. It was found that above a thin near - interface layer the epilayers have a local atomic and electronic structure bearing a close similarity to that of bulk yttria; however, there is an increase in static disorder with decreasing thickness which can be correlated to an increase of the defectivity. Yttrium -silicon bonds are present in the interface layer, forming the precursors to the formation of yttrium silicide which develops into a long range ordered phase at higher deposition temperatures. These observations were compared to available theoretical predictions on the thermodynamic stability of yttria in comparison to silicon dioxide, yttrium silicide, and yttrium silicate; the predictions were not confirmed by experiment as far as the 2 nm thick interface layer is concerned. A related study was performed on two similar rare earth oxide ultra – thin films on Si, Yb_2O_3 and Lu_2O_3 [Malvestuto et al. 2006]; XAFS recorded at GILDA was complemented by grazing incidence XRD. It was found that the films maintain the overall structure of the bulk oxides, but exhibit significant distortions of the local structure depending on thickness and thermal treatment. Finally, with the same motivation, HfO_2 – SiO_2 thin films were studied with particular attention to their thermal stability [Afify et al. 2006b], a crucial issue for semiconductor processing; Hf K – edge XAFS was combined with in-house XRD; nucleation of HfO_2 nanocrystals in the tetragonal phase after heat treatment at 1000 °C for 30 min and a partial phase transformation to the monoclinic phase (m-HfO_2) after heat treatment at 1200 °C for 30 min were detected.

B - Nanoscience and Nanotechnology

B1. Semiconductor nanoparticles

The research on semiconductor nanostructures has continued at GILDA, after the studies carried out in the previous years, paying particular attention to SiGe quantum dots and II-VI nanoparticles obtained by electrochemical way. In these fields the use of the EXAFS technique revealed to be extremely useful [Boscherini 2008, Lamberti 2004] because, permitting the retrieval of local structural parameters on a vast population of nano-objects, it provides a well averaged description of the material. Moreover, the technique is applicable also to extremely small particles (where the diffraction technique fails due to the broadening of the lines), to buried objects and to the case where unexpected amorphous phases are occasionally formed. Also in these topics, all characterized by a noticeable dilution of the absorber under investigation, the beamline resulted to be particularly well adapted to the data collection due to the high beam intensity, stability, and availability of an ancillary equipment (detector, cryostat, vibrating sample holder) and complementary characterization techniques (AFM) suited for this kind of investigations.

Ge_xSi_{1-x} islands on Si

The topic of GeSi dots on Si has received a great attention in the latest years due to the possibility of obtaining light emitting systems fully compatible with the well developed Silicon technology. This is of paramount importance as pure crystalline Si, possessing an indirect gap, is unsuited for the realization of light emitting devices. The main issues linked to the GeSi islands on Si are about the intermixing between Ge and Si and the strain state of the islands. These issues have been addressed the case of Ge islands as a function of the thickness of the Si capping [Capellini et al. 2005, D'Acapito et al. 2006d, De Seta et al. 2006] or in the case of different thicknesses of the Ge deposition [Motta et al. 2007] and a theoretical model on the interdiffusion has been derived. In the first case it has been evidenced that, upon covering Ge islands with Si , this element is at first incorporated in the islands up to a critical concentration of about 25% Ge. Successively, further Si addition results in the formation of a capping layer with the island composition remaining constant.

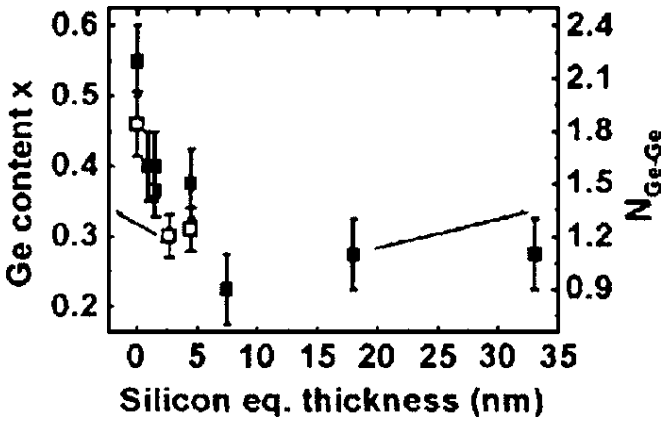

Figure 11. Evolution of the Ge content of the SiGe islands upon coverage with Si. The composition saturates at roughly 25% Ge and then remains constant. In the microscopy images this regime corresponds to the total coverage of islands.

.

The change in composition is accompanied by a change of the morphology of the islands that transform from domes, prior the Si covering, to pyramids and eventually to mesa-shaped islands just before the complete covering. This means that the driving force for intermixing is the surface diffusion and that the bulk diffusion plays a minor role in determining the island composition. From the study of the island composition as a function of the Ge coverage [Motta et al. 2007] it has been possible to confirm the minor role played by bulk diffusion and to define a quantitative model for the intermixing based on a Gaussian distribution of Si in the islands starting

from the base and with a time-independent standard deviation σ. This means that the chemical composition of the single layer deposited is frozen at the moment of its completion and no longer changed during the following deposition.

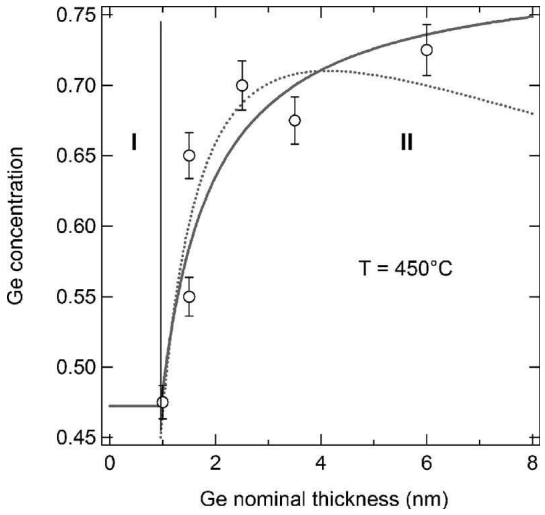

Figure 12.

Ge concentration as a function of Ge deposited nominal thickness (open circles) for samples prepared at 450 ºC. The experimental data are compared with the prediction of the model for intermixing described in [Motta et al. 2007]: line=σ constant, dots σ time-dependent.

In both cases also the strain state of the particles has been investigated finding a different behavior with strained islands in the case of non Si-covered Ge dots and relaxed islands in the case of Si covering. The strain state was studied by comparing the first shell distances Ge-Ge and Ge-Si with the results of, between others, a theoretical model developed by us [Dacapito 2004c].

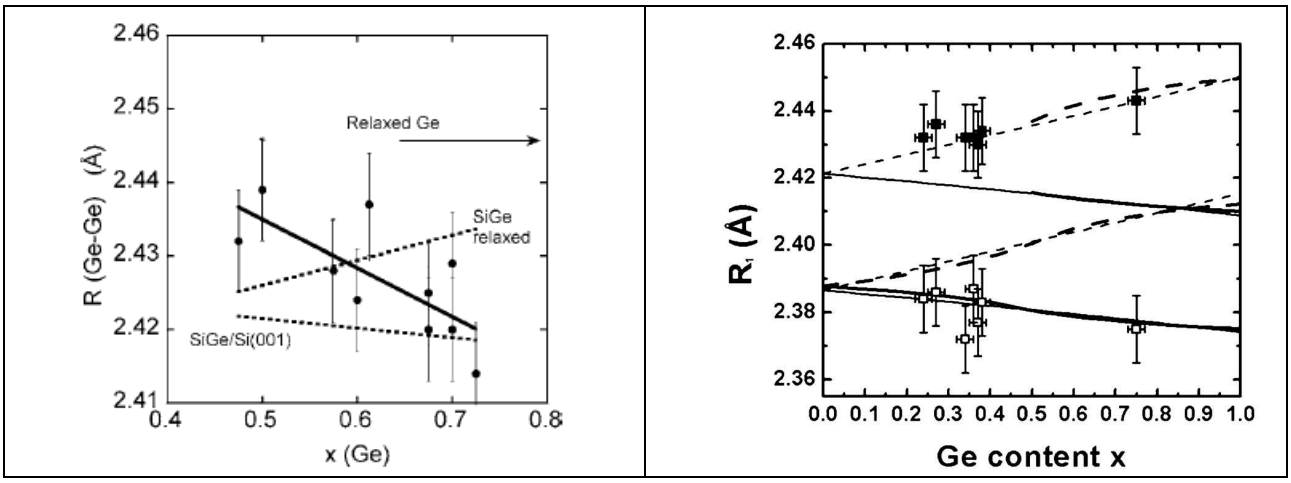

Figure13.

Ge-Ge and Ge-Si bond distances in the case of uncapped Ge islands on Si [Motta 2007 left] or Si capped islands [De Seta et al. 2006, right]. The experimental data are compared with some theoretical models for relaxed and strained alloys and an opposite trend is observed in the two cases.

The uncapped islands resulted to be strained from the Ge-Ge bond whereas the capped islands exhibited a strained behavior for the Ge-Si bond and a relaxed behavior for the Ge-Ge bond. This was explained by supposing a lattice parameter distribution in the island more strained at the base (where the particle is richer in Si) and more relaxes at the top (where the particle is richer in Ge).

<u>Ternary $Cd_xZn_{1-x}Se$ dots on Ag(111)</u>

Among the various methods for the production of semiconductor nanoparticles the Electro Chemical Atomic Layer Epitaxy revealed to be an effective way in the deposition of II-VI particles on conducting substrates. By adjusting the electrochemical parameters the composition of the nanoparticles can be controlled and consequently their physical properties like the bandgap. On the GILDA beamline we have investigated the ECALE process for producing ternary compounds $Cd_xZn_{1-x}Se$ deposited on Ag(111) and characterized by the EXAFS technique, at the Se and Zn-K edges,the nanoparticles so produced [Loglio et al. 2005, Loglio et al. 2008]. The samples produced were analyzed by Atomic Force Microscopy (AFM) using the microscope available at the local INFM-OGG laboratory. From the EXAFS analysis, and in particular from the investigation of the number and nature of nearest neighbors and the bond length, we found that the produced particles were pseudobinary compounds with the Zn-Se and Cd-Se bond length following the calculated values [Dacapito 2004c] for relaxed zincblende alloys. In general we found a lower Zn content in the particles than expected from the preparation procedure and we evidenced a significant part of Zn present as an amorphous oxide.

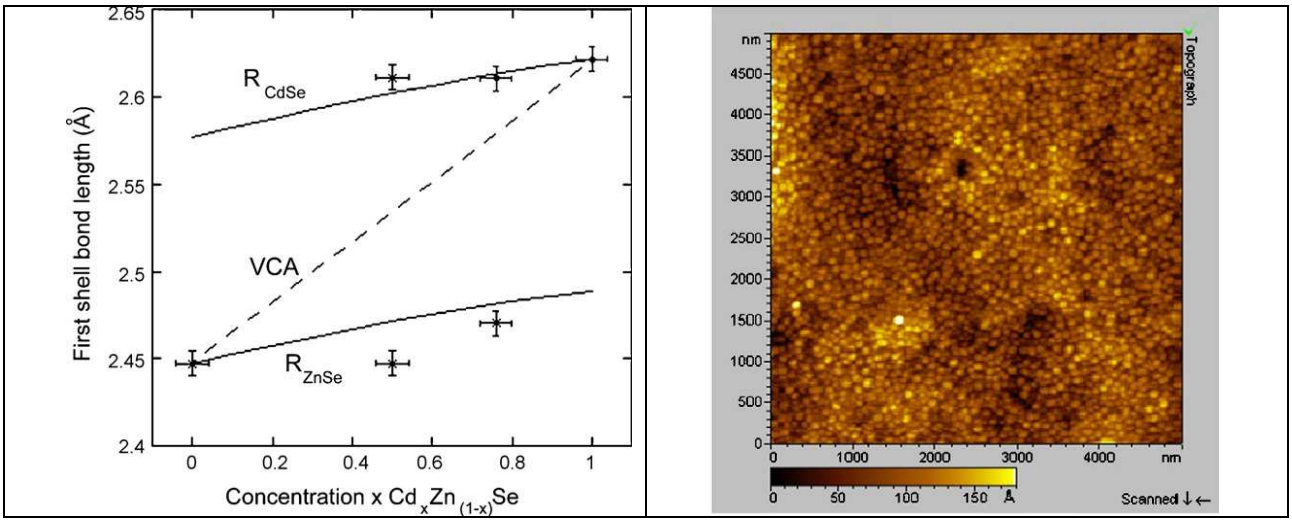

*Figure14. Left: Experimental EXAFS data (dots and crosses with error bars) for the particle composition x and the related first shell bond length R_{ZnSe} and R_{CdSe}. The data follow the values espected (lines) for a pseudobinary relaxes alloy as calculated by the method proposed in [Dacapito 2004]. The dashed line shows the value of the bond length if supposing that the local bonds scalein the same way as the lattice parameter (Virtual Crystal Approximation, VCA). The deviation from this latter mode underlines the necessity of having a local description of the material when dealing with semiconductor alloys. Right: AFM image on a 5*5 μm^2 region of a sample of composition $Cd_{0.39}Zn_{0.61}Se$ and clearly shows the nanoparticles with a roughly square base.*

B2. Metallic nanoparticles

The goal of nanoscience is to investigate size, shape, core-shell dependent electronic and geometric properties of nanoparticles in order to tune their specific catalytic, photoconductive, medical properties by varying their size and/or shape. In the last decades the need for a deep understanding of the very challenging properties of metallic nanoparticles, pushed by many technical applications, has stimulated a growing interest and a large number of experiments.

The nanoparticles, due to their specific and size dependent electronic, magnetic, structural and optical properties show a non-linear behavior and are a bridge between single molecules and infinite bulk systems.

The investigation of their properties is important to fully exploit their potential applications in

technology, since they can indicate the route for new devices and technologies. The quantification of the unique characteristics of individual nanostructures pertains to size effects and synchrotron radiation together with extended X-ray absorption fine structure (EXAFS) and X-ray absorption near-edge structure (XANES), are surely powerful tools for studying the structures and dynamics of these nano-scale materials. EXAFS and XANES techniques do not require the materials to have a long-range order and are well suited for determining the local structures of both amorphous and crystalline materials, which is a very important feature while studying nanomaterials.

Many different technologies and techniques have been explored to fabricate nanostructures and nanomaterials and different systems have been studied at the GILDA beamline; to take into account all the publications performed in this field in the last five years it is worth to classify the nanoparticles as liquid metal, monoelemental, and bielemental nanoparticles.

Liquid metal nanoparticles.

Several low melting point alloys are liquid at room temperature. The gallium-based systems are finding increased use in various applications as a replacement for toxic mercury, which has a high vapor pressure at room temperature, since they have reduced toxicity and lower vapor pressure. These systems have also a high thermal conductivity, far superior to ordinary nonmetallic liquids and this results in the use of these materials for specific heat conducting and/or dissipation applications. Other advantages of these liquid metal systems are their inherent high densities and electrical conductivities.

Among pure metals, Ga shows by itself peculiar properties that have stimulated many computational and experimental investigations. Among these properties there are a complex polymorphism and, for the main solid phase (α-Ga), a structure made of diatomic molecules with a marked pseudogap at Fermi level and strongly anisotropic conduction while the other crystalline phases show strictly comparable and nearly free-electron-like DOS, a normal melting point close to room temperature 303 K, and a lower density at the melting point than that of the liquid.

Using x-ray absorption fine structure spectroscopy (XAFS) for the structural characterization coupled with transmission electron microscopy (TEM) to characterize the deposited Ga layers, two very interesting studies have been performed one on the Extreme undercooling achieved using 3-15 nm Ga droplets deposited onto an amorphous substrate [Parravicini et al. 2006] and the second on the metallic versus covalent bonding as a function of temperature and particle size [Ghigna et al. 2007].

Liquid nanoparticles: Extreme undercooling (down to 90 K) of liquid metal nanoparticles

Ga nanodroplets were obtained by thermal evaporation, under ultrahigh vacuum, of ultrapure Ga 99.999% and condensation on carefully cleaned amorphous silica substrates (18x7x1) mm^3 kept at T=323 K. At that temperature, liquid Ga self-organizes (Volmer-Weber growth mode) in islands, whose shapes are truncated spheres with a contact angle of about 130°. The nanodroplets had a low size dispersion $\Delta D/D \approx 0.2$ and were covered after preparation with a thin layer of SiOx, to prevent Ga oxidation. Fluorescence x-ray absorption fine structure (XAFS) data were collected at GILDA beamline at the Ga K-edge. Two films have been investigated, differing in their thickness: the thicker film is continuous, while the thinner film consists of nanodroplets with a 9 nm mean diameter. The measurements were performed from 90 to 350 K after cooling the films down to 88 K.

The absence of any contributions of GaO_2 to the XAFS spectra is a proof of the effectiveness of the synthetic procedure and the electron diffraction pattern of the thinner film at 97 K shows only a diffuse halo typical of a disordered phase being also this a direct evidence that crystalline Ga is not formed down to this very low temperature.

As it is well known, simple thermodynamic considerations, predict that nanoparticles should display a depression of both the melting point and the latent heat of fusion depending on the particle

size.

Previous works on liquid Ga undercooling have been done either on micron-sized droplets in form of emulsion in alcohol or epoxy resin or on nanodroplets obtained under ultrahigh vacuum by thermal evaporation. All these works agree in that large undercoolings up to $\Delta T/T_m \approx 0.5$ are achieved, but a crystalline phase or a mixture of crystalline phases is eventually recovered from the melt, thus indicating the metastable state of the undercooled liquid, and that nature and polymorphism of these crystalline phases strongly correlate with droplet size. In the present work case, no signs of crystallization were obtained on cooling down to liquid nitrogen temperature. The particular result is related to the size of liquid droplets, which is significantly smaller than the droplets obtained from emulsions but also smaller than the nanodroplets previously investigated by the same authors. A direct experimental evidence is given, that an extreme undercooling, $\Delta T/Tm \approx 0.7$ can be achieved using Ga droplets with sizes in the 3–15 nm range deposited onto amorphous substrates, and that these nanoparticles can be kept at 90 K for times of the order of days without showing the onset of crystallization. These findings stress the importance of interfacial interactions and of finite-size effects on the thermodynamic properties at the nanoscale.

Liquid nanoparticles: Metallic versus covalent bonding: Ga nanoparticles as a case study

Interest toward the chemistry of elemental gallium arises for many, variously related aspects. The density of the liquid higher than that of the main solid phase (α) places Ga into the minority set of substances that show increasing stability of the liquid with increasing pressure and generically indicates an anomalous bonding behavior with respect to other metals. α-Gallium is indeed a very particular metal made of diatomic units with a marked pseudogap in the density of states at the Fermi level and strongly anisotropic electronic conductivity.

In spite of its high reactivity with oxygen, Ga is indeed a nice experimental model for investigating the properties of liquid metals particularly because the crystal melts slightly above room temperature (303 K). The element, however, shows a complex polymorphism that has been deeply investigated experimentally and computationally: the other crystalline phases have significantly different structures based on different local arrangements and building units, which are made, for instance, of zigzag chains of atoms (β phase) or five different coordination environments (δ phase). Remarkably, these crystal structures do not show the "anomalous" properties of α-Ga.

A systematic X-ray absorption spectroscopy investigation of the local coordination in gallium nanostructures has been performed as a function of temperature and particle size. It is shown that the nanostructure strongly affects the polymorphism of solid gallium and the (meta)stability range of the liquid phase (in agreement with previous works) and that the surface tension acts in the same direction as hydrostatic pressure in stabilizing the Ga solid phases. The effect of surface free energy is first to favor the metallic arrangement of the δ phase and then to stabilize a liquid-like phase based on dimeric molecules even at 90 K. The Ga-Ga distance in the dimers is lower in the liquid phase than in the α solid. The experimental results are discussed in comparison with molecular dynamic calculations to assess the presence of covalent character of the dimeric Ga_2 units in liquid nanostructured gallium.

Monoelemental nanoparticles

Monometallic nanoparticles show a variety of novel and fascinating electrical, magnetic, and chemical properties arising both from the presence of a large percentage of low coordinated surface atoms and from the confinement of electrons to dimensions shorter than the electron mean free path and the Fermi length. From the structural point of view, monometallic nanoclusters often undergo a contraction of the lattice distances with respect to bulk materials because of surface stress tension. At the GILDA beamline monometallic nanoparticles prepared using different techniques were studied using XAFS and X-ray powder diffraction. These studies can be grouped as:

Size, temperature dependence [Comaschi et al. 2008] *and modeling* [Longo et al. 2008] *of the structural parameters of gold nanoparticles.*

Structural studies as a function of temperature of monometallic particles embedded in dielectric matrices [Maurizio et al. 2007; Dubiel et al. 2005]

Kinetics of hydrogen absorption and desorption: Nb clusters formation in Nb-doped magnesium hydride [Checchetto et al. 2005; Bazzanella et al. 2006].

Monoelemental nanoparticles: Temperature dependence of the structural parameters of gold nanoparticles investigated with EXAFS

From the structural point of view, gold nanoclusters often undergo a contraction of the lattice distances with respect to Au bulk because of surface stress tension. According to Laplace's law, the lattice parameter is foreseen to linearly decrease with the inverse particle dimension *D*. Recently, temperature dependent x-ray diffraction measurements on a gold nanoparticle powder with mean dimension of about 4 nm showed for the first time an additional effect, i.e., the occurrence of a *crossover* in the temperature dependence of the cell parameter, which changes from an initial thermal expansion at low temperatures to a thermal contraction for *T* 125 K.

This result is not due to changes in the structure of the nanoparticle, which continues to show a fcc atomic arrangement as the bulk metal but can be attributed to the contribution of electronic excitations to the total energy of the system. Indeed, for a bulk system, the electronic contribution to the total energy results slowly varies with temperature and, for this reason, bulk materials generally show a thermal expansion, originating from the anharmonicity of the lattice potential. On the other hand, in nanoparticles, the presence of electronic discrete energy levels separated by only a few meV implies a relevant variation of the electronic energy with *T*. In the present paper, this effect is deeply explored to assess its presence and to quantify it even in smaller clusters, where localization effects are expected to become stronger and stronger. At very low sizes, x-ray diffraction does not allow measuring of the cell parameter of the nanoparticle with sufficient accuracy; therefore, XAFS spectroscopy at the GILDA beamline was used, to get a very accurate estimate of the nearest-neighbor distance as a function of temperature.

The L_3 edge of Au nanoparticles, having sizes ranging from 2.4 to 5.0 nm, have been investigated in the temperature range of 20–300 K. To achieve a very high accuracy in the determination of the first shell distance, a very careful data analysis was performed also taking into account the presence of asymmetry effects. In all samples, the temperature dependence of the first neighbor distance results was different from that of the macrocrystalline counterpart. In the largest size samples, a reduction of the thermal expansion was found, whereas in the smallest ones, the presence of a crossover from an initial thermal expansion to a thermal contraction was observed. Calculations based on a simple Grüneisen-like model showed that localization effects, that increase as the nanoparticle size decreases, can explain the reported thermal effects.

Monoelemental nanoparticles: Distorted f.c.c. arrangement of gold nanoclusters: a model of spherical particles with microstrains and stacking faults

Among nanomaterials, f.c.c. (face-centred cubic) metal nanoclusters find application in a range of different fields, for example in catalysis, in nanoelectronics, as components of optical and magnetic materials, or coupled with biomolecules to produce functionalized bioinorganic systems.

The outstanding catalytic performance of nanocrystalline Au in the selective oxidation of CO in a hydrogen-rich environment and in the water gas shift reaction probably constitutes one of the most striking examples of size-dependent properties of an f.c.c. metal. Actually, numerous experimental and theoretical studies have investigated the size and structure of Au nanoclusters and, for heterogeneous catalytic systems, the effect of the support (inert, as with silica, or reducible, as with ceria or titania) on oxidation state and electronic charge distribution.

The aim of this study was to perform a careful structural analysis of silica-supported Au catalysts and to contribute to the scientific debate on the atomic arrangement of f.c.c. metal

nanoclusters. The structures of two samples of gold nanoclusters supported on silica were studied by X-ray powder diffraction (XRD) and X-ray absorption spectroscopy.

The data relative to both techniques were analysed by an approach involving simulation based on structural models and fitting. The XRD model concerned a distorted f.c.c. (face-centred cubic) arrangement, with microstrains and parallel stacking faults in approximately spherical particles; as an alternative possibility, a linear combination of ordered f.c.c. and noncrystalline (decahedral and icosahedral) particles was also taken into account. Both approaches gave calculated patterns closely resembling the experimental data. X-ray absorption spectra were fitted on the basis of f.c.c. and noncrystalline arrangements. The best results were obtained by the f.c.c. motif, while a simulation consisting in the superposition of f.c.c. and noncrystalline components in the relative amounts determined by XRD analysis gave a poor agreement with the experimental data.

It was concluded that the good XRD fitting obtained by linear combination of lognormal size-distributed f.c.c. cuboctahedral, decahedral and icosahedral contributions was a result of the flexibility of the basis set of functions, but that the complementary analysis of X-ray absorption data did not confirm the presence of a noteworthy fraction of noncrystalline particles.

Monoelemental nanoparticles: Investigation of stress state of silver nanoparticles in silicate glasses by means of EXAFS (optical properties) and Thermal evolution of cobalt nanocrystals embedded in silica (magnetic properties)

Concerning the optical properties recently, the preparation and characterization of glasses containing metal nanoparticles, has been further stimulated by peculiar nonlinear optical properties, especially an increased third-order susceptibility, making such glass a promising candidate for application in integrated optics and photonics. Previous studies indicated that the optical properties of nanoparticle/glass composites strongly depend on the size, the structure and the concentration of the embedded nanoparticles as well as their interaction with the host matrix. Therefore, different preparation methods like ion implantation, sol-gel and ion exchange, possibly followed by reducing atmosphere treatments, ion or laser irradiation have been used to fabricate specific configurations of nanoparticles in glasses. Structural information down to the atomic scale on the nanoparticulate composites may be obtained by high resolution electron microscopy (HREM). This does not only allow to determine size, size distribution, external shape and internal structure of metal particles, but also to evaluate surface/interface effects on their lattice parameter. X-ray absorption spectroscopy is another structure sensitive method. From the extended X-ray absorption fine structure (EXAFS) spectra of the corresponding metal atoms the lattice parameter may be determined, even with more accuracy than HREM. However, the EXAFS results are averaged parameters of atom-atom correlations summed up for all detected particles, different from data determined by HREM for individual particles. The combination of both methods should be advantageous for a precise structural characterization.

Nanosized spherical silver particles were formed in silicate glass by sodium/silver ion exchange and subsequent annealing in air or hydrogen atmosphere at elevated temperatures. Furthermore, the sol-gel procedure was used to prepare embedded Ag particles. Structural characterization of these composite materials by temperature dependent EXAFS-spectroscopy with transmission and fluorescence (taken at the GILDA beamline) experiments revealed distinct differences of the particle/matrix interaction across the interface. The Ag-O and Ag-Ag correlations could be separated by fit procedures. The Ag-Ag bond length of the crystalline particles sensitively reflects their state of stress depending on the formation conditions. It was found an increase as well as a decrease of the Ag-Ag distance, i.e. tensile and compressive stress states were formed, for ion-exchanged glasses as a result of different cooling procedures and after hydrogen treatments, respectively, and for sol-gel samples. The combination with high-resolution electron microscopy (HREM) experiments confirmed such effects. Furthermore, the size dependent parameters of nanoparticles could be determined. The results can be interpreted by the size effect of nanoscaled particles and the influence of the surrounding matrix.

Concerning the magnetic properties, composites formed by magnetic nanoparticles embedded in dielectric matrices draw much interest for their potential application in magnetic recording. Basic questions concerning the composite formation and stability are far from being understood and modelized. In particular, Co nanoparticles can occur in multiple crystalline phases, which can result in large differences in the magnetic properties such as the crystalline anisotropy, so affecting the possible application in magnetic recording. The bulk equilibrium phase of Co at room temperature is hcp, whereas the fcc structure is more stable at T>420 °C (at normal pressure).

The structural evolution of cobalt nanoclusters synthesized in silica glass by ion implantation has been investigated upon thermal annealing. The samples were characterized by in-situ grazing incidence X-ray diffraction at the GILDA beamline, exploiting a synchrotron radiation beam and following their evolution during thermal treatments in vacuum up to T=800 °C. Before heating, the system was composed of hcp Co nanocrystals. The transition from hcp to fcc structure that in the bulk phase occurs around 420 °C was not detected and this result could be likely related to the finite cluster size as well as to the cluster matrix interaction. Nevertheless, the differences in the diffraction pattern recorded at T=800 °C with respect to the corresponding one at room temperature suggested the presence of a second crystalline phase.

Monoelemental nanoparticles: Nb clusters formation in Nb-doped magnesium hydride

Fast hydrogenation and dehydrogenation reaction kinetics in Mg can be achieved by using catalysts in the form of metallic nanoparticles (Nb, $PdFe_3$, Pd) dispersed at the Mg and MgH_2 surface. Nanoparticles favor the H_2 dissociation and jump of H atoms towards the Mg subsurface layers. However, the microscopic mechanisms of catalysis are not fully understood. In a previous study it was shown that Nb acts as a very efficient catalyst in the H_2 desorption from the β-MgH_2 matrix also when the metallic additive is dispersed in the hydride layers. The desorption process in the Nb-doped Mg hydride was controlled by the formation of the interconnected path of *h*-Mg where H diffusion preferentially occurs.

In order to fully understand the role of the Nb doping element, a study on the evolution of the chemical-physical state of the Nb atoms dispersed in the Mg matrix upon hydrogen absorption and desorption cycles was performed. The analyses were carried out by EXAFS spectroscopy at the GILDA beamline, x-ray diffraction and transmission electron microscopy on three representative Nb-doped (5 at. %) *h*-Mg film samples deposited by rf magnetron sputtering: (i) as-deposited *h*-Mg sample, (ii) activated β-MgH_2 samples after partial β-MgH2 to *h*-Mg phase transition (hydrogenated sample), and (iii) activated sample after complete β-MgH_2 to *h*-Mg phase transition.

Results showed that the catalytic effect of the Nb doping in the H_2 absorption and desorption kinetics is connected with the formation of Nb nanoclusters dispersed in the host matrix. The H_2 desorption from β-MgH_2 is favored by local elastic stresses produced by β-$NbH_{0.89}$ clusters on the MgH_2 matrix that reduces the stability of the hydride phase and by preferential paths in the nanocomposite hydride

Bielemental nanoparticles

The formation of bimetallic nanoclusters has been the subject of much research work, because by controlling the cluster composition the composite properties could be further tailored. In the study of multielemental metal nanoclusters in dielectrics, many points are still unknown or under debate, in particular about the way to control the alloy formation, composition, and stability upon post-preparation treatments, such as heating in selected atmospheres and laser or ion irradiation.

One of the techniques largely employed in the synthesis of alloy-based nanocomposites is ion implantation, possibly coupled with suitable thermal treatments, which has demonstrated to be very useful because, the sequential ion implantation in silica of two different ion species, eventually followed by suitable heating treatments, can lead to the formation of bielemental nanoclusters if the implantation parameters, such as the energy and fluence, are chosen to maximize the overlap of the

two concentration depth profiles.

On the other hand, another technique like radiofrequency magnetron co-sputtering deposition allows to easily obtain homogeneous thicker films doped with nanoclusters which can be useful for the fabrication of optical waveguides.

At present, the research on nanoclusters embedded in dielectric matrices goes in at least three directions that are strictly correlated: the complete understanding of physical and chemical properties of the systems, the control of the different synthesis methods for obtaining predefined structures, and the development of further complex characterization methods for achieving detailed information on the systems examined.

It is evident that the understanding of the alloy cluster formation and growth, as well as possible de-alloying processes, is needed to exploit these systems for technological purposes.

At the GILDA beamline, the research in this field was focused on the formation of bielemental clusters that have metallic and semiconductive character. These studies regarded bimetallic nanoparticles namely the dynamics of compositional evolution of bimetallic alloy nanoclusters upon heating in selected atmospheres [Mattei et al. 2005 ; Mazzoldi et al. 2005; Maurizio et al. 2004a; Mattei et al. 2004a,b] and the synthesis by co-sputtering of Au-Cu alloy nanoclusters in silica [Mattei et al. 2007] and in III-V semiconductor nanoclusters, namely the formation of GaN, GaAs and InN nanoclusters by ion implantation [Maurizio et al. 2004a].

Bielemental nanoparticles: Dynamics of compositional evolution of bielemental alloy nanoclusters upon heating in selected atmospheres

In the last years, a great interest has grown on nanoclusters embedded in dielectric matrices; these systems are the subject of much research work, with much physical, chemical and technological literature dedicated. Their potential technological application is widespread over different fields, such as catalysis for the large surface to volume ratio typical of nanostructures, magnetic recording and optoelectronics. About the latest, the enhanced third-order optical susceptibility of metal nanocluster composite glasses could be exploited in the all-optical switching device technology; recently, some effort has been done to evaluate the figures of merit that must be satisfied for ultrafast all-optical switching application of metal nanocluster composite glasses. In addition, semiconductor clusters embedded in dielectrics could be exploited for fabricating tunable light emitting devices: because of the quantum confinement effect, the emission wavelength could be tuned by properly controlling the cluster size.

For all these reasons different studies have been performed on *metal alloy nanoclusters* and *III-V semiconductors nanoclusters* with the aim of enlighten the effects of both the implantation dose and heating in different atmosphere on the nanocluster compositions.

Concerning the *bimetallic systems* it is known that the sequential ion implantation in silica of Pd+Cu, or of Au+Cu ions determines the formation of solid solution alloy nanocrystals. Detailed structural investigations of the modification induced by selected heating treatments, which both recover the matrix from the radiation damage and deeply modify the composite structure by their chemical interaction with the matrix, have been performed.

The dynamics of the compositional and structural evolution of solid solution Pd-Cu metal nanoclusters obtained by sequential ion implantation in silica, upon heating in selected atmospheres as a function of the annealing time has been investigated and a correlated diffusion of the dopants has been evidenced for both reducing or oxidizing atmospheres, mostly triggered by the Cu atom diffusion (such migration is absent in silica implanted only with Pd). In particular, upon annealing in reducing atmosphere a preferential migration of Pd towards the sample surface was observed and aggregation of large bimetallic clusters was favoured near the implantation range, as also found in the case of Au-Cu alloy clusters in silica. On the other hand, upon annealing in air, the Pd-Cu alloy nanoclusters have shown to undergo a progressive oxidation process in which the Cu atoms are oxidized mostly as CuO oxide partial shell around a Pd-rich core.

This behaviour is different from the one observed for Au-Cu clusters in silica under the same

annealing conditions: in this case, Cu atoms were extracted through the surface of the alloy clusters as Cu_2O aggregates with their crystallographic axes coherently oriented with those of the fcc Au-rich alloy nanocrystals. For what concerns Pd-Cu this process is not energetically favourable due to the large lattice mismatch between Pd-Cu solid solution alloy and the cubic Cu_2O, therefore indicating that the structural constraint given by the lattice mismatch between the core and oxide shell is crucial for controlling the stoichiometry of the oxide.

Bielemental nanoparticles: Synthesis by co-sputtering of Au-Cu alloy nanoclusters in silica

Silica films containing metal nanoclusters exhibit peculiar optical properties that have made them attractive in several application fields. As an example, metal quantum dot composite glasses exhibit an enhanced optical Kerr susceptibility, i.e., the most important physical process for applications in all-optical switching devices. The most promising metals for constituting the nanoparticles embedded in the dielectric matrix are the noble metals.

Copper + gold -containing silica films have been synthesized by radiofrequency co-sputtering deposition technique. In order to obtain the formation of metallic nanoclusters, as deposited samples have been annealed in reducing atmosphere at 900 °C. A good agreement with the bulk alloy phase diagram has been found: in particular the fcc cubic alloy solid solution is present in all the investigated compositions from pure Au to pure Cu, with a lattice parameter following the modified Vegard's law typical of the bulk alloy. Three ordered phases have also been found corresponding to the Au:Cu atomic ratios of 3:1, 1:1 and 1:3.

The linear and non-linear optical properties of the nanocomposites have been measured and it was found that the surface plasma resonance red-shifts with increasing the Cu content in the alloy and spans the entire region from that of pure Au (530 nm) to that of pure Cu (570 nm).

Bielemental nanoparticles: Formation of GaN, GaAs and InN nanoclusters by ion implantation

Concerning the *semiconductor nanocluster* formation by synthesis routes based on ion implantation, significant information are available on GaN while for InN and GaAs more investigations must be performed. It has been clearly observed that the sequential ion implantation of Ga +N in dielectric matrices, such as silica, quartz or alumina, does not determine the formation of GaN structures. GaN nanoclusters are formed in both quartz and alumina only after heating the double implanted samples in NH_3 for 1 h at T = 900 °C. The results of the EXAFS data taken at the GILDA beamline indicate that the quartz substrate favors the aggregation of Ga atoms in large GaN nanoclusters. In fact, not only the fraction of Ga atoms that do not aggregate is low (less than 30%, since the coordination number of the Ga–Ga coordination shell is 8.5 instead of 12), but also the local environment of Ga atoms that are in the clusters is ordered in a multishell structure that reproduces that one of GaN bulk up to R = 6.5 Å. The effect of lattice opening by the radiation damage is likely to promote the formation of larger clusters. In alumina matrix, the clusterization is less favored [Maurizio et al. 2004a].

C - Materials for Energy Production and Transport

In this section the studies on materials involved in various aspects of the production of energy are collected. These investigations are mostly performed by X-ray absorption spectroscopy, in some cases taking advantage of the possibility of carrying out experiments in controlled temperature and chemical environment. Two of the reports included in this section exploit the Translating Imaging Plate of GILDA to measure X-ray diffraction patterns during the structural evolution of a Pt/ceria-zirconia oxide in reducing environment. The matter of this section is divided into nuclear materials, three-way catalysts, fuel cell electrolyte materials and fast ion conductors.

Nuclear materials

The only paper of this section is concerned with an important aspect of the nuclear sources of energy production, that is the release of fission gas from irradiated UO_2 fuels [Garcia et al., 2006]. X-ray absorption spectroscopy experiments are performed on a set of xenon implanted uranium dioxide samples and the size of Xe bubbles is determined from the Xe coordination number. Results indicate that the gas forms highly pressurised inclusions as a result of temperature anneals or an external ion irradiation. Estimated bubble pressures were found to be in the region of 2–5 GPa at low temperature. The consequences of such high pressures developing within intra-granular bubbles in irradiated fuels are interpreted by a model enabling the computation of the sink strengths of bubbles as a function of the pressure of the rare-gas they contain. The model forecasts that for pressure values found in the experiments fission gas bubbles do not act as sinks for diffusing rare-gas atoms.

Three-way catalysts

This topic, although concerning catalysts, is closely related to the problematics of energy production and in particular to the fundamental issue of controlling the emission of pollutants involved in automotive transport. Three-way catalysts (TWC) are constituted of a metal nanophase supported on modified CeO_2. Due to the peculiarity of ceria that acts as an oxygen buffer, the

TWCs are employed for the exhaust treatment in gasoline-fuel vehicles to achieve simultaneous control of CO, hydrocarbons and NO emissions. In [Liotta et al. 2004], the steady-state activity of NO reduction by C3H6, was studied on a $Pt(1\%)/Ce_{0.6}Zr_{0.4}O_2$ catalyst, in a plug-flow reactor, in the temperature range 100–500 °C. Analyses by temperature programmed reduction (TPR), small-angle X-ray scattering (SAXS), X-ray photoelectron spectroscopy (XPS) and X-ray diffraction (XRD) performed at the diffraction hutch of GILDA supported the occurrence of a strong metal–support interaction (SMSI) effect between platinum and ceria and the important role of the platinum in promoting the ceria-zirconia structural reorganization.

The structural evolution during redox treatments in CO of Pt-supported and bare ceria-zirconia is specifically investigated in a paper exploiting the GILDA instrumentation for in-situ XRD (Martorana et al., 2004). The experiment is based on the change of lattice constant of ceria-zirconia (CZ) as an outcome of the reduction of Ce(IV) to Ce(III) by CO fed during the XRD experiment. The structural modification of CZ is monitored by the Translating Imaging Plate XRD detector of GILDA while the simultaneous CO2 production originated by the oxidation of CO is followed with a mass quadrupole spectrometer. In a first phase, oxygen coming from the surface layers of the ceria–zirconia mixed oxide is consumed and no structural variation of the support is observed. After this induction time, bulk reduction of Pt/ceria–zirconia takes place as a step-like process, while the CO_2 production continues at a nearly constant rate. This behavior is totally different from that of the metal-free support in similar reaction conditions, that show a gradual bulk reduction. In repeated oxidation–reduction cycles, it is observed that the induction time in Pt/ceria–zirconia is a function of the thermal history, of the amount of supported Pt and of the structural evolution of the samples.

The issue of the interaction of supported Pt with CZ is addressed in an XAS study specifically projected to investigate the Pt-CZ interface [Deganello et al. 2006]. XAS analysis allows to

evidence the formation of a platinum−cerium alloy in redox-aged samples and the stability of the metal particles toward oxidation and sintering during high-temperature treatments. Under CO flux at 773 K, bare ceria-zirconia shows a continuous drift of diffraction peaks toward smaller Bragg angles, due to a progressive increase of Ce(III) content. Under the same treatment, the structural rearrangement of Pt-supported ceria-zirconia starts after an induction time and takes place with an abrupt change of the lattice constant. The experimental evidence points to the role of supported Pt in modifying the redox properties of ceria-zirconia with respect to the bare support. It is proposed that the much faster bulk reduction observed by in situ XRD for redox-aged Pt/ceria-zirconia can be attributed to an easier release of reacted CO_2, producing a more effective turnover of reactants at the catalyst surface. The much faster bulk reduction observed by in situ XRD for Pt/CZ has been attributed to a beneficial effect of the supported metal, and in particular to an easier release of reacted CO_2, producing a more effective turnover of reactants at the catalyst surface. The formation of a Pt−Ce alloy, demonstrated by EXAFS analysis, is the source of the size and oxidation state stability of the Pt metal particles in r-Pt1CZ and, in all probability, also of the peculiar reactivity properties of redox-aged Pt/ceria-zirconia.

Fuel cell electrolyte materials

This issue is concerned with one of the forefront challenges of the research on new materials, that is the development of new proton conductors for the fabrication of oxide electrolyte membranes to be used in intermediate-temperature fuel cells. Theoretical approaches investigating the vibrational dynamics of the oxygen sublattice in perovskite-type proton conducting oxides have demonstrated that for each proton hopping event between adjacent lattice oxygens the oxygen−oxygen distance shortens to assist the proton transfer from one oxygen to the next. Experimental data about local structure are a necessary reference for theoretical calculations to develop a reliable diffusion mechanism for proton conduction and to tailor new generation high-temperature proton conductors.

In [Longo et al. 2006] the local structure of yttrium in Y-doped $BaCeO_3$ compounds is studied using X-ray absorption spectroscopy (XAS) at the Y K-edge. XAFS experiments on $BaCe_{1-x}Y_xO_{3-\delta}$ ($x = 0.02, 0.1$) compounds have been performed on dry and water bearing samples to investigate the local environment of yttrium. The main results can be summarized as follows: the local environment of yttrium is a distorted octahedron of oxygens, characterized by at least two Y−O distances; a significative structural modification in the neighborhood of yttrium takes place under hydration, pointing out a preferential insertion of the hydroxyls in the immediate environment of the dopant; the Debye−Waller factors are larger in protonated samples, and it is likely that also static disorder is effective when water is introduced in the host matrix structure; in situ XAFS experiments performed in O_2/H_2O atmosphere on the 10% Y-doped samples show that the distortion in the YO6 octahedra observed at liquid nitrogen temperature is retained also at 753 K.

The local structure investigation on Y-doped barium cerate is concluded in a further paper [Giannici et al. 2007a] concerning, besides Y, also the local environment of Ce and Ba. It is demonstrated that the insertion of yttrium in the site of cerium produces a remarkable local distortion of the dopant first-shell octahedral environment that affects also the next coordination shells by a static disorder increasing with dopant amount. For a dopant concentration estimated as $x > 0.17$, a poorly crystallized yttrium oxide phase that cannot be detected by X-ray diffraction is observed by XANES analysis. The structural analysis carried out at the K-edges of cerium and barium in Y-doped barium cerate compounds, at a nominal doping level varying from 2% to 30% of the available B sites of $BaCeO_3$, demonstrates a substantial agreement of the observed local arrangement with the crystallographic structure determined by neutron scattering. However, the local structure is sensitive to the doping level by an increasing effect of the static disorder with dopant amount. The origin of this static disorder is related to the local distortion introduced in the barium cerate matrix by the insertion of the dopant Y^{3+} species in the site of Ce^{4+}.

The increase with dopant amount of static disorder around Ce and Ba and the configuration of the Y octahedral environment are essentially independent of sample hydration and therefore is ascribed to the peculiar interaction of Y with the matrix, giving rise to a distorted oxygen octahedral arrangement. On the contrary, the static disorder around Y noticeably increases in the protonated samples and is then related to a distortion of the local structure of yttrium originated by the preferential location of protons near the dopant sites.

The local structure around indium is correlated with the proton conduction properties in the solid solution series $Ba(In,Ce)O_{3-\delta}$ in the paper [Giannici et al. 2007b]. Compared to the limited solubility of Y_2O_3 in $BaCeO_3$ and $BaZrO_3$, the complete solubility of In_2O_3 is suggested to reflect a relation between absolute hardness of the dopant and the ease of insertion into the hosting lattices. The EXAFS analysis used to probe the local environment of In_{3+} in barium cerate demonstrates that, in the surroundings of the dopant, the orthorhombic barium cerate structure is strongly modified, resulting in an increase of local symmetry. Actually, the InO_6 octahedra are very regular and, moreover, there is no indication for any defect clustering. This is suggested to be the main reason for the low entropy of formation of protonic defects by water dissolution. The mobility of such defects is lower than in Y-doped $BaCeO_3$, but a higher concentrations of protonic defects is allowed. This leads to high proton conductivities, which renders In^{3+} an attractive dopant for $BaCeO_3$-based proton conductors. The results of this paper demonstrate also that ionic radius matching is only one and not the most important criterion for tailoring a good proton-conducting ceramic material.

Fast Ion Conduction in Glasses

Fast-ion-conducting (FIC) glasses, whose values of ionic conductivity at room-temperature (RT) can be as high as 10^{-2} Ω^{-1} cm^{-1}, are interesting for potential applications in solid state electrochemical devices such as batteries, smart windows and sensors, owing to their stability, ease of preparation and large non-stoichiometric compositional ranges.

The understanding of transport properties in FIC glasses is a challenging problem both from applied and basic research point of view. Although many experimental and theoretical efforts have led to some general rules and empirical relations for high ionic conductivity, there is not yet any satisfactory and widely accepted transport model.

The structural characterization of FIC has been object of many proposals since the beginning of the GILDA activity, mainly with X-Ray Absorption as a function of temperature by the Italian Trento's group at BM08-GILDA (Ag environment) and at BM29 (I environment) and with XRD by the Swedish Goteborg's group.

A particular attention has been devoted to FIC glasses containing the doping salt AgI. The continuous experimental progress, based on the use of many experimental techniques, like nuclear magnetic resonance, infra-red and Raman spectroscopies, x-ray absorption fine structure (XAFS), x-rays and neutron diffraction, has led to the development of more and more refined models and to some commonly accepted ideas. There is a clear evidence that the high ionic conductivity of these system is due to a balance between three different effects: a) the possibility of modifying the glass network in order to accommodate a high quantity of the dissolved doping salt in a convenient way; b) a mixed environment for the mobile cation, because the cations responsible for high ionic conductivity are those which share bonds with both iodine and oxygen atoms; c) a possible interference between mobile species.

These conclusions have been confirmed on the grounds of experiments performed at ESRF on many FIC glasses: the so called "expansion of the network" has been monitored by a careful analysis of diffraction experiments, while a clear correlation between the first shell I-Ag distance and the activation energy for ion conduction in an extended range of composition has been demonstrated by EXAFS recently (Sanson 2008a).

The papers published in the years 2004-2008 from the activity at GILDA regarded:

- Modeling of the global structure of FIC glasses and interpretation of conductivity data (Karlsson 2004, Sanson 2007a, Sanson 2007b, Sanson 2008a);
- Local structure and dynamics around single components of FIC glasses (Kuzmin 2006, Sanson 2008b);
- Interpretation of X-ray Absorption data on strongly disordered glasses [Sipr et al. 2004, Dalba et al. 2005, Dalba et al. 2008].

Fast Ion Conduction in Glasses: Modeling of the global structure of FIC glasses and interpretation of conductivity data

The interpretation of the FIC on the basis of a network expansion due to the insertion of the doping salt has been proposed in previous papers based on a Reverse Monte Carlo modeling of XRD and Neutron diffraction data. [Karlsson et al. 2004] have concentrated the attention on the conductivity and structure of $(CsI)_x$-$(AgPO_3)_{1-x}$ glasses (where 0 <= x <= 0.2). In this system two mobile species are present: thus, evidence for a partial dissociation of Ag ions from oxygen sites into iodine-rich environments upon addition of CsI has been found. A similar dissociation effect has previously been found in PbI_2-doped $AgPO_3$ glasses, where it, together with network expansion, was considered to cause a much higher dc conductivity of PbI_2-doped $AgPO_3$ glasses as compared to AgI-doped $AgPO_3$ glasses. However, the dc conductivity is much lower in the present CsI-doped glasses than in Pbl_2-doped glasses. This is due to the high mobility of Cs ions, because the mixed mobile ion effect reduces the measured ionic conductivity.

Even though the "network expansion" monitored by Diffraction data is easily understood in terms of more empty space available for the dissolution of the doping salts (AgI, CsI, PbI_2) in very different glass matrices (borate, phosphate, molybdates are structurally different in terms of network and basic units rearrangement), this is a not sufficient condition for FIC.

The analysis as a function of temperature [Sanson et al. 2007a,b] and composition [Sanson et al. 2008a] of the first shell distance I-Ag has allowed to monitor by EXAFS a continuous modification of this shell (in shape, intensity and position) and to identify a correlation between the activation energy for conduction and the distance: glasses with longer I-Ag distances display higher ionic conductivity, independently from the kind of the host glassy matrix.

Fast Ion Conduction in Glasses: Local structure and dynamics around single components of FIC glasses

By EXAFS the group of University and IFN-CNR of Trento has deeply studied at GILDA the local environment of Molybdenum [Sanson et al. 2008b] and of Silver [Kuzmin et al. 2006].

The short-range order around molybdenum has been investigated in AgI-doped silver molybdate glasses $(AgI)_x(Ag_2MoO_4)_{1-x}$ (with x = 0.67 and 0.75) by Mo–K edge EXAFS measurements as a function of temperature up to the glass transition temperature. The difference from crystalline Ag_2MoO_4 is weak. A softening of the Mo–O nearest-neighbors bond has been detected, but the MoO_4 units still exhibit high rigidity. Above the Tg temperature, no meaningful evidence of local structural and dynamical modifications has been observed around molybdenum.

The local structure around Ag ions in silver borate glasses g-$Ag_2O{\cdot}nB2O_3$ n=2,4 was studied by x-ray absorption spectroscopy at the Ag K edge for temperatures from 77 to 450 K. The RDFs consist of about eight atoms, oxygens and borons, and exhibit relatively weak temperature dependence, mostly due to the presence of strong static disorder. Two main components can be identified in RDFs, located at about 2.3–2.4 Å and 2.5–3.4 Å, respectively.

Fast Ion Conduction in Glasses: Interpretation of X-ray Absorption data on strongly disordered FIC glasses

In the last decades, X-ray Absorption Spectroscopy (XAS) has recorded a remarkable interest in the study of glass structure for its sensitivity to the Short Range Order (SRO) around a selected atomic species. However, thanks to the improvement of quality of data and to modern modeling

techniques, it is evident that in the case of FIC glasses, where the cations are mobile and present in different local sites, a reliable interpretation of XAS experiments could be carried out only with a careful comparison with results of modeling techniques. This is due to the strong decreasing effect of disorder on the EXAFS signal, but mainly to the intrinsic disorder present in these systems, that can not be described in terms of simple Gaussian averaging.

[Sipr et al. 2004] reported the local coordination of Ag cations in silver borate glasses $Ag_2O.nB_2O_3$ by comparing the experimental x-ray absorption near edge structure (XANES) at the Ag K edge with results of theoretical simulations. They demonstrated that simple models which describe the local structure around Ag with a single geometric configuration cannot be reconciled with experimental XANES spectra. In order to obtain a satisfactory agreement between theory and experiment, it was necessary to include the disorder also at the short range. Structural information was extracted from XANES data using an empirical approach, based on the presence of a multiplicity of atomic structural configurations around photo absorbing atoms. This approach is particularly suited for describing the local environment of atomic species belonging to glass network modifiers. The same approach was used in [Dalba et al. 2005, Dalba et al. 2008] for the EXAFS analysis in describing the Silver environment of the same FIC glasses, when even that based on cumulant expansion or multishell Gaussian model failed. The radial distribution functions (RDFs) around Ag ions were reconstructed using a method based on the direct inversion of the EXAFS expression. The chemical types of atoms contributing to the RDF were determined via a simulation of configurationally averaged x-ray absorption near-edge structure (XANES) and EXAFS signals. The analysis shows that the immediate neighborhood of Ag contains mostly oxygens while borons dominate at larger distances. The combination of EXAFS and XANES techniques has thus allowed determining a more complete structural model than would be possible by relying solely on either EXAFS or XANES alone.

D - Environment

D1: Earth Science

X-Ray powder diffraction (XRPD) and X-Ray absorption spectroscopy (XAS) techniques have been successfully used in order to investigate relevant topics in Earth Science and related fields. The XRPD beamline set-up is particularly dedicated to time resolved studies, whilst XAS experimental setup is suitable for XAS studies on concentrated and diluted samples. The studies performed at the Gilda beamline can be divided into two main topics: 1) fundamental mineralogical and geological studies and 2) applied mineralogical studies.

Fudamental mineralogical and geological studies

The XRPD studies comprises structural studies [Colella and Gualtieri, 2007; Scordari et al., 2004] and non ambient behaviour of minerals, particularly at high temperature [Cattaneo et al., 2003; Cruciani, 2006; Cruciani et al., 2003; Merlini et al., 2005, 2008; Tribaudino et al., 2005]. New structures of zeolites and sulphates have been refined by XRPD, and phase diagrams of rock forming minerals have been descript.

The translating image plate setup available at the Gilda beamline, allowed a continuous diffraction recording during any dynamical process, in particular during a heating ramp [Merlini et al. 2005,2008; Tribaudino et al. 2005]. In this way it was possible to monitor continuously the lattice parameter evolution across phase transitions, together with very accurate thermal expansion measurement. In melilite it has been evidenced the tricritical behaviour across the incommensurate/normal structure transition, which occurs in akermanite around 80 °C. The thermal expansion in melilite is affected by cations in tetrahedral sites, in particular Mg-Al substitution, and moreover by interlayer cations (Ca-Na substitution). Single site elasticity affect trace element partitioning, and the presence of Na in melilite can explain different trace element pattern observed, for example, in melilite present in meteorites with different thermal history and metamorphic evolution.

Cruciani et al. [Cruciani et al. 2006] presents a review on high temperature behaviour of zeolites, based on data collected at the Gilda Beamline. This review attempts to rationalize the results concerning the zeolite structural changes due to heating treatments. A new parameter, namely the Stability Index, was introduced to quantify the thermal stability of zeolites. Such an index is based on the zeolite breakdown temperatures from X-ray diffraction studies. The correlation between the stability index and the Si/Al ratio confirmed the importance of the latter ratio in controlling thermal stability of zeolites. It was observed that: (i) zeolites with Si/Al3.80 are very stable; (ii) zeolites with Si/Al1.28 are quite unstable; and (iii) zeolite stability in the intermediate Si/Al range cannot directly be predicted from the Si/Al ratio. In the present study, the inverse relationship between thermal stability and the ionic potential, (Z/r)wt, was also confirmed: (i) zeolites with (Z/r)wt<0.072 are very stable; (ii) the ones with (Z/r)wt>0.187 are unstable, but (iii) the (Z/r)wt ratio does not allow a discrimination in the intermediate region. The maximum volume contraction of the zeolite unit cell appears to be controlled by the weighted ionic potential. Among different factors related to the framework topology, the expected relationship between the framework density and the Stability Index was not found

XAS absorption studies are mainly dedicated to investigate the local environment of doping and trace elements in minerals and glasses [Brigatti et al., 2004; Cardelli et al., 2003; Giuli et al., 2004; Quartieri et al., 2004; Sani et al., 2004; Tarantino et al., 2005]

The knowledge of the incorporation mechanisms of trace elements into rock-forming and accessory minerals is fundamental to understand and model the roles of the various factors (such as structure type, bulk chemistry, pressure, temperature, oxygen fugacity) which rule the partitioning of elements at equilibrium (either solid/solid or solid/liquid partitioning). Hence, this information is of particular relevance to understand petrologic and geochemical processes. The role of the crystal-chemical control on the trace-element partitioning behaviour between mineral and melt is

still poorly known in many mineral structures, and sometimes also the mechanisms ruling trace-element incorporation are not completely controlled, especially in the case of complex structures undergoing multiple solid solutions.

Garnets are a group of rock-forming minerals of great relevance for petrogenetic studies, since they are stable over a wide range of physico-chemical conditions and are able to incorporate several trace elements commonly used in geochemical modelling. For these reasons, aluminosilicate garnets ($X_3Al_2Si_3O_{12}$, X = Fe^{2+}, Mn^{2+}, Mg, Ca) have received much attention, regarding either their complex major-element crystal-chemistry or their thermodynamic properties or trace-element behaviour. Modelling of Rare Earth Elements (REE) incorporation in garnets as a function of the composition, temperature and pressure of crystallisation is particularly relevant for petrogenetic purposes. In particular, there is a need for direct information on the local coordination of the various cations substituting at the X site in garnet solid-solution.

The site location and geometry of trace amounts of dysprosium (299 ppm) in a natural melanite garnet from carbonatitic rocks have been studied by high energy fluorescence-detected XAFS. Measurements done at the Dy K-edge (53789 eV), show that Dy is hosted in the dodecahedral X site. The local geometry of Dy, which is compatible with its ionic radius, is compared to that of Ca, the major element at the X site, as determined by single-crystal X-ray refinement, and with that of other trace RE elements as determined by previous XAFS studies.

The results so far obtained at GILDA beamline by XAFS investigations on REE behaviour in natural garnets confirm that these elements (Yb, Dy, Nd) substitute for Ca at the X site, and that different degrees of local lattice relaxation may occur as a consequence of this substitution, in response to the different dimensions of the substituting cation. However, incorporation of the various trace elements is expected to be also affected by the nature of the major constituents. In particular, the larger REE are expected to be more easily incorporated in the large X site of grossular (occupied by Ca) than in the smaller X site of pyrope (occupied by Mg). Also, indicate that the local environment of a given element is dependent on the overall garnet composition, i.e., on the population of all the structural sites.

Applied mineralogical studies

The applied mineralogical studies performed comprise different materials: a) zeolites [Berlier et al., 2005a; Dalconi et al., 2006; Lassinanti et al., 2007; Martucci et al., 2005, 2007; Millini et al., 2007; Regli et al., 2007a], b) cements [Merlini et al., 2007a,b, 2008], c) oxides and ceramic materials [Beukes et al, 2007; El Habra et al., 2007; Gemmi et al., 2005; Kulkharni et al., 2007; Meneghini et al., 2004; Sacerdoti et al., 2004], d) clay minerals [Brigatti et al., 2005; Malferrari et al., 2007]. Zeolites are important materials especially in catalysis, and high temperature activation have been studied in-situ, by XRPD and XAS studies, in order to monitor the crystallographic phase changes and the local structure of active sites.

Cements hydration process have been monitored by XRPD and the hydration of ordinary Portland cements (OPC) was investigated with X-ray powder diffraction (XRPD) technique, mainly using synchrotron radiation. In situ experiments were performed during the first hours of hydration to study the evolution of the crystalline phases in the system. The hydration was carried out with pure water and in the presence of additives such as superplasticizers and setting accelerating agents. As soon as water is added to the cement, the main clinker alluminate phases (Ca3Al2O6) dissolve and react with gypsum, and ettringite (a comlex sulpho-aluminate hydrate) crystallizes. Its evolution appears to be very complex, and lattice parameters change as a function of setting time, indicating a possible chemical evolution of ettringite with time and as a function of pH. After few hours, the induction period (i.e. the period when cement is workable), the main silicate phases, mainly Ca3SiO5 dissolve and react with water, to form poor crystalline CSH (Ca-Si-hydrate) phase. Its formation and microstructure is responsible of mechanical strength of cements and concrete. CSH can be indirectly quantified, using the refined scale factor of the crystalline phases and its rescaling with Rietveld phase fraction [Merlini et al. 2007] and its evolution studied. It appears that in the

first period the volumetric evolution of CSH is function of nucleation process, and after some hours, its increase can be described by a diffusion limited process. The qualitative evolution of CSH is similar in different system investigated, and additives and admixtures, mainly superplasticizers, on the contrary, strongly alter the induction time and the ettringite crystallisation, i.e. the workability period of cement and concrete.
Ceramic material properties (such as thermal expansion) or crystallisation process have also been monitored in situ by XRPD [Kulkharni et al. 2007; Meneghini et al. 2004].
Local structure of polluting metal elements (Hg, Cd) in clay minerals have been studied by XAS techniques [Brigatti et al., 2005; Malferrari et al., 2007].

D2: Environmental Pollution

In this section we have grouped a number of studies that have implications for specific environmental issues. From a traditional disciplinary standpoint, the majority pertains to the field of Earth sciences (mineralogy and geochemistry), and only one can be assigned to biological sciences (botany – plant physiology). On the other hand, they all have in common what is probably the most diffuse application of synchrotron sources to environmental studies: the attempt, through the use of X-ray absorption spectroscopy, and in particular of EXAFS, to define the local atomic structure of an ecotoxic element in a specific matrix, to try and predict the behaviour of this element in ecosystems (e.g., mobility, retention). Based on the specific topics we can group the contributions in the following subsections

Studies of "heavy metal" interactions with clay minerals
Uptake of arsenic by gypsum and calcite
Removal of Cu from solutions by hydroxyapatite
Uptake of Pb by plants

Studies of "heavy metal" interactions with clay minerals

The environmental importance of clay minerals cannot be overstressed. They are major constituents of many soils and sediments, and have truly remarkable physical and chemical properties, notably adsorption and exchange capacities, that allow them to interact with both inorganic ions and organic molecules. For these reasons, they are important regulators of the mobility of "heavy metals" in soils and sedimentary basins. In a series of papers, Brigatti and coworkers have examined some interactions between clay minerals and metals. In the first contribution [Brigatti et al. 2004], they studied the retention of Cu and Cu-amino acid complexes by montmorillonite and beidellite, before and after repeated aqueous solution treatments, using X-ray diffraction, chemical and thermal analyses, mass spectrometry, and X-ray absorption spectroscopy (XAS). The results indicate that the extraction of metal complexes from smectites depends on the nature of the layer charge and on the kind of organic species. Cu-cysteine complexes are strongly retained in the interlayer position, whereas Cu-glycine complexes are mostly adsorbed in cationic form, which can be easily removed from the silicate layer. X-ray absorption spectroscopy was used to assess the relationships between the structure of the Cu complexes and their desorption from smectites. In Cu-exchanged smectites, the first coordination shell agrees with the hypothesis that Cu coordinates to oxygen atoms to form monomer and/or dimer complexes. The first coordination shell of Cu in smectites treated with glycine shows four atoms at distances of ~ 2 Å. Two of these bonds are with nitrogen, and two with oxygen atoms. For copper-cysteine complexes XAS data are compatible with the existence of Cu-N clusters, thus suggesting that Cu links to the amino acid by the aminic group. In the second paper [Brigatti et al., 2005], the influence of mercury on two 2:1 expandable clay minerals (montmorillonite and vermiculite) was investigated by extended X-ray absorption fine structure spectroscopy (EXAFS), X-ray diffraction at room and high temperature, thermal and chemical analyses. The adsorbed Hg amount was higher for montmorillonite than for vermiculite. Thermal analyses suggest that Hg was

released at *T* ~230 °C and 600 °C for montmorillonite, but at 550, 800 and 860 °C for vermiculite. The effect of temperature on Hg release is also apparent when the basal spacing at 230 °C for montmorillonite (d_{001}=10.3 Å) is compared to that for vermiculite (d_{001}=11.8 Å). EXAFS analyses provide qualitative evidence that oxygen atoms occupy the first coordination shell of Hg in both clay minerals. The best fit between observed and calculated spectra is obtained when montroydite (HgO) is assumed as the reference model compound. Finally, the interaction between Cd(II)in aqueous solution and montmorillonite and vermiculite was addressed via batch sorption experiments on powdered clay minerals, both untreated and cysteine-treated (Malferrari et al., 2007). Reaction products were characterized via X-ray powder diffraction (XRDP), chemical analysis, thermal analysis combined with evolved gasses mass spectrometry, and EXAFS. Sorption isotherms for Cd(II) in presence of different substrates shows that Cd(II) uptake depends both on Cd(II) starting concentration and the nature of the substrate. The results of thermal analysis, consistent with XRDP data both at room and at increasing temperature, further stress the influence of the substrate, in particular cysteine, on the interlayer. EXAFS studies suggest that Cd(II) coordinates with oxygen atoms, to give monomer complexes or CdO molecules, either on the mineral surface and/or in the interlayer. For CdÐcysteine complexes, EXAFS data agree with the existence of CdÐS clusters, thus suggesting a predominant role of the thiol group in the bonding of Cd with the amino acid.

Uptake of arsenic by gypsum and calcite

Arsenic is one of the most feared inorganic pollutants. Therefore, studies of mineral reactions controlling its mobility are of the utmost environmental importance. In recent years, much attention has been given to the possibility that calcite and gypsum can trap arsenic in their lattice in the form of an oxyanion substituting for carbonate in calcite, and for sulphate in gypsum. While the amount of substitution is expected to be low (especially in a rigid structure such as that of gypsum), it can be nonetheless of environmental significance, because both calcite and gypsum are widespread and stable phases in many surface environments. This study is being conducted independently by an Italian and a French-Spanish group; they share the participation of a GILDA staff member. (Thanks to this link, the two groups started a cooperation that produced a joint application for a new experiment at the ID22 ESRF beamline). The French-Spanish group (Fernandez-Martinez et al., 2006) worked with synthetic phases (coprecipitation experiments), by applying a combination of neutron (D20-ILL) and X-ray (ID11-ESRF) diffraction data, and EXAFS (GILDA). The combined Rietveld analysis of neutron and X-ray diffraction data, in agreement with DFT-based simulations, shows an expansion of the unit cell volume proportional to the As concentration in the samples. Interpolation of the experimental Rietveld data allows distinction of As substituted within the structure from that adsorbed on the surface of both minerals. Results obtained by EXAFS analysis of calcite samples show good agreement with the hypothesis of replacement of As into the C crystallographic site. The Italian group [Costagliola et al., 2008] worked on natural, As-bearing calcite (bulk As content ~ 250 mg/kg). Previous studies by electron spin echo spectroscopy[7] provided indirect evidence for an As for C substitution in this material. X-ray absorption spectroscopy of the same samples showed, from analysis of the XANES part, that at least part of As is present in the trivalent state, while EXAFS analysis pointed out, in samples where As(III) is present, a well defined As-Ca second shell. The results support the concept that the arsenite group can replace the carbonate group in the lattice of natural calcite.

Removal of Cu from solutions by hydroxyapatite

The ability of hydroxyapatite (HA) [$Ca_{10}(PO_4)_6(OH)_2$] to remove “heavy metals” such as Pb, Zn, Cu, Cd, Co, and Sb from water is well documented. Various uptake mechanisms have been described, including ion exchange, surface adsorption, and coprecipitation. In the paper [Corami et

[7] Di Benedetto et al., Earth Plan. Sci. Lett., 2006

al. 2008], the sorption of aqueous Cu on synthetic HA was investigated by means of a combined structural simulation and EXAFS analysis. The sorption of Cu in batch experiments follows Langmuir behaviour, and was attributed to a two-step mechanism involving surface complexation and ion exchange with Ca, resulting in the formation of a copper-containing HA. EXAFS results suggest that the metal is present in the Cu^{2+} form, and is bound to four O atoms at a distance of ~ 1.95 Å. The fixation of Cu occurs in the surface sites of hydroxyapatite, whereas sorption in the Ca sites in the inner part of the structure is unlikely.

Uptake of Pb by plants

A critical step in the assessment of the environmental hazard posed by a specific contaminant is the evaluation of its potential transfer to the biosphere, notably to plants. This information is important because 1) it is the main pathway of introduction in the food chain, 2) some plants have the ability of concentrate some elements from the soil; this ability may be potentially used for soil cleanup (phytoremediatrion). In the paper [Marmiroli et al. 2005], European walnut (*Juglans regia*) plants were grown for four years in pots on peat soil contaminated with lead. The metal was mostly taken up by roots (up to 450 mg of Pb in 50 g); concentration in the aerial parts was about 1000 times less. Pb L_{III} EXAFS spectroscopy was performed on root powder from Pb-exposed plants, Pb-impregnated cellulose, and lignin. The results evidenced the presence of PbÐO bindings within the ligno-cellulosic structure in roots. This suggests that the plant disposal strategy for Pb consists in establishing links with large organic molecules in the cell walls. The very limited translocation to the aerial parts give to walnut plants an added asset in Pb phytostabilization.

D3: Archaeological and Cultural Heritage

The use of materials science techniques has long been exploited to address questions posed by archaeologists, particularly those of provenance of ancient materials and technological aspects of production. Identification of the chemical content of ancient objects and of their structures is an important step in these studies and any non-destructive technique that can give this type of information is of particular relevance. Synchrotron radiation based X-ray techniques, which have enabled the technological advancement of many fields in materials science, have been recently applied to archaeology and cultural heritage problems. Among these techniques, those most largely applied are X-ray diffraction and X-ray Absorption Spectroscopy.

In particular, X-ray Absorption Spectroscopy (XAS) has revealed to be a powerful and flexible technique in archaeological studies. It provides for a selected chemical species quantitative information like the local geometrical parameters, number and nature of neighbours, amorphous systems or impurities. It can be applied in air, it virtually does not require any restriction on the type and size of the sample, which can be metal, ceramic, glass, cloth, wood, etc. and, finally, it is applicable to most of the elements of interest, even in very low concentrations. All these characteristics are particularly important in archaeological applications, in which samples are precious cultural heritage made of many different materials.

The archaeometrical studies developed at GILDA beamline can be divided into three categories, on the basis of the investigated materials: glasses, lustre, and pigments pigments.

Glasses

Most of XAFS applications to historical glass research have been devoted to unravel the origin of the artefact colour. In fact, scientific analysis on this topic may provide important information on

the ancient production technology and on the selection of the ingredients responsible for colour and opaque effects.

The colour exhibited by glass can depend on the oxidation state and the electronic configuration of the metal ions in them. These are usually elements belonging to the transition row of the periodic table, which absorb characteristic frequencies of the visible region as a result of d-d electronic transitions. Concerning opaque vitreous materials, the colour and opaque effects were obtained by means of many different substances (*i.e.* calcium and lead antimonates, lead stannate, quartz, wollanstonite), depending on the age and on the desired effects. In particular, regarding ancient red glass, colour and opacity are generally ascribed to the presence of copper under different speciation (metallic clusters or cuprite dendritic aggregates or cations incorporated in the glass matrix).

To characterize colorant, decolorant, and opacifying components, to better understand the manufacturing techniques of the ancient glass, and to provide information on the weathering and alteration phenomena, XAFS, and powder X-ray diffraction, potentialities were exploited by our group in the following investigations, aimed to study:

1- iron and manganese: in a number of transparent or opaque glass samples of Iron, Roman, Byzantine and Medieval ages, characterized by different colours [Quartieri et al. 2005; Arletti et al. 2008a,b,c.]

2- copper: in a series of opaque red and orange musive tesserae and game counters of Roman age [Arletti et al. 2006a,b, Santagostino Barbone et al. 2007]

3- Ca-and Sb antimonates in iron-age vessels [Arletti et al. 2008b]

Glasses:Iron and Manganese in glass fragments and musive tesserae

In ancient glass, iron is typically present at levels which can impart, when in the reduced form, a well known green coloration. To minimize this problem and to obtain transparent uncoloured glass, from around the middle of the first millennium BC, substances were added which tended to neutralize the effects of iron and/or to confer different colours. The main decolourant used before the Roman period was antimony oxide, while - from the second century BC - manganese oxide was more frequently used. The topic connected to the colouring and decolouring roles of Fe^{2+} and Mn^{4+}, respectively, and of their redox interactions during glass production is central in a number of studies performed by XAFS.

The first case study regards the glass-wares from the Medieval Val Gargassa glasshouse (Genova, Italy) [Quartieri et al. 2005]. The Fe and Mn K-edge XANES spectra and the detailed structure of the pre-edge peak of these samples and of the reference compounds showed that in the uncoloured ancient glasses iron is always present mainly as Fe^{3+}, while manganese is present in the reduced form Mn^{2+}, validating the hypothesis of a redox interaction between iron and manganese ($Fe^{2+} + Mn^{4+} \rightarrow Fe^{3+} + Mn^{2+}$), as a result of a deliberate addition of pyrolusite as decolourant during the melting procedure. The investigated glass-wares have been grouped into two main categories. The main, largely diffused production, from yellow-green to green in colour and characterized by a detectable - even if limited - variability in the Fe^{2+}/Fe^{3+} ratio, could be the result of the ”standard” melting procedure, in which a certain variability in the oxidizing and reducing conditions could account for the way in which furnace was conducted (*i.e.*, alternating of refuelling and burning) during the glass melting and working. The second, subordinate colourless artefact group, evidences the intentional adding of manganese oxide as bleaching agent.

A recent XANES investigation [Arletti et al. 2008a] has been performed on a series of early Byzantine glass (dated from the late IV cen. A.D. to the middle VII cen. A.D.), mainly vessels and beakers, recovered during excavations carried out in the Ganzirri village (Sicily-Italy). All the analysed fragments resulted to be natron-based silica-lime glass, typical of this period. Concerning minor elements, the finds of Ganzirri can be clearly divided into two groups: i) glass with high Fe, Ti, Mn contents (HIMT glass), characteristic of the Mediterranean area after the IV century A.D.; ii) glass characterized by low levels of Fe, Ti and Mn. The samples were examined by Fe- and Mn-K-edge XANES to provide information on Fe and Mn speciation and to understand whether Mn

was intentionally added to control the colour of the glass, or was present as an impurity in the sands. Contrary to the case studies previously discussed, XANES data of Ganzirri artefacts suggest that the high level of Mn in the HIMT glass is not due to a deliberate adding of pyrolusite, but to the abundant presence of this element in the sand used for the glass production.

[Arletti et al. 2008b] also recently performed the characterization of a suite of very rare, highly decorated and coloured glass vessels and beads from the VII to IV century B.C, found in Etruscan contexts. The most serious difficulty in developing this study was that any - even micro- sampling was absolutely forbidden. As a consequence, the mineralogical and chemical nature of chromophores and opacifiers present in these Iron age finds were identified by means of strictly non-destructive synchrotron-based techniques: micro X-Ray Fluorescence (μ-XRF) and Fe and Mn K-edge μ-XANES (ID21) and X-Ray Powder Diffraction (XRPD) (GILDA beamline). The combination of these techniques made it possible the identification of lead and calcium antimonates in the decorations, whereas no crystalline phases were detected in the bulk glass. Fe and Mn K-edge μ-XANES were collected at several points, thus enabling the mapping of the oxidation state of these elements across the samples. Iron is in general present in the reduced form Fe^{2+} in the bulk glass of all the vessels, and in the oxidised form Fe^{3+} in the decorations, indicating that these glass artefacts were produced in at least two distinct processing steps under different furnace conditions.

Glasses: study of Cu in musive tesserae and game counters

Several recent XAFS investigations performed on red-coloured (copper ruby red and opaque red) ancient Cu-bearing vitreous artefacts (Roman glasses and enamels, game counters, mosaic tesserae, etc) have shown that nanoparticles of metallic Cu are at the origin of the red colour, which arises from the light scattering by the colloidal metallic particles. This scattering phenomenon is not only related to the size of the nanoparticles but also to their shape, resulting in a variety of colours for human eyes (round shape for red, elongated shape for blue etc.).

The most Interesting result obtained during the XAS studies of opaque game counters from Pompeii excavations and of mosaic tesserae from Sicily [Arletti et al. 2006a,b] is the speciation of copper in the red and green samples. In particular, the chemical analysis and the SEM (Scanning Electron Microscopy) and TEM (Transmission Electron Microscopy) studies of two opaque red artifacts (a mosaic tessera from Tusa and a game counter from Pompeii) revealed the presence of an anomalously high content of Cu, finely dispersed in the glass ground mass, but did not allow to determine its oxidation state. The absence of cuprite peaks in the X-ray diffraction patterns and of any dendritic agglomerates in the SEM images suggested to rule out the presence of this species. The XAS investigation at the Cu *K*-edge and the analyses of the high-resolution spectra indicated the presence of monovalent copper cations incorporated in the glass matrix, accompanied by Cu nano-clusters. These conclusions are congruent with the red color and the opaque aspect of the samples.

A XANES/EXAFS study of the speciation of copper in reported in the paper [Santagostino Barbone et al. 2007] on selected red, orange and yellow glass slabs of sectilia panels from Faragola settlement (Ascoli Satriano, Foggia, Italy), in order to determine the chemical state of Cu. The results indicate that, with the exception of the red samples, all slabs were made by mixing a siliceous sand with natron. The red slabs show significant compositional differences with respect to K_2O and MgO contents, probably linked to the use of plant ashes as a source of alkali. The red, orange and yellow slabs are coloured by metallic copper, cuprite and Pb antimonates, respectively. The comparison between the chemical composition of the Faragola samples and several glass reference groups did notprovide conclusive evidence of provenance.

Glasses: Ca-and Sb antimonates in vessels from Etruscan contests

It has been performed the characterization of a suite of very rare, highly decorated and coloured glass vessels and beads from the VII to IV Century B.C [Arletti et al. 2008b]. The most serious difficulty in developing this study was that any - even micro- sampling was absolutely forbidden.

As a consequence, the mineralogical and chemical nature of chromophores and opacifiers present in these Iron age finds were identified by means of the following synchrotron-based strictly non destructive techniques: micro X-Ray Fluorescence (μ-XRF), Fe and Mn K-edge micro X-ray Absorption Near Edge Spectroscopy (μ-XANES) performed at ID22 beamline and X-Ray Powder Diffraction (XRPD), performed at GILDA beamline. The μ-XRF mapping evidenced high levels of Pb and Sb in the yellow decorations and the presence of only Sb in the white and light blue ones. Violet and black glass show high amounts of Mn and Fe, respectively. The XRPD analyses confirmed the presence of lead and calcium antimonates in the decorations, whereas no crystalline phases were detected in the bulk glass. The data reported in this paper allows us to conclude that the main colouring and opacifing agents used in the Iron Age were the same employed in the subsequent Roman age.

Lustre

Lustre is one of the most important decorative techniques of the Medieval and Renaissance pottery of the Mediterranean basin, capable of producing brilliant metallic reflections and iridescence. Recent works demonstrated that lustre is characterized by a heterogeneous metal-glass nanocomposite film, some hundreds nanometers thick. Silver and copper quasi-spherical nanoparticles are dispersed within the outer layers of the glaze, conferring to the whole system specific optical properties an colour. Following these recent findings, the local environment of copper and silver atoms has been studied by EXAFS spectroscopy at GILDA on original samples of gold and red lustre of Italian and Iranian origin [Padovani et al. 2004, 2006; Capellas Espuny 2006].

It has been found that, in gold lustre, whose colour is attributed mainly to the silver nanocluster dispersion, silver is only partially present in the metallic form and copper is almost completely oxidised. In the red lustre, whose colour is attributed mainly to the copper nanocluster dispersion, only a fraction of copper is present in the metallic form. EXAFS measurements on red lustre, carried out in the total electron yield mode to probe only the first 150 nm of the glaze layer, indicated that in some cases lustre nanoclusters may be confined in a very thin layer close to the surface. Metal ions in oxidized form are bound to O atoms with a bond length of about 1.84 Å for Cu and 2.01 Å for Ag, similarly to what observed in soda-lime glasses doped with Cu and Ag by the ion-exchange process. The typical metallic fraction is about 10 - 30% and an increase of this fraction up to 80% is observed when collecting data in TEY mode. This evidences as the reduction of the metal was induced by agents in the furnace atmosphere and interested a surface portion of the metal doped layer.

These findings are in substantial agreement with previous results on Italian Renaissance pottery. In spite of the large heterogeneity of cases, the presence of copper and silver ions in the glaze confirms that lustre formation is mediated by a copper- and silver-alkali ion exchange, followed by nucleation and growth of metal nanoparticles.

Pigments

XAS has been applied as a non-destructive technique for the characterization of pigments on decorated pottery fragments [Barilaro et al. 2007]. The samples were a series of pottery shards excavated from the archeological site of Caltagirone (Sicily, Italy), a well-known ceramic production center. Aesthetical criteria and morphological observations allowed attributing the samples to quite different historical periods, starting from the 18th century B.C. up to the 16th century A.D. An extensive time interval led to suppose that different materials and techniques were used for the production of the ceramic paste and also for the preparation of pigments. XAS measurements were performed at the Cu and Fe *K*-edges. The analysis was carried out both XANES and EXAFS region. The results indicate that Fe oxides is the main pigmenting agent most of the ancient fragment, while in the other ceramic shards, besides Fe oxides, copper oxides were also found. Copper is present as Cu^{2+}.

Investigations of the darkening phenomenon of copper resinate observed in a XV century easel painting were carried out by X-ray absorption near edge structure and extended X-ray absorption fine structure measurements were collected at the Cu *K*-edge on an original painting sample, as well as on fresh pigment standards and on painting models [Cartechini et al. 2008]. The study was aimed at providing structural information of the oxidation states and the local chemical environment (neighboring atoms and bond distances) of copper in the unaltered and blackened pigments in order to elucidate the discoloration mechanism. EXAFS analysis evidenced that the local chemical environment of Cu in copper resinate can be described using neutral copper acetate as a model. It consists, essentially, of bimetal Cu^{2+} carboxylate complexes with a distorted octahedral coordination. Such a structure is retained in the blackened pigment, although some differences were observed. It has been found that the alteration takes place without change of the valence state of Cu(II) ions, while the formation of the copper oxides CuO and Cu_2O responsible for the embrownment is excluded. On the basis of the XAS results it is deduced that discoloration of copper resinate may be related to local modification of the copper coordination structure as evidenced by the observation of an increase of the Cu–Cu and Cu–C distances in the EXAFS spectra.

E – Life Sciences

The GILDA beamline has been successfully exploited in a significant number of XAFS studies on biological systems. These investigations have mainly focused on metal binding sites in proteins (including structural sites of metallo-proteins as well as inhibitory sites to which exogenous metal is bound). XAFS is an invaluable tool in structural biology, because of its equal applicability to crystalline, amorphous and liquid state. It can provide the high-resolution local structure of a metal ion embedded in a biological system in terms of accurate bond lengths, metal site geometry and coordination number, yielding at the same time, through the Debye-Waller factors, information on the thermal fluctuations and static disorder that contribute to the relative mean-square displacements between the absorbing and backscattering atoms. These abilities have been used to address different biological problems and topics which include:

1) the mechanism by which Zn ions inhibit electron and proton transfer in photosynthetic [Giachini et al., 2005] and respiratory protein complexes [Francia et al., 2007, Giachini et al., 2007a];

2) the role of Zn in enhancing the stability of the myelin membrane by interacting with the myelin basic protein [Benfatto et al., 2004];

3) the relevance of protein-matrix interaction in determining the local structure and dynamics of protein metal-sites, with special emphasis for the bioprotective effects of disaccharides in glassy matrices [Giachini et al., 2007b, Veronesi et al., 2008];

4) the stereochemical characterization of catalytic and structural metal sites, among which the heme iron site of different hemoglobin complexes [Girasole et al., 2005; Pozzi et al., 2005], the binuclear copper sites of hemocyanins (Borghi et al., 2005) and a previously unknown Zn binding site in the respiratory complex NADH-Q oxidoreductase [Giachini et al., 2007c].

From a methodological point of view, the above mentioned studies, as a whole, have highlighted:

(i) the importance of taking full account of multiple scattering effects when performing *ab initio* EXAFS analyses of relatively disordered systems, as protein metal sites;

(ii) the potentiality offered by a quantitative analysis of the near edge region (XANES) in structural studies of biological metal sites;

(iii) the possibility of characterizing and localizing protein metal sites even in the absence of specific crystallographic data, using a synergic approach which combines multiple scattering EXAFS analysis, ab-intio XANES simulations, Debye-Waller factors evaluated on the basis of Density Functional Theory calculations, and statistical structural information on metal binding clusters provided by the Protein Data Bank.

In the following we report in more detail on the results obtained, which are grouped according to the lines described above.

Zn^{2+} binding sites in photosynthetic reaction centers and respiratory complexes.

Zn^{2+} metal ions bind specifically to a number of charge translocating membrane protein complexes, strongly inhibiting electron and/or proton transport. Among these protein complexes are the bacterial photosynthetic reaction center (RC) and two key enzymes of the respiratory electron transfer chain: the cytochrome (cyt) bc_1 complex and cytochrome c oxidase.

The high-affinity binding of Zn^{2+} has been characterized with great detail in the bacterial photosynthetic reaction center (RC). This pigment-protein complex, which catalyses a light-induced electron transfer across the membrane dielectric, can be considered as a model system when examining more complex redox enzymes. Structural and spectroscopic studies of Zn-RC

complexes[8] have revealed that Zn^{2+} inhibits the rate of proton transfer from the protein surface to the final electron acceptor of the RC by competing with protons for the same binding site which involves two histidine residues. This finding allowed determination of the entry point of H^+ and led to a full definition of the proton pathway from the aqueous phase to the acceptor quinone molecule bound to the RC[9]. The location of the RC Zn^{2+} binding site has suggested that the Zn inhibitory effects observed in other redox enzymes share the same mechanism, i.e. binding of a divalent metal ion blocks competitively an entry or exit proton pathway close to the protein surface. Location of Zn binding sites and resolution of their local structure becomes therefore a powerful tool in tracing proton pathways in an entire class of membrane proteins.

In view of the above considerations a systematic project has been undertaken, aimed at determining by XAFS the local structure of bound Zn^{2+} in the photosynthetic reaction center purified from the bacterium *Rhodobacter sphaeroides*, in prokaryotic and eukariotic cyt bc1 complexes, and in the cytochrome c oxidase. The objective was to determine the location of the binding sites, defining at high resolution the coordination geometries, in order to clarify the common, structural origin of the inhibitory effects observed.

X-ray absorption spectroscopy of stoichiometric Zn-RC complexes, embedded into polyvinyl alcohol films [Giachini et al., 2005] allowed a clear-cut determination of the local structure of the high affinity Zn^{2+} binding site previously identified by x-ray diffraction at 2.5 Å resolution. XAFS data were analysed by combining *ab-initio* simulations and multiparameter fitting; structural contributions up to the fourth coordination shell and multiple scattering paths (involving three atoms) have been included. The results indicated that Zn^{2+} binds two O and two N atoms in the first coordination shell. Higher shell contributions are consistent with a binding cluster formed by two His, one Asp residue and a water molecule. Analysis of complexes characterized by approximately 2 Zn ions per RC reveals a second structurally distinct binding site, involving one O and three N atoms, not belonging to a His residue. The local structure obtained for the higher affinity site nicely fitted the coordination geometry proposed on the basis of XRD data while the first shell distances resulting from XAFS analysis were considerably contracted in comparison with those determined by XRD.

Cyt bc_1 complexes are electrogenic quinol:cyt c oxidoreductases, encountered in a broad variety of prokaryotic and eukaryotic organisms. These widespread membrane integral enzymes play a crucial role during photosynthesis and respiration[10]. In all cases these energy transducing enzymes transfer electrons from a hydroquinone derivative (QH_2) to a soluble electron carrier (a c-type cyt). The bc_1 complex is one of the major contributors of the transmembrane electrochemical proton gradient used for ATP synthesis. The mechanism of redox coupled H^+ translocation by the bc_1 involves two catalytic sites facing the two opposite sides of the energy transducing membrane: the Q_o site, at which QH_2 oxidation is coupled to proton release and cyt c reduction, and the Q_i site, where quinone reduction is coupled to H^+ uptake. A complete catalytic cycle requires two turnovers of the Q_0 site, so that 4 H^+ are released to one side and 2 H^+ are taken up from the other side of the membrane. Various XRD structures of the mitochomdrial bc_1 complex are available; recently an XRD structure of the simpler bacterial cyt bc_1 at 3.8 Å has been published[11] (Berry et al., 2004).

---

[8] Axelrod, H.L., Abresch, E.C., Paddock, M.L., Okamura, M.Y., Feher, G. (2000) Proc. Natl. Acad. Sci. USA 97, 1542-1547.
Paddock, M.L., Sagle, L., Tehrani, A., Beatty, J.T., Feher, G., Okamura, M.Y. (2003) Biochemistry 42, 9626-9632.

[9] Adelroth, P., Paddock, M.L., Sagle, L.B., Feher, G., Okamura, M.Y. (2000) Proc. Natl. Acad. Sci. USA 97, 13086-13092

[10] Berry,E.A., Guergova-Kuras,M., Huang,L.S., Crofts, A.R. (2000a) Ann. Rev. Biochem. 69, 1005-1075

[11] Berry, E.A., Huang, L.-S., Saechao, L.K., Pon, N.G., Valkova-Valchanova, M., F. Daldal (2004) Photosynth. Res. 81, 251-275.

Zn^{2+} is a well established inhibitor of the bovine mitochondrial cyt bc_1, in which it competes with H^+ ions. In bacterial bc_1 complexes Zn^{2+} has been recently shown to decelerate specific electron transfer steps and the generation of transmembrane voltage[12]. These observations have been tentatively explained by proposing that Zn^{2+} binds close to the Q_0 site, blocking the proton release channel(s). In agreement with this suggestion two potential inhibitory Zn^{2+} binding sites have been revealed in the XRD structure of the avian cyt bc_1: one of them, (Zn01), located in a hydrophilic area between cyt b and c_1, might interfere with the egress of H^+ to the aqueous medium. Although a number of putative Zn ligands (including histidines) were identified, the coordination geometry could not be resolved[13].

Using Zn K-edge XAFS the local structure of Zn^{2+} bound stoichiometrically to non crystallized cyt bc_1 complexes has been investigated [Giachini et al., 2007a]. In a comparative study the avian, the bovine and the bacterial enzymes were examined. A large number of putative clusters, built by combining information from first-shell analysis and metalloprotein databases, were fitted to the experimental spectra by using *ab initio* simulations. This procedure led to the identification of the binding clusters with high levels of confidence. In both the avian and bovine enzyme a tetrahedral ligand cluster formed by two His, one Lys and one carboxylic residue was found, and this ligand attribution fit the crystallographic Zn01 location of the avian enzyme. In the chicken enzyme the ligands were the His121, His268, Lys270 and Asp253 residues, and in the homologous bovine enzyme they were the His 121, His267, Lys269 and Asp254 residues. Zn^{2+} bound to the bacterial cyt bc_1 complex exhibited quite different spectral features, consistent with a coordination number of six. The best fitting octahedral cluster was formed by one His, two carboxylic acids, one Gln or Asn residue and two water molecules. Interestingly, by aligning the crystallographic structures of the bacterial and avian enzyme, this group of residues was found to be located in the region homologous to that of the Zn01 site. This cluster included the His276, Asp278, Glu295 and Asn279 residues of the cyt *b* subunit. The conserved location of the Zn^{2+} binding sites at the entrance of the putative proton release pathways, and the presence of His residues pointed out to a common mechanism of inhibition. As previously shown for the photosynthetic bacterial reaction center, zinc would compete with protons for binding to the His residues, thus impairing their function as proton donor/acceptors.

Cytochrome c oxidase is the terminal component of the respiratory chain: it catalyses the oxidation of cyt c reduced by the bc_1 complex, reducing O_2 to H_2O and pumping 4 protons across the mytochondrial membrane. Definition of the proton transfer pathways is an open question, crucial for understanding the complex catalytic mechanism of the enzyme. XRD structures of cyt oxidase have helped identify two putative channels for H^+ uptake, referred to as the D and K channels. The roles of these channels are still debated in terms of the number and destination of the protons they conduct and how the individual proton uptake events are coupled to electron transfer[14]. Zn^{2+} inhibits bovine heart cyt c oxidase[15]. In analogy with the scenario observed with the photosynthetic RC, it has been proposed that in cyt c oxidase Zn^{2+} binds near the entry point of the D-pathway at which a cluster of histidine residues and carboxylates is found[16].

XAFS analysis performed according to the procedure described above for the cytochrome bc1 complex, allowed to identify tetrahedral coordination site(s) for Zn^{2+} with two N histidine

[12] Klishin, S.S., Junge, W., Mulkidjanian, A.Y. (2002) Biochim. Biophys. Acta 1553, 177-182

[13] Berry, E.A., Zhang, Z., Bellamy, H.D., Huang, L. (2000b) Biochim. Biophys. Acta 1459, 440-448

[14] Brzezinski, P. (2004) Trends in Biochem. Sci. 29, 380-387.

[15] Nicholls, P., Singh, A.P. (1988) Life Sci. Adv. 7, 321-326

[16] Aagaard, A., Namslauer, A., Brzezinski, P. (2002) Biochim. Biophys. Acta 1555, 133-139

imidazoles, one N histidine imidazol or N lysine and one O-COOH (glutammate or aspartate), most likely located at the entry site of the proton conducting D pathway, and involved in inhibition of the oxygen reduction catalysis [Francia et al., 2007].

Analysis of XANES spectra of Zn interacting with phospholipid multilayers and with the myelin basic protein

The myelin sheath, a system of lipid bilayers wrapped around the nerve axon, plays a central role in the transduction of the nervous signal. Its stability, ensured by the presence of the myelin basic protein (MBP)[17], is enhanced by Zn ions[18]. In order to clarify the interaction of Zn ions with myelin sheath components, XAFS spectroscopy has been employed to characterize the local environment of Zn ions inserted in Langmuir-Blodgett multilayers (LBMLs). These phospholipid systems model quite accurately the myelin sheath[19].

A quantitative analysis has been performed of the X-ray absorption near-edge structure (XANES) spectra at the Zinc K-edge of systems formed by LBMLs in the presence and in the absence of myelin basic protein and in two hydration conditions [Benfatto et al., 2004]. These spectra have been analyzed by Minuit XANes (MXAN), a procedure able to perform a quantitative fit of XANES data in terms of structural parameters[20]. Using this method, the significant differences between the spectra observed in the XANES spectra have been correlated with the coordination changes due to reduction of the space around the Zinc when the level of hydration was lowered and/or the myelin basic protein was added. These spectral differences appeared to be peculiar of the XANES energy range, and were not present in the extended X-ray absorption fine structure (EXAFS) energy range where the analysis was previously performed. This investigation has provided an unambiguous answer to the question of the role of Zn in such complexes by showing that the metal interacts with both the phospholipid heads of the substrate and the myelin basic protein.

Protein-matrix structural-dynamical interactions probed by XAFS: studies in cytochrome c and in photosynthetic reaction centers embedded in polyvinyl alcohol films and in dehydrated treahlose glasses.

Trehalose, a non reducing disaccharide of glucose, is found in large amounts in organisms (like some desert plants) that can survive conditions of extreme drought and high temperature in a state of suspended metabolism (anydrobiosis). This property has been put in relation with the peculiar efficacy of trehalose in the preservation of isolated proteins, membranes and tissues[21]. The effects of embedding carboxy-myoglobin in trehalose have been recently studied by a number of techniques which are sensitive to atomic motion including temperature-dependent optical absorption spectroscopy[22] and neutron scattering[23] which showed that trehalose traps the protein in

[17] Riccio, P.L., Masotti, L., Cavatorta, P., De Sanctis, A., Juretic, D., Bobba, A., Pasquali-Ronchetti, I., Quagliarello, E. (1986) Biochem. Biophys.Res. Commun. 134, 313– 319.

[18] Earl, C.E., Chantry, A.C. Mohammad, N., Glynn, P. (1988) J. Neurochem. 51, 718– 724.

[19] Haas, H., Torrielli, M., Steitz, R., Cavatorta, P., Sorbi, R., Fasano, A., Riccio, P., Gliozzi, A. (1998) Thin Solid Films 327– 329, 627– 631.

[20] Benfatto, M., Della Longa, S. (2001) J. Synchr. Rad. 8, 1087-1094.

[21] Crowe L.M., Reid D.S., Crowe J.H. (1996). Biophys. J. 71, 2087-2093.

[22] Cordone, L., Galajada, P., Vitrano, E., Gassmann, A., Ostermann, A. and Parak, A. (1998). Eur. Biophys. J. 27, 173-176.

[23] Cordone L., Ferrand M., Vitrano E., and Zaccai G. (1999). Biophys. J. 76, 1043-1047.

a harmonic potential. These experimental results have been rationalized by molecular dynamics simulations which showed that: (a) the amplitude of anharmonic motions stemming from the interconversion among the protein's conformational substates is greatly reduced in a dehydrated trehalose matrix; (b) structures are formed which confine the protein within a network of hydrogen bonds connecting protein groups, residual water molecules and trehalose molecules[24].

In agreement with these observations a study of spectral diffusion dynamics, performed on trehalose-coated cytochrome c suggests that also in this heme protein diffusive-like motions are strongly reduced in trehalose matrices as compared to glycerol-water glasses and that the solvent changes some structural features of the protein[25]. As a whole, the results summarized above suggest that changes in atomic motion induced by incorporation in trehalose matrices are accompanied by sizeable structural distortions.

This hypothesis has been tested by using Fe K-edge XAFS to examine the effect of the solvent/matrix environment on the structure and dynamics of the Fe ligand cluster of reduced horse heart cytochrome c in solution, in a dried polyvinyl alcohol (PVA) film and in two trehalose matrices characterized by a different content of residual water [Giachini et al., 2007b]. XAFS data were analysed by combining *ab-initio* simulations and multiparameter fitting, attempting to disentangle structural from disorder parameters. Essentially the same structural and disorder parameters accounted adequately for the XAFS spectra measured in solution, both in the absence and in the presence of glycerol, and in the PVA film, showing that this polymer interacts weakly with the embedded protein. Instead, incorporation in trehalose leads to severe structural changes, more prominent in the more dried matrix, consisting in: (a) an increase up to 0.2 Å of the distance between Fe and the imidazole N atom of the coordinating histidine residue; (b) an elongation up to 0.16 Å of the distance between Fe and the fourth shell C atoms of the heme pyrrolic units. These structural distortions are accompanied by a substantial decrease of the relative mean square displacements of the first ligands. In the extensively dried trehalose matrix extremely low values of the Debye Waller factors were obtained for the pyrrolic and for the imidazole N atoms. This finding has been interpreted as reflecting a drastic hindering in the relative motions of the Fe ligand cluster atoms and an impressive decrease in the static disorder of the local Fe structure. It appears therefore that the dried trehalose matrix perturbs dramatically the energy landscape of cyrochrome c, giving rise, at the level of local structure, to well resolved structural distortions and restricting the ensemble of accessible conformational substates.

The study of protein-matrix structural-dynamic interaction has been extended to an integral membrane complex, by performing a XAFS analysis of the Fe^{2+} site in photosynthetic reaction centers (RC) from *Rhodobacter sphaeroides* [Veronesi et al., 2008]. Crystallographic studies show that Fe^{2+} is ligated with four N_ε atoms from four His residues and two O_ε atoms from a Glu residue. By considering multiple scattering contributions to the XAFS function the structural resolution of the site could be improved: His residues were split in two groups, characterized by different Fe-N_ε distances, and two distinct Fe-O_ε bond lengths resolved. The effect of the environment was studied by embedding the RC into a polyvinyl alcohol (PVA) film and into a dehydrated trehalose matrix. Incorporation into trehalose caused elongation in one of the two Fe-N_ε distances, and in one Fe-O_ε bond length, as compared to the PVA film. The asymmetry detected in the cluster of His residues and its response to incorporation into trehalose have been ascribed to the hydrogen bonds between two His residues and the quinone acceptors. The structural distortions observed in the trehalose matrix indicated a strong interaction between the RC surface and the water-trehalose matrix, which propagates deeply to the interior of the protein. The absence of matrix effects on the Debye-Waller factors has been related to the static heterogeneity and rigidity of the ligand cluster.

---

[24] Cottone G., Ciccotti G., Cordone L. (2002). J. Chem. Phys. 117 (2002) 9862-9866.

[25] Ponkratov, V.V., Friedrich, J. and Vanderkooi, J.M. (2002). J. Chem. Phys. 117, 4594-4601.

Characterization of catalytic metal sites in hemoglobins and hemocyanins, and identification of a structural Zn binding site in the NADH-Q oxidoreductase.

The haemoglobin (Hb) molecule, a heterotetramer, consists of two α and two β subunits, each of which contains as a co-factor a haem group. These four subunits are paired as two dimers. Structural studies showed that deoxy haemoglobins and liganded haemoglobins have two different modes of packing of the two dimers (the quaternary structures) with no major changes in the gross conformation of each of the subunits (the tertiary structures). Perutz assigned deoxy and oxy haemoglobins to T and R quaternary states, which exhibited low and high O_2 affinity, respectively[26]. In the unliganded T-state haemoglobin, the five-coordinated irons lie outside the plane of the pyrrole nitrogen atoms of the haems on the proximal side, whereas in the liganded (with O_2, CO or NO) R-state molecule all irons are six-coordinated and lie in the haem plane, displaying octahedral geometry.

In the last few years, physiological implications have given rise to a large number of studies on HbNO[27]. In particular, interest in NO has considerably increased since it was discovered that this gas provides a unique way to transmit biological signals, thus behaving as a universal second messenger.

The haem stereochemistry has been investigated in the nitrosylated derivative of two amphibian haemoglobins, from *Xenopus laevis* and *Ambystoma mexicanum*, by means of XAFS with the aim to explain the relationships between the active site structure and physiological function of these proteins, compared to that from humans [Pozzi et al., 2005]. The results have shown that while the Fe site local structure of human HbNO is modulated by an allosteric effector such as inositol hexakisphosphate (IHP), shifting the T-R equilibrium towards the T-state, the Fe site local structure of amphibians HbNO is stabilized in a particularly tensed T-state also without IHP.

Among the different Hbs, the ones of annelids are giant extracellular aggregates (M.W. between 2500 and 4200 kD) which present interesting peculiarities and pose a challenge to understand the mechanisms by which different structural units, forming a complex macromolecule, communicate with each other, thus attaining greater efficiency and regulatory control of the biological processes.

From the structural point of view, it is known that a single protein carries 144 Fe-heme containing subunits. The macroprotein also contains linker chains which do not contain Fe-heme but are involved in the protein assembly. Such a huge number of myoglobin-folded subunits are arranged in 12 dodecamers aggregated in an hexagonal bilayer[28]. The critical residues around heme are the same as in vertebrates, however, little is known about the active site structure or about the structural mechanism involved in the oxygen binding/release.

The active site structure of the oxygenated derivative of the main subassemblies (whole protein, dodecamers, and trimers) of the giant haemoglobin from *Eisenia foetida* has been characterized by XANES [Girasole et al., 2005]. The data revealed a remarkable effect of the hierarchic assemblies on the active site of the subunit. Specifically, the whole protein has the same site structure of the dodecamer, while a sharp conformational transition occurs when the dodecamer is disassembled into trimers (and monomers) revealing that constraints due to the protein matrix determine the active site geometry and, consequently, the protein function in these large complexes.

Hemocyanins (Hcs), which are dioxygen transport proteins, belong to an important class of copper proteins characterized by a binuclear active site. The large dimensions of these molecules and/or the difficulties in their isolation have hampered their structural characterization by X-ray diffraction (XRD). As a result, up to now only the crystal structures of four Hcs have been resolved.

---

[26] Perutz, M.F., Fermi, G., Luisi, B., Shaana, B., Liddington, R.C. (1987) Acc. Chem. Res. 20, 309-

[27] Gross, S.S., Wolin, M.S. (1995) Annu. Rev. Physiol. 57, 737

[28] Royer, W.E., Strand, K., van Hell, M., Hendrickson, W.A. (2000) Proc. Natl. Acad. Sci. USA 97, 7107.

XAFS was used very early to characterize the active site of type-3 copper proteins, particularly in the EXAFS region[29]. However, most of these early investigations were carried out in the frame of the single scattering approximation, which has proven to be erroneous, especially in the case of active sites surrounded by histidines.

Studies on the met- and met-azido-Hc forms from *Octopus vulgaris* (mollusc) and *Carcinus aestuarii* (arthropod) and on some related binuclear models without XRD have considered and resolved some fundamental structural aspects of their binuclear type-3 copper site[30]. More recently multiple scattering (MS) calculations have been performed in order to refine the EXAFS interpretation of the absorption spectra [Borghi et al., 2005]. It is only with a composite and advanced approach that some difficult problems, mainly deriving from the presence of two absorbing atoms and from the fact that the metal-metal contribution in the absorption spectra overlaps with the Cu-His signals, have been overcome. Results have been obtained which indicate the role of the MS calculations in the XANES edge region, and which show how it is possible to extract quantitative information from this part of the spectrum in order to refine the structure of the site also in the case of a binuclear centre.

The NADH-quinone oxidoreductase (complex I) plays a central role in energy transduction, coupling electron transfer from NADH to ubiquinone with proton pumping across the inner mitochondrial membrane in eukaryotic organisms or across the cytoplasmic membrane in prokariots. Mitochondrial complex I is one of the largest membrane-bound protein assemblies, being formed by 14 central subunits and up to 32 accessory subunits, and including as cofactors a non-covalently bound flavin mononucleotide (FMN) molecule, 2 binuclear and 6 tetranuclear iron-sulfur clusters[31]. By using inductively-coupled plasma atomic-emission spectroscopy and XAFS spectroscopy, evidence has been recently provided that Complex I posses a tighly-bound Zn ion [Giachini et al., 2007c]. By combining information from first-shell analysis and from metalloprotein data bases, putative binding clusters have been built and fitted to the experimental spectrum using *ab initio* simulations. The best fitting binding cluster is formed by 2 histidine and 2 cysteine residues arranged in a tetrahedral geometry. This previously undetected Zn binding site displays a local structure typical of a constitutive, structural metal site.

[29] See for example Brown, J.M., Powers, L., Kincaid, B., Larrabee,J.A., Spiro, T.G. (1980) J. Am. Chem. Soc. 102, 4210-4216.

[30] Borghi, E., Solari, P.L., Beltramini, M., Bubacco, L., Di Muro, P., Salvato, B. (2002) Biophys. J. 82, 3254-3268.

[31] Brandt, U. (2006) Annu. Rev. Biochem. 75, 69-92.

F – Soft Condensed Matter

In addition to the classic techniques used for basic structural investigation, since several years the synchrotron radiation based X-ray methodologies gave a strong impulse in scientific advancement for various field of material science and also the soft matter took advantage of this. Investigation about the chemical structure of organic, organometallic or polymeric materials provides good knowledge of the structure around metal atoms and allows for exploration about modifications occurring upon sample treatments. Among the synchrotron based methodologies, X-ray Absorption Spectroscopy and X-ray Diffraction turn out to be the most commonly applied in material science for soft matter at GILDA.

More specifically, EXAFS appear as the method most extensively used as applied to systems containing heavy metals as in organometallic polymer films or macrocycle coordination compound macromolecules. The method resulted fairly suitable, supplying structural information concerning the number of first and second neighbours around the metal centres and therefore local geometry factors for materials lacking structural order. X-ray Absorption Spectroscopy is feasible in high or low vacuum conditions as well as in air, without limitations then simplifying the accomplishment of experimental set up as well resulting applicable to every kind of soft matter species. Besides, soft matter samples not containing suitable metal atoms, however presenting crystalline order, can be conversely investigated by X-ray Diffraction technique thus producing data relative to the structure.

In the framework of this class of materials (i.e. soft matter) the general objective of the researchers is essentially the rationalization of the chemical structure, for materials with short or long range order or underprovided of structural order, and generally also the inspection of the modifications occurring after interaction with chemical species, attempting to analyze either, the involved species and the nature of interaction.

An additional remark worth to be mentioned, about the GILDA soft matter research projects developed in the period 2004-2008, concerns the observation that nearly all the investigated soft materials deal with their sensing specificity towards specific chemical species both, in gas phase producing non covalent interaction with reproducibility of the process, or by trapping selected ionic chemicals.

The Soft Matter research projects so far performed at the GILDA Beamline during 2004-2008 can be grouped in few classes based on the kind of material specificity: 1) Polymers; 2) Organometallics; 3) Organic based solids; 4) Polymer templated oxides.

Polymers

As for the scientific cases falling in this class, a further subdivision can also be applied considering that, even if all the contributions are dealing with absorption EXAFS spectroscopy nevertheless, some of these have been achieved classically in transmission but some have been attained in total reflection mode (reflEXAFS). Among the five reports of this section, four contributions within this topic can be grouped in a general research project on Pt and Pd containing rod-like organometallic polymers; the fifth one is on an amphoteric polyamidoamine based sorbing hydrogel.

Polymers: Pt and Pd containing rod-like organometallic polymers

The systems of interest are polymers containing metal in the main chain (Pd or Pt), then producing a rod-like organometallic polymers for which the authors were interested in analyzing the chemical structure around the metal sites. These materials exhibit good peculiar properties useful for applications in the framework of sensors and NLO technology.

Using EXAFS exploration in transmission mode, [Battocchio et al. 2006a] have approached the problem using a simplified molecular system as a model for the more complex extended structure. The absorption method was assessed to be reliable in the case of such kind of materials, as supported by comparison with XRD data analysis; the extension of the analysis to ten-unit long

oligomers was also successful, opening a new scenario relative to the use of EXAFS to these systems. The Pt containing model system (Pt-DEBP oligomer, see the figure with Pt atoms in pink colour) was analyzed at the Pt L_{III} edge and the structural achievements were used as a basis for the resolution of the rod-like decanuclear oligomer structure.

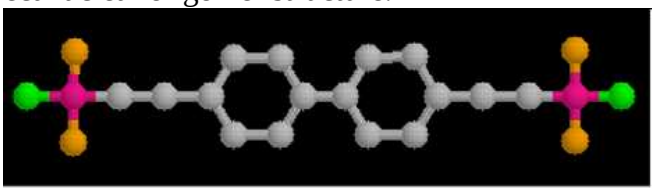

The dinuclear transition metal dialkynyl bridged Pt (II) square planar complex trans and also squared cyclic tetranuclear systems were studied by EXAFS at the Pt L_{III} edge by [Battocchio et al. 2008] with the intention of achieving from structural EXAFS data analysis elucidation about the interaction occurring at the interface with H_2S molecules. The work deals with the requirement to accomplish a system for the detection and monitoring the sulphur containing compounds in several environments. Sulphur containing compounds are originating from fossil-derived fuels and spoil the air, producing SO_x compounds which are major air pollutants giving rise to the acid rain, H_2S is also a toxic gas harmful for the human body. In this framework the GILDA beamline capability allowed for measurement by a gas cell device in H_2S atmosphere. EXAFS signals, obtained by subtracting the signal in *k* space achieved for the pristine poly-ynes to the *k* signal of the corresponding samples as exposed to H_2S allowed for evidencing a residual oscillation ascribable to the new Pt-S bond formation. Insight into the spectral features analysis gave, in addition, quantitative evaluation concerning the involved metal sites. The metal coordination increases from four to five leading to a pentacoordinated pyramidal Pt centers.

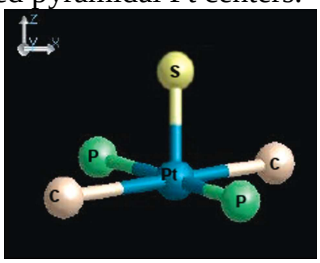

One of the peculiarities at the GILDA beamline is the availability of X-ray absorption measurements with the radiation impinging onto the sample surface at grazing angle in a total reflection mode (REFLEXAFS). This experimental set up has been probed as a method for the enhancement of data relatively to the sample surface. [D'Acapito et al 2004d] have searched for structural answers relative to the dialkynyl bridged Pd (II) square planar complex rod-like polymer. Attempts to achieve data relative to the Pd centres relative arrangement was made, studying sample films nearly one monolayer thickness or multilayer thick; comparison with data relative to the bulk sample as measured in transmission mode was performed. [Battocchio et al. 2006b] extended the investigation by reflEXAFS at the Pt L_{III} edge applied to Pt (II) organometallic polymers of the same family as above, deposited as thick films onto Au and Cr flat surfaces. In this case the reliability of the method was confirmed and assessed; both EXAFS and NEXAFS regions were investigated. The use of a new data analysis program was accomplished for the NEXAFS region of the spectrum with the choice of clusters atoms, which resulted enough to reproduce the spectrum. The dependence of XANES as a function of clusters size was studied. There is a high sensitivity of XANES spectrum on the average first shell distance (a 0,2 Å increase of first shell radius corresponds to 6,2 eV contraction of energy separation between spectral features).

Polymers: Amphoteric polyamidoamine based sorbing hydrogel

A further application of EXAFS Spectroscopy to polymeric system was performed by [Ferruti et al. 2006] which investigated a amphoteric polyamidoamine based sorbing hydrogel with an

innovative molecular architecture, as derived by the use of a crosslinking agent carrying a side primary amino group, by XAS, verifying the atoms relative position, the coordination number, interatomic distances and the modifications occurring to the structure as a consequence of Cu^{2+}, Ni^{2+} and Co^{2+} metal ions adsorption. In this report the authors applied EXAFS spectroscopy to the characterization of metal/hydrogel complexes. For the Co^{2+}containing system the results indicated an asymmetric octahedral metal coordination structure; the asymmetric structure being consistent with the involvement in Co^{2+} coordination of two different functional groups. A final remark about this study was relative to the occurrence of a fast metal ion adsorption and therefore environmental applications of such polymeric material for heavy metal detection.

Organometallics

Macrocyclic compounds coordinated by centred transition metal ions occur also in nature, in the case the macrocycle is built by benzene rings surrounding the four linked and nitrogen containing five atomic rings, these occurs as Me-phthalocyanines (Me-Pcs) macromolecules. Since several decades, Me-Pcs raised a widespread attention by the scientific community because of their peculiar properties in the framework of photoconductivity, biocompatibility, semiconduction, vacuum compatibility and also because of their thermal and chemical stability. Metal-Pcs show presence of radiation absorption in the VIS range, as expected for coordination compounds and exhibit intense and dazzling colour in the range from blue to red originating from the d-d electron transition due to the degeneracy removal by the ligands field. Me-Pcs along the years have found important applications in many technological fields as chemical sensing, photoconducting agents, photovoltaic cell, nonlinear optics and electrocatalysis. In the gas sensing domain Me-Pcs films have been widely studied as electrical gas sensors: the sensing mechanism is based on the conductivity changes induced by the chemical-physical adsorption of oxidizing or reducing gases.

Organometallics: $(Ru\text{-}Pc)_2$

The first study about these systems concerns the interaction at the interface NO_2 / $(Ru\text{-}Pc)_2$ in the framework of gas sensors. EXAFS experiments were performed on the evaporated film of the dimeric ruthenium complex [Alagna et al. 2006]. Absorption spectra analysis gave evidence for the modifications occurring upon interaction between $(Ru\text{-}Pc)_2$ and NO_2 giving rise to formation of radical species due to the macrocycle oxidation. EXAFS measurements carried on before and after NO_2 exposure confirmed that also the coordinating Ru metal is involved in the oxidation process. The authors attempted also to verify the reversibility of the sensing process however, the complete recover of the $(Ru\text{-}Pc)_2$ could not be completely attained.

Organometallics: Cu-Pc

A second scientific case approached at GILDA concerns X-ray absorption investigation about Cu-Pc complex [Maggioni et al. 2006]. In this case the investigation mostly deals with structural analysis of the material as a consequence of thermal treatments; however, the ultimate objective was once more related to the sensing behaviour of Cu-Pc towards NO_2 molecules. Glow-discharge thin sublimated Cu-Pc films onto aluminium substrate were used for EXAFS measurements at the Cu K-edge (8979 eV). The authors found that the first Cu-N shell was substantially unperturbed by the heat treatments, with the four nitrogen atoms at a distance of 1, 91-1, 94 Å; nevertheless, the response of Cu-Pc sample to NO_2 was strongly modified after heating. A close analysis of the XANES part of the absorption spectrum brought these authors to evidence the changes occurring at the Cu coordination sites after heating to 290 ºC, and connected to partial Cu-Pc decomposition and copper oxide formation, with a final evaluation of 75% (CuO)-25%(Cu-Pc) sample composition. On the basis of the XANES findings, the fitting of the sample heated up to 290 ºC included also Cu-O and Cu-Cu correlations at 1, 98 and 2, 93 Å, typical of very disordered or amorphous CuO, as confirmed by the large Debye-Waller factors. XANES analysis was very useful in this experiment

allowing highlighting structural differences upon heat treatment of Cu-Pc samples prepared in two different way (e.g. GDS and evaporated) therefore giving useful indications about the working parameters for the best way of preparing stable and reliable electrical gas sensing material.

Organic based solids

X-ray diffraction methodology has been used at GILDA for investigations relative to the chemical structure of organic macromolecules. Alfa-ciclodextrine in water solution containing varius methylpyridines molecules, in particular 4-methylpyridine, undergoes reversible liquid-solid transition upon heating, with the solid phase involved in a further phase modifications with higher temperatures [Plazanet et al. 2006]. X-ray powder diffraction allowed for the identification of five crystalline phases. The unit cell parameters and corresponding changes with temperature indicated a scenario for the crystallization process. On the basis of the XRD data it has been attempted to propose a model for the mimics of the observed disorder-order transition.

[Comotti et al. 2007] used XRD to investigate the structure and properties of the mesoporous hybrid p-phenylenesilica endowed with crystalline order in the walls. The structure resulted open-pore like with an easy accessibility of the nanochannels to the gas phase, with the host molecules confined in the channels along the matrix walls. The main objective of this work was the capability of chemical species removal from a vapour mixture by a mesoporous material. The full carbon dioxide loading in the channels could be detected by synchrotron radiation X-ray diffraction experiments. The XRD analysis performed at GILDA allowed stating that, the selective adsorption of carbon dioxide vs that of oxygen and hydrogen, together with the permanent porosity, high thermal stability, and high degree of order makes the investigated material a suitable matrix for purifying hydrogen in clean-energy generation.

Polymer templated oxides

Vanadium oxide (VO*x*) thin films are investigated for several applications ranging from optical switching devices, thermal and gas sensors, to catalysis. The use of particular structure-directing agents as template can significantly increase the interlayer distance between adjacent layers. 2D VO*x* have the ability to intercalate a greater percentage of ions between adjacent layers. The higher surface area to volume ratio of the 2D networks compared to the corresponding 3D allows faster kinetics and improved response when ions are intercalated or when gases are adsorbed. In this framework, a study on sol-gel derived vanadium oxide thin films by EXAFS upon templating using polyethylene glycol (PEG) was reported spectroscopy in [Cremonesi et al. 2007]. The XAFS spectra of films with different molar ratio of PEG could be grouped according to the similarity of the features suggesting the presence of two different phases during the annealing process for the analyzed samples. One organization, obtained at 400°C, is characterized by a nearly 3D network with both axial and planar order, while the second phase, obtained at 450°C, has a 2D character with a short range order.

G – Catalysis

The research in catalysis performed at GILDA takes advantage of the instrumentation allowing in situ experiments both for XAS and XRD, and of the possibility of measuring diluted samples by fluorescence XAS. The possibility of monitoring products and reactants by chemical techniques such as mass spectrometry during in situ XAS and XRD experiments allows to correlate catalytic activity with the structural properties of the investigated materials. GILDA offers also the opportunity of analyzing by ReflEXAFS model systems constituted of catalytic centers supported on monocrystals cut along a lattice plane, so allowing to perform structural studies on thoroughly controlled samples. The papers produced by exploiting the experimental facilities of GILDA are of very high quality and are usually published on the most important journals hosting contributions on catalysis. They are classified in the broad categories of: 1) Zeolites/molecular sieves; 2) Phillips catalysts; 3) Catalysts for pollution control.

Zeolites/molecular sieves

Metal catalysts supported on zeolites or micro- macroporous aluminosilicates present a number of interesting peculiarities, in particular involving the possibility of selective control of the allowed reactions, on the basis of the hindrance of reagents, reaction intermediate and/or products. Catalysis over zeolites/molecular sieves-supported systems is then of overwhelming importance for a number of industrial processes, often concerning organic molecules.

One of the worldwide lieding groups in this field comes from the University of Turin and exploits for his investigations, besides a number of complementary in-house techniques, the experimental resources provided at GILDA. Prestipino et al. [Prestipino et al. 2004] presented a very interesting in situ XANES study on an industrial Ti-silicalite-1 catalyst active in the selective oxidation of a number of organic compounds using an environmental friendly oxidant such as acqueous H_2O_2. The research on Ti-silicalite-1 is also the matter of a review [Bordiga et al. 2007] intended to underline how the most-advanced experimental and theoretical physical chemistry tools can be used synergistically to understand the reactivity of Ti-silicalite-1 (TS-1) in an important number of low-temperature oxidation reactions with aqueous H_2O_2 as the oxidant. Literature results are carefully reviewed and accompanied with new, unpublished highlights of both experimental and computational origin. A summary of the experimental Ti-K-edge EXAFS and XANES literature concerning the activated material in vacuo conditions is presented and compared to the corresponding Ti geometries obtained by ab initio calculations. From such a comparison, the excellent agreement between experiment and theory for water and ammonia is shown. The interaction with hydrogen peroxide is also discussed, underlining the problems faced in reaching a common view between experimental and theoretical results, owing to the difficulties in performing experiments where anhydrous H_2O_2 is dosed on TS-1, and in taking into account the role played by the aqueous medium in the reactivity of Ti(IV) centres toward H_2O_2 using ab initio calculations.

The paper by Berlier et al. [Berlier et al. 2005b] reports about the characterization of an isomorphously substituted Fe-MCM-22 sample with high iron content (Si/Fe = 18) using FTIR, XANES and EXAFS spectroscopies. The catalyst is tested for de-NO_x reaction. Template burning and subsequent activation in vacuo caused the migration of a fraction of framework Fe^{3+} species to extraframework positions, accompanied by the reduction of a fraction of Fe^{3+} to Fe^{2+}. A fraction of extraframework Fe^{2+} sites is able to adsorb NO, forming $Fe^{2+}(NO)_n$ complexes (n=1,2,3), which indicates a high coordinative unsaturation of such sites. The X-ray absorption spectroscopies demonstrate that this fraction is however small, as both EXAFS and XANES spectra are almost unperturbed by NO adsorption, while the corresponding FTIR bands are highly broad and asymmetric, not allowing to detect the presence of $Fe^{3+}(NO)$ complexes. The effect of red-ox treatments with O_2 and H_2 is also investigated. Adsorbed oxygen efficiently shields the Fe centers and does not rapidly nor efficiently react with NO. Upon H_2 treatment, the reduction of extraframework Fe^{3+} (likely present on the surface of small oxidic clusters) to Fe^{2+} takes place.

A Cu-ZSM-5 catalysts is investigated in the paper by Prestipino et al. (Prestipino et al. 2005a). EXAFS spectroscopy, analysed in the frame of the multiple scattering theory, has been able to determine the local structure of $[Cu(CO)_2]^+$ complexes hosted inside ZSM-5 channels upon contacting the activated zeolite with CO from the gas phase at room temperature. It is found that the number of coordinated CO molecules (1.8 ± 0.3) is in good agreement with the $[Cu(CO)_2]^+$ stoichiometry suggested by IR. The Cu-C distance obtained for the $[Cu(CO)_2]^+$ complex is 1.88 ± 0.02 Å , with a C-O distance of 1.12 ± 0.03 Å. An increase of the Cu-C distance of 0.05 Å by moving from $[Cu(CO)_2]^+$ to $[Cu(CO)^3]^+$ complexes has been observed, which is the local rearrangement needed to accommodate a third CO ligand in the first coordination shell of copper. EXAFS determined that the Cu-C-O bond angle is linear within error bars of (170 ± 10)°, while IR and XANES indicate that intrazeolitic $[Cu(CO)_2]^+$ complexes have C_{2v} symmetry. The experimentally obtained moieties are in good agreement with the values obtained with advanced quantum mechanical methods. A catalytic system based on ZSM-5 is also taken into consideration in the review by Zecchina et al. [Zecchina et al. Phys. Chem. Chem. Phys. 2007], dealing with an examination of the literature on Fe-ZSM-5 and summarizing the most widely accepted views on the structure, nuclearity and catalytic activity of the iron species. By comparing the results obtained with the various characterization techniques, it is concluded that Fe-ZSM-5 and Fe-silicalite are not ideal samples and that many types of species are present, some active and some other silent from adsorptive and catalytic point of view.

The high density of framework Ti(IV) centers makes ETS-10 a promising photocatalyst. Its advantage, with respect to the classical high-surface-area TiO_2 oxide, consists of a threedimensional microporous structure that provides to ETS-10 a shape selectivity toward the photodegradation of large organic molecules. Its structure is formed by chains of corner-sharing TiO_6 octahedra linked to each other by tetrahedral SiO_4 units, generating a large-pore and forming a three-dimensional channel structure. Although the material is crystalline, it is characterized by a high level of disorder and actually the crystal is built with different stacking arrangements, resulting in an inherently disordered structure. In the paper by [Prestipino et al. 2005b] the Ti K-edge EXAFS and XANES analysis of the ETS-10 molecular sieve structure is performed on high-resolution data collected at GILDA. A model of ETS-10 where the Ti atoms are bonded with two equivalent axial oxygen atoms is supported. This model is also able to reproduce the edge and the post-edge region of the XANES spectrum. A weak but well-defined pre-edge peak at 4971.3 eV is explained by assuming that a fraction of Ti atoms are in a local geometry similar to that of the pentacoordinated Ti sites in the ETS-4 structure. It is argued that these Ti atoms in ETS-10 should be the terminal of the -Ti-O-Ti-O-Ti- chains, whose actual number is strongly increased by the high crystal defectivity.

The importance of methanol-to-light-olefins industrial process using H-SAPO-34 as a catalyst, has stimulated the investigation of new zeolitic material with the same CHA topology but characterized by a different acidic strength. The paper by Regli et al. [Regli et al. 2007b] reports a detailed IR investigation on the symmetry, accessibility, acidic strength, and reactivity of B sites in a CHA framework. The as prepared material exhibits $[B(OSi)_4]$ units in a T_d-like geometry. The template burning process is monitored by in situ XRD carried out at GILDA, and the break of a B-O-Si bond results in $[B(OSi)_3]$ units in a D_{3h}-like geometry, confirmed by the appearance of the IR fingerprint at 1390 cm-1. Interaction with H_2O allows the T_d-like geometry to be reversibly restored, while weak bases, such as H_2 and CO, are unable to displace B species from the D_{3h}-like geometry but testify the weak Brönsted acidity of internal OH species.

Phillips catalyst for ethylene polymerization

Phillips catalysts are composed of a chromium oxide supported on an amorphous material, typically silica. The Cr/SiO_2 Phillips catalysts are nowadays responsible for the commercial production of more than one-third of all of the PE sold worldwide, allowing to polymerize more than 50 different types of polyethylene, without the intervention of any activators, a fact that simplifies the catalyst preparation and production process. The industrial importance of the Phillips

catalyst for olefin polymerization has attracted a great deal of academic and industrial research over the last 50 years as it is described in a review by the research group of the University of Turin [Groppo et al. 2005a], also reporting their first EXAFS an XANES evidences on this important industrial catalyst. In their following papers, Groppo et al. carried out detailed studies on the structure of model and actual Phillips catalysts, contributing to shed light on the structure and oxidation state of the Cr active centers.

In [Groppo et al. 2005b], reporting about in situ EXAFS and XANES studies on the Phillips ethylene polymerization Cr/SiO_2 catalyst, two polymerization routes are investigated and compared. The former mimics the process adopted in industrial plants, where ethylene is dosed directly on the oxidized catalyst, while in the latter the oxidized catalyst is first reduced by CO at 623 K. On this reduced catalyst C_2H_4 polymerization has been investigated at room temperature and at 373 K. To allow experiments in transmission mode, a Cr loading of 4 wt% has been adopted. At this loading a fraction of clustered Cr_2O_3 particles has been observed and quantified. The high energy resolution and signal-to-noise ratio of the XANES data allowed to determine the fraction of Cr sites involved in the polymerization reaction. Preliminary ReflEXAFS experiments have been performed on a model catalyst prepared by impregnation of Cr on a flat Si(100) substrate covered by a thin layer of amorphous silica. Experiments have been performed ex situ on the grafted catalyst (i.e., after impregnation and thermal activation) and at the end of the polymerization stage demonstrating that, as a counterpart of a similar behavior during polymerization, this model system shows also similar XANES features as the standard Cr/SiO2 catalyst.

In the subsequent paper [Groppo et al. 2006] the Cr(VI) precursors are reduced by C_2H_4 (industrial process) or by CO (model laboratory process), with the formation of Cr(II) species. The reduced species react further with C_2H_4, leading to the direct formation of polymer chains anchored to the Cr sites. This characteristic differentiates the Phillips catalyst from the classical Ziegler–Natta and from metallocene-based catalysts, which require an activator. Due to the amorphous nature of the support the Cr(II) sites, although characterized by the same divalent state, are heterogeneous and characterized by different catalytic activity. Three main questions are addressed in this paper: (i) the initiation mechanism; (ii) the structure of the active sites on the silica surface and (iii) the number of actually active sites. An estimation of the fraction of Cr(II) sites involved in the C_2H_4 polymerization on a $Cr(II)/SiO_2$ Phillips catalyst is obtained by means of in situ alternated CO adsorption and C_2H_4 polymerization FTIR experiments, showing that about 28% of the total surface sites react fast with C_2H_4, while a lower fraction, which depends upon the temperature reaction conditions, is more slowly involved, according to the XANES results. The idea of investigating a model catalyst grafted of a monocrystal surface is thoroughly exploited in the paper by Agostini et al. [Agostini et al. 2007], by carrying out an X-ray absorption experiment with the ReflEXAFS equipment available at GILDA. In situ (XANES/EXAFS) experiments are conducted on a highly diluted $Cr/SiO_2/Si(100)$ system (2 Cr/nm^2), representing a model of the Phillips catalyst for ethylene polymerization. This experiment demonstrated that it is possible to follow the reversible red-ox reactivity of surface species grafted on a single well-defined surface, at a concentration limit that is far below the monolayer coverage level. The main outcome of the experiment is that the red-ox ability of the isolated surface Cr species is not enough to make a polymerization active species and that XANES spectroscopy can be diagnostic in discriminating between active and inactive isolated Cr(II) sites owing to the presence/absence of a characteristic preedge feature around 5996 eV.

Supported catalysts for pollution control

Effective oxidation of hydrocarbons and/or control of CO emissions are one of the major topics of the research on catalytic materials. Quite often, the active centers of supported heterogeneous catalysts are so dispersed on a carrier material, usually an inert oxide, that laboratory XRD experiments are not able to characterize the investigated catalytic systems. Moreover, it is possible that the active site for a given reaction is constituted of a cluster of a few atoms exposed to the

interaction with the reactants and that both structure and oxidation state crucially determine the catalytic properties. For these systems X-ray absorption spectroscopy constitutes a precious tool for structural characterization and assessment of structure-reactivity relationships. In the paper by Pettiti et al. [Pettiti et al. 2004] δ-Al_2O_3 supported La, Mn, Co and Fe containing catalysts are prepared by impregnation of δ-Al_2O_3 with citrate-type precursors and calcination at 1073 K. The catalysts were preliminarly characterized by various spectroscopies and X-ray diffraction (XRD), and then investigated by XAS at GILDA. XAS demonstrates, also for the most diluted samples, the formation of oxide phases. In particular, Mn-containing samples revealed the formation of α-Mn_2O_3, while the 30 wt.% La-Mn bimetallic sample showed the formation of $LaMnO_3$ perovskite. All Co containing samples revealed the presence of $CoAl_2O_4$ spinel. Fe containing samples showed the formation of α-Fe_2O_3, while La-Fe containing ones, that of $LaFeO_3$ perovskite. Catalytic tests of CO oxidation, performed in the temperature range 300-800 K, demonstrate that the sample containing La and Mn in the form of $LaMnO_3$ perovskite is the most active among all the examined catalysts. Most of the Co containing catalysts are found active at RT, but they rapidly deactivate. None of the Fe-based samples is active at RT and these catalysts were found, on average, to be substantially less active than the Mn- and Co-based ones.

The catalytic partial oxidation of methane to synthesis gas over ruthenium catalysts is investigated by thermogravimetry coupled with infrared spectroscopy (TGA-FTIR) and in situ X-ray absorption spectroscopy (XAS) at GILDA by Rabe et al. [Rabe et al. Phys 2007]. It is found that the oxidation state of the catalyst influences the product formation. On oxidized ruthenium sites, carbon dioxide is formed. The reduced catalyst yielded carbon monoxide as a product. The influence of the temperature is investigated, finding that at temperatures below the ignition point of the reaction the catalyst is in an oxidized state. At temperatures above the ignition point, the catalyst is reduced. This is also confirmed by in situ XAS spectroscopy. The results indicate that both a direct reaction mechanism as well as a combustion-reforming mechanism can occur. The importance of knowing the oxidation state of the surface is discussed and a method to determine it under reaction conditions is presented.

H – Miscellanea: Thermal Expansion, phase transition and local lattice distortions

Thermal Expansion

The recent discovery of compounds exhibiting negative thermal expansion (NTE) over very large temperature intervals has renewed the interest for a deeper understanding of the mechanisms of NTE. The macroscopic expansion of crystals results from a competition between a positive contribution due to bond stretching and a negative contribution due to tension effects. The ability of EXAFS of measuring the real expansion of inter-atomic distances and the corresponding parallel and perpendicular mean square relative displacements (MSRDs) represents an effective tool for directly monitoring the local behaviour of NTE materials. This potential of EXAFS has been exploited to study some NTE crystals with different structures: diamond-zincblende, cuprite and delafossite.

Three main features appear evident from a comparative analysis of all the investigated systems

(1) The expansion of the nearest-neighbour distance measured by EXAFS is always positive. Within the same family of isostructural compounds, the stronger is the negative crystallographic expansion, the larger is the positive EXAFS expansion. The positive EXAFS expansion and the perpendicular MSRD can be connected to the bond-stretching and to the tension effects, respectively.

(2) Within the same family of isostructural compounds, a stronger NTE corresponds to a larger perpendicular to parallel anisotropy of the MSRD. The MSRD anisotropy seems to be more relevant for NTE than the anisotropy of absolute atomic vibrations measured by diffraction.

(3) The comparison between EXAFS and diffraction gives information on the correlation of vibrational motion, in both parallel and perpendicular directions. The perpendicular correlation is always weaker than the parallel correlation.

The results up to now obtained represent significant constraints for NTE theoretical models, and facilitate the search for a comprehensive phenomenological picture. Besides, the results obtained for bulk materials allow a calibration of the technique for further works on nanocrystalline materials.

The relevance of an accurate interpretation of thermal effects on EXAFS spectra has been quite early recognized[32]. For a long time, however, the attention has been focused only on the mean square relative displacement along the bond direction (parallel MSRD). The development of the cumulant expansion method has then given the possibility of effectively taking into account the effects of anharmonicity for moderately disordered systems.

More recently, some basic differences between EXAFS and Bragg diffraction have been experimentally detect. While Bragg diffraction measures the distance between average atomic positions, EXAFS measures the average interatomic distances; the two quantities, as well as their temperature dependences, are intrinsically different, due to the effect of atomic vibrations perpendicular to the bond. From the difference between the thermal expansions measured by EXAFS and by Bragg diffraction, one can evaluate the perpendicular MSRD.

The relevance of this kind of EXAFS studies is twofold. On the one hand, it allows a deeper understanding of the relationship between the EXAFS parameters and the local structural and dynamical properties of materials. On the other hand, peculiar information and original insights can be gained on the mechanisms of intriguing phenomena, such as negative thermal expansion.

Thermal Expansion: Local lattice dynamics, the case of copper

EXAFS spectra sample the one-dimensional distributions of instantaneous scattering paths lengths, that, for single scattering events, correspond to inter-atomic distances. In moderately disordered systems, the distributions can be parametrised in terms of their leading cumulants,

[32] G. Beni and P. M. Platzman, Phys. Rev. B14 (1976) 1514.

corresponding to average value, variance and asymmetry. The EXAFS cumulants can be connected to the force constants of effective one-dimensional pair potentials. The relationships between the one-dimensional EXAFS cumulants and the structural and dynamical properties of three-dimensional crystals are being investigated by several researchers, by both experimental and theoretical approaches.

EXAFS measurements have been performed on copper, in the temperature interval from 4 to 500 K. The results for the first shell can be summarized as follow: (a) The distance variations can be appreciated with resolutions better than 0.001 Å, so that the bond thermal expansion can reliably be measured; it is larger than the crystallographic expansion, and the difference has been exploited to evaluate the perpendicular MSRD. (b) The ratio between perpendicular and parallel MSRDs is about 2.5, say larger than the value 2 of a perfectly isotropic system. (c) The thermal expansion evaluated from the 3rd cumulant (asymmetry of the distribution) differs from both the bond thermal expansion and the crystallographic thermal expansion.

The analysis of the outer shells was globally performed by comparison with theoretical simulation, including multiple scattering paths. A unique average expansion coefficient could be reasonably obtained, without possibility of disentangling the differences between different shells and evaluating the perpendicular MSRDs. Accurate values were instead obtained for the parallel MSRDs, whose Debye temperatures are in good in agreement with the diffraction and specific heat values, as well as with recent dynamical calculations of fcc metals.

The experimental results for copper represent a new, accurate reference for checking ab-initio calculations[33]. Path-integral Monte Carlo (PIMC) simulations succeeded in reproducing the results of the experiment on copper, and gave new hints on the connection between effective pair potential and bond thermal expansion [a Becara et al. 2003, a Becara et al. 2008]. According to PIMC calculations, the asymmetry, measured by the third cumulant, is much stronger for the first shell than for the outer shells. The thermal expansion of the Cu-Cu distance, which for the first shell can be accounted for by a joint effect of asymmetry and shift of the effective pair potential, is quite solely due to the effective potential shift for the outer shells. This progressive reduction of the anharmonicity effect in going from the bare pair interaction potential to the effective pair potentials of the first and of the outer shells is supported also by recent calculations based on the use of a Morse potential[34].

Thermal expansion: Negative Thermal Expansion materials

It is known since long time that several crystals with the diamond-zincblende structure are affected by negative thermal expansion (NTE) in limited low-temperature intervals. More recently, strong NTE extending over very large temperature intervals has been observed in crystals with framework structures, such as ZrW_2O_8 or Ag_2O. These findings, besides their technological interest, have renewed the attention towards a deeper understanding of the NTE mechanisms. The net macroscopic thermal expansion of crystals is the sum of a positive contribution due to bond stretching and a negative contribution due to tension effects; when the negative contribution prevails, NTE is observed.

The possibility of measuring by EXAFS the real expansion of selected inter-atomic distances and the corresponding parallel and perpendicular MSRD represents an effective tool for directly monitoring the local behaviour of NTE materials, complementary to Bragg diffraction and alternative to the less simple analysis of diffuse scattering in total scattering experiments. A research program is under way to to investigate the local mechanisms of NTE in crystals with different structures.

(a) Crystals with the diamond-zicblende structure are affected by isotropic NTE in limited low-temperature intervals. NTE is weak in Ge, and the strongest in CuCl. The results of EXAFS

[33] F. D. Vila, J. J. Rehr, H. H. Rossner, H. J. Krappe, Phys. Rev. B76 (2007) 014301
[34] Van Hung N., Fornasini P., J. Phys. Soc. Jpn. 76 (2007) 084601.

measurements performed on Ge and on CuCl [Vaccari et al. 2007] reveal some basic features that characterize all NTE materials up to now studied by EXAFS or diffuse scattering. The nearest-neighbour bond thermal expansion measured by EXAFS is positive at all temperatures; besides, the positive expansion is much stronger in CuCl, where stronger is the crystallographic negative expansion. The ellipsoids of relative displacements are anisotropic; the stronger the negative expansion, the stronger is the anisotropy (the atomic thermal factors, measured by Bragg diffraction, are instead isotropic in cubic crystals, for symmetry reasons). The anisotropy of relative atomic vibrations can reasonably be connected to the tension effect responsible for the negative contribution to thermal expansion. The relatively open structure of tetrahedral crystals facilitates the movements perpendicular to given bonds. However, the non-linear character of the A–B–A links and the coordination of each atom to four neighbours make the interpretation of results more complicated than for simpler linear links A–B–A.

(b) Linear A–B–A links are present in some crystals $CuMO_2$ (M=Al, Sc, In, La) with the layered structure of delafossite, which are affected by NTE along the *c* axis in non-negligible temperature intervals. Each Cu ion is coordinated to two O atoms belonging to the two adjacent O–M–O layers, the linear O–Cu–O link being always parallel to the *c* axis. According to Bragg diffraction, the NTE along the *c* axis is due to the contraction of the distance between the Cu and O average positions. EXAFS at the Cu K edge in $CuScO_2$ and $CuLaO_2$ [Ahmed et al. 2009] has revealed that the expansion of the Cu–O bond is positive within the entire temperature interval. The thermal ellipsoids of Cu atoms evaluated from diffraction patterns exhibit a stronger anisotropy in $CuLaO_2$, where the NTE is weaker, while the anisotropy of the MSRD from EXAFS is stronger in $CuScO_2$, where the NTE is stronger. This result suggests that NTE is better correlated to the anisotropy of the MSRDs than to the anisotropy of the diffraction ellipsoids.

(c) Most systems that exhibit NTE in large temperature intervals are framework structures, where polyhedral structural units centered on A atoms are connected at the corners by linear A–B–A links. The framework structures of ZrW_2O_8, $Zn(CN)_2$ and Ag_2O undergo isotropic NTE within the full explored temperature interval. Cuprite Cu_2O, in spite of having the same structure of Ag_2O, exhibits instead a behaviour similar to the zincblende CuCl, NTE prevailing only in a limited low-temperature interval. In the cuprite structure, shared by Cu_2O and Ag_2O, each metal atom is linearly coordinated to two O atoms, while each O atom is tetrahedrally coordinated to four metal atoms. Accurate EXAFS and Bragg diffraction measurements have been done on Cu_2O and Ag_2O [Sanson et al. 2005, Artioli et al. 2006, Sanson et al. 2006]. A positive expansion of the nearest-neighbor M–O bond has been measured by EXAFS in both compounds; the positive expansion is stronger in Ag_2O, where stronger is the crystallographic NTE. The motion of M atoms, measured by diffraction, and the relative motion of the M–O pair, measured by EXAFS, are both anisotropic; the amplitude of motion perpendicular to the M–O bond is larger than the amplitude of motion parallel to the bond. The anisotropy is stronger in Ag_2O than in Cu_2O.

The results of EXAFS studies NTE have been recently summarized in ref. [Fornasini et al. 2008].

Local lattice distortions

Selectivity of atomic species and sensitivity to the short-range order make XAFS particularly suited to study the local distortions in crystalline lattices of high-temperature superconductors (HTS) and of random ternary alloys.

Local lattice distortions: High-temperature superconductors

Superlattices based on thin layers of the (Ca, Sr, Ba) CuO_2 compounds have been produced, in order to understand the mechanism by which the charge transfer among different layers can give rise to superconductivity[35]. Polarized XANES and EXAFS measurements have been performed at the Cu and Ba K edges on the infinite layer compounds $CaCuO_2$ and $SrCuO_2$, as well as on the superconducting $(BaCuO_2)_2/(CaCuO_2)_n$ and non-superconducting $(BaCuO_2)_2/(SrCuO_2)_n$ superlattices[36]. The results have shown that in the superconducting superlattice the charge reservoir block ($BaCuO_2$ infinite layer) contains 0.6 oxygen vacancies per unit cell, randomly distributed in the CuO_2 plane sandwiched between the BaO planes, and that the two apical oxygens are not in the Ba plane, but are shifted towards Cu by 0.21 Å.

Local order and lattice distortions around the dopant Ce atoms have been studied in the superconducting compound $Nd_{2-x}Ce_xCuO_{4\pm\delta}$ by analyzing EXAFS at the Ce and Nd K edges in samples with different dopant concentrations [Ghigna et al. 2004]. The results have shown that the oxygen cuboid around each Ce dopant atom is mainly shrunk along the z crystallographic direction, and the CuO_4 planes bocomecorrugated. The lattice distortion is localized around Ce atoms and is largely independent of temperature and of Ce and O content. The Nd environment is undistorted. Difference electron density maps from X-ray diffraction data have further revealed the presence of interstitial oxygen atoms in two non-equivalent sites, next to Nd or Ce atoms. Interstitial sites near Ce atoms are 3 to 4 times more populated than the Nd ones, demonstrating that interstitial oxygens tend to form cluster defect with Ce substitutional defects.

Local lattice distortions: Random ternary alloys $U_xLa_{1-x}S$

US, as other uranium chalcogenides, orders ferromagnetically below T_c=180 K. The magnetic exchange is indirect, and either mediated by the S p electrons or by the conduction electrons. Understanding the electronic and magnetic properties is facilitated by the replacement of U with the La, which does not carry a magnetic moment. EXAFS has been measured at the La *K* and U L_3 edges in the $U_xLa_{1-x}S$ system, at 11 values of *x*, from 0 to 1 [Bombardi et al. 2003]. The measurements reveal a complex local variation of the first- and second-neighbor distances. The La-S distances are systematically larger than the U-S distances and almost concentration independent for $x<0.5$. Around this concentration the La-S distance starts to decrease linearly with *x*. The study of the second-neighbor distances confirms a non-Vegard behavior of the lattice parameter evolution with La substitution. Near $x\sim0.5$, the static disorder in the solid solution strongly increases. The important differences in distances found by EXAFS show that at the atomic level the anion sublattice does not follow the virtual crystal approximation; this fact could affect band calculations, so that these studies stimulate the development of more realistic theroetical models.

Phase transitions

The availability of the image plate detector allows to monitor the kinetics of phase transitions by x-ray powder diffraction.

Phase transitions: XRPD kinetic study of the $PbGeO_3$ solid-solid phase transition

$x\mathrm{PbO}(1-x)\mathrm{GeO}_2$ glasses are interesting for their promising optical applications when doped with rare earths. The study of phase equilibria is, however, complicated by devitrification processes. For

[35] Balestrino G., Tebano A., Supercond. Sci. Technol. 16 (2003) R29.
[36] Colonna S., Arciprete F., Balzarotti A., Balestrino G., Medaglia P.G., Petrocelli G., Physica C **334** 64, 2000.

instance, devitrification of the $x = 0.50$ glass produces monoclinic lead metagermanate $PbGeO_3$ via the formation of a metastable phase, unknown in the literature. A kinetic study of the solid–solid transition between the metastable and the monoclinic $PbGeO_3$ phases has been performed by means of differential scanning calorimetry (DSC) and time-resolved X-ray powder diffraction (XRPD) with image plate detector [Tomasi et al. 2005]. XRPD patterns measured at the rate of 1°/min show the transition occurring between 558 and 585°C. The quantitative analysis has allowed the evaluation of the transformed fraction as a function of temperature. The global DSC and XRPD results point out that the assumptions of the Arrhenian behaviour are fulfilled for both the growth and nucleation rates.

I - Instrumentation and data treatment methods

A part of the scientific activity of the GILDA beamline has been devoted to the development of new techniques for data collection and methods for data analysis. As a general rule, these studies have been carried out in tight collaboration with scientific groups deeply involved in the related activity. This can be divided in 3 main sectors: studies on new detectors and signal processing, development of new sample environment / data collection methods, development of new data analysis methods.

The beamline GILDA revealed to be well suited for the development of new instrumentation or data analysis methods thanks to a marked flexibility of all its major components. This property was common both to the X-ray optics that demonstrated the capability of working in different conditions (wide energy range, possibility of changing the beam intensity, size, ..) as well as to the hardware/software environment that permitted an easy implementation of non standard instrumentation or data collection modes.

New detectors and signal processing

The advent of 3rd generation synchrotron radiation sources with increased beam intensity have represented a tough challenge for detector technology. Namely, there is still a lack in the availability of detectors that result to be at the same time fast and capable of resolving energies with a resolution $\Delta E/E$ better than 10^{-2}. This justifies the activity in testing new ways for detector technology. In collaboration with the Department of Physics of the Genova University we have carried out feasibility tests for the use of superconducting Transition Edge Sensor (TES) micro-calorimeters in Synchrotron Radiation. These devices are widely used in astronomy and have the advantage that they can achieve an energy resolution extremely pushed (theoretically about 1 eV at 10 keV) avoiding the geometrical constraints that are typical of crystal analyzers. In principle they could find several applications in synchrotron radiation science [D'Acapito et al. 2004e].

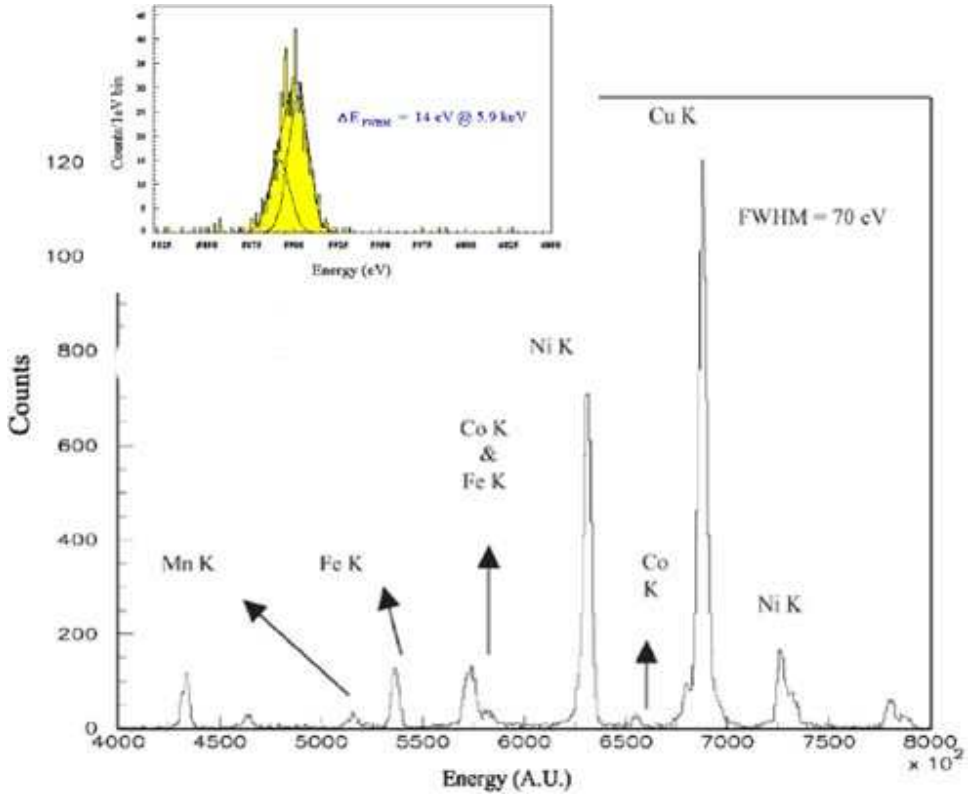

Figure 15. Fluorescence spectrum of a complex sample (here a renaissance ceramic specimen, courtesy of prof. B. Brunetti, Univ. Perugia) collected with the TES detector. The relevant energy resolution (here about 70 eV FWHM)

permits to separate the lines of neighboring chemical species in the periodic table. In the inset we show the spectrum from a Fe55 source collected with the same detector in a shielded environment and showing that the energy resolution was in that case of about 14 eV FWHM.

The detector was successfully tested on the beamline where a resolution of 70 eV at 9 keV was observed [Maurizio et al. 2004b] predominantly due to the ambient electrical noise; the same detector in laboratory yielded 14 eV at 5.9 keV. The severe limitations of sensitivity to ambient noise and low count rate achievable (estimated to be max 1kcps/element) together with the complexity of the associated cryogenic circuit has prevented us from using this kind of devices on the beamline.

A further explorative study on new detectors has been carried out on diamond based devices [De Sio et al. 2008]. This kind of detector has the advantage of being transparent and to be capable to stand high radiation load as required by the future 4th generation sources. Our test revealed that this kind of detectors is sufficiently linear to permit the collection of EXAFS data in a way comparable to Ion Chambers.

For what concerns the more conventional Germanium detectors we carried out studies devoted to the improvement of the quality of the collected data with particular attention to 2 aspects:

- data correction in the case of moderate pileup [Ciatto et al. 2004b, Ciatto et al. 2004c].
- extraction of the fluorescence contribution from the total emission spectrum [Dacapito et al. 2007e]

Indeed the signal from a Ge detector, being the collection electronics totally in digital form, can be easily processed from a numerical point of view. In particular, with this method it is possible to correct the nonlinear response of the device in the case of XAS data collected in fluorescence mode. The nonlinearity leads to severe errors in the determination of amplitude parameters in EXAFS data, in particular number of neighbors and Debye-Waller factors. In the papers devoted to this issue [Ciatto et al. 2004b, Ciatto et al. 2004c] 3 correction methods were proposed (numerical inversion of the detector readout based on a supposed response function, correction by comparing fast and slow readout channels, local linearization of the response function) and their effects were checked on real spectra collected on the beamline (Figure 16)

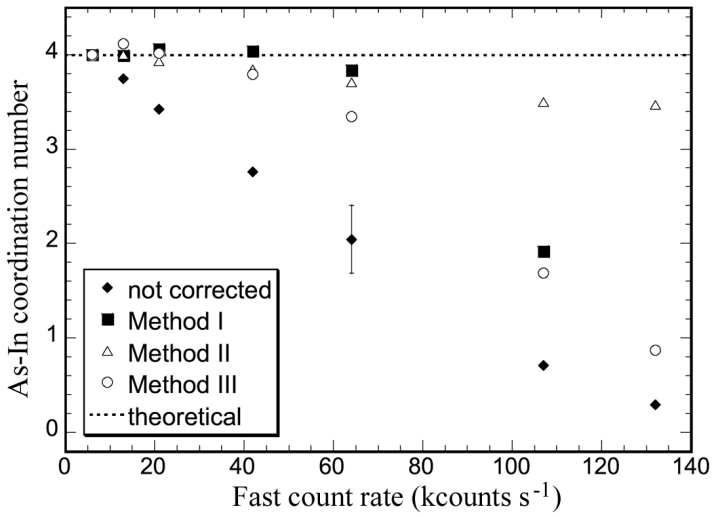

Figure 16. Number of nearest neighbors in InAs derived from EXAFS spectra collected at the As-K edge in fluorescence mode with the Ge detector operative on the beamline. 3 data correction methods are compared with the aim to test their capability of reproducing the correct value (4 in the zincblende structure) at the highest count rate.

Another advantage from the digital form of the data processing comes from the fact that complete fluorescence spectra are available for processing. In particular it is possible, during

EXAFS spectra, to store these data at each energy point and then using them for a finer analysis. Indeed when collecting data in fluorescence mode the conventional method consists in integrating all counts in a Region Of Interest (ROI) that includes the emission from a dominating line (K_α or L_α) [Dacapito et al. 2007e]. When the element under analysis is particularly diluted the same ROI is likely to contain other contributions like the low energy tail of the elastic emission or the Compton line. This results in a variable background that could affect the subsequent data processing. By carrying out a fit of the emission spectrum the contribution of the sole fluorescence line can be isolated providing cleaner data for the analysis.

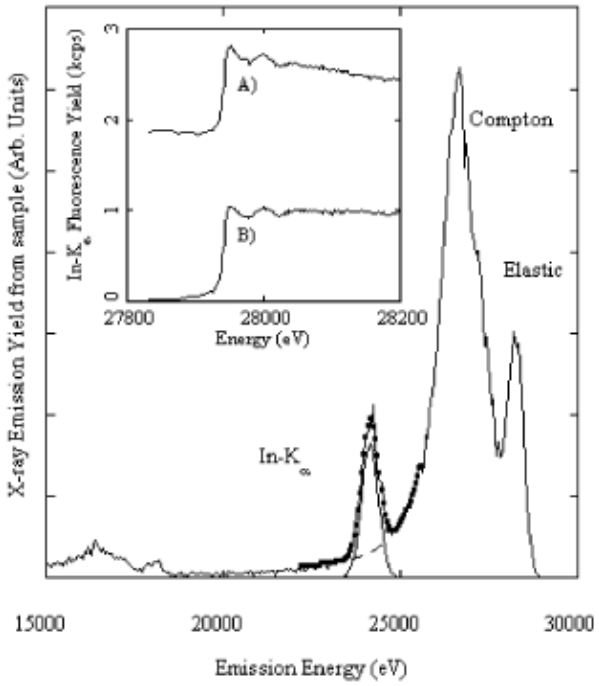

Figure 17. X-ray emission with an excitation at 28250 eV from a thin layer of Indium doped Si with a doping level of 10^{13} at/cm^2.The In-K_α line lays on the tail of the Compton line and a conventional data extraction method should lead to the spectrum labeled by A) in the inset. Note that no vertical shifting has been applied to this spectrum, the signal below the edge being due to the scattering. By carrying out a fit of the emission data in the ROI indicated by the dots with suitable lineshapes (here a Gaussian for the K_α line and an exponential for the background), the more regular spectrum B) in the inset is obtained.

Both methods can be applied to data collected to the beamline and specific processing codes are made available to the users.

Sample environment / data collection methods

In order to provide to the users an instrument for the in-situ analysis of reacting materials a cell for studying in situ gas-solid chemical reactions has been developed [Longo et al. 2005]. The sample is in pellet form, hold by a gold-plated copper frame and contained in a steel chamber thus resulting in a particularly clean environment. The cell permits measurements in both transmission and fluorescence mode and the sample can be heated up to 770 K or cooled down to 170K. The treating gas after reaction is send to an external mass spectrometer that realizes the analysis of the reacted species.

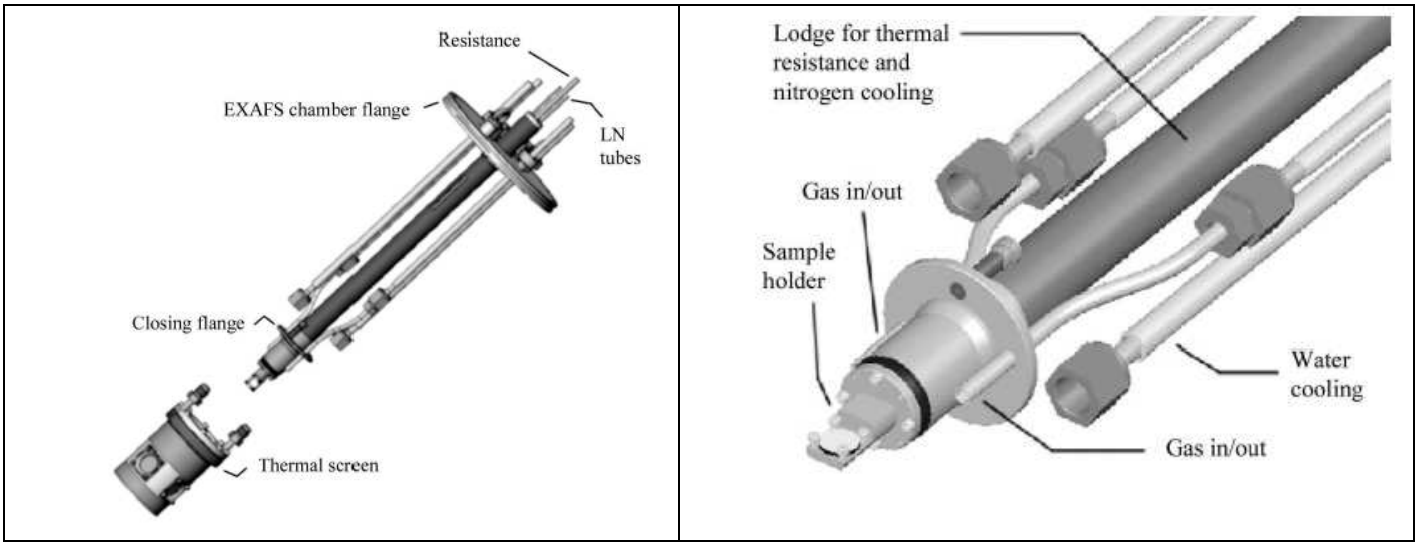

Figure 18. Drawings of the cell for in-situ gas-solid reactions. From [Longo-JSR-05].

The cell has been used in studies on Three-way catalysts and is currently available for users.

Among the data collection methods we have investigated the possibility of setting up procedures capable to provide depth-sensitive EXAFS data. In particular, we concentrated on methods based on the total external reflection of x-rays on smooth surfaces [D'Acapito et al. 2007c, D'Acapito et al. 2008] or on the standing waves in multilayers [Rovezzi et al. 2006, Patelli et al. 2004]. In the first case, the method consists in comparing EXAFS data collected below and above the critical angle for total external reflection: this changes the penetration depth of the probe beam from a few nm to several μm to permitting the to obtain information on the surface or on the deep bulk of the sample. The procedure was applied to the study of Arsenic dopants in Si: in this case it has been possible to distinguish surface sites characterized by a strong disorder and possible As-As correlations from the bulk sites where As is inserted in an ordered Si matrix.

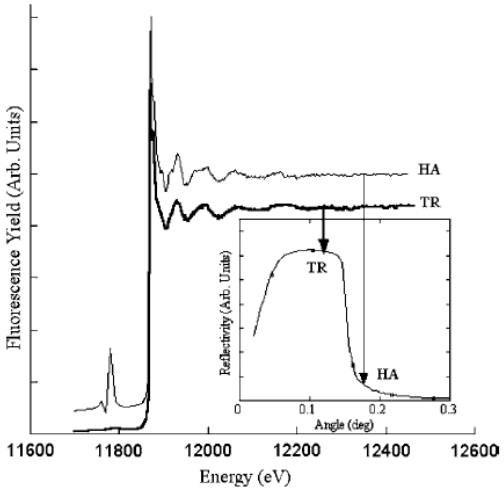

Figure 19.. Comparison of the As-K edge spectra relative to an Arsenic doped Si sample. The TR spectrum was collected in Total Reflection condition as indicated by the reflectivity spectrum shown in the inset whereas the HA spectrum was collected at High incidence Angle on the lower part of the reflectivity. The two spectra exhibit clear differences (in particular absence of the higher frequency modulations in the TR spectrum) that are linked to different incorporation sites for As in surface or in the bulk of trhe matrix.

A more complex procedure was set up in the analysis of multilayers. Here it is known that it is possible to achieve spatial sensitivity by exploiting the standing wave that sets up in the material near a Bragg peak. Thus an automatic data collection code was prepared that scanned the sample incidence angle in order to cross the Bragg peak at each energy point of the exafs spectrum. For each angular point the intensity of the fluorescence yield from the sample was collected and a further code realized the analysis of these data with the extraction of the fluorescence intensity at the minimum and maximum positions. The former dataset contains information on the interfaces whereas the latter contains information from the central zone of the fluorescing layer. From these spectra EXAFS spectra were extracted and analyzed in the standard way. The method was applied in the investigation of Mo-Si multilayers for applications in soft X-ray mirrors and differences were found between the two sets of data.

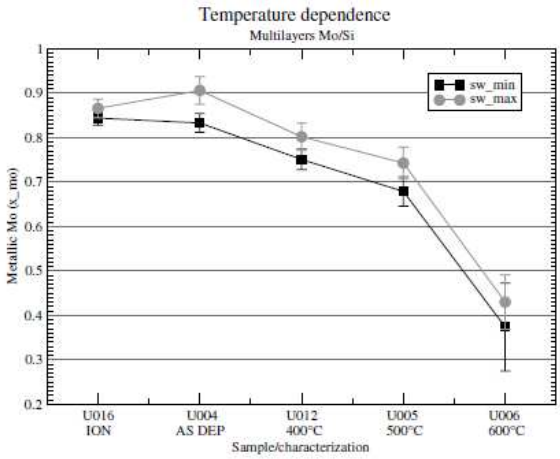

Figure 20. Fractional content of metallic Mo (x_{Mo}) in the exafs spectra collected at the Mo-K edge in MoSi multilayers. The spectra were collected by using the standing wave originated at a Bragg Peak as a probe and datasets at the maximum and minimum for the Mo-Ka fluorescence yield are stored and analyzed. The result shows that the metallic Mo fraction in data collected ad the minimum is systematically smaller in samples treated at different annealing temperature values.

The method revealed to be effective in distinguishing the *interface* from the *bulk* part of the structure as shown in the picture above.

New data analysis methods

Together with technical upgrades we have also collaborated in the development of new data analysis procedures in order to provide to the users better performing data analysis codes. One of the major result in this field has been the development of a quantitative analysis code for EXAFS data collected in total reflection mode [Benzi et al. 2008]. Indeed, whereas the analysis of ReflEXAFS spectra collected on diluted samples can be carried out with the standard codes (Feff, GNXAS, ..) the same is not true for concentrated samples. This is because in this case the absorber is sufficiently concentrated to significantly contribute to the total refractive index of the material so determining the extinction length, the critical angle and the reflectivity itself . Moreover this dependence is variable in energy and takes contributions from both the real and imaginary parts of the refractive index. This means that it is not possible to easily extract the absorption coefficient of a material from the reflectivity data operation that is necessary for the analysis of the EXAFS spectra with conventional methods. For this reason we have developed a method based on a different concept i.e. it transforms the theoretical EXAFS paths accordingly to the reflectivity behavior of the material. In this way the new theoretical paths are directly usable on the ReflEXAFS data.

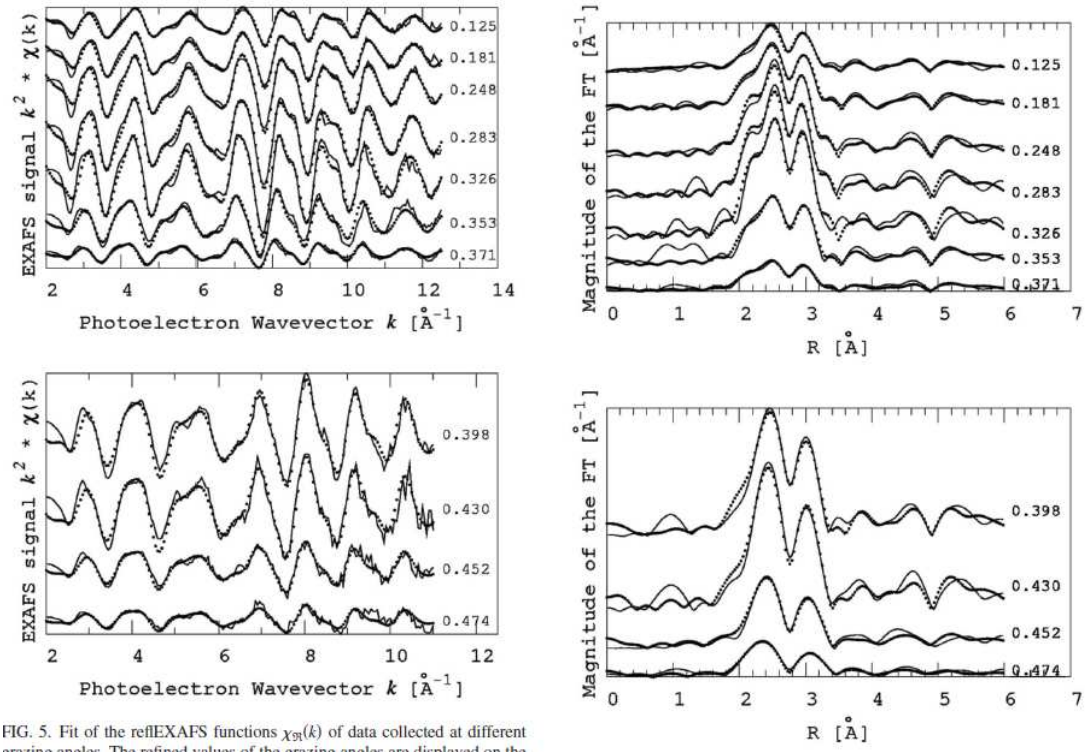

FIG. 5. Fit of the reflEXAFS functions $\chi_{\mathrm{Bl}}(k)$ of data collected at different

Figure 21. Examples of experimental ReflEXAFS data (dots) and best fits (lines) relative to a thin Au film on silicon. Data collected at different incidence angles are shown (here the critical value is at about 0.36 deg) and the fits are carried out for the first 4 coordination shells around the absorber.

The method has been tested on a model case (Gold thin film on silicon) and resulted to be capable to provide correct quantitative structural parameters at angles above and below the critical value and to permit data analysis with single and multiple scattering paths in the first few coordination shells around the absorber. At present the program is being developed in collaboration with the SciSoft group of ESRF and is available on request for all users.

A final example has been the work done in collaboration with the Rostov State University (RU) on the development of a new method for the quantitative analysis of XANES spectra [Smolentsev et al. 2006].

VI. Selection of 5 publications

Manganese-induced growth of GaAs nanowires
Martelli F., Rubini S., Piccin M., Bais G., Jabeen F., De Franceschi S., Grillo V., Carlino E., d'Acapito F., Boscherini F., Cabrini S., Lazzarino M., Businaro L., Romanato F., Franciosi A.
Nano Letters **6**, 2130-2134, 2006.
Abstract:
GaAs nanowires have been grown on SiO2 and GaAs by molecular beam epitaxy using manganese as growth catalyst. Transmission electron microscopy shows that the wires have a wurtzite-type lattice and that r-Mn particles are found at the free end of the wires. X-ray absorption fine structure measurements reveal the presence of a significant fraction of Mn-As bonds, suggesting Mn diffusion and incorporation during wire growth. Transport measurements indicate that the wires are p-type, as expected from doping of GaAs with Mn.

Iron Oxidation, Interfacial Expansion, and Buckling at the Fe/NiO(001) Interface
P. Luches, V. Bellini, S. Colonna, L. Di Giustino, F. Manghi, S. Valeri, and F. Boscherini
Physical Review Letters **96**, 106106, 2006.
Abstract:
In order to provide a structural basis for a physical understanding of exchange bias in metal/magneticoxide interfaces, we have determined the structure of the Fe=NiO(001) interface by means of x-ray absorption spectroscopy and *ab initio* density functional theory calculations. A Fe-Ni alloyed phase on top of an interfacial FeO planar layer is formed. The FeO layer exhibits a 7% expanded interlayer distance and a 0.3Å buckling; its presence is predicted to increase the spin magnetic moment of the interface Fe atoms by $0.6\mu_B$, compared to the ideally abrupt interface.

Metallic versus covalent bonding: Ga nanoparticles as a case study
Ghigna P., Spinolo G., Parravicini G.B., Stella A., Migliori A., Kofman R.,
Journal of the American Chemical Society **129**, 8026-8033, 2007.
Abstract:
A systematic X-ray absorption spectroscopy investigation of the local coordination in gallium nanostructures has been performed as a function of temperature and particle size. It is shown that the nanostructure strongly affects the polymorphism of solid gallium and the (meta)stability range of the liquid phase (in agreement with previous works) and that the surface tension acts in the same direction as hydrostatic pressure in stabilizing the Ga solid phases. The effect of surface free energy is first to favour the metallic arrangement of the δ phase and then to stabilize a liquid-like phase based on dimeric molecules even at 90 K. The Ga-Ga distance in the dimers is lower in the liquid phase than in the α solid. The experimental results are discussed in comparison with molecular dynamic calculations to assess the presence of covalent character of the dimeric Ga_2 units in liquid nanostructured gallium.

Indium doping in barium cerate: The relation between local symmetry and the formation and mobility of protonic defect.

Giannici F., Longo A., Balerna A., Kreuer K.D., Martorana A.

Chemistry of Materials, 19, 5714-5720, 2007b

Abstract:

The solid solution series $Ba(In,Ce)O_{3-\delta}$ has been investigated with respect to structure, formation, and mobility of protonic defects. Compared to the limited solubility of Y_2O_3 in $BaCeO_3$ and $BaZrO_3$, the complete solubility of In_2O_3 is suggested to reflect a relation between absolute hardness of the dopant and the ease of insertion into the hosting lattices. Extended X-ray absorption fine structure (EXAFS) was used to probe the local environment of In^{3+} in barium cerate: in the surroundings of the dopant, the orthorhombic structure is strongly modified, resulting in an increase of local symmetry. The InO_6 octahedra are very regular, and there is no indication for any defect clustering. This is suggested to be the main reason for the low entropy of formation of protonic defects by water dissolution. The mobility of such defects is slightly lower than in Y-doped $BaCeO_3$, but at high dopant levels the high local symmetry allows for formation of very high concentrations of protonic defects. This leads to high proton conductivities, which render In^{3+} an attractive dopant for $BaCeO_3$-based proton conductors.

In situ Cr K-edge XAS study on the Phillips catalyst: Activation and ethylene polymerization

Groppo E., Prestipino C., Cesano F., Bonino F., Bordiga S., Lamberti C.,Thüne P, Niemantsverdriet J.W., Zecchina A.

Journal of Catalysis **230**, 98-108, 2005.

Abstract:

In this in situ EXAFS and XANES study on the Phillips ethylene-polymerization Cr/SiO_2 catalyst, two polymerization routes are investigated and compared. The first mimics that adopted in industrial plants, where ethylene is dosed directly on the oxidized catalyst, while in the second the oxidized catalyst is first reduced by CO at 623 K. On this reduced catalyst C2H4 polymerization has been investigated at room temperature and at 373 K. To allow experiments in transmission mode, a Cr loading of 4 wt% has been adopted. At this loading a fraction of clustered Cr2O3 particles has been observed and quantified. The use of a third-generation synchrotron radiation source has allowed us to improve the energy resolution and signal-to-noise ratio of the XANES data, allowing us to determine the fraction of Cr sites involved in the polymerization reaction. This number represents an upper limit of the active sites. Preliminary ReflEXAFS experiments have been performed on a model catalyst prepared by impregnation of Cr on a flat Si(100) substrate covered by a thin layer of amorphous silica. Experiments have been performed ex situ on the grafted catalyst (i.e., after impregnation and thermal activation) and at the end of the polymerization stage.

VII. Highlights of the scientific activity of GILDA: 2004 – 2008

In this section some highlights of the scientific activity of GILDA are reported; the papers are classified according to the following main research fields:

A. Information and Communication technologies,
B. Nanoscience and Nanotechnology
C. Materials for energy production and transport;
D. Environment
E. Life Science;
F. Soft Condensed Matter;
G. Catalysis;
H. Miscellanea with the topics of thermal expansion, phase transition and local lattice distortions;
I. Instrumentation and data treatment methods.

In the following the single contributions are marked as IHR, STAFF&USER or USER to differentiate between the research of the staff, research of the staff in collaborationwith external users and research of the external user only.

A - Information and Communication Technologies

Er site in Er-implanted Si nanoclusters embedded in SiO_2 (STAFF&USER)
C. Maurizio, F. Iacona, F. D'Acapito, G. Franzò, F. Priolo
Phys. Rev. B. ***74****, (2006) 205428 1-7.*

Er-doped Si nanoclusters represent one of the most promising materials to be used as efficient light emitters in a Si-based optoelectronics. When Er is introduced in an insulating matrix containing Si nanoclusters, a strong interaction occurs, with the excitation energy preferentially transferred from the Si nanoclusters to the rare earth ions, which subsequently de-excite radiatively by emitting 1.54 μm photons. Among the structural factors that can drive the Er optical properties into this composite system, the local structure around Er atoms is expected to play a major role. In this work, the authors focussed on the determination by EXAFS measurements of the local order around Er atoms introduced by ion implantation in substoichiometric silica films prepared by plasma enhanced chemical vapor deposition, where Si nanoclusters have been formed by different high temperature annealing processes. They prepared two set of samples. The first one (samples T1, T2, T3) was annealed at increasing temperature (from room temperature, sample T1, to 1250 °C, sample T3) prior to the Er implantation, to induce the formation of Si nanoclusters; in this case the Er concentration was about 4.5×10^{19} Er/cm^3, i.e. below the known threshold for the PL quenching. In the second set of samples (C1, C2, C3), an extensive phase separation between Si clusters and SiO2 was present in the matrix, and the Er concentration was varied in the range 4.5×10^{19}-1.0×10^{21} Er/cm^3, i.e. below and above the concentration threshold for the PL quenching. All of the samples underwent a suitable annealing after ion implantation to eliminate the residual defects left over by the implantation process and to optically activate Er. The EXAFS experiment was performed at the Er L_{III} edge at the GILDA beamline: the monochromator was equipped with a couple of 311 Si crystals and the harmonic rejection was achieved by a couple of Pd-coated mirrors, working at an incidence angle of 3 mrad. Due to low Er concentration, the x-ray absorption spectra were measured in fluorescence mode with a 13-element high-purity Ge detector; the EXAFS spectrum of Er_2O_3 crystalline powder was also measured (in transmission mode) as a standard reference; the samples

were cooled down at 77 K to reduce thermal vibrations. The analysis of the EXAFS spectra was performed by the FEFF8-FEFFIT 2.98 package. The main results are here summarized:

- The Er atoms are mainly surrounded by O atoms at a distance lower than what found in Er_2O_3; no Er-Si coordination is detected. The Er-O distance and the coordination number of the O shell are strictly related: longer is the first, higher is the second, in agreement with the general trend predicted by the bond-valence theory (see Figure 1).
- The pre-implantation annealing temperature has mainly no effect on the Er site (see data of samples T1, T2 and T3, Figure 1).
- The Er implantation dose affects the Er site: the increase of the implantation dose (from sample C1 to C3) determines an Er site closer to the site in the crystalline Er_2O_3 (6 O atoms at a distance of about 2.27 Å), see Figure 1. The radiation damage is most likely responsible for this behaviour that is still present after a post-implantation annealing.
- In the presence of an extensive phase separation between Si and SiO_2 (sample C1, C2, C3), the efficiency of the photoluminescence process is significantly increased when the first shell of atoms around Er is closer to that one of Er_2O_3 (Figure 1).

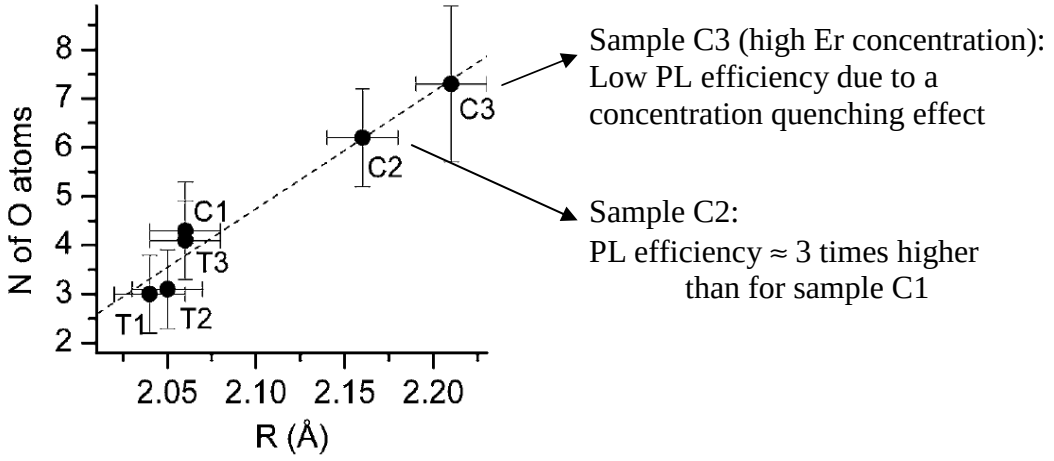

Figure 1
Coordination number of the first shell of O atoms around Er versus the corresponding Er-O distance, as obtained from the EXAFS analysis (as a comparison, in the crystalline Er_2O_3 the first O shell is formed of 6 O atoms at a distance of about 2.27 Å). The dashed line is a guide for the eye.

Experimental determination of the local geometry around In and In–C complexes in Si (STAFF&USER)

F. d'Acapito, Y. Shimizu, S. Scalese, M. Italia, P. Alippi, and S. Grasso
*Applied Physics Letters **88**, 212102 (2006)*

In the recent years the research on doping methods suitable for the realization of shallow junctions has received a great impulse. Among *p*-type dopants In is particularly interesting as it possesses a low diffusion coefficient that makes it ideal for the realization of steep doping profiles[37]. The main drawbacks linked to In are the low solubility in Si (around $1.8*10^{18}$ at./cm^3)[38] and the high ionization energy (0.150 eV)[1] that, however, should not represent a major problem if

[37] R. Baron, M. H. Young, J. K. Neeland, and O. J. Marsh, Appl. Phys. Lett. **30**, 594 (1977).

[38] S. Solmi, A. Parisini, M. Bersani, D. Giubertoni, V. Soncini, G. Carnevale, A. Benvenuti, and A. Marmiroli, J. Appl. Phys. **92**, 1361 (2002).

using In to dope a metal-oxide semiconductor (MOS) channel.3 However, an acceptor state with an appreciably lower energy (0.111 eV) has been detected and identified as an In–C complex[39]. In the presence of these complexes the electrical activation of In is greatly enhanced. In this contribution we have used the x-ray absorption spectroscopy (XAS) technique to determine in a quantitative way the site of In dopants in pure or C-doped silicon and to compare the results with *ab initio* calculations based on the Density Functional Theory (DFT).
Measurements at the In–K edge (*E*=27940 eV) were carried out at the Italian CRG beam line GILDA at the European Synchrotron Radiation Facility. It is worth to underline that working at such high energy on a highly diluted sample ($5*10^{13}$ In/cm^2 in the most dilutes specimens) buried in a matrix represent a particularly challenging aspect of the experiment. Due to the extreme dilution of the absorber in the sample data were collected in grazing incidence geometry in the dedicated experimental chamber operative on the beam line. Measurements were carried out at room temperature. The incidence angle was chosen at ϕ =0.075° slightly above the critical value for total external reflection on Si at 28 keV (ϕ_c=0.064°); in this condition the extinction length of the probe beam to 2 μm instead of 2.7 mm in the case of normal incidence. The signal was collected in fluorescence mode and the contribution of the In-K□ line to the spectrum was extracted from the background via a fitting procedure.

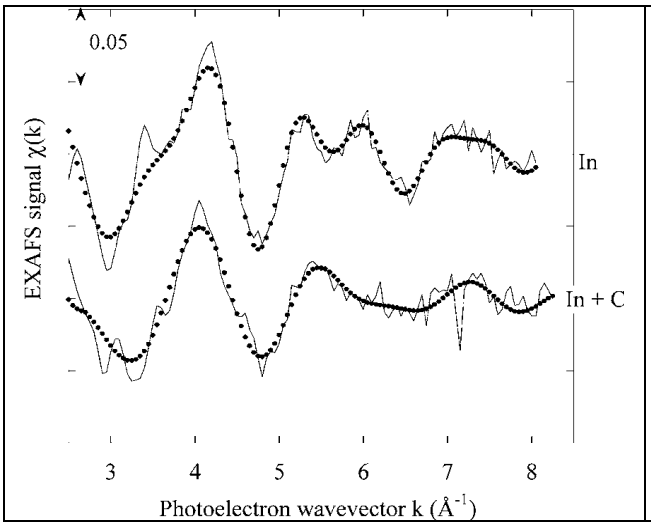

Parameter	In (XAS)	C–In (XAS)	In (DFT)	C–In (DFT)
R^{In-Si}±0.02 Å	2.53×4	2.58×3	2.53×4	2.59×3
R^{In-C}±0.02 Å		2.31×1		2.31×3
σ_1^2±0.003 Å^2	0.005	0.006		
R_2^{In-Si}±0.05 Å	3.88×12	3.34×3	3.89×12	3.38×3
		3.85×6		3.89×6
		4.10×3		4.14×3
R_3^{In-Si}±0.05 Å	4.37×12	4.22×6	4.52×12	4.26×6
		4.54×3		4.59×3
		4.77×3		4.81×3
σ_2^2±0.003 Å^2	0.004	0.008		

Figure1
Left Experimental EXAFS data (lines) compared with the best fitting curces (dots) in the case of pure In and In+C doped Si. In concentration in both cases was $5*10^{13}$ at/cm^2. **Right**: comparison between the local structure parameters derived from the XAS analysis and from the DFT calculation.

The data analysis confirms the findings of the DFT calculation, i.e., that In in Si occupy substitutional sites with four equivalent I shell In–Si distances $R_{In–Si}$=2.53 Å, slightly smaller than the sum of tetrahedral covalent radii $R_{In–Si}$ =2.578 Å. In pure Indium implanted samples, the matrix around the dopant is quite ordered as indicated by the presence of high frequency signals coming from the higher coordination shells that split the oscillations at 4 and 5.5 Å^{-1}. On the contrary the introduction of C induces a dramatic disordering of the In site. Indeed, DFT calculations show that both atoms are off the ideal *Ts* sites by 0.1 Å, causing II and III shells to split in approximately three subshells each.. The In–C interatomic distance is longer than the sum of the tetrahedral covalent radii $R_{In–C}$=2.179 whereas the In–Si distance becomes identical to the sum of the respective tetrahedral radii. The presence of the C neighbour and the increase of the disorder in a large zone around In is a direct confirmation of the pairing between the two chemical species. In the case of

[39] [Baron-APL-79] 5R. Baron, J. P. Baukus, S. D. Allen, T. C. McGill, M. H. Young, H. Kimura, H. V. Winston, and

more concentrated sampes (In implantation fluence = $5.5*10^{14} at/cm^2$) the solubility limit is locally overcome and In-In pairs are detected[40].

Controlled aggregation of magnetic cations in a semiconductor nitride matrix (STAFF&USER)
Bonanni, A. Navarro-Quezada, T. Li , M. Wegscheider, Z. Matey, V. Hol'y, R.T. Lechner, G. Bauer, M. Rovezzi, F. D'Acapito, M. Kiecana , M. Sawicki and T. Dietl
Phys. Rev. Lett. **101**, 135502 (2008).

The origin of the ferromagnetic behaviour persisting above room temperature (RT) and discovered in semiconductors doped with transition metals and rare earths may certainly be considered as one of the most controversial issues in today's materials science. Many misleading assumptions and conclusions on the actual magnetic interactions in magnetically doped semiconductors and oxides have been, until recently, caused by lack of a proper correlation between fabrication parameters and structural characterisation at the nanoscale. Now, there is an increasing amount of evidence that, owing to specific features of magnetic impurities in semiconductors and oxides, the epitaxial growth of these systems can result in the self-organised aggregation of magnetically robust nanocrystals embedded in the host paramagnetic matrix. This finding holds enormous potential for the fabrication of a range of multifunctional nanosystems relevant to spintronics, nanoelectronics, photonics, and plasmonics. However, it has also been realised that difficulties in the experimental resolution and identification of the embedded nanostructures endure and hamper the progress in the control of the mechanisms accounting for associated and hitherto unexplored nanoassembly processes. Synchrotron radiation microprobe[41] and other nanoanalytical synchrotron tools, in combination with high-resolution transmission electron microscopy (HRTEM)[42], represent a suitable blend of techniques that, when complemented by magnetic measurements, can lead to a thorough characterisation of magnetically doped semiconductors. The model system (Ga,Fe)N has been found from SQUID magnetometry data to be ferromagnetic at RT for a concentration of magnetic ions above 0.4% under the employed growth conditions. While laboratory high-resolution X-ray diffraction (XRD) does not evidence any phase separation in these samples, powder diffraction XRD measurements carried out at the beamline **ID31** by using a photon energy of 15.5 keV reveal the presence of new diffraction peaks identified as the (002) and (111) of the phase - Fe3N with a Curie temperature $TC \sim 575$ K. Moreover, it has been possible to confirm a recent theory[43],according to which it is possible to modify the chemical valence of transition metal cations by doping with shallow acceptors (Mg in the case of GaN) or donors (Si for GaN), and, consequently, affect their aggregation in the semiconducting matrix. Figure 1 indicates that doping with Si does indeed hinder the formation of Fe-rich regions: panel (a) reproduces the full /2 scan and panel (b) a reduced scan with focus on the range with the diffraction peaks originating from the embedded nanocrystals. This is confirmed by the HRTEM images in the inset of the figure 1.

[40] d'Acapito F., Golosio B., Shimizu Y., Scalese S., Italia M., Alippi P., Grasso S. *The site of In dopants in Si* AIP Conference Proceedings – 882 (2007) 375-377.

[41] G. Martinez-Criado, A. Somogyi, S. Ramos, J. Campo, R. Tucoulou, M. Salome, J. Susini, M. Hermann, M. Eickhoff, and M. Stutzmann, *Appl. Phys. Lett.* **86**, 131927 (2005).
[42] M. Jamet, A. Barski, T. Devillers, V. Poydenot, R. Dujardin, P. Bayle-Guillmaud, J. Rotheman, E. Bellet-Amalric, A. Marty, J. Cibert, R. Mattana and S. Tatarenko, *Nature Mater.* **5**, 653 (2006).
[43] T. Dietl, *Nature Mater.* **5**, 673 (2006).

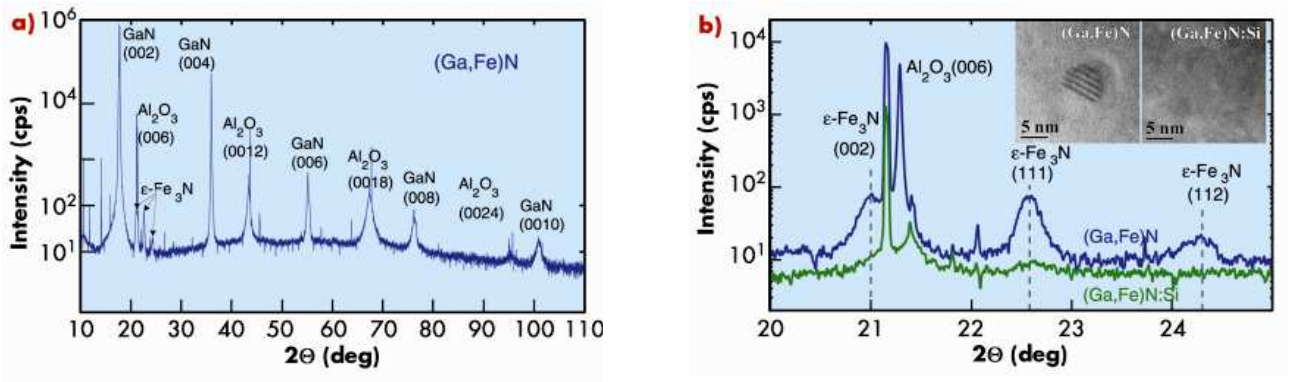

Figure 1

The results on the effect of Si on the aggregation of the Fe ions in the GaN matrix are also corroborated by X-ray absorption near-edge structure (XANES) measurements at the Fe K-edge carried out at the GILDA beamline (**BM08**). As evidenced in Figure 2, XANES data point to the expected presence of Fe in the Fe3+ charge state in the nominally undoped (Ga,Fe)N samples, whereas they confirm the coexistence of Fe3+ and Fe2+ ions in the case of doping with Si, supporting the onset of a shift of the Fermi level and consequent modification of Fe charge state in the system.

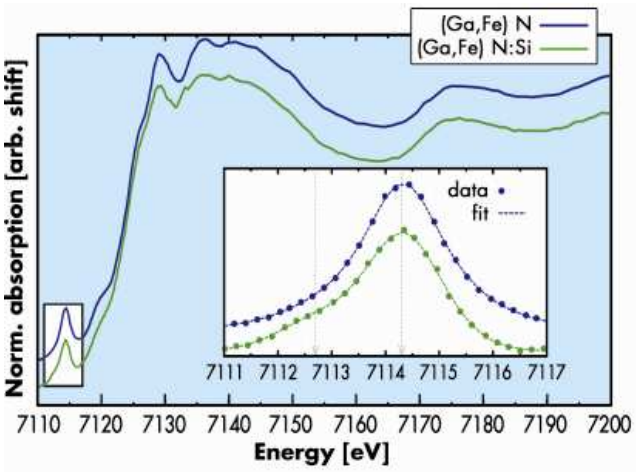

Figure 2

An analogous effect has been verified in the case of doping with Mg. By combining HRTEM with synchrotron XRD and XANES it has been possible to identify the distinct ways by which Fe incorporates into the GaN lattice giving an important contribution to the elucidation of the origin of the ferromagnetic features in magnetically doped semiconductors. Importantly, the doping with either acceptors or donors hampers the nanocrystal assembling and offers a way to functionally control the aggregation of magnetic elements in a non-magnetic host.

Structure of the Fe/NiO(001) interface measured by polarization dependent XAFS.(STAFF&USER)
Luches P., Bellini V., Colonna S., Di Giustino L., Manghi F., Valeri S., Boscherini F.
Phys. Rev. Lett. ***96****, 106106/1-4 (2006).*

Interfaces between ferromagnetic (FM) and antiferromagnetic (AFM) materials constitute one of the active elements of new magneto-electronic devices, which exploit the electron spin rather than its charge for information processing and transfer. The exchange interactions at the interface formed between the FM and the AFM layers result in an unidirectional magnetic anisotropy, the so

called exchange bias, of which a quantitative explanation is presently lacking[44]. Exchange bias leads to a shift of the magnetic hysterisis curve. In many cases, real FM/AFM interfaces are not ideal in their structure and chemistry and their atomic configuration is expected to have a very strong influence on the magnetic couplings between the two materials.

We investigated the case of an epitaxial system, Fe/NiO(001), taken as a model for a FM metal / AFM oxide interface, and obtained a combined experimental and theoretical description for it, which provides new insight in the understanding of magnetic couplings in such systems.

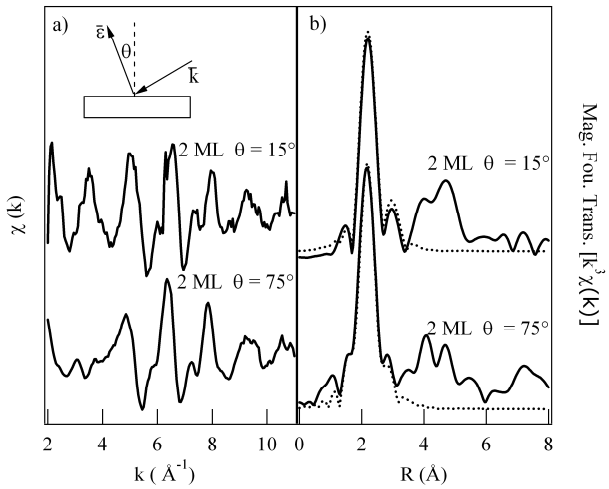

Figure 1
a) Background subtracted Fe K-edge EXAFS spectra for the 2 ML Fe film in the two geometries. b) Corresponding k^3 weighted magnitude of the Fourier transforms (solid line) and fit (dashed line).

The sample used for this study was a UHV grown 2 ML Fe/10 ML NiO/Ag(001) multilayer, capped by a 10 nm thick Au layer to prevent the sample contamination by the atmosphere. Fe K-edge x-ray absorption fine structure (XAFS) measurements were performed at the BM08 "GILDA" beamline. We exploited the polarization dependence of the XAFS cross section in order to separately probe the in-plane and out-of-plane structure.

The background subtracted XAFS spectra in the two geometries are shown in Figure1a. Figure 1b shows the corresponding magnitude of the Fourier transforms and the results of structural fits.

The fitting of the extended range spectra was performed assuming the formation of a planar FeO-like layer at the Fe/NiO interface (see model in Figure 2). The FeO-like layer exhibits a buckling, with O and Fe atoms respectively shifted towards and away from the underlying NiO substrate. Moreover, the distance between the last NiO plane and the average position of the FeO plane is 7 % larger than the interplanar distance of bulk NiO. A body-centered-tetragonal (bct) Fe-Ni phase is present on top of the interfacial FeO layer.

We have compared the structural parameters obtained by the XAFS analysis to the results of density functional theory calculations performed by means of the all-electron linearized augmented plane wave method + local orbital in the generalized gradient approximation. The atomic configurations of the structurally relaxed system compare very well with the experimental ones. In particular, the numerical agreement between the values for the buckling of the FeO layer (experiment: 0.29 ± 0.07 Å; theory: 0.34 Å) and for the expanded distance between the FeO layer and the underlying NiO (exp. 2.24 ± 0.08 Å; th. 2.25 Å) is notable. Our calculations also allowed to evaluate the spin magnetic moment of the Fe atoms at the interface, providing original insight into

[44] J. Nogués and I.K. Schuller, J. Magn. Magn. Mater. **192** 203 (1999).

the relation between structure and magnetic properties. We compared the values obtained assuming the presence of a pure, pseudomorphic, Fe layer and the formation of an oxidized FeO layer.

A significant increase of approximately 0.6 μ_B (from 2.6 μ_B to 3.2 μ_B) in the presence of the distorted FeO layer was found. The origin of this change lies in a depopulation of minority spin *d* orbitals involved in the Fe-O bonds. The Fe atoms of the interfacial FeO layer assumed in our model are in fact more coordinated with oxygen atoms than Fe atoms situated in the first layer of the ideal Fe/NiO interface, therefore a higher spin polarization is achieved. Uncompensated moments coming from the interfacial FeO layer, which may couple ferromagnetically with the Fe layer, are expected to influence dramatically the exchange interaction at the Fe/NiO interface, with significant consequences also on the exchange bias mechanism.

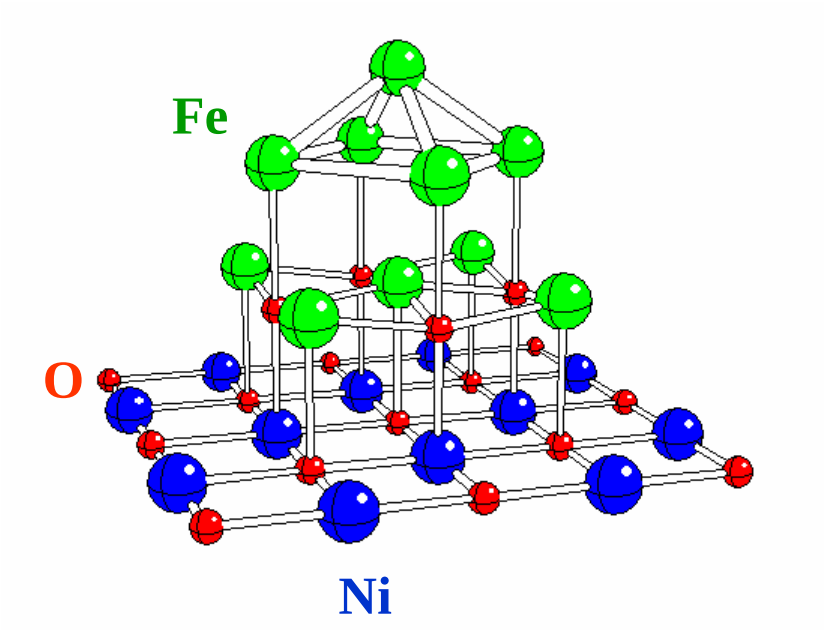

Figure 2.
Model of the Fe/NiO(001) interface

In summary, we give evidence for the presence of a structurally distorted FeO layer at the Fe/NiO(001) interface, in which the spin magnetic moment of Fe atoms is increased compared to the abrupt interface. This work provides the atomic level characterization necessary in order to provide a structural basis for a physical understanding of exchange bias in FM / AFM interfaces.

Depth-resolved study of impurity sites in low-energy ion-implanted As in Si. (STAFF&USER)
F. d'Acapito, S. Milita , A. Satta , L. Colombo
J. Appl. Phys. **102**, 043524 (2007).

The electrical and diffusion properties of dopant atoms in silicon are of primary importance for the realisation of ultra-shallow junctions for transistors in the semiconductor industry. In arsenic-doped Si:As, important phenomena appear when the doping level reaches volumes as high as 10^{21} cm^{-3}, namely: (i) the concentration of free carriers does not increase linearly with the doping level; (ii) rapid thermal annealing (RTA) enhances the concentration of active carriers, while further annealing decreases the number of electrically-active impurities to saturation levels; (iii) the As diffusion coefficient starts to increase rapidly. Furthermore, upon RTA the original implant profile is modified significantly by the transient enhanced diffusion effect, generating long tails of dopants into the substrate and their accumulation near the surface. To explain the electrical As deactivation and its enhanced diffusion one can use X-ray measurements and computer simulation techniques.

The extended X-ray absorption fine structure (EXAFS) technique has been widely used since it characterises the local atomic structure around the dopant atom. The efficacity of ab initio calculations to reproduce the local structure of point defects has also been demonstrated.

In this work we combine EXAFS measurements and *ab initio* total energy calculations to investigate these phenomena. In particular, we investigated four crystalline Si:As samples, obtained by implanting Si (001) substrates with As^+ ions at an energy of 5 keV and a fluence of $1x10^{15}cm^{-2}$ and treated by different thermal budgets.

The EXAFS measurements were carried out at the arsenic K edge (E = 11867 eV) in glancing angle geometry, at BM08, the GILDA CRG beamline. For each sample, spectra were collected *in total reflection* (TR), and *high angle* (HA) modes. TR uses an incident beam below the critical angle for the total reflection, and the latter above, so that the As site in surface part (about 6 nm in TR mode) or in the bulk (300 nm in HA mode) of the sample are probed.

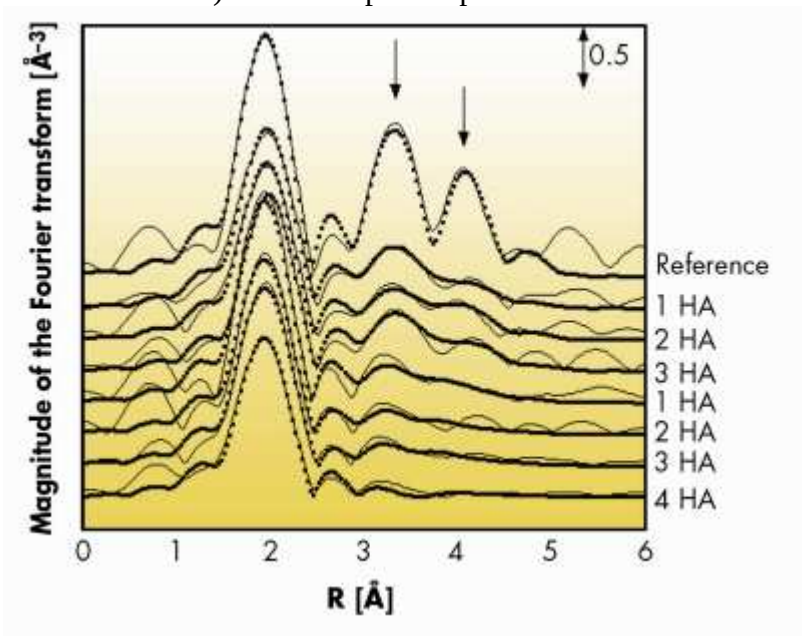

Figure 1

The experimental findings were supported by our theoretical study based on the density functional theory (DFT). Figure 1 shows the Fourier Transform pattern of the EXAFS spectra of the samples measured both in TR and HA. The *reference* used for As in a substitutional position is the spectrum of an Si (001) wafer implanted with As+ ions at an energy of 70 keV and a fluence of $3x10^{15}$ cm^{-2} and annealed at 1100°C in N2 for 100 s. Arrows indicate the peaks that exhibit the more marked change when passing from HA to TR series. In our case, the peaks located in the region from 3.0 to 4.5 Å correspond to the second and third coordination shells. They are weaker in the HA spectra than those in the reference spectrum and they disappear in the TR spectra. This indicates an increase of the disorder in all the samples, which is more evident in the shallow region.

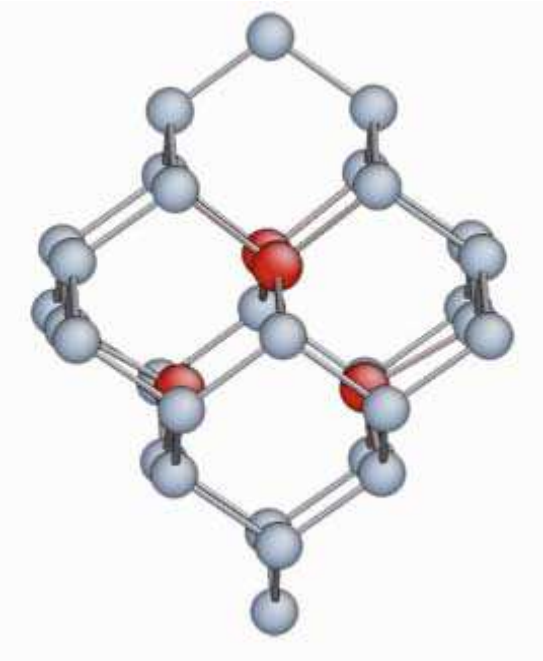

Figure 2

The HA data, relative to all the As content, also in the deeper part of the implant, reveal the presence of As in the Si matrix linked to a vacancy. Only by comparing the value of the distance for Si second neighbours resulting from the fit of the experimental data and those obtained by DFT calculations for various complexes V-Asn (n=1 to 4) we could identify V-As3 and V-As4 as those present in the material. Figure 2 represents a model of the V-As4 complex.

In the TR case we found a very disordered environment with possible presence of As precipitates. This is due to the crystallisation front that, initiating from the amorphous/crystalline interface during the annealing, transports dopants towards the Si/SiO_2 interface (snowplough effect) creating in this zone an increased concentration of As impurities and defects.

In this work we have carried out a depth-selective EXAFS investigation in grazing incidence geometry on arsenic doped silicon samples. Evidence of different environments of the impurity along the concentration profile has been found and the experimental findings have been compared with an *ab initio* study. In summary, As occupies predominantly substitutional positions and it is linked to vacancies forming As3V and/or As4V complexes. Conversely, near the surface, the local structure appears to be extremely disordered, plausibly as a consequence of the As accumulation at the surface due to the thermal annealing treatment.

B - Nanoscience and Nanotechnology

Metallic versus covalent bonding: Ga nanoparticles as a case study[(USER)]

Ghigna P., Spinolo G., Parravicini G.B., Stella A., Migliori A., Kofman R.

Journal of the American Chemical Society **129**, 8026-8033 (2007)

In this study a systematic X-ray absorption spectroscopy investigation of the local coordination in gallium nanostructures has been performed as a function of temperature and particle size. The main goal of this study was to show how nanostructures affect the polymorphism of solid gallium and the (meta)stability range of the liquid phase and that the surface tension acts in the same direction as hydrostatic pressure in stabilizing the Ga solid phases.

Interest toward the chemistry of elemental gallium arises for many, variously related aspects.

The *density of the liquid higher than that of the main solid phase* (α) places Ga into the minority set of substances that show increasing stability of the liquid with increasing pressure and generically indicates an anomalous bonding behavior with respect to other metals.

α-Gallium is indeed a very particular metal made of *diatomic units* with a marked pseudo-gap in the density of states at the Fermi level and strongly anisotropic electronic conductivity. In spite of its high reactivity with oxygen, Ga is indeed a nice experimental model for *investigating the properties of liquid metals* particularly because the α-crystal *melts slightly above room temperature* (303 K).

Gallium however, shows a complex polymorphism that has been deeply investigated experimentally and computationally: the other crystalline phases have significantly different structures based on different local arrangements and building units, which are made, for instance, of zigzag chains of atoms (β phase) or five different coordination environments (δ phase). Remarkably, these crystal structures do not show the "anomalous" properties of α-Ga.

Evidence of the influence of interfaces on Ga bonding is given by a large amount of experiments available from recent or older literature on the effect of confinement on gallium polymorphism.

The same authors recently found a more extreme behavior for Ga nanoparticles below 5 nm in diameter, which can be undercooled down to liquid nitrogen temperature and kept at that temperature for times on the order of days without showing the onset of crystallization.

All these results strongly suggest that the condensed phases of elemental gallium represent a kind of test case where the bonding behavior can be easily modified, and the effect can be achieved by acting on the surface free energy contribution.

To that purpose, a systematic investigation of the local coordination in gallium nanostructures in the size range between 5 and 150 nm from 90 to 350 K was performed.

Ga films have been obtained by thermal evaporation under ultrahigh vacuum of ultrapure Ga (99.999%) and condensation on a carefully cleaned amorphous silica substrate kept at 323 K. At that temperature, liquid Ga self-organizes in islands, whose shapes are truncated spheres with a contact angle of about 130°. Three of the investigated films consist of nanodroplets with 5, 10, and 30 nm mean radius, respectively. The nanodroplets have a low size dispersion and have been covered after preparation with a thin layer of SiO_x (15 nm thick), to prevent Ga oxidation.

A continuous 150 nm thick Ga film, was prepared by condensing Ga vapor on a silica substrate cooled to liquid nitrogen temperature under UHV and also this film was covered by a protective layer of SiO_x. Fluorescence XAFS data were collected at GILDA beamline at the Ga-K edge.

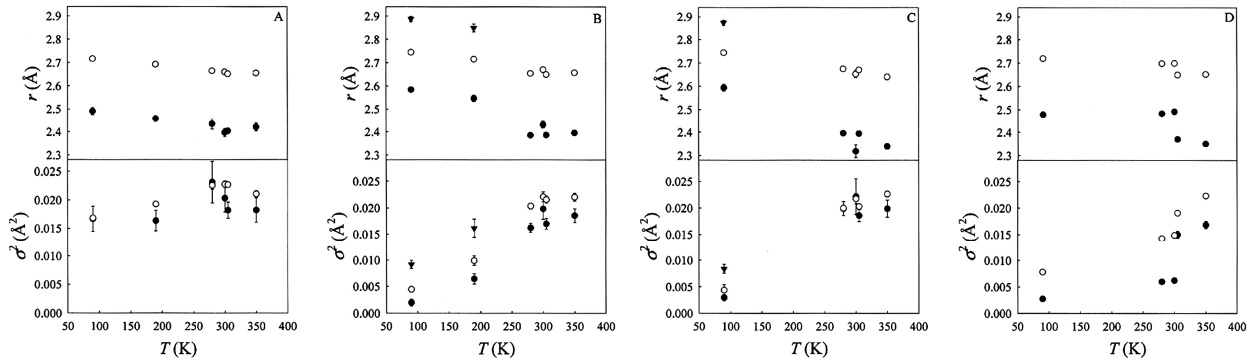

Figure 1
Ga-neighbours distances and their variances as obtained by the EXAFS fitting, plotted as a function of T: (A) 5 nm sample; (B) 10 nm sample; (C) 30 nm sample; (D) 150 nm sample.

The main conclusion that can be drawn from the experimental results are the following:
(1) The nanostructure size strongly affects the polymorphism of solid gallium and the (meta) stability range of the liquid phase. The results nicely combine with those, more specifically pertinent to the β and δ phases, typically obtained on larger particles.
(2) Concerning the local structure and/or bonding behavior, the effect of the surface free energy is first to favor the metallic arrangement of the δ phase and then to stabilize a liquid-like phase based on dimeric molecules even at 90 K.
(3) In this respect, the surface tension acts in the same direction as hydrostatic pressure.
(4) The Ga-Ga distance in the dimers in the liquid phase (near 2.4 Å or below) is lower than in the α solid (near 2.46Å), and therefore one is tentatively induced to infer that in the liquid phase the Ga-Ga dimer bonding character is more covalent than in the solid R Ga phase.
Remarkable conclusions of this work, in particular, are that (1) liquid Ga is made of Ga atoms and Ga_2 dimers in chemical equilibrium with each other, (2) the bond length of the dimer is between 2.25 and 2.5Å, and (3) the map of electronic density distinctively shows that *the bond is a truly covalent bond* not simply a *metallic charge overlap forced by ionic proximity.*

Sub-nanometric metallic Au clusters as efficient Er^{3+} sensitizers in silica(STAFF&USER)
E. Trave, G. Mattei, P. Mazzoldi, G. Pellegrini, G. Scian, C. Maurizio, G. Battaglin
Appl. Phys. Lett. 89 (2006) 151121.

During the last few decades, telecommunication technology has been largely attracted to Er doped materials, since the rare earth ion shows a characteristic optical emission at 1540 nm allowing for application as the active element for light generation and amplification in optical devices. To overcome the intrinsic small cross section for Er excitation, a useful strategy is represented by the interaction with sensitizing species such as other rare earths, semiconductor nanostructures, organic complexes, and more recently, metals. Concerning metallic species, recently an enhancement of the Er photoluminescence (PL) has been reported in sol-gel silica samples triggered by the surface plasmon resonance (SPR) of 20 nm Au nanoclusters and by the gettering of the OH groups at the Au clusters surface[45]. On the other hand, it has been shown that an Er PL increase through Ag clusters in silica can be attained without development of SPR, i.e., without large metallic clusters

[45] Fukushima et al, J. Appl. Phys. 2005

(Stronhofer et al., Appl. Phys. Lett. 2002). So, the aim of this work is to clarify the possibility of an energy transfer process mediated by ultra-small metallic clusters.

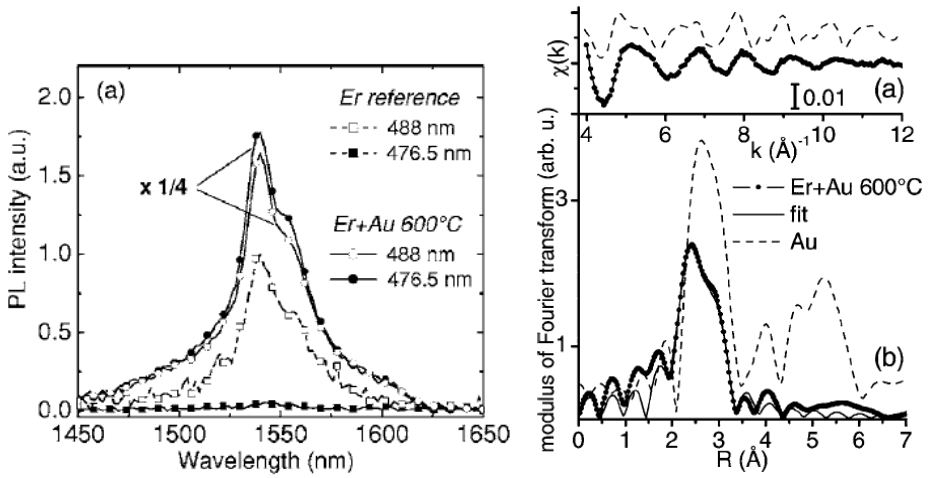

Figure 1. Right: In resonance (488 nm) and out of resonance (476.5 nm) Er PL emission around 1540 nm for the Er reference sample before and after Au implantation followed by a thermal treatment at 600 °C; the PL intensity is normalized to one for the Er reference sample and consequently rescaled for the co-implanted one. Left: EXAFS analysis of the Au L_{III}-edge spectrum for Er+Au 600 °C, compared to that one of metallic Au. (a) EXAFS spectra. (b) k^3-weighted Fourier transform moduli (in the range k=4–11 $Å^{-1}$) of the EXAFS spectra in (a); the Au-Au first shell fit for the sample is also reported; the spectra are not corrected for the phase shift.

The reference sample is an Er-implanted silica (Er concentration = 10^{20} Er/cm^3, corresponding to a total fluence of 6.8×10^{14} Er/cm^2) that underwent a N_2- annealing to repair the radiation damage and to activate the Er PL emission. A set of samples was then obtained by a subsequent Au^+ implantation of the Er-implanted silica (the reference sample); as for the Er implantation, a multiple set of implants was made to obtain an homogeneous dopant concentration (about 10^{21} Au/cm^3, corresponding to a total fluence of 6.1×10^{15} Au/cm^2), and the implantation energies were chosen to maximize the overlap between the concentration depth profiles of the two species. Post Au-implantation treatments were then carried out in the temperature range 400-900°C in N_2 atmosphere for 1h. The effect of N_2 annealing is to both wash out the implantation-induced defects and to promote the Au aggregation in clusters.

The occurrence of an energy transfer process after the introduction of gold ions in Er implanted silica has been evidenced by a PL study of the Er^{3+} emission around 1540 nm both in resonant (λ = 488 nm) and nonresonant (λ = 476.5 nm) pumping conditions. The Figure 1 (left panel, (a)) compares the PL spectra of the Au-implanted sample annealed at 600 °C (Er +Au 600 °C) and of the Er reference. Exciting both samples at 488 nm, resonantly with the $^4F_{7/2}$ Er^{3+} level, Er +Au 600 °C sample shows a PL signal sensibly higher than the Er reference one, with an enhancement factor of about seven. Moreover, only the co-implanted sample shows the Er emission when excited nonresonantly 476.5 nm: this is the fingerprint of an indirect Er excitation mechanism mediated by Au-related sensitizing centers. It is worth noting that for the sample heated at 600 °C, the SPR of the Au nanoclusters was not observed. The EXAFS experiment has clarified the structures responsible for this energy transfer effect. The EXAFS experiment was performed at the L_{III}-edges of Au and Er, at the GILDA beamline of the ESRF. Due to sample dilution, the spectra were recorded in fluorescence mode by a 13-element high purity Ge detector; the samples were cooled at 80 K to reduce the thermal vibrations. In Figure 1 (right panel, (a)) the Au-edge EXAFS spectrum of the Er+Au 600 °C sample is compared to that of metallic Au foil: one main oscillation is evident, extending up to k=12 $Å^{-1}$. This signal is related to an Au-Au coordination (see Figure 1, right panel, (b)), proving the presence of Au metallic aggregates, with an estimated Au-Au distance R =2.78±0.01 Å. This value is about 3% shorter than the first shell distance in the bulk fcc Au (R_{bulk}=2.88 Å): this is consistent with the presence of small (about 1 nm in size) Au clusters, that

are known to exhibit a contraction of the interatomic distances.16 The measured coordination number of the first Au shell is N=3.9±0.4 (N=12 for bulk Au): this decrease is due to the reduced dimension of the Au aggregates (1 nm fcc cluster with the same interatomic distance as the measured one would give N≈8, the exact value depending on the cluster geometry and possibly to the fraction of single Au atoms dispersed into the matrix). Considering that the measured Au-Au interatomic distance contraction suggests a sub-nanometer average size for the aggregates, the coordination number indicates that a large fraction of the Au atoms are present as metallic aggregates. This picture is further supported by the lack of significant correlation peaks in the EXAFS signal at distances larger than that one described. The EXAFS analysis of the samples heated at higher temperature indicates a growth of the Au clusters.
The EXAFS analysis at the Er L_{III}-edge indicates that Er atoms are dispersed into the oxide matrix and correlated in the first shell with O atoms; moreover no Er-Er correlation is detected, so the formation of extended phases such as metallic Er or Er oxides can be ruled out.
In summary, from the PL and EXAFS analysis, it is concluded that: (i) gold plays an effective role in Er sensitization, promoting a broadband increase of the Er PL emission at 1540 nm; (ii) the energy transfer process should be mostly triggered by 5d to 6sp interband absorption occurring in Au nanoaggregates; (iii) small (subnanometric) Au clusters seem to be more efficient sensitizers than larger ones.

Temperature dependence of the structural parameters of gold nanoparticles investigated with EXAFS(STAFF&USER)

T. Comaschi, A. Balerna and S. Mobilio
Physical Review B ***77****, 075432, 2008*

Metal nanoparticles show a variety of novel and fascinating electrical, magnetic, and chemical properties arising both from the presence of a large percentage of low coordinated surface atoms and from the confinement of electrons to dimensions shorter than the electron mean free path and the Fermi length. From the structural point of view, metallic nanoclusters often undergo a contraction of the lattice distances with respect to bulk materials because of surface stress tension. According to Laplace's law, the lattice parameter is foreseen to linearly decrease with the inverse particle dimension *D*. Recently, temperature dependent x-ray diffraction measurements on a gold nanoparticle powder mean dimension of about 4 nm showed for the first time an additional effect, i.e., the occurrence of a *crossover* in the temperature dependence of the cell parameter, which changes from an initial thermal expansion at low temperatures to a thermal contraction for *T* around 125 K[46]. This result is not due to changes in the structure of the nanoparticle, which continues to show a fcc atomic arrangement as the bulk metal but can be attributed to the contribution of electronic excitations to the total energy of the system. Indeed, for a bulk system, the electronic contribution to the total energy results slowly varies with temperature and, for this reason, bulk materials generally show a thermal expansion, originating from the anharmonicity of the lattice potential. On the other hand in nanoparticles, the presence of electronic discrete energy levels separated by only a few meV implies a relevant variation of the electronic energy with *T*. At GILDA, we explored more deeply this effect to assess its presence and to quantify it even in smaller clusters, where localization effects are expected to become stronger and stronger. At very low sizes, x-ray diffraction does not allow measuring of the cell parameter of the nanoparticle with sufficient accuracy; at this purpose, we used EXAFS spectroscopy at the Au L_3 edge to get a very accurate estimate of the nearest-neighbour distance as a function of temperature.

[46] W.-H. Li, S. Y. Wu, C. C. Yang, S. K. Lai, K. C. Lee, H. L. Hunag, and H. D. Yang, Phys. Rev. Lett. **89**, 135504, 2002.

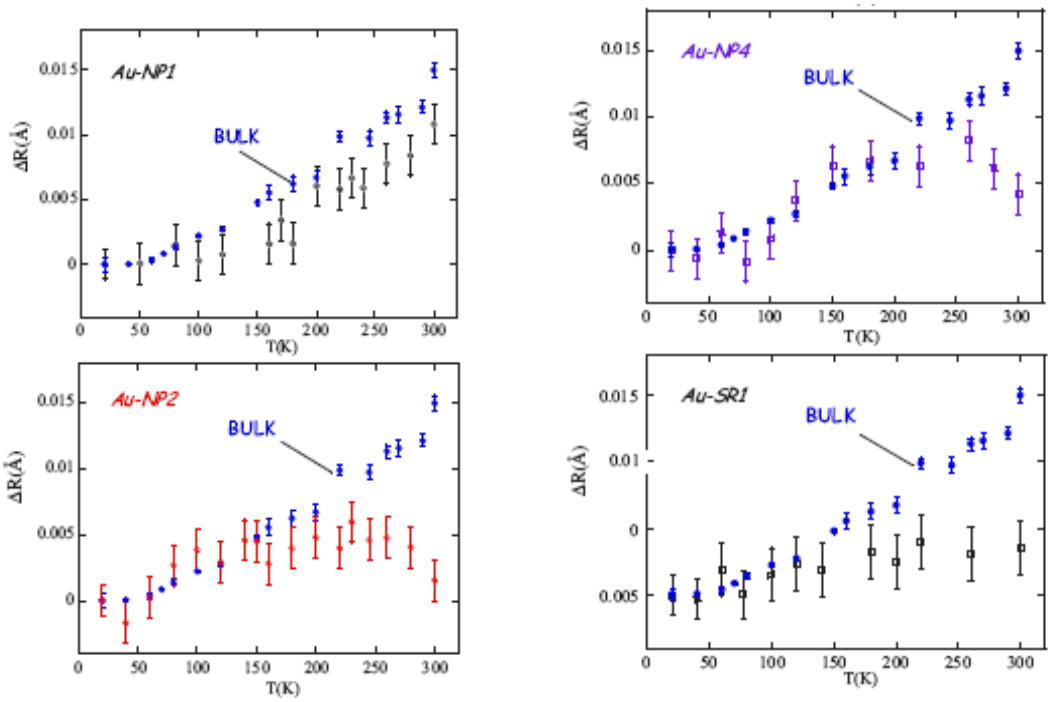

Figure 1.

The EXAFS results are shown in figure 1, which report the first shell distance for different Au metallic cluster samples of diameter ranging from 25 to 50 Å. Quite marked differences between the different samples are evident. Au-NP1, the sample with the greatest nanoparticle size, has a bulk-like trend with slightly lower *R* values. On the contrary, Au-NP2 at low *T* has a bulk-like behaviour, while over 170 K, its *R* values do not grow as in the bulk case and become much lower than the bulk ones as the temperature increases up to 300 K. Au-NP3, the greatest sample of the two produced using evaporation, shows a thermal behaviour similar to Au-NP1. As Au-NP2, Au-NP4 also follows the bulk behaviour at low temperatures, while over 200 K, the achieved *R* values are quite lower than the bulk ones. Finally, the Au-SR1 sample shows a nearly zero expansion in the investigated temperature range.

In order to have an understanding of the thermal behaviour of our samples, we have calculated the thermal behaviour of the nearest-neighbour distance for approximately spherical gold nanoclusters of different sizes. We considered the total energy of the system as sum of three main contributions:

$$E_{tot} = U + E_{vib} + E_{el}$$

where U, E_{vib}, and E_{el} are the static, the vibrational, and the electronic energy of the nanoparticle, respectively. The temperature-independent part of the total energy is represented by the static term U. E_{vib} was calculated as the energy of a finite series of harmonic oscillators and introducing anharmonicity effects by considering the volume dependence of the phonon frequencies, described by the Grüneisen parameter γ. The electronic contribution to the total energy was treated according to Kubo[47]. In this approach, the discrete energy level distribution, *En*, induced by the finite particle size, which also depends on the particle shape and surface conditions, is averaged and assumed to be an equally spaced energy level distribution.

[47] R. Kubo, J. Phys. Soc. Jpn. **17**, 975, 1962.

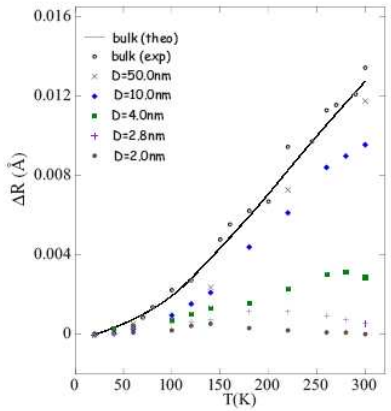

Figure 2

Comparison between the experimental thermal expansion of gold bulk and thermal expansion predicted from our calculations for a bulklike system together with the theoretical trends with *T* of the relative values of the mean interatomic distance for different nominal sizes of the nanocluster.

In Figure 2, the excellent agreement between the so calculated thermal expansions of the bulk with the values experimentally observed is clearly visible, which confirms that anharmonic effects are properly taken into account by our model. We observe that for clusters our calculations foresee three regimes:

1. for high cluster dimensions, a bulk-like behaviour with a reduced thermal expansion;
2. for intermediate cluster sizes, a crossover from a reduced thermal expansion at low *T* to a negative thermal expansion at high *T* with a crossing temperature which lowers at smaller dimensions;
3. a nearly zero thermal expansion for low sizes.

We underline that such behaviours are in qualitative agreement with those experimentally observed, reported in Figure 1.

C - Materials for Energy Production and Transport

Indium Doping in Barium Cerate: the Relation between Local Symmetry and the Formation and Mobility of Protonic Defects[(USER)]

Giannici, F., Longo, A., Balerna, A., Kreuer, K.-D., Martorana, A.

Chemistry of Materials, 19, 5714-5720 (2007).

The solid solution series $Ba(In,Ce)O_{3-\delta}$ has been investigated with respect to structure, formation, and mobility of protonic defects. XRD demonstrates that indium is soluble in any ratio in barium cerate, anyway maintaining the perovskite structure of the parent oxide. Compared to the limited solubility of Y_2O_3 in $BaCeO_3$ and $BaZrO_3$, the complete solubility of In_2O_3 is suggested to reflect a relation between absolute hardness of the dopant and the ease of insertion into the hosting lattices. Extended X-ray absorption fine structure (EXAFS) was used to probe the local environment of In3+ in barium cerate: in the surroundings of the dopant, the orthorhombic structure is strongly modified, resulting in an increase of local symmetry, as it is sketched in figure 1.

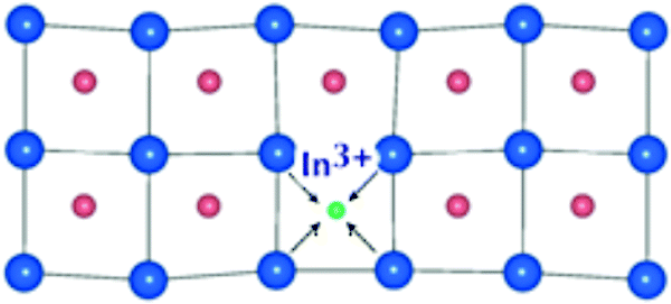

Figure 1
Schematic drawing showing the increase of local symmetry around the In dopant in In-doped barium cerate.

This result could be achieved by a detailed analysis of the local structure around indium, performed at GILDA. In the figure 2 the reliability of such analysis is demonstrated:

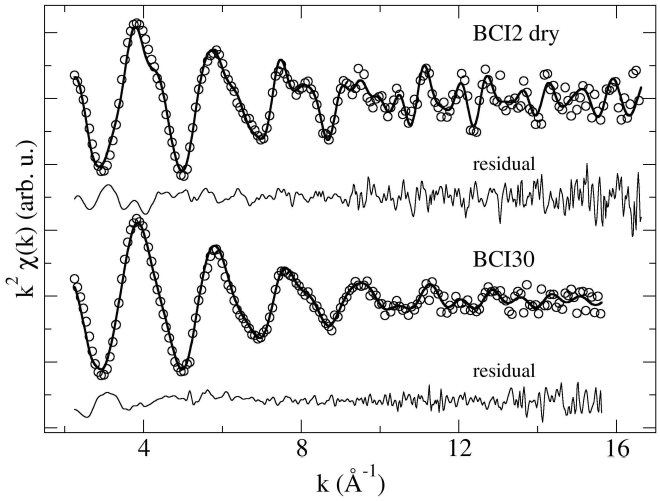

Figure 2
Experimental k^2-weighed EXAFS spectra, best fits and residual functions for BCI2 dry and for BCI30 as-prepared samples.

Then, it is concluded that the InO6 octahedra are very regular, and that there is no indication for any defect clustering. This is suggested to be the main reason for the low entropy of formation of protonic defects by water dissolution. The mobility of such defects is lower than in Y-doped $BaCeO_3$, but at high dopant levels the high local symmetry allows for formation of very high concentrations of protonic defects, which may balance the lower proton mobility compared to Y:BaCeO3. This doping behavior is also suggested to be the consequence of the lower Pearson absolute hardness of In^{3+} compared to Y^{3+}. Contrary to $Y:BaCeO_3$, protonic defects do not referentially reside in the vicinity of the dopant, demonstrating a quite different rearrangement of the O-H chemical bond as a consequence of In insertion. The results of this paper demonstrate that ionic radius matching is only one and probably, as is confirmed by the behavior of other perovskites, not the most important criterion for tailoring a good proton-conducting ceramic material. Actually, chemical matching is even more important than the structural one. The high dopant solubility is a further parameter to be taken into account for development of perovskite oxides for electrochemical applications.

Metal−Support Interaction and Redox Behavior of Pt (1 wt %)/$Ce_{0.6}Zr_{0.4}O_2$.[(USER)]
Deganello, G., Giannici, F., Martorana, A., Pantaleo, G., Prestianni, A., Balerna, A., Liotta, L.F., Longo, A.
Journal of Physical Chemistry B, 110, 8731-8739 (2006).

This paper reports a study of the interaction of ceria-zirconia (CZ) with Pt nanoparticles supported onto the mixed oxide surface. The material is a three-way catalyst, designed to limit the impact of pollutants, CO, NOx and hydrocarbons, produced by car engines.
Pt supported on ceria-zirconia gives rise to peculiar properties of the resulting composite material: (i) CO2 coming from anaerobic CO oxidation is produced in larger amount and at lower temperature with respect to metal free CZ; (ii) redox-aged Pt/ceria-zirconia shows evidence of a direct Pt−Ce interaction; and (iii) Pt/CZ bulk reduction is much faster and starts with an induction time with respect to CZ. It is proposed that the reduction mechanism of Pt/CZ consists of two steps: initially, the preferential reduction of the support surface takes place; afterward, bulk reduction is accomplished. As demonstrated by in situ XRD performed at GILDA, the overall lattice oxygen amount that CZ and Pt/CZ can deliver at 773 K for the oxidation of CO is about the same for the two materials, but the much faster bulk reduction observed by in situ XRD for Pt/CZ has been attributed to a beneficial effect of the supported metal, and in particular to an easier release of

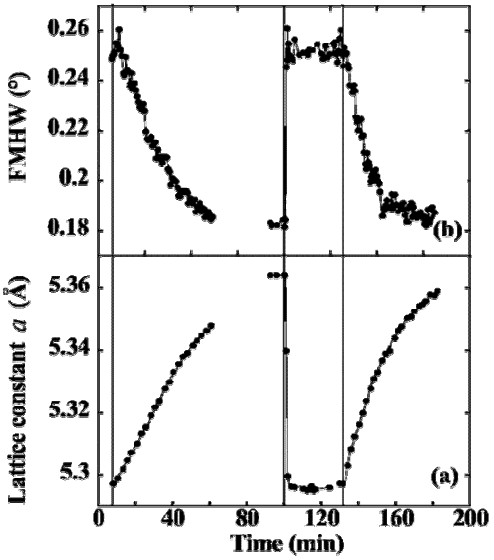

Figure 1
(a) (Lattice constant a as a function of in situ treatment;
(b) 220 peak fwhm of r-CZ. The changes of gases fed to the sample are indicated by vertical lines at 10‘ (switching on of CO/He), 100‘ (change to O2/He), and 130‘ (second reductive treatment). The variation, both of lattice constant and fwhm, is progressive during reduction. During oxidation, these parameters vary very rapidly, and two phases, one still reduced and one oxidized, can be detected. The corresponding values of lattice constant and fwhm are weighted averages of these two phases.

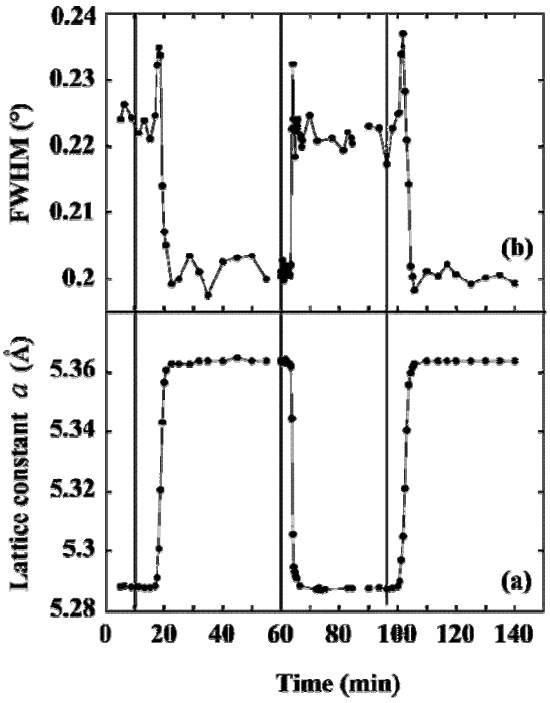

Figure 2
(a) Lattice constant a as a function of in situ treatment; (b) 220 peak fwhm of r-Pt1CZ. The changes of treatment gases are indicated by vertical lines at 10‘ (switching on of CO/He), 60‘ (change to O2/He), and 90‘ (second reductive treatment). The variation of both lattice constant and fwhm is very quick. Outside the transition regions, the powder patterns are fitted with a single phase. During the transitions from the oxidized to the reduced phase and vice versa, two phases, one oxidized and one reduced, are necessary to perform the Rietveld refinement; the corresponding values of lattice constant and fwhm are weighted averages of these two phases.

reacted CO2, producing a more effective turnover of reactants at the catalyst surface. The figure 3 shows the EXAFS analysis, that evidences the presence of a Pt5Ce alloy in reduced Pt/CZ that actually demonstrates envisaged the strong metal-support interaction (SMSI) in this material.

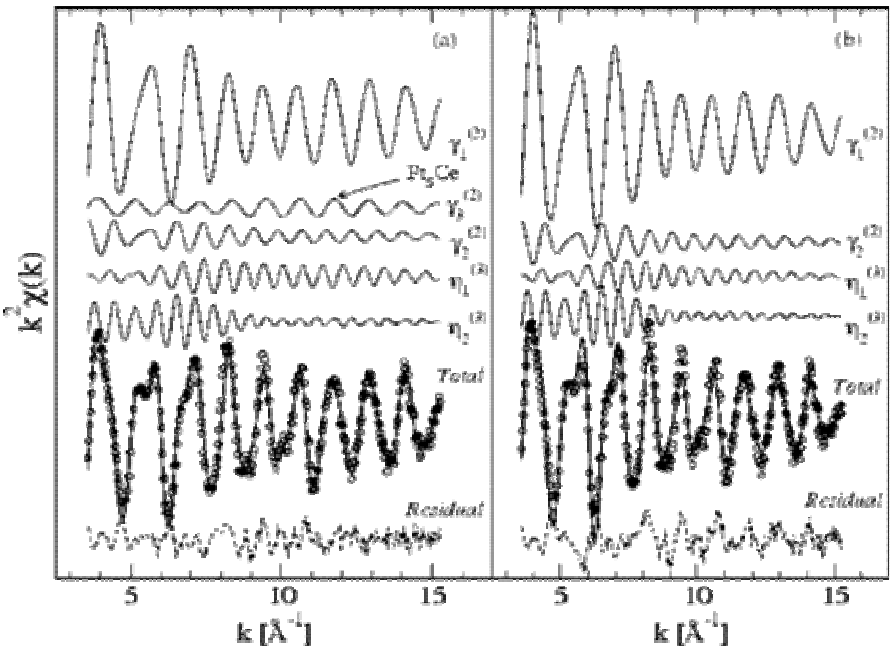

Figure 3
Component signals and overall fitting to the r-Pt1CZ EXAFS data. Two-body components are indicated by γi(2) and three-body components by ηi(3). (a) Allowing for a Pt−Ce contribution; (b) without Pt−Ce. The residual in panel b clearly shows that a well-defined frequency is missing.

D - Environment

In situ Study of Methane Anaerobic Combustion on Iron Oxides: Towardsa Clean Hydrogen Production Process(USER)

M. Gemmi, M. Merlini, U. Cornaro, D. Ghisletti, G. Artioli

J. Appl. Cryst (2005) **38**, 353-360.

Hydrogen will be one of the most important fuels in a future sustainable economy. In the medium term, hydrogen production will still rely on fossil fuels, whose environmental impact has to be lowered both by modifying actual technologies and/or developing new ones capable of mitigating CO2 emissions. ENI is developing a clean process for H2 production from fossil fuels based on the properties of selected oxides that, once reduced with hydrocarbons, are capable of being re-oxidised by splitting H2O into H2 and [O], which in turn re-oxidises the solid closing the loop[48].

$4MexOy + CH4 \rightarrow 4MexO(y-1) + 2H2O + CO2$

$4MexO(y-1) + 4\ H2O \rightarrow 4MexOy + 4H2$

$CH4 + 2\ H2O \rightarrow 4H2 + CO2;\ \Delta H = 39.5$ Kcal

A redox solid circulating among three fluidised bed reactors is the asset developed to exploit the reaction scheme **(Figure 1).**

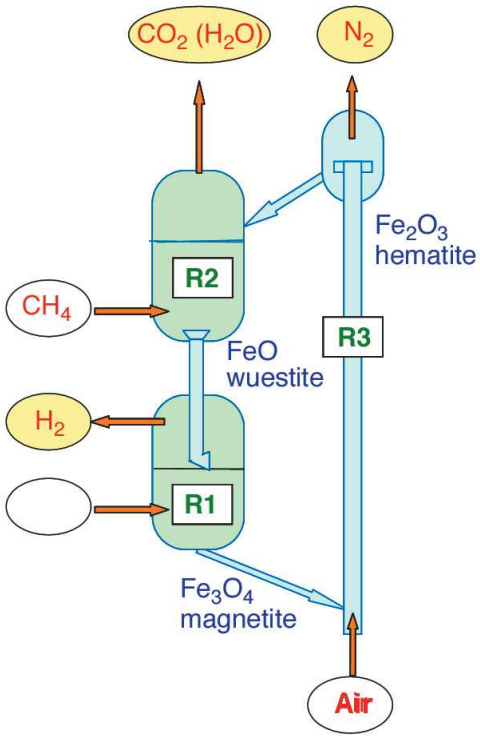

Figure1. Conceptual reactors design to exploit the redox concept on iron oxide based circulating solid. A concentrated stream of CO2/H2O (ready to be buried) is produced in reactor 2, when the solid is reduced by methane (Fe2O3/FeO). A stream of H2 (virtually carbon free) is produced in reactor 1, when the solid is partly oxidised with water (FeO/Fe3O4). Thermal balance is achieved in reactor 3, where the solid is fully reoxidised (Fe3O4/Fe2O3).

We carried out a combined X-ray diffraction (XRD) / mass spectrometry (MS) experiment at the Italian CRG BM08 “GILDA” beamline, to study the structural evolution of an iron based solid exposed to methane under anaerobic combustion conditions as a first step of such a redox cycle. The CeO2/Fe2O3 solid investigated was exposed to a high temperature (~ 1000 K) CH4 reducing flux followed by a re-oxidation in air. The sample was contained in an open quartz capillary. One side was connected to a gas injecting system (CH4/Ar mixture, air and Ar for purging cycles), the other to a mass spectrometer (MS). X-ray powder diffraction was collected by a translating image plate system with a time resolution of one minute. All the collected powder patterns were analysed by the Rietveld method, obtaining a complete structure characterisation of the process in terms of

[48] U.Cornaro, D.Sanfilippo US2004152790-A1

quantitative analysis of the crystal phases involved (see Figure 2a). As soon as the CH4 enters the capillary, a series of redox reactions take place. Iron present as Fe3+ in Fe2O3 is progressively reduced to Fe+2Fe+32O4 (magnetite), Fe+2O (wuestite) and finally to Fe. The appearance of metallic iron in the XRD signal coincides with the H2 emission and the decrease of the flow of outgoing CH4 (Figure 2b) detected by MS. This is direct evidence of methane cracking (CH4 → C + 2H2) catalysed by iron. The carbon produced by this reaction appears two minutes later as Fe3C, which replaces iron in catalysing the cracking, and as a polymorph of graphite. We have clear evidence that CeO2 participate to the reduction process. It is known that in a reducing environment ceria may convert into a non-stoichiometric reduced form (CeO2-x), whose crystal structure has the same symmetry but a larger unit cell.

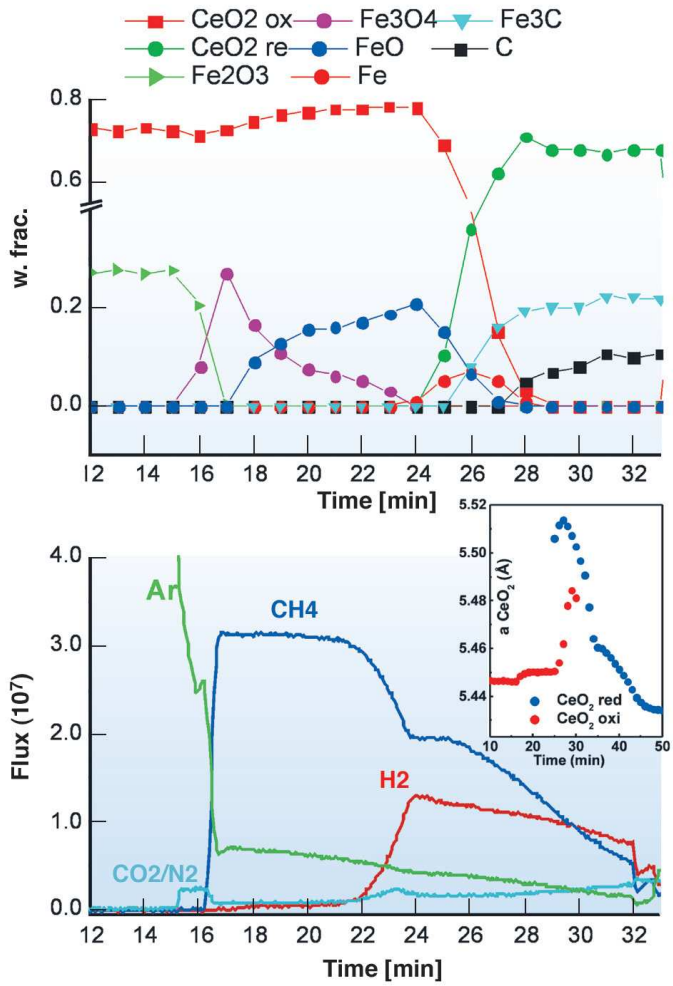

Figure 2. Evolution during the reduction cycle:
a) Quantitative phase analysis;
b) Evolved gases;
c) Plot of the CeO2 cell parameter.

By mapping the variation of CeO2 unit cell parameter, a small jump corresponding to CH4 injection and a large jump corresponding to H2 emission can be detected. The latter hange is simultaneous with a splitting of the ceria diffraction peaks that can be interpreted as a mixture of two reduced ceria phases with different defectivity (Figure 2c). The stoichiometry of the reduced ceria is proportional to the unit cell variation and seems to be temperature independent[49]. The estimated compositions are CeO1.99 after the CH4 injection and CeO1.88 for the most reduced form appearing after H2 emission. Peak shape analysis demonstrates that during CH4 combustion CeO2 undergoes re-crystallization since the full width half maxima of CeO2 peaks constantly decrease. The oxidation follows the reverse path of the reduction except for the direct oxidation of Fe3C to FeO without the intermediate formation of iron. The final solid has the same composition as the starting mixture demonstrating that the cycle is totally reversible.

[49] H. Chiang, R. N. Blumenthal, R. A. Fournelle, *Solid State Ionics* **66**, 85-95 (1993).

X-ray absorption investigations of copper resinate blackening in a XV century Italian painting.[(USER)]

Cartechini L. Miliani C. Brunetti B.G. Sgamellotti A. Altavilla C. Ciliberto E. d'Acapito F.
*Applied Physics A, **92**, 243-250, 2008.*

This paper reports the study of the darkening of copper resinate, a green copper-based pigment, observed in a XV century easel painting of the Italian artist Niccolò Liberatore.The painting revealed serious problems of conservation due to the blackening of green and blue areas containing the copper-based pigments azurite, malachite and copper resinate. In particular, it has been observed that while azurite and malachite painting layers still contain unaltered crystals of the pigments, the copper resinate layer has undergone a complete blackening.

Copper resinate is a transparent green glaze which was obtained by mixing copper pigments, usually verdigris, with terpenic resins, often in the presence of drying oils. The resulting pigment consisted of a complex mixture of copper carboxylate complexes of resin and fatty acids which was used fresh to produce a transparent amorphous green layer, or in the form of dried powder dispersed in a binder (drying oil or tempera grassa). Copper resinate was particularly appreciated for its glassy brilliant optical effects, but unfortunately it has the tendency of discolouring to brown in a relatively short time. **Understanding the role of copper-based pigments in the alteration processes of painting layers is of great interest for conservation science.**

XANES and EXAFS measurements were collected at the Cu *K*-edge on an original painting sample, as well as on fresh pigment standards and on painting models, with the aim of providing structural information on the oxidation states and the local chemical environment of copper in the unaltered and blackened pigments, and to elucidate the discoloration mechanism. XAS measurements were performed on the original painting sample ($1.5\times1.5 mm^2$) and on the painting models in the X-ray fluorescence yield mode (XFY), using a high-purity 13-element Ge detector. This experimental configuration allowed to collect the Cu signal by probing the first tens of μm through the depth of the painting layer. Moreover, measurements in the total electron yield (TEY) mode were collected for the blackened copper resinate sample, limiting the probed depth to the first hundreds of nanometres of the painting layer . The strong analogy of the spectral features in XFY and TEY modes allowed to assess that the copper local environment does not change across the depth of the blackened layer and no surface effects are present.

EXAFS analysis evidenced that the local chemical environment of Cu in copper resinate can be described using neutral copper acetate as a model. It consists, essentially, of bimetal Cu^{2+} carboxylate complexes with a distorted octahedral coordination. Such a structure is retained in the blackened pigment, although some differences were observed. It has been found that the alteration takes place without change of the valence state of Cu(II) ions, while the formation of the copper oxides CuO and Cu_2O responsible for the embrownment is excluded. On the basis of the XAS results it is deduced that discoloration of copper resinate may be related to local modification of the copper coordination structure as evidenced by the observation of an increase of the Cu–Cu and Cu–C distances in the EXAFS spectra.

Copper ions have been demonstrated to play a primari reactive role in oxidation processes of drying oil. Thus, the copper chemical environment, especially in a lipid binder, can undergo local molecular rearrangements, which, in specific conditions, may lead to a change of the chromatic properties. As a matter of fact, the results of this work strongly suggest that copper complexes are primarily involved in pigment embrownment. It is reasonable to assume that discoloration takes place as result of strong copper–organic matrix interactions (copper-ion extraction and/or metal-catalysed oxidation of the organic matrix) followed by the modification of the Cu coordination structure, as demonstrated by the EXAFS spectra. These modifications could be due, during the past history of the paint, to specific environmental conditions (undocumented cleaning procedure, exposure to light or heat, etc.), which drastically influenced the copper chemistry.

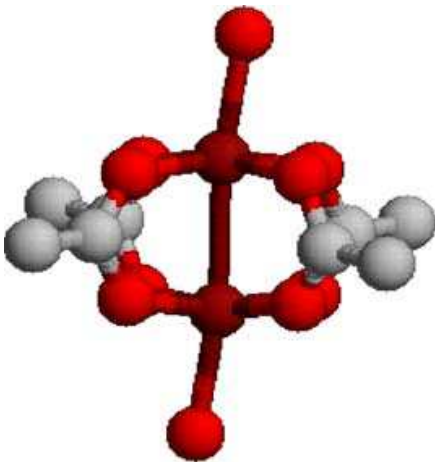

Figure 1.
Scheme of the bridging bidentate coordination of Cu ions in copper acetate (Cu = *dark red*, C = *grey*, O = *red*). Apical oxygen atoms are also shown

E – Life Science

Zn^{2+} binding sites in photosynthetic reaction centers and respiratory complexes(USER)

Giachini, L., Francia, F., Mallardi, A., Palazzo, G., Carpenè, E., Boscherini, F., Venturoli, G.
Multiple scattering X-ray absorption studies of Zn2+ binding sites in bacterial photosynthetic reaction centers
Biophys. J. **88**, 2038-2046, 2005.
Giachini, L., Francia, F., Veronesi, G., Lee, D.W., Daldal, F., Huang, L.S., Berry, E.A., Cocco, T., Papa, S., Boscherini, F. and G. Venturoli
X-Ray Absorption Studies of Zn^{2+} Binding Sites in Bacterial, Avian, and Bovine Cytochrome bc_1 Complexes
Biophys. J. **93**, 2934-2951, 2007.
Francia, F., Giachini, L., Boscherini, F., Venturoli, G., Capitanio, G., Martino, P.L., and S. Papa:
*FEBS Lett. **581**, 611-616, 2007.*

Zn^{2+} metal ions bind specifically to a number of charge translocating membrane protein complexes, strongly inhibiting electron and/or proton transport. Among these protein complexes are the bacterial photosynthetic reaction center (RC) and two key enzymes of the respiratory electron transfer chain: the cytochrome (cyt) bc_1 complex and cytochrome c oxidase.

The high-affinity binding of Zn^{2+} has been characterized with great detail in the bacterial photosynthetic reaction center (RC). This pigment-protein complex, which catalyses a light-induced electron transfer across the membrane dielectric, can be considered as a model system when examining more complex redox enzymes. Structural and spectroscopic studies of Zn-RC complexes[50] have revealed that Zn^{2+} inhibits the rate of proton transfer from the protein surface to the final electron acceptor of the RC by competing with protons for the same binding site which involves two histidine residues. This finding allowed determination of the entry point of H^+ and led to a full definition of the proton pathway from the aqueous phase to the acceptor quinone molecule bound to the RC[51]. The location of the RC Zn^{2+} binding site has suggested that the Zn inhibitory effects observed in other redox enzymes share the same mechanism, i.e. binding of a divalent metal ion blocks competitively an entry or exit proton pathway close to the protein surface. Location of Zn binding sites and resolution of their local structure becomes therefore a powerful tool in tracing proton pathways in an entire class of membrane proteins.

In view of the above considerations a systematic project has been undertaken, aimed at determining by XAFS the local structure of bound Zn^{2+} in the photosynthetic reaction center purified from the bacterium *Rhodobacter sphaeroides*, in prokaryotic and eukariotic cyt bc1 complexes, and in the cytochrome c oxidase. The objective was to determine the location of the binding sites, defining at high resolution the coordination geometries, in order to clarify the common, structural origin of the inhibitory effects observed.

X-ray absorption spectroscopy of stoichiometric Zn-RC complexes, embedded into polyvinyl alcohol films [Giachini et al., 2005] allowed a clear-cut determination of the local structure of the high affinity Zn^{2+} binding site previously identified by x-ray diffraction at 2.5 Å resolution. XAFS data were analysed by combining *ab-initio* simulations and multiparameter fitting; structural contributions up to the fourth coordination shell and multiple scattering paths (involving three atoms) have been included. The results indicated that Zn^{2+} binds two O and two N atoms in the first coordination shell. Higher shell contributions are consistent with a binding cluster formed by two His, one Asp residue and a water molecule. Analysis of complexes characterized by approximately 2 Zn ions per RC reveals a second structurally distinct binding site, involving one O and three N atoms, not belonging to a His residue. The local structure obtained for the higher affinity site nicely

[50] Axelrod, H.L., Abresch, E.C., Paddock, M.L., Okamura, M.Y., Feher, G. (2000) Proc. Natl. Acad. Sci. USA 97, 1542-1547.
Paddock, M.L., Sagle, L., Tehrani, A., Beatty, J.T., Feher, G., Okamura, M.Y. (2003) Biochemistry 42, 9626-9632.

[51] Adelroth, P., Paddock, M.L., Sagle, L.B., Feher, G., Okamura, M.Y. (2000) Proc. Natl. Acad. Sci. USA 97, 13086-13092

fitted the coordination geometry proposed on the basis of XRD data while the first shell distances resulting from XAFS analysis were considerably contracted in comparison with those determined by XRD.

Cyt bc_1 complexes are electrogenic quinol:cyt c oxidoreductases, encountered in a broad variety of prokaryotic and eukaryotic organisms. These widespread membrane integral enzymes play a crucial role during photosynthesis and respiration[52]. In all cases these energy transducing enzymes transfer electrons from a hydroquinone derivative (QH_2) to a soluble electron carrier (a c-type cyt). The bc_1 complex is one of the major contributors of the transmembrane electrochemical proton gradient used for ATP synthesis. The mechanism of redox coupled H^+ translocation by the bc_1 involves two catalytic sites facing the two opposite sides of the energy transducing membrane: the Q_o site, at which QH_2 oxidation is coupled to proton release and cyt c reduction, and the Q_i site, where quinone reduction is coupled to H^+ uptake. A complete catalytic cycle requires two turnovers of the Q_0 site, so that 4 H^+ are released to one side and 2 H^+ are taken up from the other side of the membrane. Various XRD structures of the mitochomdrial bc_1 complex are available; recently an XRD structure of the simpler bacterial cyt bc_1 at 3.8 Å has been published[53].

Zn^{2+} is a well established inhibitor of the bovine mitochondrial cyt bc_1, in which it competes with H^+ ions. In bacterial bc_1 complexes Zn^{2+} has been recently shown to decelerate specific electron transfer steps and the generation of transmembrane voltage[54]. These observations have been tentatively explained by proposing that Zn^{2+} binds close to the Q_0 site, blocking the proton release channel(s). In agreement with this suggestion two potential inhibitory Zn^{2+} binding sites have been revealed in the XRD structure of the avian cyt bc_1: one of them, (Zn01), located in a hydrophilic area between cyt b and c_1, might interfere with the egress of H^+ to the aqueous medium. Although a number of putative Zn ligands (including histidines) were identified, the coordination geometry could not be resolved[55].

Using Zn K-edge XAFS the local structure of Zn^{2+} bound stoichiometrically to non crystallized cyt bc_1 complexes has been investigated [Giachini et al., 2007a]. In a comparative study the avian, the bovine and the bacterial enzymes were examined. A large number of putative clusters, built by combining information from first-shell analysis and metalloprotein databases, were fitted to the experimental spectra by using *ab initio* simulations. This procedure led to the identification of the binding clusters with high levels of confidence. In both the avian and bovine enzyme a tetrahedral ligand cluster formed by two His, one Lys and one carboxylic residue was found, and this ligand attribution fit the crystallographic Zn01 location of the avian enzyme. In the chicken enzyme the ligands were the His121, His268, Lys270 and Asp253 residues, and in the homologous bovine enzyme they were the His 121, His267, Lys269 and Asp254 residues. Zn^{2+} bound to the bacterial cyt bc_1 complex exhibited quite different spectral features, consistent with a coordination number of six. The best fitting octahedral cluster was formed by one His, two carboxylic acids, one Gln or Asn residue and two water molecules. Interestingly, by aligning the crystallographic structures of the bacterial and avian enzyme, this group of residues was found to be located in the region homologous to that of the Zn01 site. This cluster included the His276, Asp278, Glu295 and Asn279 residues of the cyt *b* subunit. The conserved location of the Zn^{2+} binding sites at the entrance of the putative proton release pathways, and the presence of His residues pointed out to a common mechanism of inhibition. As previously shown for the photosynthetic bacterial reaction center, zinc

[52] Berry,E.A., Guergova-Kuras,M., Huang,L.S., Crofts, A.R. (2000a) Ann. Rev. Biochem. 69, 1005-1075

[53] Berry, E.A., Huang, L.-S., Saechao, L.K., Pon, N.G., Valkova-Valchanova, M., F. Daldal (2004) Photosynth. Res. 81, 251-275.

[54] Klishin, S.S., Junge, W., Mulkidjanian, A.Y. (2002) Biochim. Biophys. Acta 1553, 177-182

[55] Berry, E.A., Zhang, Z., Bellamy, H.D., Huang, L. (2000b) Biochim. Biophys. Acta 1459, 440-448

would compete with protons for binding to the His residues, thus impairing their function as proton donor/acceptors.

Cytochrome c oxidase is the terminal component of the respiratory chain: it catalyses the oxidation of cyt c reduced by the bc_1 complex, reducing O_2 to H_2O and pumping 4 protons across the mytochondrial membrane. Definition of the proton transfer pathways is an open question, crucial for understanding the complex catalytic mechanism of the enzyme. XRD structures of cyt oxidase have helped identify two putative channels for H^+ uptake, referred to as the D and K channels. The roles of these channels are still debated in terms of the number and destination of the protons they conduct and how the individual proton uptake events are coupled to electron transfer[56]. Zn^{2+} inhibits bovine heart cyt c oxidase[57]. In analogy with the scenario observed with the photosynthetic RC, it has been proposed that in cyt c oxidase Zn^{2+} binds near the entry point of the D-pathway at which a cluster of histidine residues and carboxylates is found[58].

XAFS analysis performed according to the procedure described above for the cytochrome bc1 complex, allowed to identify tetrahedral coordination site(s) for Zn^{2+} with two N histidine imidazoles, one N histidine imidazol or N lysine and one O-COOH (glutammate or aspartate), most likely located at the entry site of the proton conducting D pathway, and involved in inhibition of the oxygen reduction catalysis [Francia et al., 2007].

[56] Brzezinski, P. (2004) Trends in Biochem. Sci. 29, 380-387.

[57] Nicholls, P., Singh, A.P. (1988) Life Sci. Adv. 7, 321-326

[58] Aagaard, A., Namslauer, A., Brzezinski, P. (2002) Biochim. Biophys. Acta 1555, 133-139

F – Soft Condensed Matter

H_2S gas interaction with Pt(II)-containing polymetallaynes of selected chain length: an XPS and EXAFS study(USER)

Battocchio Chiara, Fratoddi Ilaria, Russo Maria Vittoria, Polzonetti Giovanni

Journal of Physical Chemistry A, 112, 7365-7373, 2008.

Sulfur-containing compounds are common impurities in fossil-derived fuels and chemical feed stocks[59], and damage the quality of the air by forming sulfur oxides SO_x, during the burning of fuels, that are major air pollutants leading to acid rain[60]. Therefore, the detection and monitoring of sulfur – containing compounds are highly attractive. In this framework, the main objective of this research was to establish a relationship between chemical, geometrical and electronic structure of small Pt containing organometallic systems (no more than four repetitive units) and their sensitivity and selectivity with regard to a sulfur containing molecule as H_2S. Poly-ynes consisting of Pt or Pd square planar complexes in the chain between organic spacers have been synthesized and characterized in our group. Our systems have been successfully used in sensors and optical devices[61]. Structural data have been achieved on these materials by means of SR-XPS, NEXAFS[62], reflEXAFS and EXAFS [C. Battocchio et al. 2006a, C. Battocchio et al. 2006b].

The simpler related model molecules, recently synthesized to have model systems whose characterization would be crucial for the interpretation of the polymers chemical physical properties, have been studied by XPS and EXAFS and a square planar structure around the metal, together with a charge transfer interaction between units were assessed.

The here considered samples are the binuclear transition metal dialkynyl bridged Pt(II) complex *trans, trans*-[ClPt(PBu_3)$_2$(C≡C-C_6H_4-C_6H_4-C≡C)Pt(PBu_3)$_2$Cl] (**1**), the tetranuclear linear oligomer *trans*-{Cl-[Pt(PBu_3)$_2$(C≡C-C_6H_4-C_6H_4-C≡C)]$_3$Pt(PBu_3)$_2$Cl} (**2**), the tetranuclear cyclic oligomer *cis*-[Pt(PBu_3)$_2$(C≡C-C_6H_4-C_6H_4-C≡C)]$_4$ (**3**) and the multinuclear (ten Pt containing units) linear oligomer *trans*-{Cl-[Pt(PBu_3)$_2$(C≡C-C_6H_4-C_6H_4-C≡C)]$_9$Pt(PBu_3)$_2$Cl} (**4**) (molecular structures are reported in Figure 1).

EXAFS spectroscopy was performed at the Pt LIII edge to investigate the interaction between Pt-DEBPn (Pt-diethynylbiphenyl, n = 2,4) oligomers of different length and geometry (linear and cyclic, depending on the Pt square planar complex configuration, *trans* or *cis* respectively) and H_2S molecule. The hypothesized chemical interaction occurring between Pt(II) and S was verified and investigated. We believe that this chemical interaction is responsible for the high sensitivity and selectivity of Pt-DEBPn based mass sensor devices towards sulfur-containing compounds [3]. The experiments were carried out by EXAFS measurements on Pt-DEBPn pellet samples, both in low vacuum conditions (P = 10^{-3} mBar) and in presence of H_2S gas (P = 500 mBar) using the chemical cell. Detection of the transmission signal was done at the Pt L_{III}-edge (11564 eV). *In situ* treatments were made possible at GILDA by a small chamber equipped with input and output gas lines, that allows to perform EXAFS measurements on samples in controlled chemical environment [A. Longo et al. 2005] .

[59] Speight, J. G. *The Chemistry and Technology of Petroleum*, 2nd ed. , Dekker, New York, **1991**.

[60] Stern, A. C.; Boubel, R. W.; Turner, D. B.; Fox, D. L. *Fundamentals of Air Pollution*, 2nd ed., Academic Press, Orlando, FL, **1984**.

[61] C. Caliendo, G. Contini, I. Fratoddi, S. Irrera, P. Pertici, M. V. Russo, G. Scavia, Nanotech. 18 (2007) 125504.

[62] C. Battocchio, I. Fratoddi, M. V. Russo, G. Polzonetti, Chem. Phys. Lett. 400 (2004) 290.

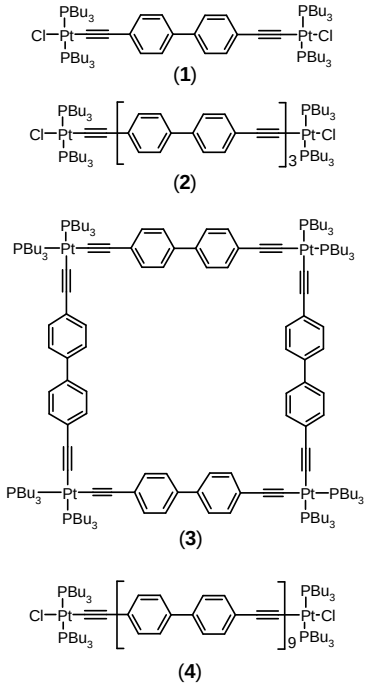

Figure 1.
Molecular structures of trans, trans-[ClPt(PBu3)2(-C≡C-C6H4-C6H4-C≡C-Pt(PBu3)2Cl] (1), trans-{Cl- [Pt(PBu3)2 -C≡C-C6H4-C6H4-C≡C-]3 Pt(PBu3)2 -Cl} (2), cis-{[Pt(PBu3)2 -C≡C-C6H4-C6H4-C≡C-]3 Pt(PBu3)2] (3) and trans-{Cl-[Pt(PBu3)2 -C≡C-C6H4-C6H4-C≡C-]9 Pt(PBu3)2 -Cl} (4).

The interaction of Pt containing organometallic poly-ynes with H_2S molecules has been investigated for one complex and three oligomers differentiated in both chain length (4, 9 repetitive units) and conformation (*cis* or *trans*). EXAFS, XPS, and UV-visible absorption spectroscopies, have been employed on purpose to perform an extensive characterization of the four samples before and after exposure to H_2S.

EXAFS measurements gave evidence for the interaction between the metal and the H_2S gaseous molecules showing a S-Pt coordination; structural modifications at the Pt coordination center have been detected as a consequence of this interaction. XAS data analysis suggested the change of Pt coordination from a square planar structure into a square-pyramidal geometry around the transition metal with H_2S in the apical position for the pentacoordinated platinum units, as depicted in Figure 2.

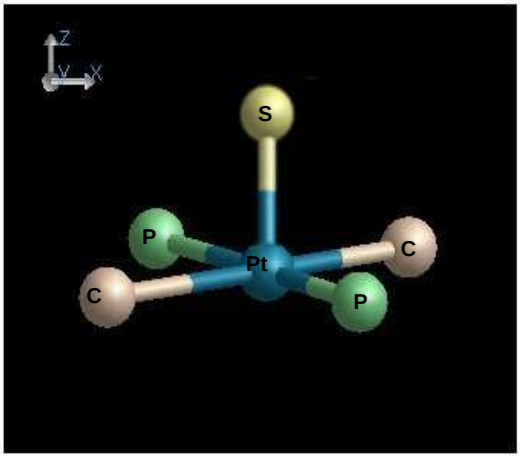

Figure 2
Tridimensional structure of the pentacoordinated Pt(II) cluster; the sulfur atom is in apical position, on the z axis; the two P atoms and the two acetylene units are in the xy plane.

-

The chemical interaction arising between Pt(II) centers and sulfur atoms has been assessed by the XPS Pt4f and S2p core levels analysis (see Figure 3).

	$Pt4f_{7/2}$ (Pristine Sample)		$Pt4f_{7/2}b$ (Sample + H_2S)	
	B.E. (eV)	FWHM (eV)	B.E. (eV)	FWHM (eV)
(**1**)	73.00	1.90	73.10	1.96
(**2**)	73.10	2.00	73.13	1.92
(**3**)	73.10	2.03	73.09	1.95
(**4**)	73.13	1.90	73.13	1.92

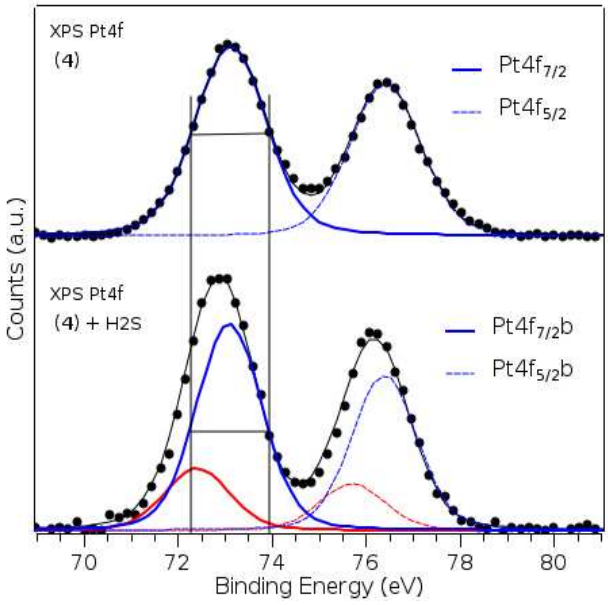

Figure 3.
Pt4f XPS spectra collected on sample (4) prior and after exposure to H_2S. For all the treated samples the overall signal is wider, and a small asymmetry, arising by the new spectral component, is detectable at lower BE. The component ascribed to the pristine Pt poly-yne ($Pt4f_{7/2}b$, higher BE values) in the treated sample spectrum shows the same BE and FWHM values of the pristine sample spectrum. Pt4f BE and FWHM values of all samples, both pristine and interacting with H_2S (b component), are reported in the table.

No interaction between Pt and S has been evidenced for samples exposed to SO_2 in the same conditions, thus confirming the selectivity of Pt-DEBPn as sensors.

Furthermore, the S/Pt atomic ratio of 1/3 for all samples, as estimated by XPS, suggests that in the here considered experimental conditions (Pt-poly-ynes samples exposed to H_2S gas at 500mBar) the adsorption undergo saturation.

G – Catalysis

Coordination and oxidation changes undergone by iron species in Fe-MCM-22 upon template removal, activation and red–ox treatments: an in situ IR, EXAFS and XANES study.[(USER)]
Berlier, G., Pourny, M., Bordiga, S., Spoto, G., Zecchina, A., Lamberti, C.
Journal of Catalysis, 2005, 229, 45-54

Extraframework iron cations embedded in zeolites can show different valence states (Fe2+, Fe3+ and even Fe4+) depending upon the reducing or oxidising character of the reagents present in the catalyst environment. An example of catalytic activity associated with the interplay between different oxidation states of Fe is given by the de-NOx catalysis on an isomorphously substituted Fe-MCM-22 sample. The paper reports its characterization by FTIR, XANES and EXAFS spectroscopies. Template burning and subsequent activation in vacuo causes the migration of a fraction of framework Fe^{3+} species to extraframework positions, accompanied by the reduction of a fraction of Fe^{3+} to Fe^{2+}. This conclusion is achieved by analysis of the EXAFS and XANES data collected at GILDA on the templated Fe-substituted MCM-22 sample, after template burning and after NO treatment.

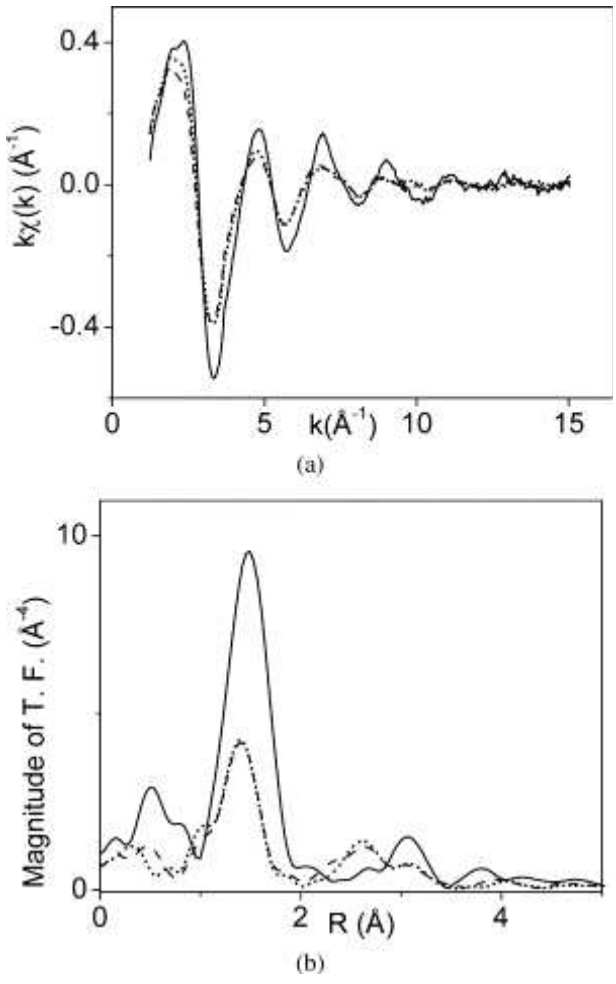

Figure 1
(a) Experimental kχ(k) of the Fe-MCM-22 sample in the presence of template (full line), after removing template and subsequent activation at 773 K (dashed line), and after subsequent interaction with 15 Torr of NO at RT (dotted line); (b) Corresponding k^3-weighted, phase uncorrected FT.

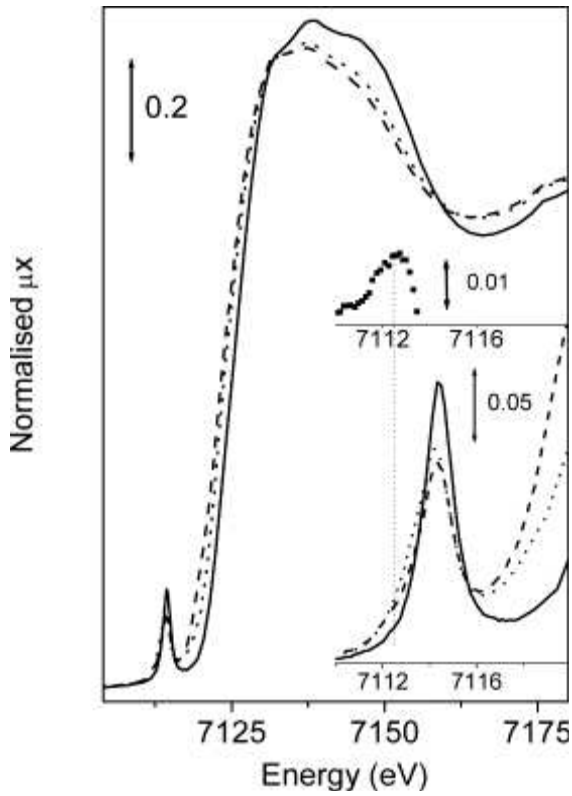

Figure 2
XANES spectra of sample Fe-MCM-22 with template (solid line), after removal of template and subsequent activation at 773 K (dashed line) and subsequent adsorption of 15 NO at RT (dotted line). The inset shows the magnification of the pre-edge peaks. The scattered curve in the upper part of the inset is the difference between the spectrum of the activated sample and that of the sample with template.

A fraction of extraframework Fe^{2+} sites is able to adsorb NO, forming $Fe^{2+}(NO)_n$ complexes (n=1,2,3), which indicates a high coordinative unsaturation of such sites. The X-ray absorption spectroscopies demonstrate that this fraction is however small, as both EXAFS and XANES spectra are almost unperturbed by NO adsorption. The corresponding FTIR bands are highly broad and asymmetric, not allowing to detect the presence of $Fe^{3+}(NO)$ complexes. The broad character of the nitrosyl bands suggests the presence of small oxidic clusters, in agreement with XANES and EXAFS evidences. The nature and distribution of extraframework Fe species are influenced by water preadsorption, which causes the increase of the amount of the most coordinatively unsaturated Fe^{2+} sites, able to form $Fe^{2+}(NO)_3$ complexes. The effect of red-ox treatments with O_2 and H_2 is also investigated. Upon oxidation, adsorbed oxygen is formed, which efficiently shields the Fe centers and does not rapidly nor efficiently react with NO. Upon reduction, the intensity of nitrosyl complexes increases, indicating the reduction of extraframework Fe^{3+} (likely present on the surface of small oxidic clusters) to Fe^{2+}.

In situ, Cr K-edge XAS study on the Phillips catalyst: activation and ethylene polymerization.[(USER)]

Groppo, E., Prestipino, C., Cesano, F., Bonino, F., Bordiga, S., Lamberti, C., Thüne, P.C., Niemantsverdriet, J.W., Zecchina, A.

Journal of Catalysis, 2005, 230, 98-108

In this paper, two ethylene polymerization routes on the Phillips Cr/SiO_2 catalyst are investigated and compared by in situ EXAFS and XANES. The former process mimics the process adopted in industrial plants, where ethylene is dosed directly on the oxidized catalyst, while in the latter the oxidized catalyst is first reduced by CO at 623 K. On this reduced catalyst C_2H_4 polymerization has been investigated at room temperature and at 373 K. To allow experiments in transmission mode, a Cr loading of 4 wt% has been adopted. At this loading a fraction of clustered Cr_2O_3 particles has been observed and quantified. The high energy resolution and signal-to-noise ratio of the XANES data allowed to determine the fraction of Cr sites involved in the polymerization reaction. So, it was possible to discriminate the presence of different Cr(II) sites on the basis of the observation of different XANES features in the samples reduced by CO and by C_2H_4.

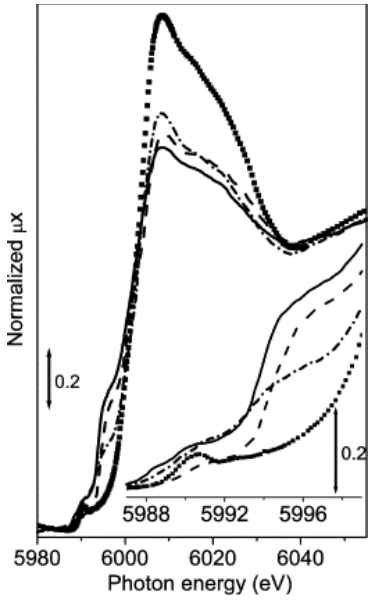

Figure 1

High resolution XANES spectra of the catalyst after in situ polymerization. The dashed line and the dash-dotted line spectra refer to the CO reduced sample, subsequently contacted with C_2H_4 at RT and at 373 K, respectively. The scattered square line refers to the Cr/SiO2 catalyst directly reduced in C_2H_4 at 523 K for 1 h (ethylene-reduced catalyst). As an example of unengaged Cr(II) species, the spectrum collected on the CO reduced catalyst (prior contact with ethylene) is also reported (full line). The inset reports a magnification of the pre-edge features.

In particular, figure 1 allows to notice a characteristic shoulder at about 5996 eV that was demonstrated to be diagnostic of isolated Cr(II) species, so allowing to discriminate Cr(II) centers involved in the ethylene plymerization. Preliminary ReflEXAFS experiments have been performed

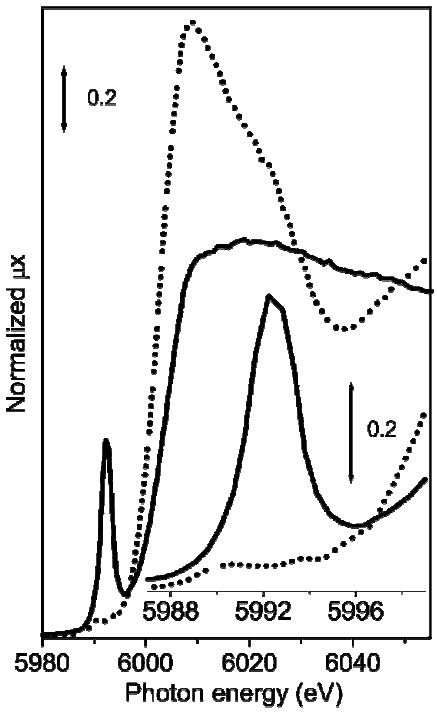

on a model catalyst prepared by impregnation of Cr on a flat Si(100) substrate covered by a thin layer of amorphous silica. Experiments have been performed ex situ on the grafted catalyst (i.e., after impregnation and thermal activation) and at the end of the polymerization stage demonstrating that, as a counterpart of a similar behavior during polymerization, this model system also shows similar XANES features as the standard Cr/SiO2 catalyst.

Figure 2.
XANES spectra of CrOx /SiO2/Si(100) model catalyst after thermal activation (full line) and after polymerization (dotted line), collected ex situ in ReflEXAFS mode.

The ReflEXAFS XANES pattern demonstrates that also in the model catalyst after polymerization the shoulder at 5996 eV, typical of isolated Cr(II) species, is absent (dotted line). The presence of the diagnostic shoulder at 5996 eV allowed to determine that fractions of about 25 and 55% of the original Cr(II) sites are involved when ethylene polymerization is performed on the model catalyst at room temperature and at 373 K, respectively.

H. Miscellanea

Negative thermal expansion in CuCl: An extended X-ray absorption fine structure study. (STAFF&USER)

Vaccari M., Grisenti R., Fornasini P., Rocca F., Sanson A.
Phys. Rev. B 75 (2007) 184307

The recent discovery of compounds exhibiting negative thermal expansion (NTE) over very large temperature intervals has renewed the interest for a deeper understanding of the mechanisms of NTE. The macroscopic expansion of crystals results from a competition between a positive contribution due to bond stretching and a negative contribution due to tension effects. The ability of EXAFS of measuring the real expansion of inter-atomic distances and the corresponding parallel and perpendicular mean square relative displacements (MSRDs) represents an effective tool for directly monitoring the local behaviour of NTE materials.

It is well known since long time that many tetrahedrally bonded semiconductors with the diamond or zinc-blende structure - such as Si, Ge, GaAs, ZnTe, CuCl - undergo NTE at very low temperatures, strength and temperature interval of NTE increasing with ionicity. In view of the relative simplicity of these structures and of the large amount of information available on them, a systematic exploration of diamond/zincblende crystals is particularly useful to search for correlations between the NTE properties and the quantities measured by EXAFS, and to gain a deeper insight into the local mechanisms of NTE.

Germanium, affected by very weak NTE, had already been thoroughly studied by EXAFS. CuCl exhibits the strongest NTE among tetrahedral semiconductors: the thermal expansion coefficient is minimum at about 30 K ($\alpha_{min} \sim -8 \times 10^{-6}\ K^{-1}$), and is negative up to 100 K. The EXAFS structure at the *K* edge of copper in CuCl has been studied as a function of temperature, from 6 to 300 K.

The main results can be summarized as follows:

- While the distance between the average positions of copper and chlorine, measured by Bragg diffraction, undergoes negative expansion below 100 K, the expansion of the Cu-Cl bond length is positive at all temperatures. The difference between EXAFS and Bragg diffraction expansions is due to relative vibrations perpendicular to the Cu-Cl bond. By comparing with the previous results for germanium, one can see that the positive expansion measured by EXAFS is larger for the crystal affected by the stronger NTE.
- The relative thermal vibrations exhibit a marked perpendicular to parallel anisotropy, in contrast with the isotropy of the absolute thermal factors of single atoms measured by Bragg diffraction. The relative anisotropy is reasonably connected to the tension mechanism responsible for NTE. Again, by comparing with the results for germanium, one can see that the anisotropy is larger for the crystal affected by stronger NTE.
- A connection can be established between perpendicular mean square relative displacements (MSRD) and low-energy transverse acoustic modes, which are known to be responsible for NTE in zinc-blende structures.
- The Cu-Cl bond thermal expansion cannot be obtained from the third cumulant. A similar result was found for the nearest-neighbor distances in copper and germanium.

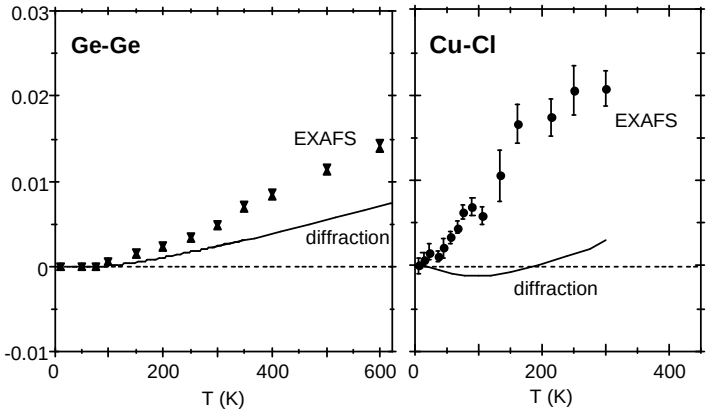

Figure 1
Thermal expansions of the nearest-neighbors distance measured by EXAFS and by Bragg diffraction in Ge and in CuCl.

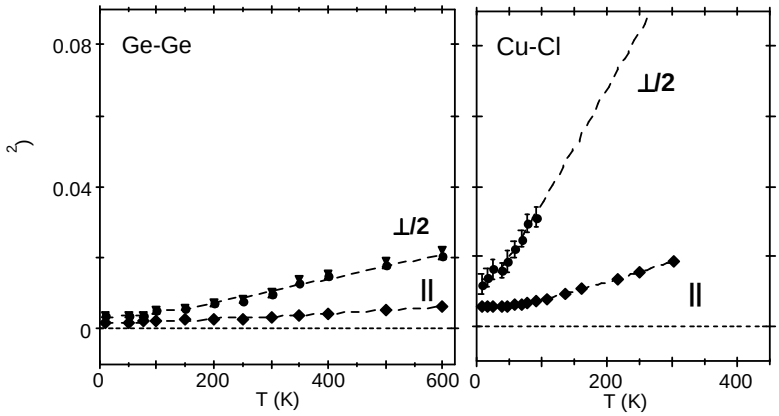

Figure 2
Parallel and perpendicular mean square relative displacements of the nearest-neighbours atomic pair measured by EXAFS in Ge and in CuCl.

I - Instrumentation and data treatment methods

A new procedure for the quantitative analysis of extended x-ray absorption fine structure data in total reflection geometry [IHR]

F. Benzi, I. Davoli, M. Rovezzi, and F. d'Acapito

Review of Scientific Instruments ***79****, 103902 (2008).*

Extended x-ray absorption fine structure (EXAFS) in total reflection mode (reflEXAFS) is an experimental technique that provides local order information around a given atom with high surface sensitivity. This is due to the extremely small extinction length (a few tens of Å) of the evanescent wave appearing when the probe beam shines the sample in total reflection conditions. The noticeable advantage of this technique is that we may use the x-ray absorption spectroscopy (a bulk probe) to investigate surface effects. In particular, the technique permits the analysis of buried interfaces. Applications of reflEXAFS can be found in literature on a variety of fields, namely, chemical reactions at the solid state, surface treatments, and structural studies of thin films. A variety of spectrometers dedicated to this method is available on the major synchrotron radiation sources.

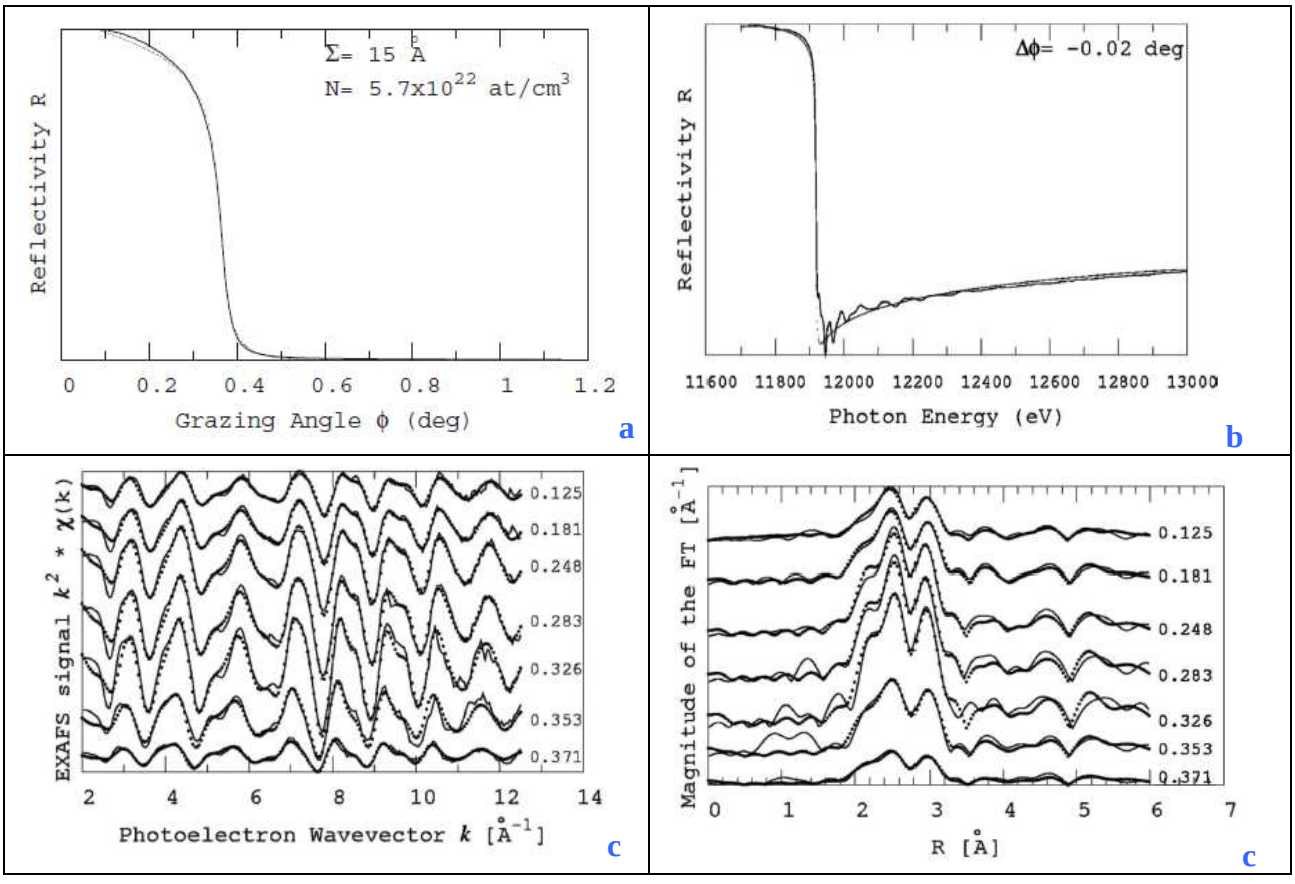

Figure 1

Example of working flow of the program. **a)** fit of the reflectivity at fixes energy **b)** fit of the reflectivity at fixed angle. From these fits the parameters describing the surface (the roughness S, the angular error Δϕ, the density N) are derived. Successively the theoretical EXAFS signals are generated and the fit of the data at any angle are carried out (**c** left and right).The example is relative to a 2000 Å gold film on Si and the nominal collection angle is shown aside. The structural fits are

carried out with a model consisting in Single and Multiple scattering paths up the fourth coordination shell.

The theory of x-ray absorption spectroscopy is presently well understood and it permits the quantitative determination of local structure parameters both from the near edge region as well as from the extended zone. On the other hand no straightforward analysis procedure has been developed for ReflEXAFS data because spectra collected in total reflection mode (i.e., at an incidence angle ϕ smaller than the critical angle for total external reflection ϕ_c) are less straightforward to analyze, since the sample reflectivity R as a function of the photon energy *E* depends in a complex way on both the real δ and imaginary β parts of the refractive index.

A novel general approach has been developed by our group which allows the complete fit of the experimental data. The proposed method consists in three basic steps:

1. determination of sample specific parameters (namely, density and roughness) permitting to reproduce the sample reflectivity both at fixed angle and energy (Fig 1a and 1b).
2. computation of EXAFS theoretical scattering paths with an *ab initio* code and subsequent generation of modified *refl-EXAFS* theoretical scattering paths based on the reflectivity of the sample. Both single- and multiple- scattering paths can be generated.
3. The newly calculated theoretical paths are later used for the fitting of the oscillating part of the reflectivity (Fig. 1c).

With this method multi-shell fits can be carried out permitting a detailed structural description of the sample.

The method is implemented as a PYTHON code and is based on the theoretical calculations of the FEFF program although the procedure is quite general and could be ideally used as well in conjunction with different *ab initio* codes and fitting programs. As a test case the application of this method to reflEXAFS data collected on a gold film, at incidence angles below and above the critical value, is presented in Fig 1. The code is presently being further developed in collaboration with the SciSoft group of ESRF.

VIII. 2004 – 2008 GILDA Publications

a Beccara S., Dalba G., Fornasini P., Grisenti R., Pederiva F., Sanson A., Diop D., and Rocca F.
Local thermal expansion in copper: extended x-ray-absorption fine-structure measurements and path-integral Monte Carlo calculations
Phys. Rev. B 68 (2003) 140301.

a Beccara S., Fornasini P.
Path-integral Monte Carlo calculation of the effect of thermal disorder in EXAFS of copper
Phys. Rev. B 77 (2008) 172304.

Afify N.D., Grisenti R., Dalba G., Armellini C., Ferrari M., Larcheri S., Rocca F., Kuzmin A.
Short-range order around Er^{3+} in silica waveguides containing aluminium, titanium and hafnium
Optical Materials **28**, 864-867, 2006a.

Afify N.D., Dalba G., Mahendra Kumar Poppolu U., Armellini C., Jestin Y., Rocca F.
XRD and EXAFS studies of HfO_2 crystallisation in SiO_2-HfO_2 films.
Materials Science in Semiconductor Processing **9**, 1043, 2006b.

Afify N.D., Dalba G., Rocca F., Ferrari M.
Er^{3+}-activated SiO_2-based glasses and glassceramics: from structure to optimisation
Physics and Chemistry of Glasses **48**, 229-234, 2007a.

Afify N.D., Dalba G., Ferrari M., Rocca F., Armellini C., Kuzmin A.
Local structure around Er3+ in SiO2-HfO2 glassy waveguides using EXAFS
Physical Review B, 24114, 2007b.

Agostini G., Groppo E., Bordiga S., Zecchina A., Prestipino C., d'Acapito F., Van Kimmenade E., Thüne P.C., Niemantsverdriet J.W., Lamberti C.
Reactivity of Cr species grafted on SiO2/Si(100) surface: A reflection extended X-ray absorption fine structure study down to the submonolayer regime
Journal of Physical Chemistry C, **111**, 16437-16444, 2007.

Ahmed S.I., Dalba G., Fornasini P., Vaccari M. Rocca F., Sanson A. Li J., Sleight A.W.
Negative thermal expansion in crystals with the delafossite structure: an EXAFS study of CuScO2 and CuLaO2
Phys. Rev. B 79 (2009) 104302.

Alagna L., Capobianchi A., Paoletti A.M., Pennesi G., Rossi G., Casaletto M.P., Generosi A., Paci B., Albertini V.R.
The effect of NO_2 on spectroscopic and structural properties of evaporated ruthenium phtalocyanine dimer
Thin Solid Films, **515**, 2748-2753, 2006.

Arletti R., Dalconi M.C., Quartieri S., Triscari M., Vezzalini G.
Roman coloured and opaque glass: A chemical and spectroscopic study.
Applied Physics A, **83**, 239-245, 2006°.

Arletti R., Ciarallo A., Quartieri S., Sabatino G. and Vezzalini G.
Archaeometric analyses of game counters from Pompeii,
in Geomaterials in Cultural Heritage, edited by Maggetti M. and Messiga B. Vol. 257, Geological Society, London, Special Publications (The Geological Society of London, London UK) pp. 175-186, 2006b.

Arletti R. Vezzalini G. Quartieri S. Ferrari D. Merlini M. Cotte M.
Polychrome glass from Etruscan sites: First non-destructive characterization with synchrotron μXRF, μXANES and XRPD.
Applied Physics A, **92**, 127-135, 2008a.

Arletti R., S. Quartieri, G. Vezzalini, G. Sabatino, M. Triscari, and M.A. Mastelloni
Archaeometrical analyses of glass cakes and vitreous mosaic tesserae from Messina (Sicily, Italy)
J. non-cryst. Solids **354**, 4962-4969, 2008b.

Arletti R., C. Giacobbe, S. Quartieri, G. Sabatino, G. Tigano, M. Triscari and G. Vezzalini
Archeometrical investigation on Sicilian early bizantine glass: chemical and spectroscopic data

Archaeometry, **50**, 1-12, 2008c.

Artioli G., Dapiaggi M., Fornasini P., Sanson A., Rocca F., Merli M.
Negative thermal expansion in cuprite-type compounds: A combined synchrotron XRPD, EXAFS, and computational study of Cu2O and Ag2O
J. Phys. Chem. Solids, **9-10** (2006) 1918.

Bardelli F., Meneghini C., Mobilio S., Castellano C., Dediu V.
Charge ordering and local structure in manganese oxide perovskites studied by EXAFS
Nucl. Inst. and Methods in Phys. Res. B**200**, 226-230, 2003.

Bardelli F., Meneghini C., Mobilio S., Ray S., Sarma D.D.
Local structure of $Sr_2FeMo_xW_{1-x}O_6$ double perovskites studied by EXAFS
Physica Scripta **T115** 457-458 (2005).

Bardelli F., Meneghini C., Mobilio S., Ray S., Sarma D.D.
XAFS study on $Sr_2FeMo_xW_{1-x}O_6$ double perovskite series
Mat. Sc. and Eng. B **126**, 226-229 (2006).

Barilaro D., V. Crupi, D. Majolino, V. Venuti, G. Barone, F. D'Acapito F. Bardelli F. Giannici.
Decorated pottery study: Analysis of pigments by x-ray absorbance spectroscopy measurements.
Journal of Applied Physics. **101**, 64090, 2007 .

Battocchio C., D'Acapito F., Smolentsev G., Soldatov A.V., Fratoddi I., Contini G., Davoli I., Polzonetti G., Mobilio S.
XAS study of a Pt-containing rod-like organometallic polymer
Chemical Physics, **325**, 422-428, 2006a.

Battocchio C., D'Acapito F., Fratoddi I., La Groia A., Polzonetti G., Roviello G., Russo M.V.
Platinum (II) dialkynyl bridged binuclear complex and related multinuclear oligomer: comparison of EXAFS and X-ray crystal structure studies
Chemical Physics, **328**, 269-274, 2006b.

Battocchio C., Fratoddi I., Russo M.V., Polzonetti G.
H_2S gas interaction with Pt(II)-containing polymetallaynes of selected chain lenght: an XPS and EXAFS study
Journal of Physical Chemistry A, **112**, 7365-7373, 2008.

Bazzanella N., Checchetto R., Miotello A., D'Acapito F., Maurizio C., Barucca G., Majni G., Mengucci P.
Kinetics of hydrogen absorption and desorption in magnesium: role of the structure and of catalysts.
in Advanced materials for energy conversion III, Warrendale, Pa.: TMS, p. 89-99, ISBN: 978-0-87339-610-3, 2006.

Benfatto, M., Della Longa, S., Qin, Y., Li, Q., Pan, G., Wu, Z., Morante, S.
The role of Zn in the interplay among LangmuirÐBlodgett multilayer and myelin basic protein: A quantitative analysis of XANES spectra
Biophys. Chem. **110**, 191-201, 2004.

Benzi, I. Davoli, M. Rovezzi, F. d'Acapito
A new procedure for the quantitative analysis of extended x-ray absorption fine structure data in total reflection geometry
Rev. of Sci. Instrum. **79**, 103902, 2008.

Berlier G., Prestipino C., Rivallan M., Bordiga S., Lamberti C., Zecchina A.
Behavior of extraframework Fe sites in MFI and MCM-22 zeolites upon interaction with N2O and NO.
Journal of Physical Chemistry B **109**, 22377-22385, 2005a

Berlier G., Pourny M., Bordiga S., Spoto G., Zecchina A., Lamberti C.
Coordination and oxidation changes undergone by iron species in Fe-MCM-22 upon template removal, activation and redDox treatments: An in situ IR, EXAFS and XANES study
Journal of Catalysis, **229**, 45-54, 2005b.

Beukes J.A., Mo F., van Beek W.
X-Ray induced radiation damage in taurine: a combined X-ray diffraction and Raman study
Physical Chemistry - Chemical Physics **9**, 4709-4720, 2007.

Bombardi A., d'Acapito F., Mattenberger K., Vogt O., Lander G.H.
Non-Vegard behavior of the $U_xLa_{1-x}S$ system
Phys. Rev. B **68**, 104414, 2003.

Bonanni A., A. Navarro-Quezada, Tian Li, M. Wegscheider, Z. Matěj, V. Holý, R. T. Lechner, G. Bauer, M. Rovezzi, F. D'Acapito, M. Kiecana, M. Sawicki, and T. Dietl
Controlled Aggregation of Magnetic Ions in a Semiconductor: An Experimental Demonstration,
Phys. Rev. Lett. **101**, 135502, 2008a.

Bonanni A., A. Navarro-Quezada, T. Li, M. Wegscheider, Z. Matey, V. Holy, R.T. Lechner, G. Bauer, M. Rovezzi, F. D'Acapito, M. Kiecana, M. Sawicki, and T. Dietl,
Controlled aggregation of magnetic cations in a semiconductor nitride matrix
ESRF Highlights, **2008**, 93-94, 2008b.

Bordiga S., Bonino F., Damin A., Lamberti C.
Reactivity of Ti(IV) species hosted in TS-1 towards H2O2-H2O solutions investigated by ab initio cluster and periodic approaches combined with experimental XANES and EXAFS data: a review and new highlights
Physical Chemistry - Chemical Physics, **9**, 4854-4878, 2007.

Borghi, E., Solari, L.
Multiple-scattering XAS calculations for the characterization of the binuclear (type 3) copper sites of hemocyanins and related model compounds
J. Synchrotron Rad. **12**, 102-110, 2005.

Boscherini F., M., Ciatto G., d'Acapito F., Bisognin G., De Salvador D., Berti M., Felici M., Polimeni A., Nabetani Y.
X-ray absorption and diffraction study of II-VI dilute oxide semiconductor alloy.
Journal of Physics Condensed Matter **19**, 446201, 2007.

Boscherini F.
X-ray absorption fine structure in the study of semiconductor heterostructures and nanostructures,
in: "Characterization of Semiconductor Heterostructures and Nanostructures", chapter 9, Lamberti C. (Ed.), Elsevier 2008.

Brigatti M.F., Colonna S., Malferrari D., Medici L.,
Characterization of Cu-complexes in smectite with different layer charge location: Chemical, thermal and EXAFS studies.
Geochim. Cosmochim. Acta **68**, 781-788, 2004.

Brigatti M.F., Colonna S., Malferrari D., Medici L., Poppi L.
Mercury adsorption by montmorillonite and vermiculite: A combined XRD, TG-MS, and EXAFS study.
Applied Clay Science **28**, 1-8, 2005.

Buscaglia M.T., Buscaglia V., Ghigna P., Viviani M., Spinolo G., Testino A., Nanni P.
Amphoteric behaviour of Er^{3+} dopants in $BaTiO_3$: An Er L_{III}- edge EXAFS assessment
Physical Chemistry - Chemical Physics 6, 3710-3713, 2004.

Capellas Espuny M.
Different minerals dictate colour of glass.
ESRF Newsletter, 44, 13 (2006)

Capellini G., M. De Seta, L. Di Gaspare, F. Evangelisti, and F. D'Acapito
Evolution of Ge/Si(001) islands during Si capping at high temperature,
J. Appl. Phys. **98**, 124901-124908, 2005.

Cardelli A., Cibin G., Benfatto M., Della Longa S., Brigatti M.F., Marcelli A.
A crystal-chemical investigation of Cr substitution in muscovite by XANES spectroscopy.
Physics and Chemistry of Minerals, **30**, 54-58, 2003

Cartechini L. Miliani C. Brunetti B.G. Sgamellotti A. Altavilla C. Ciliberto E. d'Acapito F.
X-ray absorption investigations of copper resinate blackening in a XV century Italian painting
Applied Physics A, **92**, 243-250, 2008.

Cattaneo A., Gualtieri A.F., Artioli G.
Kinetic study of the dehydroxylation of chrysotile asbestos with temperature by in situ XRPD.
Physics and Chemistry of Minerals. **30**, 177-183, 2003.

Cattaruzza E., Battaglin G., Gonella F., Maurizio C., Ali S., Trave E.
Doping of silicate glasses with erbium by a field-assisted solid-state ion exchange technique
Journal of Physics D: Applied Physics **47**, 045301-5, 2009.

Cesca T., Gasparotto A., Mattei G.,Rampazzo V., Boscherini F.,Fraboni B., Priolo F., Ciatto G., d'Acapito F., Bocchi C.
Atomic environment of Fe following high-temperature implantation in InP
Physical Review B **68**, 224113-1-224113-11, 2003.

Cesca T., Gasparotto A., Mattei G., Fraboni B., Boscherini F., Longo M., Tarricone L.
Local structure of Fe incorporated in GaInP layers by high temperature ion implantation
Nuclear Instruments and Methods in Physics Research B **257**, 332-335 (2007).

Checchetto R., Bazzanella N., Miotello A., Maurizio C., d'Acapito F., Mengucci P., Barucca G., Majni G.
Nb clusters formation in Nb-doped magnesium hydride
Applied Physics Letters **87**, 061904-1, 2005.

Ciatto G., d'Acapito F., Fraboni B., Boscherini F., El Habra N., Cesca T., Gasparotto A., Moreira E.C., Priolo F.
Local structure of iron implanted in indium phosphide.
Nuclear Instruments and Methods in Physics Research B **200**, 100-104, 2003a.

Ciatto G., Boscherini F., d'Acapito F., Mobilio S., Baldassarri H.V.H.G., Polimeni A.,Capizzi M., Gollub D., Forchel A.
Atomic ordering in (InGa)(AsN) quantum wells: An In K-edge X-ray absorption investigation.
Nuclear Instruments and Methods in Physics Research B **200**, 34, 2003b.

Ciatto G., d'Acapito F., Grenouillet P., Mariette H., De Salvador D., Bisognin G., Carboni R., Floreano L., Gotter R., Mobilio S., Boscherini F.
Quantitative determination of short-range ordering in InGaAsN.
Physical Review B **68**, 161201 [Rapid Communication] 2003c.

Ciatto G.
Structure locale des nitrures d'elements III-V et effets des traitements post-croissance.
Universitè de Grenoble PHD thesis, 2004a.

Ciatto G., d'Acapito F., Boscherini F., Mobilio S.
Treatment of EXAFS data taken in the fluorescence mode in non-linear conditions
Journal of Synchrotron Radiation **11**, 278-283, 2004b

Ciatto G., d'Acapito F., Boscherini F., Mobilio S.
Response to W. K. Warburton's Comments on Treatment of EXAFS data taken in the fluorescence mode in non-linear conditions by G. Ciatto et al. (2004). J. Synchrotron Rad. 11, 278–283
Journal of Synchrotron Radiation **11**, 509, 2004c

Ciatto C., d'Acapito F., Sanna S., Fiorentini V., Polimeni A., Capizzi M., Mobilio S., Boscherini F.
Comparison between experimental and theoretical determination of the local structure of the GaAsN dilute nitride alloy.
Physical Review B **71**, 115210, 2005a.

Ciatto G., Renevier H., Proietti M.G., Polimeni A., Capizzi M., Mobilio S., Boscherini F.
Effects of hydrogenation on the local structure of InGaAsN quantum wells and GaAsN epilayers.
Physical Review B **72**, 085322, 2005b.

Ciatto G., Harmand J., Glas F., Largeau L., LeDu M., Boscherini F., Malvestuto M., Floreano L., Glatzel P., Mori R.A.
Anion relative location in the group-V sublattice of GaAsSbN/GaAs epilayers: XAFS measurements and simulations.
Physical Review B **75**, 245212, 2007.

Colella C., Gualtieri A.F.
Cronstedt's zeolite.
Microporous and Mesoporous Materials, **105**, 213-221, 2007

Comaschi T. Balerna A. Mobilio S.,
Temperature dependence of the structural parameters of gold nanoparticles investigated with EXAFS
Physical Review B **77**, 075432-1, 2008.

Comotti A., Bracco S., Valsesia P., Ferretti L., Sozzani P.
2D multiniclear NMR, hyperpolarized xenon and gas storage in organisilica nanochannels with crystalline order in the walls
Journal of the American Chemical Society, **129**, 8566-8576, 2007.

Corami A., d'Acapito F., Mignardi S., Ferrini V.
Removal of Cu from aqueous solutions by synthetic hydroxyapatite: EXAFS investigation.
Materials Science and Engineering B **149**, 209-213, 2008.

Costagliola P., Bardelli F., Benvenuti M., Di Benedetto F., Lattanzi P., Meneghini C., Romanelli M.
Arsenic uptake by natural calcite: a XAS study.
1st SIMP-AIC Joint Mtg, Sestri Levante (GE), 7-12 Sept. 2008

Cremonesi A., Calestani G., Antonioli G., Bersani D., Lottici P.P., Djaoued Y., BrYning R
XAS analysis on mesoporous vanadium oxide thin films by sol-gel
X-ray Spectrometry, **36**, 226-229, 2007.

Cruciani G., Martucci A., Meneghini C.
Dehydration dynamics of epistilbite by in situ time resolved synchrotron powder diffraction.
European Journal of Mineralogy. **15**, 257-266, 2003.

Cruciani G.
Zeolites upon heating: Factors governing their thermal stability and structural changes.
Journal of Physics and Chemistry of Solids **67**, 1973-1994, 2006.

D'Acapito F., Mobilio S., Scalese S., Terrasi A., Franzò G., Priolo F.,
Structure of Er-O complexes in crystalline Si
Physical Review **B69**, 153310-1-4, 2004a.

D'Acapito F., Maurizio C., Malvestuto M.
The atomic site of As implanted in Si at ultra-low energies
Materials Science and Engineering B **114-115**, 386-389, 2004b.

D'Acapito F.
Nearest-neighbor distances in strained thin films of random pseudobinary semiconductor alloys: A calculational methodology,
J. Appl. Phys. **96** , 369-373, 2004c

D'Acapito F., Fratoddi I., D'Amato R., Russo M.V., Contini G., Davoli I., Mobilio S., Polzonetti G.
Structure of a monolayer of Pd-diethynylbiphenyl deposited on chromium studied by total reflection EXAFS
Sensors and Actuators B **100**, 131-134, 2004d.

D'Acapito F., Maurizio C.
Applications of low-temperature detectors to synchrotron radiation
Nuclear Instruments and Methods in Physics Research A **520**, 602-605, 2004e.

D'Acapito F., Mobilio S., Terrasi A., Scalese S., Franzò G., Priolo F.
Local order around Er3+ ions in thin silicon oxide layers grown in Si by MBE
Physica Scripta 2005, **T115**, 384-386.

D'Acapito F., Shimizu Y., Scalese S., Italia M., Alippi P., Grasso S.
The effect of thermal treatments on the local geometry around indium in In and In + C high dose implanted Si.
Nuclear Instruments and Methods in Physics Research B **253**, 59, 2006a.

D'Acapito F., Shimizu Y., Scalese S., Italia M., Alippi P., Grasso S.
Experimental determination of the local geometry around In and In – C complexes in Si.
Applied Physics Letters **88**, 212102, 2006b.

D'Acapito F., G. Smolentsev, F. Boscherini, M. Piccin, G. Bais, S. Rubini, F. Martelli, and A. Franciosi
Site of Mn in Mn-doped GaAs: X-ray absorption spectroscopy
Phys. Rev. B **73**, 035314 (1-6), 2006c.

D'Acapito F., M. de Seta, G. Capellini, L. di Gaspare, F. Evangelisti
Relaxed state of $Ge_xSi_{1\_x}$ islands embedded in Si
Nucl. Instrum. and Meth. B **246**, 64–68, 2006d

D'Acapito F., Francini R., Pietrantoni S., Barbier D.
The site of Er in phosphate glasses studied by K-edge EXAFS'
AIP Conference Proceedings 2007, 882, 401-403, 2007a.

D'Acapito F., S. Milita, A, Satta, L. Colombo
Depth resolved study of impurity sites in low energy ion implanted As in Si,
ESRF Highlights 2007b.

D'Acapito F., S. Milita, A, Satta, L. Colombo
Depth resolved study of impurity sites in low energy ion implanted As in Si
J. Appl. Phys. **102**, 43524, 2007c

D'Acapito F, Maurizio C, Brunetti B, Cartechini L, Sgamellotti A, Quartieri S, Arletti R..
Archaeometric studies at the GILDA beamline at the European Synchrotron Radiation Facility.
Nuovo Cimento C, **30**; 1, 2007d.

D'Acapito F., Golosio B., Shimizu Y., Scalese S., Italia M., Alippi P., Grasso S.
The site of In dopants in Si
AIP Conference Proceedings **882**, 375-377, 2007e.

D'Acapito F., Maurizio C., Paul M.C., Lee T.S., Blanc W., Dussardier B.
Role of CaO addition in the local order around Erbium in SiO_2-GeO_2-P_2O_5 fiber preforms
Material Science Engeneering B146, 167-170, 2008.

Dalba G., Fornasini P., Kuzmin A., Monti F., Sanson A., Sipr O., Rocca F.
XANES and EXAFS Modeling of Configurational Disorder in Silver Borate Glasses
Physica Scripta, **T115**, 149, 2005.

Dalba G., Afify N.D., Rocca F.
X-ray absorption spectroscopy studies of glass structure
Phys. Chem. Glasses: Eur. J. Glass Sci. Technol. B, 49, 149–159, 2008c.

Dalconi M.C., Cruciani G., Alberti A., Ciambelli P.
Over-loaded Cu-ZSM-5 upon heating treatment: A time resolved X-ray diffraction study
Microporous and Mesoporous Materials **94**, 139-147, 2006.

De Seta M., G. Capellini, L. Di Gaspare, F. Evangelisti, F. D'Acapito
Freezing shape and composition of Ge/Si(001) self-assembled islands during silicon capping,
J. Appl. Phys. **100**, 093516, 2006.

De Sio A. Bocci A. Pace E. Castellano C. Cinque G. Tartoni N. d'Acapito F.
Diamond solid state ionization chambers for x-ray absorption spectroscopy applications
Applied Physics Letters **93**, 083503, 2008.

Deganello G., Longo A., Prestianni A., Liotta L., Macaluso A., Pantaleo G., Balerna A., Mobilio S.
Structural evolution of Pt/ceria-zirconia TWC catalysts during the oxidation of carbon monoxide.
Journal of Solid State Chemistry, **177**, 1268-1275 (2004).

Deganello G., Giannici F., A., Pantaleo G., Prestianni A., Balerna A., Liotta L.F., Longo A.

Metal-support interaction and redox behavior of Pt(1 wt %)/Ce0.6Zr0.4O2.
Journal of Physical Chemistry B **110**, 8731-8739, 2006.

Del Bianco L. Boscherini F. Fiorini A.L. Tamisari M. Spizzo F. Vittori Antisari M. Piscopiello E.
Exchange bias and structural disorder in the nanogranular Ni/NiO system produced by ball milling and hydrogen reduction
Phys. Rev. B**77,** 094408/1-12 (2008).

Del Bianco L. Boscherini F. Tamisari M. Spizzo F. Vittori Antisari M. Piscopiello E.
Exchange bias and interface structure in the Ni/NiO nanogranular system
J. of Phys. D **41**, 134008/1-7 (2008).

Dezanneau G., Audier M., Vincent H., Meneghini C., Djurado E.
Structural characterization of $La_{1-x}Ca_xMnO_{3\pm\square}$ by X-ray diffraction and X-ray absorption spectroscopy
Phys. Rev. B **69,** 014412/1-11, 2004.

Diaz J., Morales R., Valvidares S.M., Alameda J.M.
Phase separation in Fe-Si and Co-Si sputtered ferromagnetic alloys and the origin of their magnetic anisotropy
Phys. Rev. B **72**, 144413/1-15 (2005).

Dubiel M., Yang X.C., Brunsch S.
Investigation of stress state of silver nanoparticles in silicate glasses by means of EXAFS
Physica Scripta T **115**, 729-732, 2005.

El Habra N., Crociani L., Sada C., Zanella P., Casarin M., Rossetto G., Carta G., Paolucci G.
MOCVD of CoAl2O4 thin films from {Co[Al(OiC3H7)4]2} as precursor.
Chemistry of Materials **19**, 3381-3386, 2007.

Falciola L., Longoni G., Mussini P.R., Mussini T.
Thermodynamics of the amalgam cells {Cs-amalgam|CsX (m)|AgX|Ag} (X = Cl, Br, I) and primary medium effects in (methanol + water), (acetonitrile + water), and (1,4-dioxane + water) solvent mixtures
Journal of Chemical Thermodynamics 38 (2006) 788.

Fernandez-Martinez A., Roman-Ross G., Cuello G.J., Turrillas X., Charlet L., Johnson M.R., Bardelli F.
Arsenic uptake by gypsum and calcite: Modelling and probing by neutron and X-ray scattering.
Physica B**385-386**, 935-937, 2006.

Ferruti P., Ranucci E., Bianchi S., Falciola L., Mussini P.R., Rossi M.
Novel polyamidoimine-based hydrogel with an innovative molecular architecture as a Co^{2+} -, Ni^{2+} - and Cu^{2+} -sorbing material:cyclovoltammetry and extended X-ray absorption fine structure studies
Journal of Polymer Science A: Polymer Chemistry, **44**, 2316-2327, 2006.

Fornasini P., a Beccara S., Dalba G., Grisenti R., Sanson A., Vaccari M., and Rocca F.
Extended x-ray-absorption fine-structure of copper: local dynamics, anharmonicity and thermal expansion, s Phys. Rev. B **70**, 174301, 2004.

Fornasini P., Dalba G., Grisenti R., Purans J., Sanson A., Vaccari M., Rocca F.
EXAFS studies of lattice dynamics and thermal expansion
Physica Status Solidi (c) **11**, 3085, 2004.

Fornasini P., a Beccara S., Dalba G., Grisenti R., Purans J., Sanson A., Rocca F., Diop D.
EXAFS and local thermal expansion
Physica Scripta, **T115**, 143, 2005.

Fornasini P., Dalba G., Grisenti R., Purans J., Vaccari M., Rocca F., Sanson A.
Local behaviour of negative thermal expansion materials
Nucl. Instrum. Meth. Phys. Res. B **246**, 180, 2006.

Fornasini P., Sanson A., Vaccari M., Artioli G., Dapiaggi M.
Local lattice dynamics and negative thermal expansion in crystals,
J. Phys. Conf. Series **92**, 012153, 2007.

Fornasini P., Ahmed S.I, Sanson A. Vaccari M.
EXAFS studies of negative thermal expansion materials
Phys. Stat. Sol. (b) **11**, 2497, 2008

Fortes L.M., Santos L.F., Gonzalves M.C., Almeida R.M., d'Acapito F.
Influence of Er3+ on the early stages of crystallization of chloro-tellurite glasses studied by XRD and EXAFS
Journal of Non-Crystalline Solids **348**, 11-16, 2004.

Fraboni B., Cesca T., Gasparotto A., Mattei G., Boscherini F., Impellizzeri G., Priolo F., Jakomin R., Longo M., Tarricone L.
Electrical and structural characterization of Fe implanted GaInP
Physica B **401-402**, 278-281, 2007.

Francia, F., Giachini, L., Boscherini, F., Venturoli, G., Capitanio, G., Martino, P.L., and S. Papa:

FEBS Lett. **581**, 611-616, 2007.

Garcia P., Martin P., Carlot G., Castelier E., Ripert M., Sabatier C., Valot C., d'Acapito F., Hazemann J.L., Proux O., Nassif V.
"A study of xenon aggregates in uranium dioxide using X-ray absorption spectroscopy".
Journal of Nuclear Materials, **352**, 136-143, 2006.

Gemmi M., Merlini M., Cornaro U., Ghisletti D., Artioli G.
In situ simultaneous synchrotron powder diffraction and mass spectrometry study of methane anaerobic combustion on iron-oxide-based oxygen carrier.
Journal of Applied Crystallography **38**, 353-360, 2005.

Ghigna P., Spinolo G., Santacroce E., Colonna S., Mobilio S., Scavini M., Bianchi R.:
Local structure around Ce in the $Nd_{2-x}Ce_xCuO_{4\pm\delta}$ superconductor probed by EXAFS
Eur. Phys. J. B **41**, 31, 2004.

Ghigna P., Marzola A., Amantea R., Malavasi L., Flor G., d'Acapito F., Bardelli F., Mozzati M.C
Local structure and electronic properties in colossally magnetoresistive thin film of $La_{0.87}Na_{0.13}MnO_3$ by Mn-K edge EXAFS and XANES
Nucl. Inst. and Methods in Phys. Res. B **238,** 242-247, 2005.

Ghigna P., Spinolo G., Parravicini G.B., Stella A., Migliori A., Kofman R.,
Metallic versus covalent bonding: Ga nanoparticles as a case study
Journal of the American Chemical Society **129**, 8026-8033, 2007.

Giachini, L., Francia, F., Mallardi, A., Palazzo, G., Carpenè, E., Boscherini, F., Venturoli, G.
Multiple scattering X-ray absorption studies of Zn2+ binding sites in bacterial photosynthetic reaction centers
Biophys. J. **88**, 2038-2046, 2005.

Giachini, L., Francia, F., Veronesi, G., Lee, D.W., Daldal, F., Huang, L.S., Berry, E.A., Cocco, T., Papa, S., Boscherini, F. and G. Venturoli
X-Ray Absorption Studies of Zn^{2+} Binding Sites in Bacterial, Avian, and Bovine Cytochrome bc_1 Complexes
Biophys. J. **93**, 2934-2951, 2007a.

Giachini, L., Francia, F., Cordone, L., Boscherini, F. and G. Venturoli
Cytochrome C in a dry trehalose matrix: structural and dynamical effects probed by x-ray absorption spectroscopy.
Biophys. J. **92**, 1350-1460, 2007b.

Giachini, L., Francia, F., Boscherini, F., Pacelli, C., Cocco, T., Papa, S., Venturoli, G.
EXAFS reveals a structural zinc binding site in the bovine NADH-Q oxidoreductase
FEBS Lett. **581**, 5645-5648, 2007c.

Giannici F., Longo A., Deganello F., Balerna A., Arico A.S., Martorana A.
"Local environment of barium, cerium and yttrium in BaCe1-xYxO3-delta ceramic protonic conductors".
Solid State Ionics, **178**, 587-591, 2007a.

Giannici F., Longo A., Balerna A., Kreuer K.D., Martorana A.

"Indium doping in barium cerate: The relation between local symmetry and the formation and mobility of protonic defects".
Chemistry of Materials, 19, 5714-5720, 2007b.

Girasole, M., Arcovito, A., Marconi, A., Davoli, C., Congiu Castellano, A., Bellelli, A., Amiconi, G.
Control of the active site structure of giant bilayer hemoglobin from the Annelid Eisenia foetida using hierarchic assemblies
Appl. Phys. Lett. **87**, 233901, 2005.

Giubertoni D., Pepponi G., Bersani M., Gennaro S., d'Acapito F., Doherty R., Foad M.A.
An EXAFS investigation of arsenic shallow implant activation in silicon after laser sub-melt annealing.
Nuclear Instruments and Methods in Physics Research B **253**, 38694, 2006.

Giuli G., Paris E., Mungall J., Romano C., Dingwell D.
V oxidation state and coordination number in silicate glasses by XAS.
American Mineralogist **89**, 1640-1646, 2004.

Gonella F., Quaranta A., Padovani S., Sada C., d'Acapito F., Maurizio C., Battaglin G., Cattaruzza E.
Copper diffusion in ion-exchanged soda-lime glass
Applied Physics **A81**, 1065-1071, 2005a.

Gonella F., Quaranta A., Cattaruzza E., Padovani S., Sada C., d'Acapito F., Maurizio C.
Cu-alkali ion exchange in glass: A model for the copper diffusion based on XAFS experiments
Computational Materials Science **33**, 31-36, 2005b

Groppo E., Lamberti C., Bordiga S., Spoto G., Zecchina A.
The structure of active centers and the ethylene polymerization mechanism on the Cr/SiO2 catalyst: A frontier for the characterization methods
Chemical Reviews, **105**, 115-183, 2005a.

Groppo E., Prestipino C., Cesano F., Bonino F., Bordiga S., Lamberti C.,Thüne P, Niemantsverdriet J.W., Zecchina A.
In situ Cr K-edge XAS study on the Phillips catalyst: Activation and ethylene polymerization
Journal of Catalysis **230**, 98-108, 2005b.

Groppo E., Lamberti C., Cesano F., Zecchina A.
On the fraction of CrII sites involved in the C2H4 polymerization on the Cr/SiO2 Phillips catalyst: a quantification by FTIR spectroscopy
Physical Chemistry - Chemical Physics **8**, 2453-2456, 2006.

Gunnella R., L. Morresi, N. Pinto, R. Murri, L. Ottaviano, M. Passacantando, F. D'Orazio, F. Lucari
Magnetization of epitaxial MnGe alloys on Ge(1 1 1) substrates,
Surf. Sci. **577**, 22-30, 2005.

Gupta A., Paul A., Gupta M., Meneghini C., Pietsch U., Mibu K., Maddalena A., Dal ToŽ S., Principi G.
Structural characterization of epitaxial Fe/Cr multilayers using anomalous X-ray and neutron reflectivity.
J. of Magn. and Magn. Mat. **272-276**, 1219-1220, 2004.

Karlsson C., Meneghini C., Swenson J.
Structural properties determining the ionic conductivity of CsI-doped $AgPO_3$ glasses.
Phys. Rev. B **69**, 224209, 2004.

Kulkarni S.R., Merlini M., Phatak N., Saxena S.K., Artioli G., Gupta S., Barsoum M.W.
High-temperature thermal expansion and stability of V2AlC up to 950 °C.
Journal of the American Ceramic Society **90**, 3013-3016, 2007.

Kuzmin A., Dalba G., Fornasini P., Rocca F., Šipr O.
X-ray absorption spectroscopy of strongly disordered glasses: Local structure around Ag ions in g-$Ag_2O{\cdot}nB_2O_3$.
Phys. Rev. B **73**, 174110, 2006.

Lamberti C.
The use of synchrotron radiation in the characterization of strained semiconductor heterostructures and thin films.
Surface Science Reports **53**, 1-197, 2004.

Larcheri S., Armellini C.,Rocca F., Kuzmin A.,Kalendarev R.,Dalba G., Graziola R., Purans J., Pailharey D., Jandard F.
X-ray studies on optical and structural properties of ZnO nanostructured thin films
Superlattices and Microstructures, **39**, 267-274, 2006.

Lassinanti Gualtieri M., Andersson C., Jareman F., Hedlund J., Gualtieri A.F., Leoni M., Meneghini C.
Crack formation in alpha-alumina supported MFI zeolite membranes studied by in situ high temperature synchrotron powder diffraction.
Journal of Membrane Science **290**, 95-104, 2007.

Liotta L.F., Longo A., Macaluso A., Martorana A., Pantaleo G., Venezia A.M., Deganello G.
Influence of the SMSI effect on the catalytic activity of a Pt(1%)/Ce0.6Zr0.4O2 catalyst: SAXS, XRD, XPS and TP investigations.
Applied Catalysis B: Environmental **48**, 133-149, 2004.

Liscio F., Bardelli F., Meneghini C., Mobilio S., Ray S., Sarma D.D.
Local structure and magneto-transport in Sr_2FeMoO_6 oxides
Nucl. Inst. and Methods in Phys. Res. B **246**,189-193, 2006.

Loglio F., M. Innocenti, F. D'Acapito, R. Felici, G. Pezzatini, E. Salvietti and M.L. Foresti
Cadmium selenide electrodeposited by ECALE: electrochemical characterization and preliminary results by EXAFS
Journal of Electroanalytical Chemistry, Volume **575**, Pages 161-167, 2005.

Loglio F., Innocenti M., Salvietti E., Pezzatini G., Felici R., d'Acapito
Ternary CdxZn1-xSe nanocrystals deposited on Ag(111) by ECALE: Electrochemical and EXAFS characterization.
Electrochimica Acta **53** 6978–6987, 2008.

Longo A., Balerna A., d'Acapito F., D'Anca F., Giannici F., Liotta L.F., Pantaleo G., Martorana A.
A new cell for the study of in situ chemical reactions using X-ray absorption spectroscopy
Journal of Synchrotron Radiation **12**, 499-505, 2005.

Longo A., Giannici F., Balerna A., Ingrao C., Deganello F., Martorana A.
"Local environment of yttrium in Y-doped barium cerate compounds".
Chemistry of Materials, **18**, 5782-5788, 2006.

Longo A. Martorana A.,
Distorted f.c.c. arrangement of gold nanoclusters: a model of spherical particles with microstrains and stacking faults
Journal of Applied Crystallography **41**, 446-455, 2008.

Luches P., Bellini V., Colonna S., Di Giustino L., Manghi F., Valeri S., Boscherini F.
Iron oxidation, interfacial expansion, and buckling at the Fe/NiO(001) interface
Phys. Rev. Lett. **96**, 106106/1-4 (2006).

Maggioni G., Carturan S., Tonezzer M., Bonafini M., Vomiero A., Quaranta A., Maurizio C., Giannici F., Scandurra A., D'Acapito F., Della Mea G., Puglisi O.
Effects of heat treatments on the properties of copper phtalocyanine films deposited by glow-discharge-induced sublimation
Chemistry of Materials, **18**, 4195-4204, 2006.

Malavasi L., Mozzati M.C., Di Tullio E., Tealdi C., Flor G.
Redox behavior of Ru-doped $La_{1-x}Na_xMnO_{3+\delta}$ manganites
Phys. Rev. B **71**, 174435/1-5, 2005.

Malavasi L., Mozzati M.C., Tealdi C., Azzoni C.B., Flor G.
Oxygen content variation and cation doping dependence of $(La)_{1.4}(Sr_{1-y}Ca_y)_{1.6}Mn_2O_{7\pm\delta}$ (y=0,0.25,0.5) bilayered manganites
Phys. Rev. B **74**, 064104/1-15, 2006.

Malferrari D., Brigatti M.F., Laurora A., Pini S., Medici L.
Sorption kinetics and chemical forms of Cd(II) sorbed by thiol-functionalized 2:1 clay minerals.
Journal of Hazardous Materials **143**, 73-81, 2007.

Malvestuto M., Carboni R., Boscherini F., d'Acapito F., Spiga S., Fanciulli M., Dimoulas A., Vellianitis G., Mavrou G.
X-ray absorption study of the growth of Y_2O_3 on Si(001).
Physical Review B **71**, 075318, 2005.

Malvestuto M., Scarel G., Wiemer C., Fanciulli M., d'Acapito F., Boscherini F.
X-ray absorption spectroscopy study of Yb_2O_3 and Lu_2O_3 thin films deposited on Si(100) by atomic layer deposition.
Nuclear Instruments and Methods in Physics Research B **246**, 90, 2006.

Marmiroli M., Antonioli G., Maestri E., Marmiroli N.
Evidence of the involvement of plant ligno-cellulosic structure in the sequestration of Pb: An X-ray spectroscopy-based analysis.
Environmental Pollution **134**, 217-227, 2005.

Martelli F., Rubini S., Piccin M., Bais G., Jabeen F., De Franceschi S., Grillo V., Carlino E., d'Acapito F., Boscherini F., Cabrini S., Lazzarino M., Businaro L., Romanato F., Franciosi A.
Manganese-induced growth of GaAs nanowires
Nano Letters **6**, 2130-2134, 2006.

Martucci A., Alberti A., Cruciani G., Frache A., Marchese L., Pastore H.O.
Temperature-induced transformations in CoAPO-34 molecular sieve: A combined in situ X-ray diffraction and FTIR study.
Journal of Physical Chemistry B **109**, 13483-13492, 2005.

Martucci A., Guzman-Castillo M.D.L., Di Renzo F., Fajula F., Alberti A.
Reversible channel deformation of zeolite omega during template degradation highlighted by in situ time-resolved synchrotron powder diffraction.
Microporous and Mesoporous Materials **104**, 257-268, 2007.

Mattei G., Battaglin G., BelloV., Cattaruzza E.,De Julian C.,De Marchi G.,Maurizio C.,Mazzoldi P.,Parolin M., Sada C.
Compositional evolution of Pd-based nanoclusters under thermal annealing in ion implanted SiO_2.
Nuclear Instruments and Methods in Physics Research B **218**, 433-437, 2004a

Mattei G., Maurizio C., Sada C., Mazzoldi P., de Julian Fernandez C., Cattaruzza E., Battaglin G.
Au-Cu and Pd-Cu nanoclusters obtained by ion implantation in silica: Stability under thermal annealing.
Journal of Non-Crystalline Solids **345-346**, 667-670, 2004b

Mattei G., Maurizio C., Mazzoldi P., d'Acapito F., Battaglin G., Cattaruzza E., de Julian Fernandez C., Sada C.
Dynamics of compositional evolution of Pd-Cu alloy nanoclusters upon heating in selected atmospheres
Physical Review B **71**, 195418- 1,2005.

Mattei G., Battaglin G., Cattaruzza E., Maurizio C., Mazzoldi P., Sada C., Scremin B.F.,
Synthesis by co-sputtering of Au-Cu alloy nanoclusters in silica
Journal of Non-Crystalline Solids **353**, 697-702, 2007.

Maurizio C.
Multielemental nanoclusters formed by ion implantation in dielectrics
Nuclear Instruments and Methods in Physics Research B **218**, 396-404, 2004a.

Maurizio C., Pergolesi D., Gatti F., d'Acapito F., Razeti M., Balerna A., Mobilio S.
Application of a TES micro-calorimeter as high-energy resolution detector for hard X-rays at a synchrotron beam line
Nuclear Instruments and Methods in Physics Research A **520**, 610-612, 2004b.

Maurizio C., d'Acapito F., Priolo F., Franzò G., Iacona F., Borsella E., Padovani S., Mazzoldi P.
Site of Er ions in Er-implanted silica containing Si nanoclusters
Optical Materials **27**, 900-903, 2005.

Maurizio C., Iacona F., d'Acapito F., Franzò G., Priolo F.
Er site in Er-implanted Si nanoclusters embedded in SiO_2

Physical Review **B74**, 205428-1-7, 2006.

Maurizio C., Mattei G., Canton P., Cattaruzza E., de Julian Fernandez C., Mazzoldi P., d'Acapito F., Battaglin G., Scian C., Vomiero A.,
Thermal evolution of cobalt nanocrystals embedded in silica
Materials Science and Engineering C **27**, 193-196, 2007.

Maurizio C., d'Acapito F., Sada C., Cattaruzza E., Gonella F., Battaglin G.,
Site of transition metal ions in ion-exchanged metal-doped glasses
Materials Science and Engineering B149, 171-176, 2008a.

Maurizio C., d'Acapito F., Ghibaudo E., Broquin J.E.
Tl ion-exchange borosilicate glass: investigation of the Tl site by x-ray absorption spectroscopy
Journal of Non-Crystalline Solids 354, 124-128, 2008b.

Maurizio C., Quaranta A., Ghibaudo E., D'Acapito F., Broquin J.-E.,
Ag site in Ag-for-Na ion-exchanged borosilicate and germanate glass waveguides
J. Phys. Chem. C in press, 2009.

Mazzoldi P., Padovani S., Enrichi F., Mattei G., Trave E., Guglielmi M., Martucci A., Battaglin G., Cattaruzza E., Gonella F., and Maurizio C.
Sensitizing effects in Ag-Er co-doped glasses for optical amplification
Proceedings SPIE 5451, 311-326, 2004.

Mazzoldi P., Mattei G., Maurizio C., Cattaruzza E., Gonella F.

Metal Alloy Nanoclusters by Ion Implantation in Silica
in "Engineering Thin Films and Nanostructures with Ion Beams", Emile Knystautas Editor, Optical Science and Engineering Series, Vol. 95, Taylor&Francis CRC Press, 2005.

Meneghini C., Mobilio S., Lusvarghi L., Bondioli F., Ferrari A.M., Manfredini T., Siligardi C.
The structure of ZrO2 phases and devitrification processes in a Ca-Zr-Si-O-based glass ceramic: A combined a-XRD and XAS study.
Journal of Applied Crystallography, **37**, 890-900, 2004.

Meneghini C., Liscio F., Bardelli F., Mobilio S., Ray S., Sarma D. D.
The nature of "disorder" in ordered double perovskite, Sr_2FeMoO_6
Phys. Rev. Lett. submitted, 2009.

Merlini M., Gemmi M., Artioli G.
Thermal expansion and phase transitions in Akermanite and gehlenite.
Physics and Chemistry of Minerals **32**, 189-196, 2005.

Merlini M., Artioli G., Meneghini C., Cerulli T., Bravo A., Cella F. The early hydration and the set of Portland cements: In situ X-ray powder diffraction studies. Powder Diffraction **22**, 201-208, 2007.

Merlini M., Meneghini C., Artioli G., Cerulli T. Synchrotron radiation XRPD study on the early hydration of cements. Zeitschrift fŸr Kristallographie Supplement **26**, 411-416, 2007.

Merlini M. Gemmi M. Cruciani G. Artioli G.
High-temperature behaviour of melilite: In situ X-ray diffraction study of gehlenite-åkermanite-Na melilite solid solution.
Physics and Chemistry of Minerals **35**, 147-155, 2008.

Merlini M. Artioli G. Cerulli T. Cella F. Bravo A. Tricalcium aluminate hydration in additivated systems. A crystallographic study by SR-XRPD. Cement and Concrete Research **38**, 477-486, 2008.

Millini R., Carati A., Bellussi G., Cruciani G., Parker Jr W.O., Rizzo C., Zanardi S.
Synthesis, characterization and crystal structure of EMS-2 Ð a novel microporous stannosilicate.
Microporous and Mesoporous Materials, **101**, 43-49, 2007.

Monesi C., Meneghini C., Bardelli F., Benfatto M., Mobilio S., Manju U., Sarma D. D.
Local structure in $LaMnO_3$ and $CaMnO_3$ perovskites: a quantitative structural refinement of Mn-K edge XANES data,
Phys. Rev. B **72**, 033111, 2005.

Monesi C., Meneghini C., Bardelli F., Benfatto M., Mobilio S., Manju U., Sarma D.D.
Quantitative structural refinement of Mn K edge XANES in $LaMnO_3$ and $CaMnO_3$ perovskites
Nucl. Inst. and Methods in Phys. Res. B **246**,158-164, 2006.

Motta, F. Boscherini, A. Sgarlata, A. Balzarotti, G. Capellini, F. Ratto, and F. Rosei
GeSi intermixing in Ge nanostructures on Si(111): An XAFS versus STM study
Phys. Rev. B **75**, 035337, 2007.

Noé P., Salem B., Delamadeleine E., Jalabert D., Calvo V., Maurizio C., d'Acapito F.
Effect of the Er-Si interatomic distance on the Er^{3+} luminescence in silicon-rich silicon oxide thin films
Journal of Applied Physics **102**, 103516-1-4, 2007.

Ottaviano L., M. Passacantando, A. Verna, R. Gunnella, E. Principi, A. Di Cicco, G. Impellizzeri, and F. Priolo
Direct structural evidences of Mn dilution in Ge,
J. Appl. Phys. **100**, 063528, 2006.

Padovani S., Borgia I., Brunetti B., Sgamellotti A., Giulivi A., d'Acapito F., Mazzoldi P., Sada C., Battaglin G.
Silver and copper nanoclusters in the lustre decoration of Italian Renaissance pottery: An EXAFS study.
Applied Physics A., **79**, 229-233, 2004.

Padovani S., Puzzovio D., Sada C., Mazzoldi P., Borgia I., Sgamellotti A., Brunetti B.G., Cartechini L., d'Acapito F., Maurizio C., Shokoui F., Oliaiy P., Rahighi J., Lamehi-Rachti M., Pantos E.
XAFS study of copper and silver nanoparticles in glazes of medieval middle-east lustreware (10^{th}-13^{th} century).
Applied Physics A**83**, 521-528, 2006.

Parravicini G.B., Stella A., Ghigna P., Spinolo G., Migliori A., d'Acapito F., Kofman R.,
Extreme undercooling (down to 90 K) of liquid metal nanoparticles
Applied Physics Letters **89**, 033123-1, 2006.

Patelli, V. Rigato, G. Salmaso, M. Rovezzi, F. D'Acapito
Temperature dependence of interface thickness in Mo/Si multilayers studied by Standing-Wave EXAFS
INFN – LNL Annual report 2004, pg 90, 2004.

Persson I. D'Angelo P., De Panfilis S., Sandström M., Eriksson L.
Hydration of lanthanoid(III) ions in aqueous solution and crystalline hydrates studied by EXAFS spectroscopy and crystallography: The myth of the "gadolinium break"
Chem. Eur. 14 (2006) 3056.

Pettiti I., Colonna S., De Rossi S., Faticanti M., Minelli G., Porta P.
XAS characterization and CO oxidation on delta-alumina supported La, Mn, Co and Fe oxides
Physical Chemistry - Chemical Physics **6**, 1350-1358, 2004.

Plazanet M., Dean M., Merlini M., Hyller A., Emerich H., Meneghini C., Johnson M.R., Trommsdorff H.P.
Crystallization on heating and complex phase behaviour of alfa-cyclodextrin solutions
Journal of Chemical Physics, **125**, 154504, 2006.

Pozzi, D., Amiconi, G., Arcovito, A., Girasole, M., Congiu Castellano
Haem conformation of amphibian nytrosylhaemoglobins detected by XANES spectroscopy
Eur. Phys. J. E **16**, 373-379, 2005.

Prestipino C., Bonino F., Usseglio S., Damin A., Tasso A., Clerici M.G., Bordiga S., d'Acapito F., Zecchina A., Lamberti C.
Equilibria between peroxo and hydroperoxo species in the titanosilicates: An in situ high-resolution XANES investigation
Chem.Phys.Chem., **5**, 1799-1804, 2004.

Prestipino C., Capello L., d'Acapito F., Lamberti C.

Local structure of [CuI(CO)2]+ adducts hosted inside ZSM-5 zeolite probed by EXAFS, XANES and IR spectroscopies
Physical Chemistry - Chemical Physics, **7**, 1743-1746, 2005a.

Prestipino C., Solari P.L., Lamberti C.
EXAFS and XANES investigation of the ETS-10 microporous titanosilicate
Journal of Physical Chemistry B **109**,13132-13137, 2005b.

Quartieri S., Dalconi M.C., Boscherini F., Oberti R., D'Acapito F.
Changes in the local coordination of trace rare-earth elements in garnets by high-energy XAFS: New data on dysprosium
Physics and Chemistry of Minerals 31, 162-167, 2004

Quartieri S., Pia Riccardi M., Messiga B., Boscherini F.
The ancient glass production of the Medieval Val Gargassa glasshouse: Fe and Mn XANES study.
Journal of Non-Crystalline Solids, **351**, 3013-3022, 2005.

Rabe S., Nachtegaal M., Vogel F.
Catalytic partial oxidation of methane to synthesis gas over a ruthenium catalyst: the role of the oxidation state
Physical Chemistry - Chemical Physics **9**,1461-1468, 2007.

Regli L., Bordiga S., Busco C., Prestipino C., Ugliengo P., Zecchina A., Lamberti C.
Functionalization of zeolitic cavities: Grafting NH2 groups in framework T sites of B-SSZ-13 - A way to obtain basic solids catalysts?
Journal of the American Chemical Society **129**, 12131-12140, 2007a

Regli L., Bordiga S., Lamberti C., Lillerud K.P., Zones S.I., Zecchina A.
Effect of boron substitution in chabazite framework: IR studies on the acidity properties and reactivity towards methanol
Journal of Physical Chemistry C, **111**, 2992-2999, 2007b

Rovezzi M., d'Acapito F., Patelli A., Rigato V., Salmasso G., Bontempi E., Davoli I.
Characterization of thermally treated Mo/Si multilayer mirrors with standing wave-assisted EXAFS
Nuclear Instruments and Methods in Physics Research B **246**, 127-130, 2006.

Rovezzi M., T. Devillers, E. Arras, F. d'Acapito, A. Barski, M. Jamet, and P. Pochet
Atomic structure of Mn-rich nanocolumns probed by x-ray absorption spectroscopy
Appl. Phys. Lett. **92**, 242510, 2008.

Sacerdoti M., Dalconi M.C., Carotta M.C., Cavicchi B., Ferroni M., Colonna S., Di Vona M.L.
XAS investigation of tantalum and niobium in nanostructured TiO2 anatase.
Journal of Solid State Chemistry **177**, 1781-1788, 2004.

Sani A., Quartieri S., Boscherini F., Antonioli G., Feenstra A., Geiger C.A.
Fe^{2+}-O and Mn^{2+}-O bonding and Fe^{2+} and Mn^{2+} vibrational properties in synthetic almandine-spessartine solid solutions: An X-ray absorption fine structure study
European Journal of Mineralogy, 2004, 16, 801-808

Sanson A., Dalba G., Fornasini P., Grisenti R., Rocca F., Artioli G., Dapiaggi M., Tiano W.
EXAFS and XRD study of local dynamics in Cu2O and Ag2O
Physica Scripta, **T115**, 271, 2005.

Sanson A., Rocca F., Dalba G., Fornasini P., Grisenti R., Dapiaggi M., Artioli G.
Negative thermal expansion and local dynamics in Cu2O and Ag2O
Phys. Rev. B **73**, 214305, 2006.

Sanson A., Rocca F., Fornasini P., Dalba G., Grisenti R., Mandanici A.
Thermal behaviour of the local environment around iodine in fast-ion-conducting AgI-doped glasses,
Phil. Mag., 87769–777, 2007a.

Sanson A., Rocca F., Dalba G., Fornasini P., Grisenti R.,
Influence of temperature on the local structure around iodine in fast-ion-conducting AgI:Ag_2MoO_4 glasses,
New J. Phys., **9**, 88, 2007b.

Sanson, A; Rocca, F; Armellini, C; Dalba, G; Fornasini, P; Grisenti, R
Correlation Between I-Ag Distance and Ionic Conductivity in AgI Fast-Ion-Conducting Glasses,
Phys. Rev. Lett, **101**, 155901, 2008a.

Sanson A., Rocca F., Armellini C., Ahmed S., Grisenti R.
Local study on the MoO_4 units in AgI-doped silver molybdate glasses,
Journal of Non-Crystalline Solids, **354**, 94–97, 2008b

Santagostino Barbone A., Gliozzo E., d'Acapito F., Memmi Turbanti I., Turchiano M., Volpe Giuliano
The sectilia panels of Faragola (Ascoli Satriano, southern Italy): a multi-analytical study of the red, orange and yellow glass slabs.
Archaeometry, **49**, 3-23 (2007)

Scordari F., Ventruti G., Gualtieri A.F.
The structure of metahohmannite, Fe23+[O(SO4)2].4H2O, by in situ synchrotron powder diffraction.
American Mineralogist **89**, 365-370, 2004.

Sipr O., Dalba G., Rocca F.
Ordered and disordered models of local structure around Ag cations in silver borate glasses based on x-ray absorption near-edge structure spectroscopy
Phys. Rev. B, **69**, 134201, 2004a.

Smolentsev G., Soldatov A.V., d'Acapito F., Polzonetti G., Fratoddi I.
Local structure parameters through the fitting of XANES spectra using a multidimensional interpolation: Application to the Pd K-edge of Pd-diethynylbiphenyl polymer
Journal of Physics Condensed Matter **18**, 759-766, 2006.

Spiga S., Wiemer C., Tallarida G., Fanciulli M., Malvestuto M., Boscherini F., d'Acapito F., Dimoulas A., Vellianitis G., Mavrou G.
Structural characterization of epitaxial Y_2O_3 on Si (001) and of the Y_2O_3/Si interface.
Materials Science and Engineering B **109**, 47-51, 2004.

Tarantino S.C., Ghigna P., McCammon C., Amantea R., Carpentier M.A.
Local structural properties of (Mn,Fe)Nb2O6 from Mšssbauer and X-ray absorption spectroscopy.
Acta Crystallographica B **61**, 250-257, 2005.

Tomasi C., Scavini M., Cavicchioli A., Speghini A., Bettinelli M.
Isothermal and non-isothermal kinetic study of the $PbGeO_3$ solid_solid phase transition
Thermochimica Acta **432**, 2, 2005.

Trave E., Mattei G., Mazzoldi P., Pellegrini G., Scian C., Maurizio C., Battaglin G.
Sub-nanometric metallic Au clusters as efficient Er^{3+} sensitizers in silica
Applied Physics Letters **89**, 151121-1-3, 2006.

Tribaudino M., Benna P., Nestola F., Meneghini C., Bruno E.
Thermodynamic behaviour of the high-temperature P1/1 phase transition along the CaAl2Si2O8-SrAl2Si2O8 join.
Physics and Chemistry of Minerals, 2005, 32, 314-321, 2005.

Vaccari M., Grisenti R., Fornasini P., Rocca F., Sanson A.
Negative thermal expansion in CuCl: An extended X-ray absorption fine structure study
Phys. Rev. B 75 (2007) 184307.

Veronesi, G., Giachini, L., Francia, F., Mallardi, A., Palazzo, G., Boscherini, F., Venturoli, G.
The Fe2+ site of photosynthetic reaction centers probed by multiple scattering X-ray absorption fine structure spectroscopy: Improving structure resolution in dry matrices
Biophys. J. **95**, 814-822,. 2008.

Zecchina A., Rivallan M., Berlier G., Lamberti C., Ricchiardi G.

Structure and nuclearity of active sites in Fe-zeolites: comparison with iron sites in enzymes and homogeneous catalysts
Physical Chemistry Chemical Physics 9, 3483-3499, 2007.
